COMBUSTION AND EMISSIONS OF A DIRECT INJECTION GASOLINE ENGINE USING EGR

by

Thomas Lattimore

A thesis submitted to

The University of Birmingham

for the degree of

DOCTOR OF PHILOSOPHY

The University of Birmingham

School of Engineering

December 2015

UNIVERSITY OF BIRMINGHAM

Abstract

This research has examined the combustion and emissions of a spray-guided direct-injection spark-ignition (DISI) engine using exhaust gas recirculation (EGR). The impact of EGR type, swirl and tumble intake airflows, compression ratio and fuel type were also investigated.

EGR addition resulted in significant fuel consumption improvements and differing particulate matter (PM) behaviour depending on the knock limited maximum brake torque (KLMBT) spark advance achieved. When comparing EGR types, cooled EGR achieved the best fuel consumption and cooled EGR after three-way catalyst (TWC) achieved the best gaseous emissions (NO_x and HC).

Swirl and tumble intake airflows significantly increased fuel consumption. However, these increases could be minimized with EGR addition. Swirl significantly reduced the accumulation mode particulate emissions, providing a potential solution for PM reduction. EGR addition did not significantly affect PM for the swirl and tumble intake airflow conditions.

20%vol 1-butanol addition to gasoline fuel (Bu20) resulted in significant PM reductions at 8.5 bar IMEP. At 7.0 bar IMEP, EGR addition allowed the KLMBT spark timing to be advanced, as the compression ratio was increased. Fuel consumption was improved by 0.4% due to the spark advance and reduced pumping losses, and PM improved because the formation of primary particles was reduced.

Acknowledgements

First and above all, I praise God, the most beneficent, the most merciful, for providing me with this opportunity and for granting me the capability to succeed. This thesis would not have been possible without the assistance and guidance of several people. I would therefore like to offer my sincere gratitude and thanks to them all.

I would like to give my warmest and most sincere gratitude to Professor Hongming Xu who throughout the duration of my PhD program has provided me with invaluable guidance, experience and support to enable me to successfully complete my PhD. I would like to thank my second supervisor, Professor Miroslaw L. Wyszynski for his useful comments and feedback for my research work, and I would like to thank Professor Akbar Ghafourian for his guidance, help and encouragement in my annual reviews. I would also like to thank the Engineering and Physical Sciences Research Council for providing the funding for my PhD scholarship, and I would like to thank the University Of Birmingham for facilitating the scholarship and my PhD studies, as well as Professor Kyle Jiang for awarding the scholarship to me.

Great thanks go to my PhD candidate and research assistant colleagues who have provided me with technical knowledge and a good working environment to complete my PhD studies. I would like to thank Dr. Chongming Wang, Dr. Jose Herreros, Soheil Rezaei, Dr. Changzhao Jiang, Tawfik Badawy, Dr. Xaio Ma, Dr. Dhananjay Srivastava, Dr. Isaline Lefort, Dr. Arumugam Sakunthalai Ramadhas, Dr. Mohammadreza Attar, Dr. He Ma and Maria Macias, in particular, for their technical support at various times during my studies. I would also like to thank Yasser Al Qahtani, Rafiu Olalere, Ricky Creegan and Lucas Polglase for providing a friendly productive working environment at the University.

Contents

List of Figures

List of Tables

List of Notations

AFR	Air Flow Rate
aTDC	After Top Dead Centre
BDC	Bottom Dead Centre
BOC	British Oxygen Company
bTDC	Before Top Dead Centre
Bu20	20%vol 1-butanol in gasoline
CAD	Crank Angle Degrees
CC	Cubic Capacity
CCD	Charge Coupled Device
CE	Cooled EGR
CFR	Cooperative Fuel Research
CI	Confidence Interval
CID	Combustion Initiation Duration (Crank angle from spark discharge to MFB5)
CLD	Chemiluminescence Detector
COV_{IMEP}	Coefficient of Variation of IMEP
CO	Carbon Monoxide
Comb.	Combustion
CO_2	Carbon Dioxide
DC	Direct Current
DI	Direct-Injection
DISI	Direct-Injection Spark-Ignition
$(dQ/d\theta)$	Net Heat Release Rate
EC	European Commission
EGR	Exhaust Gas Recirculation
EGT	Exhaust Gas Temperature

EPSRC	Engineering and Physical Sciences Research Council
ETCS	Engine Timing Control System
EU	European Union
EVC	Exhaust Valve Closing
E20	20%vol ethanol in gasoline
FID	Flame Ionization Detector
FTIR	Fourier Transform Infra-Red
FTP	Federal Test Procedure
GC	Gravimetric Content
HC	Unburned Hydrocarbon
HE	Hot EGR
HoV	Heat Of Vaporisation
HSDAQ	High Speed Data Acquisition
IC	Internal Combustion
ICE	Internal Combustion Engines
IMEP	Indicated Mean Effective Pressure
IN	Inputs
ISFC$_{net}$	Net Indicated Specific Fuel Consumption
IVO	Intake Valve Opening
KLMBT	Knock Limited Maximum Brake Torque
LHV	Lower Heating Value
LSDAQ	Low Speed Data Acquisition
MBT	Maximum Brake Torque
MF	Methylfuran
MFB	Mass Fraction Burned
MFB10	Crank Angle at 10% Mass Fraction Burned
MFB10-90	Combustion Duration (Crank Angle Degrees from 10 to 90% MFB)

MFB5	Crank Angle at 5% Mass Fraction Burned
MFB50	Crank Angle at 50% Mass Fraction Burned
MFB90	Crank Angle at 90% Mass Fraction Burned
MON	Motor Octane Number
$\dot{m}_{net}$	Net Mass Flow Rate of Fuel into the Combustion Chamber
NA	Naturally Aspirated
NDIR	Non-Dispersive Infra-Red
Nd:YAG	Neodynium-Doped Yttrium Aluminium Garnet
NEDC	New European Driving Cycle
NI	National Instruments
NO	Nitrous Oxide
NO$_x$	Nitrous Oxides
η	Thermal Efficiency
OUT	Outputs
PAH	Polycyclic Aromatic Hydrocarbon
PAI	Polyamid-Imide
PFI	Port Fuel Injection
PID	Proportional Integral Controller
PIV	Particle Image Velocimetry
PLIF	Planar Laser Induced Florescence
PM	Particulate Matter
PN	Particulate Number
PMEP	Pumping Mean Effective Pressure
P$_{max}$	Maximum Pressure
PRF	Primary Reference Fuel
R$_c$	Compression Ratio
RDE	Real Driving Emission

ROHR	Rate Of Heat Release
RON	Research Octane Number
RPM	Revolutions Per Minute
SI	Spark-Ignition
Sig.	Significant
SMPS	Scanning Mobility Particle Sizer
TDC	Top Dead Centre
TWC	Three-Way Catalyst
T90	90% Distillation Temperature
ULG	Unleaded Gasoline
US	United States
VAF	Volumetric Airflow
V_c	Clearance Volume
VVT	Variable Valve Timing
V_d	Swept Volume
VE	Volumetric Efficiency
VVT	Variable Valve Timing
WOT	Wide Open Throttle
γ	Heat Capacity Ratio
$\Delta_{vap}H$	Heat Of Vaporization
λ	Air-Fuel Ratio

List of Publications

1.   **Investigation of EGR Effect on Combustion and PM Emissions in a DISI Engine**, Thomas Lattimore, Chongming Wang, Hongming Xu, Miroslaw L. Wyszynski, Shijin Shuai, 2016, Applied Energy, 161, 256-267, doi:10.1016/j.apenergy.2015.09.080.

2.   **Investigation of Compression Ratio and Fuel Effect on Combustion and PM Emissions in a DISI Engine**, Thomas Lattimore, José M. Herreros, Hongming Xu, Shijin Shuai, Fuel, 169, 68-78, doi: 10.1016/j.fuel.2015.10.044.

3.   **Impacts of Low-level MF content in gasoline on DISI engine combustion behaviour and emissions,** Chongming Wang, Hongming Xu and Thomas Lattimore. 2013. SAE technical paper 2013-01-131, doi:10.4271/2013-01-1317.

4.   **Fuel Effect on Particulate Matter Composition and Soot Oxidation in a Direct-Injection Spark Ignition (DISI) Engine,** Chongming Wang, Hongming Xu, Jose Martin Herreros, Thomas Lattimore and Shijin Shuai. 2014. Energy & Fuels, 28, 2003-2012, doi: 10.1021/ef402234z.

Awards:

TI Group Scholarship (PG) for outstanding academic performance

Thomas Lattimore, School of Mechanical Engineering, University Of Birmingham, March 2013

Chapter 1

Introduction

The aim of this chapter is to provide an overview of the PhD research investigation conducted by the author. The study of fuel consumption reducing techniques of EGR (also used to reduce NO_x), swirl and tumble intake airflows, geometric compression ratio increase as well as the study of biofuels is driven by the demand for reduced fuel consumption and hence reduced CO_2 emissions from vehicles. This is in addition to, in the case of biofuels, the demand for renewable energy supply and increased energy supply security. The overall research outline, objectives and investigation approach are presented briefly, after which the outline for the thesis follows.

1.1 Overview

While many of us dream of a future where electric cars charged by renewable means are commonplace and the small demand for a traditional engine sound is met by clean hydrogen combustion, this dream is still a long way away. Crude oil supplies have at least 50 years remaining (BP, 2015), if not more, especially because of the ongoing discovery and exploitation of shale oil reserves, which has been a significant factor in the oil price slump we are experiencing in 2015-16. Therefore, there is not a strong economic incentive for industry to invest in the technology and infrastructure required for electric and hydrogen powered vehicles. There are, however, legislative factors that are driving the research and development in the automotive industry; most significantly, emissions legislation and tax incentives. The progress though is not towards wide-scale electric vehicle use. It is towards increased engine and vehicle efficiency through engine downsizing and vehicle hybridization, amongst other methods, as well as reduced vehicle emissions produced by the efficiency

improvements and improved emissions after-treatment. Thus, for the meantime, conventional spark-ignited and compression-ignited internal combustion (IC) engines are here to stay. However, they will be increasingly downsized with increasing amounts of hybridization to recover waste power from the engine and the vehicle to improve their overall efficiencies.

In spark-ignition (SI) engines, many technologies are being widely utilized to improve fuel economy and to reduce emissions. These technologies include EGR, improved combustion using swirl and tumble generated intake airflows, optimised compression ratio, DI, turbocharging, variable valve lift and timing, cam profile switching and lean-burn stratified charge combustion. These improve the fuel economy of the engine itself and reduce its emissions, although PM and some gaseous emissions can potentially be increased. More efficient catalytic converters and improved particulate filters are being utilized to reduce the emissions of the vehicle as a whole, by converting the emissions from the engine into less harmful substances.

Biofuels, particularly bio-ethanol, are also believed to be part of the solution to reduce vehicle emissions. This is due to their oxygenated nature which reduces combustion temperatures, providing decreased NO_x emissions, along with reduced HC and PM emissions through improved post-combustion oxidisation. The ability to produce bio-ethanol and similar biofuels using renewable methods greatly reduces their net CO_2 output; the CO_2 produced during combustion is absorbed from the atmosphere when the raw plant material used to produce the fuel is grown.

While EGR, swirl and tumble intake airflows, compression ratio and biofuels have been studied in detail previously by other researchers, their effect on combustion in DISI engines and their subsequent emissions has been much less thoroughly investigated, particularly

regarding their effect on PM emissions. Therefore, their impact on DISI engine combustion and emissions needs to be assessed.

1.2 Objectives and Approaches

The main research objective of this investigation was to study the impact of EGR on the combustion and emissions, in particular the PM emissions, of a DISI engine. A spray-guided single-cylinder DISI thermal research engine was used for the engine experiments. PM emissions were measured using a Cambustion DMS 500 and a TSi SMPS 3936. A Horiba MEXA-7100DEGR gas analyser was used to measure the gaseous emissions of nitrous oxides (NO_x) and hydrocarbons (HC).

The following are the areas that were investigated throughout the author's PhD study:

- The effect of EGR and its type on engine combustion and emissions

- The effect of intake airflow and EGR on engine combustion and PM emissions

- The effect of compression ratio, fuel and EGR on engine combustion and emissions

The novel ideas investigated in this thesis include:

- Investigation of the effect of different types of EGR (hot EGR, cooled EGR, hot EGR after TWC, cooled EGR after TWC) on engine combustion and gaseous emissions at the same engine load using a simulated TWC (this removes the effect of varying TWC conversion efficiencies which result in varying EGR ratios)

- Investigation of the effect of 1-butanol blending into gasoline on engine combustion and emissions (particulate and gaseous) at different compression ratios

- Unlike most other investigation, the PM analysis in this thesis has classified the particles into nucleation and accumulation modes, which have been studied individually, where appropriate

1.3 Research Outline

The research presented in this thesis was conducted by the author at the Future Engines and Fuels research laboratory at the University of Birmingham with help and support from Jaguar Land Rover and Shell Global Solutions UK. The research was mainly conducted to investigate the effects of EGR on the combustion and emissions of a DISI engine.

The study of engine combustion includes an analysis of the KLMBT spark timing achieved at different operating conditions with the engine. It includes a detailed and comprehensive analysis of the in-cylinder pressure trace and mass fraction burned (MFB) profiles. A Ricardo WAVE engine model has been utilized to calculate the in-cylinder temperature in order to assist in the engine combustion study. Fuel consumption behaviour has been analysed in detail to quantify the effect of the combustion at different engine conditions on this parameter. Pumping mean effective pressure (PMEP), exhaust gas temperature (EGT) and coefficient of variation of IMEP (COV_{IMEP}) have been analysed too in order to further quantify the combustion effects. Regulated emissions of PM, NO_x and HC were then examined in order to study the effect of the engine combustion on these critical parameters, which are the most important regarding legislative requirements.

In order for biofuels to be commercialised, their combustion and emissions must be quantified and subsequently shown to be competitive with fuels currently on the market (i.e. gasoline). Therefore, this thesis also presents research comparing gasoline and oxygenated fuels blended into gasoline.

1.4 Thesis Outline

This thesis is composed of seven chapters. A brief outline of each chapter is presented below.

Chapter 2- Literature Review

This chapter reviews the literature that is relevant to this investigation. DI and spark timing are talked about in detail as well as the phenomenon of engine knock. The current trend of engine downsizing is introduced along with fuel consumption improvement and CO_2 emission reduction, with EGR, swirl and tumble intake airflows and compression ratio explored in detail. After this, spark ignition fuels including oxygenated alternatives are discussed. Finally, a discussion into the regulated engine-out emissions and related legislation is provided.

Chapter 3- Experimental Setup and Techniques

This chapter gives detailed information of the engine and instrumentation setup, as well as detailed information of the data acquisition and recording systems. The emission analysers are introduced after which key calculations for engine parameters used in this thesis are presented. Finally, the details of the Ricardo WAVE engine model are provided along with the details of the fuels used in this investigation.

Chapter 4- The Effect of EGR and its Type on Engine Combustion and Emissions

This chapter provides details of the combustion and emissions characteristics of a DISI engine operated with hot EGR at different engine loads of 5.5, 7.0 and 8.5 bar IMEP, and with different EGR types of hot EGR, cooled EGR, hot EGR after TWC and cooled EGR after TWC. In the first part, the hot EGR addition was increased across the different engine loads, and in the second part the EGR addition was increased at a single engine load of 7.0

bar IMEP, and the EGR type is changed. The combustion and emission parameters at the different conditions are compared to quantify the effect of EGR and its type on them.

Chapter 5- The Effect of Intake Airflow and Hot EGR on Engine Combustion and PM Emissions

This chapter provides details of the combustion and PM emission characteristics of a DISI engine operated with swirl and high tumble intake airflows, and with hot EGR addition. The EGR addition was increased across the two intake airflow conditions along with a baseline low tumble condition at a single engine load of 7.0 bar IMEP. The combustion and PM emission parameters at the different conditions are compared to quantify the effect of intake airflow and hot EGR on them.

Chapter 6- The Effect of Compression Ratio, Fuel and Hot EGR on Engine Combustion and Emissions

This chapter provides details of the combustion and emissions characteristics of a DISI engine operated with different compression ratios and different fuels, and with hot EGR addition. In the first part, the two fuel splash blends of Bu20 and E20 were tested along with a baseline of gasoline at a single engine load of 8.5 bar IMEP, with the compression ratio increased after each of the fuel blends and the reference fuel were tested. In the second part, gasoline fuel was tested at a single engine load of 7.0 bar IMEP, with the hot EGR addition increased along with the compression ratio. The combustion and emission parameters at the different conditions are compared to quantify the effect of compression ratio, fuel type and hot EGR on them.

Chapter 7- Summary and Conclusions, and Recommendations for Future Work

This chapter summarizes the research conducted in this investigation and provides the key conclusions of this thesis. Recommendations for future work are then given.

Chapter 2

Literature Review

The aim of this chapter is to review the literature that is relevant to this investigation. The main areas of discussion are SI engine combustion and emissions.

2.1 Introduction

Firstly, this chapter provides a brief introduction regarding the history of IC engines and explains the key fundamental differences between spark and compression ignition engines. Spark-ignited combustion is then further discussed, after which DI and spark-timing which result in the combustion and emissions from the engine are talked about in detail. The phenomenon of knock is then discussed with the factors affecting knocking tendency explained.

Secondly, the current and ever ongoing trend of improved vehicle fuel economy and reduced CO_2 emissions is introduced followed by detailed discussion of the potential of EGR, swirl and tumble intake airflows and geometric compression ratio increase to enable these improvements to be achieved. SI fuels are then explored due to their significant effect on combustion and emissions, including oxygenated alternatives, due to their increased use in motor vehicles and due to their predicted increased future usage.

Finally, regulated engine-out emissions are discussed, including an overview of the current legislation in both Europe and the US, due to their strong influence on the research and development of automotive engines. TWCs are then briefly discussed due to their strong influence on engine-out emissions.

2.2 History of IC Engines

The concept of the IC engine can be traced back to 1680 when Dutch Physicist Christian Huygens designed a gunpowder fuelled IC engine (Stone, 1999, The Institute of Historical Research, 2004). During the next 200 years further designs were proposed and built to advance the concept further. The most significant breakthrough came with Nicolaus Otto who built the first practical four-stroke IC engine in 1876 (Wu, 2007). The Otto cycle formed the underlying working principle for the engine operation and it became the universally adopted cycle for all liquid fuelled spark-ignited IC engines to this day. Later in 1893, Rudolph Diesel achieved compression ignition in an engine operated using the Diesel cycle which is utilized to this day in diesel compression ignition engines (Bennett, 2013).

The fundamental difference between gasoline and diesel engines is not the type of ignition but the type of combustion that occurs, with spark-ignited engines typically burning with a pre-mixed flame and compression-ignited engines typically burning with a diffusion flame (Stone, 1999). In order to obtain a reliable ignition and combustion with a pre-mixed flame, the fuel-air mixture of a SI engine must always be closed to stoichiometric, which necessitates the use of a throttle valve to control the amount of air entering the combustion chamber, which in return increases engine pumping work and thus reduces cycle efficiency (Stone, 1999). SI engines also suffer from knock, which limits their compression ratio thus limiting their thermal efficiency (Gupta, 2013). However, in diffusion flames, the fuel-air mixture is only required to be approximately stoichiometric at the flame front, which allows the engine to be de-throttled and the fuel injection to be controlled to produce the required power output (Stone, 1999). Thus, there are no throttling losses, significantly increasing the cycle efficiency as compared to a gasoline engine, resulting in improved part-load fuel economy (Stone, 1999). Also, knock is not a limitation in CI engines, thus, they can be

operated with higher compression ratios, significantly improving their thermal efficiency as compared to SI engines (Reitze Jr., 2001). However, PM is a significant problem in CI engines due to the diffusion flame, necessitating the use of a diesel particulate filter, which increases pumping losses (Bennett, 2010). The pre-mixed flame produces little PM meaning the vehicle does not require a particulate trap. Thus, it does not suffer from any additional pumping losses as a result of the higher exhaust back-pressure (Agarwal et al., 2014).

Today the main goal of engine researchers is to improve engine efficiency in order to reduce engine CO_2 emissions through reduced fuel consumption, while complying with ever tighter emissions regulations (Zaccardi et al., 2009). This has led to the increased use of DI, turbocharging and increased compression ratios (Heywood and Welling, 2009, Zaccardi et al., 2009).

2.3 SI Combustion

During the compression stroke of the SI engine cycle, the piston causes the fuel-air mixture to become highly compressed before a spark ignites the mixture causing it to combust. The spark leaves a small nucleus of the flame that propagates into the unburned gas, and it is not until that nucleus grows into a size which is the same order as that of the turbulence scale that the flame propagation can be enhanced by in-cylinder turbulence (Stone, 1999). This period is often referred to as the early burn, delay period or combustion initiation duration (CID) and it comprises the initial laminar combustion and the transition to fully turbulent combustion, typically lasting 1-2ms or 9-18 CAD at 1500 rpm (Stone, 1999). The crank angle interval between the spark discharge and the MFB5 or MFB10 parameters are typically used to define this period (Stone, 1999). The duration of this period depends on the temperature, pressure and composition of the fuel-air mixture (Stone, 1999).

Between MFB10 and MFB90 is the main combustion period which is dominated by turbulent combustion, the second stage of which occurs shortly after the peak pressure and it is affected by the same parameters as the early burn period along with turbulence (Stone, 1999). The flame in the final combustion stage makes contact with more of the combustion chamber walls and consequently it makes less contact with the remaining unburned fuel-air mixture, thus resulting in a significantly slower combustion (Stone, 1999).

2.3.1 Direct-Injection

DI is a technology that was initially developed for diesel engines but it was not until relatively recently that it was incorporated into gasoline production engines, with the modern DISI engine being first produced in 1996 by Mitsubishi, although the concept was initially invented by Frenchman Léon Levavasseur in 1902 (Institution of Mechanical Engineers, 2013, Mitsubishi Motors, 1999). It has an advantage of improved fuel economy and power output in comparison to PFI because the fuel can be injected into the combustion chamber at the best time; it is not dictated by the intake valve opening time as with PFI (Harada et al., 1997). DI benefits from charge cooling; the fuel cools as it is injected into the combustion chamber, causing the knocking tendency to reduce, allowing the spark timing to be subsequently advanced, as well as improving volumetric efficiency (Shimotani et al., 1995, Yang and Anderson, 1998). This contributes to fuel economy and power output improvements at medium-high loads (Alger et al., 2000, Daniel et al., 2012b, Harada et al., 1997). Both DI and PFI provide an advantage compared to carburettor type fuel injection because much more precise fuel metering is achieved which improves fuel economy and reduces engine emissions (Institution of Mechanical Engineers, 2013, Robert Bosch GmbH, 2006). Spray-guided DI first produced by Mercedes in 2006 is the most widely used DI method due to its improved thermodynamic efficiency and fuel economy compared to other

DI systems, such as wall-guided and air-guided DI, in addition to improved HC and PM emission behaviour (Green Car Congress, 2006).

DI can be used to realize either homogenous or stratified combustion. Traditionally homogenous combustion has been used to refer to that produced by PFI and stratified combustion has been used to refer to that produced by DI. However, within DI itself there are homogenous and stratified concepts (Harada et al., 1997, Takagi and Skippon, 1998). With an early injection of fuel directly into the cylinder during the induction stroke, a more homogenous mixture of approximately λ=1 can be achieved (Harada et al., 1997, Takagi and Skippon, 1998). When the fuel is injected late into the cylinder during the compression stroke a more stratified mixture is formed with an overall lambda of ~20 and a combustible mixture of λ~1 around the spark plug (Harada, 1997, Takagi and Skippon, 1998). With homogenous mixture formation, the mixture preparation is assisted by the high flow velocities and their aerodynamic forces in the area of the opening and closing intake valves, helping the fuel to evaporate quickly, ensuring it is well homogenized (Robert Bosch GmbH, 2006). With stratified mixture formation, a mixture cloud is created which can then be transported into the area around the spark plug by the air flows in the combustion chamber and by the upward stroke of the piston (Robert Bosch GmbH, 2006). The mixture formation benefits from the higher pressures and temperatures in the combustion chamber during the compression stroke of the engine cycle (Robert Bosch GmbH, 2006).

2.3.2 Spark-Timing

Spark timing has a significant effect on engine combustion and emissions. Regarding engine efficiency and thus fuel economy, greater expansion work can be produced on the piston as the spark is advanced and the pressure is consequently increased at TDC. However, advancing the spark also increases the compression work of the engine as the in-cylinder

pressure is increased during the compression stroke. Thus, there is a trade-off between the compression and expansion work in the IC engine to achieve the best engine efficiency, and this is controlled by the spark timing (Heywood, 1988). An optimum MFB50 phase of 8-10˚aTDC is required to produce best engine efficiency and thus the best fuel economy (De O. Carvalho et al., 2012). At low to medium engine loads, the spark timing can be chosen in order to produce the optimal combustion phasing. However, at high engine loads, knock limits the spark advance that can be achieved, meaning that more retarded spark timings are required (Checkel and Dale, 1989). Emissions are also significantly affected by the engine spark timing (Heywood, 1988); something that will be discussed in detail in a later section.

2.3.3 Knocking Phenomena

2.3.3.1 Introduction to Knocking Phenomena

The phenomenon of knock has existed for the majority of the history of IC engines, with the most widely publicised solution to the problem being high octane fuels (Checkel and Dale, 1989, Kalghatgi, 2013). These increase the knock tolerance of the engine which in turn allows the spark timing to be advanced for fuel economy and torque benefits. However, they also increase the cost of the fuel because high octane fuel fractions are more expensive than those with a low octane number (Checkel and Dale, 1989). The fuel economy benefits also reduce the engine CO_2 output, which along with fuel consumption is at the forefront of the public perception (Gov UK, 2011, Kalghatgi, 2013). Therefore, it is anticipated that demand for higher octane fuels will only increase in the future (Green Car Congress, 2013, Kalghatgi, 2014, Pawlowski and Splitter, 2015).

Knock itself is a shock wave generated by the auto-ignition of the fuel-air mixture in the end-zone of the combustion chamber once it has exceeded a critical temperature of approximately 625-725˚C (Kalghatgi, 2013). This most commonly occurs when the spark timing is

advanced to an extent that the pressure and temperature in the engine cylinder are increased to a critical level where the flame front generated from the spark discharge radiates significant heat to the fuel-air mixture in the end-zone, causing its pressure and temperature to increase through compression (Heywood, 1988). This occurs because the density of the burned mixture increases by approximately a factor of four causing not only the unburned mixture to be compressed but also compressing those parts of the charge that have already burned and displacing them back towards the spark plug (Heywood, 1988). This causes the temperature of the fuel-air mixture in the end-zone to rise beyond 625-725°C resulting in auto-ignition (Kalghatgi, 2013).

The auto-ignition produces two or more flame fronts in the combustion chamber which rapidly radiate heat to the remaining unburned fuel-air mixture, causing it to combust more rapidly than in normal combustion (Rothe et al., 2006). When its resulting shock wave makes contact with the piston face, it produces structural damage rather than exerting a pressure to push it (Oppenheim, 2004). The high pressure and temperature rise rates produced by the knock produce very high mechanical and thermal loads in the pistons, bearings, cylinder head and the cylinder head gasket, causing damage and even failure to these components (Amann and Alger, 2012, Robert Bosch GmbH, 2006). The flame front of this shock wave can propagate at a rate of 10 to 100 times that of normal combustion and it resonates on the combustion chamber walls producing the audible "ping" which is characteristic of engine knock (Hamilton et al., 2008).

Whether knock occurs or not reflects the outcome of a race between the advancing flame front and the pre-combustion reactions in the unburned end gas. Knock will not occur if the flame front consumes the end gas before these reactions have time to cause the fuel-air

mixture to auto-ignite (Heywood, 1988). However, if these reactions are given sufficient time, they will produce auto-ignition before the flame front arrives (Heywood, 1988).

2.3.3.2 Factors affecting Knocking Tendency

There are several factors which affect the tendency of an SI engine to knock. The most common is substantial spark advance which produces higher in-cylinder temperatures which leads to higher temperatures in the end-zone of the combustion chamber, resulting in ever greater levels of knock as the spark is continually advanced (Ulsoy et al., 2012). As the torque and load demand from the engine increase, the charge density is increased which leads to higher temperatures during the compression stroke, causing the engine knock tendency to increase (Robert Bosch GmbH, 2006). By definition, lower octane number fuels will knock more than those with a higher octane rating, thus, knock tendency increases with their use. Increasing the compression ratio increases knock tendency because the pressures and temperatures within the fuel-air charge are increased during the compression stroke (Robert Bosch GmbH, 2006). Deposits in the combustion chamber also increase the effective compression ratio, increasing knock tendency (Rajput, 2005, Robert Bosch GmbH, 2006).

Ineffective cooling within the engine can lead to hot spots forming within the combustion chamber and it can lead to overall temperature increases; both of which increases knock tendency (Rajput, 2005). Poor turbulence and swirl characteristics of an engine, produced by the relevant engine geometries can increase knock tendency (Robert Bosch GmbH, 2006). The use of homogenous fuel injection increases knock tendency because the mixture in the end-zone of the combustion chamber is ignitable whereas with stratified injection, only the mixture around the spark plug is rich enough to ignite (Robert Bosch GmbH, 2006). NO introduced into the intake gas by EGR increases knock tendency (Hoffmeyer et al., 2009, Lewis et al., 2014, Roth et al., 2010, Takaki et al., 2014, Yuan et al., 2015), but this is

overcome by the higher heat capacity of the exhaust gas compared to fresh air (Francqueville and Michel, 2014), resulting in knock tendency reducing overall. Finally, the use of PFI injection increases knock tendency in comparison to DI because it does not benefit from the charge cooling effect that occurs with DI (Alger et al., 2000, Harada et al., 1997).

2.3.4 Downsizing, Fuel Consumption Improvement and CO_2 Emission Reduction

The current trend in gasoline engine technology is aggressive downsizing which aims to decrease the engine capacity while maintaining or improving power output, in order to improve fuel economy and reduce emissions, through reduced pumping losses and other efficiency gains (Cairns et al., 2006, Castagné et al., 2003, Lecointe and Monnier, 2003). Technologies such as turbocharging and DI are used in order to achieve these aims (Castagné et al., 2003, Lecointe and Monnier, 2003, Song et al., 2014). In addition, techniques such as EGR, swirl and tumble intake airflows and increased compression ratio are being used to improve the fuel economy and thus reduce the CO_2 output of modern engines. Therefore, EGR, swirl and tumble intake airflows and compression ratio increase have been researched further in this investigation to help develop the knowledge of engine researchers in these areas. These are discussed further in the following sections.

2.3.5 EGR

EGR, both internal and external, as well as lean mixtures, can be used to reduce the power density and thus reduce the energy deposition rate of the mixture to improve engine knock resistance (Francqueville and Michel, 2014, Galloni et al., 2013, Nishida et al., 1988), allowing increased boosting in turbocharged engines as well as increased compression ratios (Galloni et al., 2013). This however reduces the maximum engine load and torque, as well as the maximum power density, meaning that it can only be utilized at part-load conditions. It can most effectively be used in fast-burn engine designs such as the widely used four-valve

pentroof combustion chamber; the design produces significant tumble which leads to a rapid burn (Stone, 1999, Urushihara et al., 1995). It is most effective in these designs because EGR reduces the laminar flame speed of the fuel-air mixture, thus, a fast-burn balances the EGR well (Endres et al., 1992, Heywood, 1988). This allows EGR to be utilised to reduce NO_x emissions, which is particularly important for stratified combustion at low loads, or it allows it to be utilised to improve part-load fuel economy (Davis and Borgnakke, 1982, Heywood, 1988). However, EGR potentially increases particulate and HC emissions, thus, this limits its use in modern DISI engines (Alger et al., 2009a, Diana et al., 1996, Wei et al., 2012, Zhong et al., 2013).

Part-load fuel economy is improved because the throttle has to be more opened to achieve a particular load, due to the EGR gases replacing some of the fresh air volume in the combustion chamber (Stone, 1999). This reduces the pumping work required of the engine, thus improving fuel economy (Abd-Alla, 2002, Grandin et al., 1998, Robert Bosch GmbH, 2006, Wei et al., 2012). This is important at high loads because stratification for the purpose of reducing pumping losses is not possible. Thermal efficiency is also improved with EGR addition due to reduced combustion temperatures (Ratnak et al., 2015, Siokos et al., 2015), contributing to fuel economy improvements. As mentioned, the spark timing can be advanced due to the improved knock resistance with EGR addition, allowing the optimum 8-10˚aTDC MFB50 phasing to be achieved, also improving the fuel economy (De O. Carvalho et al., 2012). EGTs are also reduced with EGR which can be useful for protecting the inlet turbine of turbocharged engines (Alger et al., 2009a). However, the EGR system must be sufficiently robust to withstand the deposits that accumulate in the system due to the lower EGTs (Heywood, 1988, Robert Bosch GmbH, 2006).

Another drawback of EGR is that COV_{IMEP} is increased, and eventually some cycles become sufficiently slow burning with high EGR ratios that combustion is not completed by the time the exhaust valve opens, eventually causing engine misfire (Matsushita et al., 1985, Siokos et al., 2015, Wei et al., 2012). Thus, it is necessary to advance the spark in order to ensure that the combustion is sufficiently completed before the exhaust valve opens. Depending on the engine operating condition, the optimum 8-10°aTDC MFB50 phasing can either be achieved at a certain spark timing and EGR addition, or the combustion can degrade so much that despite advancing the spark timing, the combustion duration is too long to achieve a sufficiently advanced MFB50 combustion phasing, resulting in partial burns and misfire (Pan et al., 2014). Therefore, there is a maximum rate of EGR that can be achieved while keeping COV_{IMEP} below a 5% maximum (Dunn-Rankin, 2008). Furthermore, combustion efficiency is reduced at high EGR levels due to the increased combustion duration (Siokos et al., 2015, Wei et al., 2012).

Typically higher engine loads are more tolerant to EGR addition but again, there is a trade-off because as mentioned, the diluting effects of EGR reduce the maximum load that the engine can achieve, and no EGR addition can be achieved at full-load without using an external pump due to the equivalent intake and exhaust pressures. Thus, the maximum EGR addition that can be achieved is limited (Institution of Mechanical Engineers, 2013).

2.3.5.1 EGR Type

Cooled EGR has been shown to be more effective in suppressing engine knock than hot EGR due to reduced temperatures in the end-zone of the combustion chamber (Alger et al., 2009a), while EGR after a TWC (catalysed EGR) further reduces knocking tendency because NO present in EGR gases before a TWC induces knock (Hoffmeyer et al., 2009, Lewis et al., 2014, Parsons et al., 2015). The reduced knock allows the spark timing to be advanced

resulting in fuel economy improvements. It also allows the compression ratio to be increased, also resulting in fuel economy improvements (Su et al., 2014). Fuel economy is also improved as a result of the lower in-cylinder temperatures and thus improved thermal and volumetric efficiencies achieved by cooling the EGR gases (Su et al., 2014, Wei et al., 2012). However, the maximum EGR addition achievable with cooled EGR may be limited because of water droplet formation (Siokos et al., 2015) and it has been observed to increase COV_{IMEP} and HC emissions (Wei et al., 2012). Despite the work that has been done, much more investigation needs to be conducted into the effect of different EGR types (hot EGR, cooled EGR, hot EGR after TWC, cooled EGR after TWC) on engine combustion and emissions.

2.3.5.2 Stratified EGR

Most commonly, EGR is used in its homogenous form where the intake air is well-mixed with the EGR gases. However, some researchers have investigated stratified EGR to help overcome the reduction of burning speed, the HC emission increase and the increase in COV_{IMEP} (Wei et al., 2012). This is where the fresh air and EGR gases are separated in the combustion chamber, which improves flame propagation at the spark plug region (Wei et al., 2012). However, there are significant challenges in implementing stratified EGR. Due to the flow structure in the combustion chamber being extremely complex, it is very difficult to achieve complete separation of the fresh air and EGR gases, and it is challenging to maintain the stratification throughout the intake and compression strokes prior to ignition (Wei et al., 2012). Therefore, this is why stratified EGR is not pursued in this investigation.

2.3.6 Swirl and Tumble Intake Air Flows

Turbulence, commonly quantified as swirl and tumble, is generated as a result of the induction and compression strokes of the engine cycle, along with the geometry of the combustion chamber (Dunn-Rankin, 2008). Swirl is defined as organized rotation of the fuel-

air charge about the cylinder axis, while tumble is defined as organized rotation of the fuel-air charge around an axis perpendicular to that of the cylinder axis, at half the height of the combustion chamber (Matsushita et al., 1985, Stone and Ladommatos, 1992). While the swirl motion will undergo some decay during the engine cycle due to friction, intake swirl usually persists through the compression and combustion, and it is converted into general turbulence during the expansion processes (Lee et al., 2000, Li et al., 2001).

Swirl is typically used to improve fuel air mixing (improved mixture homogeneity) and to increase the speed of the combustion process, particularly with air-guided fuel injection in order to transport the fuel-air mixture towards the spark plug (Agarwal et al., 2014, Nagayama et al., 1977). For pre-mixed combustion in SI engines, the effect of increased in-cylinder turbulence breaks-up or wrinkles the flame front, which has the effect of increasing the area of the flame front increasing the combustion speed (Lee, 2007, Stone, 1999). Increasing the in-cylinder turbulence allows leaner mixtures to be burned which are less prone to knock, due to the reduced combustion temperatures; improving fuel economy and affecting engine emissions (Nagayama et al., 1977, Stone, 1999). PM emissions, as well as NO_x and HC emissions will be affected, even with stoichiometric conditions (Kim and Kim, 1995, Mikulec et al., 1988, Urushihara et al., 1995). Indeed, (Mehta et al., 2001) reported that the use of swirl valves resulted in significant improvements in PM mass as compared to low tumble conditions. Furthermore, swirl motion improves COV_{IMEP}, particularly as engine speed is increased by creating consistent in-cylinder flow conditions (Zeng et al., 2015).

It is commonly thought that knock is reduced as a result of the increased in-cylinder turbulence due to the faster combustion; the fuel-air charge in the end-zone of the combustion chamber is consumed before it has an opportunity to auto-ignite (Hirooka et al., 2004). However, it must be noted that a faster flame will also increase in-cylinder pressures which

will make auto-ignition more likely. In general, faster burning cycles are more prone to knock (Kalghatgi, 2013, Leppard, 1982). Furthermore, swirl allows EGR, as discussed previously, to be used at high ratios (Heywood, 1988, Nagayama et al., 1977).

A disadvantage of generating engine swirl and tumble intake airflows is that the volumetric efficiency (VE) is reduced which can cause the fuel economy to worsen (Arcoumanis and Kamimoto, 2009). This also limits the EGR addition that can be achieved, since there is a smaller pressure difference between the exhaust and intake. Although the use of lean mixtures will reduce the efficiency of a TWC causing emissions to increase, the emissions improvements produced by the lean burn combustion may be sufficient to offset this loss (Stone, 1999). Finally, excessive tumble can lead to an increase in HC emissions and an increase in fuel consumption (Stone, 1999).

2.3.6.1 Swirl and Tumble with EGR Addition

Using swirl and tumble along with EGR addition allows the engine to operate under learn burn conditions in order to improve fuel economy and NO_x emissions, while maintaining HC emissions at the same level (Endres et al., 1992). In addition, high tumble airflows can be used to achieve high EGR additions of up to 30-40% which can be used to improve fuel economy (Ikeya et al., 2015, Takahashi et al., 2015, Zhang et al., 2014a). High swirl airflows could also be used for the same purpose. COV_{IMEP} can also be reduced with a combination of tumble and EGR addition as compared to using EGR alone, due to enhanced turbulent flow in the cylinder (Zhang et al., 2014a). In particular, because EGR allows the spark timing to be advanced, it allows the point of ignition to occur earlier in the engine cycle where the turbulence is stronger. This increases the laminar flame speed allowing the combustion slowing effects of EGR to be overcome.

2.3.7 Compression Ratio

Increased compression ratios can lead to significant fuel economy improvements (Gumbleton et al., 1976, Heywood, 1988). In an engine in which the compression ratio was raised from 9.7:1 to 14.6:1, an efficiency gain of up to 15% was obtained with larger gains at part throttle, due to the improved thermal efficiency (Stone, 1999). The EGT is decreased when compression ratio is increased, due to more efficient conversion of the fuel energy into work on the piston (Heywood, 1988).

However, there are also disadvantages to increased compression ratios. The fuel consumption can worsen under low-speed, high-load conditions at high compression ratios due to spark retardation caused by heavy knocking (Okamoto et al., 2003). NO_x emissions increase due to higher in-cylinder temperatures. Large squish areas and poor surface-to-volume ratios increase the hydrocarbon emissions (Stone, 1999). This is in addition to the increased hydrocarbons resulting from the higher in-cylinder pressures which cause more HCs to be stored in the piston crevices (Heywood, 1988). When released during the expansion stroke these do not burn fully, thus contributing to HC emission increases with increased compression ratios (Heywood, 1988, Zhang et al., 2014b). They also result from the lower EGTs which reduce the rate of HC oxidation (Heywood, 1988). Finally, combustion deposits become more significant as the compression ratio is increased because the ratio of their volume compared to the volume of the combustion chamber increases (Liiva et al., 1992, Stone, 1999).

2.3.7.1 Compression Ratio and EGR

Compression ratio increase with EGR addition has been shown to significantly improve fuel economy while reducing the sum of the NO_x and HC emissions (Diana et al., 1996). The

combination of the two has also been shown to produce a relatively low COV_{IMEP} due to increased turbulence intensity and reduced cyclic variations (Pan et al., 2014).

2.4 Spark Ignition Fuels

Fuels are typically mixtures of hydrocarbons whose carbon and hydrogen bonds are broken in order to form new bonds with oxygen atoms when the fuel is burned in air. This process produces a significant amount of energy which is converted into work on the piston which then undergoes a number of conversions to produce power at the vehicle wheels.

2.4.1 Gasoline

The size and geometry of the hydrocarbon molecule has a significant effect on its chemical properties, providing a wide-range of potential fuels that can be utilized in IC engines (Stone, 1999). Indeed, gasoline is a mixture of many different sized alkane and alkene hydrocarbon molecules with varying chain lengths and isomerisation. Hydrocarbons can also form aromatic and cyclo-alkane ring structures such as benzene, which are also present in gasoline fuel in varying quantities and types.

Overall, the two most important characteristics of gasoline are its volatility and octane number (Stone, 1999). Gasoline fuel is required to vaporize well within a given temperature range that is season dependent in most countries so that it can produce an ignitable fuel-air mixture when injected into the combustion chamber. If it vaporizes too easily then it can result in problems such as vapour lock and excessive evaporative emissions (Srinivasan, 2001). However, if it is not volatile enough it will be difficult to produce an ignitable fuel-air mixture in cold conditions, leading to poor cold startability (Kalghatgi, 2013, Robert Bosch GmbH, 2006). If the fuel does not vaporize well enough it can also pass into the engine oil on the combustion chamber walls, causing it to become diluted (Kalghatgi, 2013, Robert Bosch

GmbH, 2006). Finally, poorly vaporized fuel can lead to excessive deposit formation (Liiva et al., 1992). Fuel octane number limits the spark timing advance that can be achieved with the engine, and thus the fuel economy and torque, because of engine knock, as discussed. Thus, fuel octane number requirements have increased and will continue to increase in the coming years, in order to achieve further fuel economy improvements (Green Car Congress, 2013). The fuel specifications for gasoline fuel in the EU and US are provided in Table 2-1.

Table 2-1 EU (EN 228-2012) and US (ASTM D4814 Rev B-2011) Fuel Specification (Analiit AA, 2015, Chevron, 2009)

Parameter	EU	US
Density (kg/m³)	720-775 (at 15°C)	-
RON	95[1]	-
MON	85	-
Distillation Properties		
T10 (°C)	-	≤70
T50 (°C)	-	≤77-121
T90 (°C)	-	≤190
End of distillation point (°C)	-	≤205
Evaporation Properties		
Percentage evaporated at 70˚C summer (volume %)[2]	20-48	-
Percentage evaporated at 70˚C Winter (volume %)[2]	22-50	-
Percentage evaporated at 100˚C (volume %)	46-71	-
Percentage evaporated at 150˚C (volume %)	≥75	-
Oxygenates		
Aromatics (m/m)	≤35%	≤20.9%
Olefins (%m/m)	≤18%	≤11.9%
Sulphur (ppm)	≤10	≤80

[1] Member States may decide to continue to permit the placing on the market of unleaded regular grade petrol with a minimum motor octane number (MON) of 81 and a minimum research octane number (RON) of 91.
[2]Depends on volatility class of region, country and season

The octane number scale is used to define the octane number for a given fuel; n-heptane is assigned an octane number of 0 and isooctane is assigned an octane number of 100. The octane number of a given fuel is thus defined as the mixture of n-heptane and isooctane which produces the equivalent knocking tendency of the given fuel. For example, if the fuel

has the same knocking tendency as a fuel mixture of 95% octane and 5% heptane, then it is given an octane number of 95 (Burton et al., 2000). For octane numbers above 100, a tetraethyl lead knock additive is added to the isooctane fuel in order to allow the octane number to be quantified (Heywood, 1988). This is effectively just an extrapolation of the 0-100 octane scale.

The two most widely used tests for defining the knock tendency of a given fuel are the Research Method (ASTM D-2699) and the Motor Method (ASTM D-2700), both of which are conducted in a standardized single-cylinder engine (Heywood, 1988, Kalghatgi, 2013). The test for MON differs from that used for the RON test by using pre-heated mixtures, higher engine speeds and variable ignition timing. Thus, the fuel being examined is subjected to more stringent thermal demands, which is why MON figures are typically lower than those for RON (Bradley et al., 2004, Robert Bosch GmbH, 2006). The engine itself was developed by the Cooperative Fuel Research (CFR) Committee. Thus, it is commonly referred to as a CFR engine (Bock et al., 2013). The CFR engine is a robust four-stroke overhead valve engine with a compression ratio that can be varied from 3 to 30 while operating (Heywood, 1988). The operating conditions for the two tests are shown in Table 2-2.

Table 2-2   Operating conditions for research and motor octane number test methods (Bradley, 2004, Heywood, 1988)

	Research Method	Motor Method
Inlet Temperature	52˚C	149˚C
Engine Speed	600 rpm	900 rpm
Spark Advance	13˚bTDC	19-26˚bTDC (varies with compression ratio)
Air/fuel ratio	Adjusted for maximum knock	

Overall, the test conditions are selected to represent the engine operating range where knock is most severe. The air-fuel ratio is adjusted to achieve the most severe knock, then the compression ratio is increased to produce knock of a standardized intensity as measured by a knock detector (Heywood, 1988).

However, there are some limitations of the standard tests conducted in the CFR engine; both RON and MON are evaluated at low engine speeds and the air/fuel ratio is adjusted to produce the maximum knock (Stone, 1999). All practical gasolines are mixtures of aromatics, olefins, naphthenes, oxygenates and paraffins which have auto-ignition chemistries different from those of n-heptane and isooctane (Heywood, 1988). Compared to primary reference fuels (PRF's), real fuels become more resistant to knock as pressure is increased for the same temperature, thus, the MON method of increasing the intake temperature is limited. Furthermore, because alcohols burn more rapidly than gasoline, their ignition timings in the RON and MON tests are over-advanced, leading to an underestimate of their knock performance (Heywood, 1988). Therefore, engines can behave rather differently during their daily use from what these standard tests would otherwise suggest. Due to these limitations, an average of the RON and MON values is typically taken in order to produce an antiknock index which offers an improved characterization of the antiknock properties of the fuel (Robert Bosch GmbH, 2006).

Fuel volatility is significantly affected by the chemical structure of the fuel, with shorter carbon chains having a higher volatility than longer chains, and branched carbon chains having a higher volatility than straight chains with the same number of carbon atoms (Burton et al., 2000). The chemical structure of the fuel also significantly affects its RON and MON. Fuel octane number decreases with increasing chain length, it increases with increasing numbers of side chains for the same number of carbon atoms and it increases with ring

structures such as those found in cyclo-alkanes and aromatics (Kalghatgi, 2013). This has significant effects on achieving ever higher octane number fuels, because of concerns over the carcinogenic properties of aromatics (Golding and Watson, 1999).

2.4.2 Oxygenated Alternatives

In recent years, interest in alcohol fuels has grown significantly due to their renewable nature (although many are still made from crude-oil stocks), and along with other oxygenated molecules, they are important components of modern day gasoline fuel (Hamilton et al., 2008, Heywood, 1988). The main drawback of oxygenated fuels is their lower gravimetric calorific values as compared to pure hydrocarbons, due to their partially oxygenated nature (Daniel et al., 2012a, Kalghatgi, 2013). This typically results in higher engine-out CO_2 emissions (Al-Hasan, 2003, Hsieh et al., 2002, Masum et al., 2014, Varol et al., 2014) because more fuel needs to be burned in order to achieve the same power output. The reduced power output can be overcome with compression ratio increases however, with 40-60%vol ethanol in gasoline blends being shown to have a similar performance to gasoline (Goswami et al., 2015), thus reducing the CO_2 increases. Furthermore, alcohols such as ethanol have a high octane number and high enthalpy of vaporization which allows the spark timing to be advanced as compared to regular gasoline fuel, enabling the fuel consumption penalty to be reduced and torque to be improved (Al-Hasan, 2003, Deng et al., 2013a, Irimescu et al., 2015, Poitras et al., 2015). The high enthalpy of vaporization also reduces the charge temperature which improves VE and the lower air/fuel ratios mean that more energy is released per kilogram of stoichiometric mixture burned; both of these lead to overall efficiency improvements (Ramadhas, 2011).

Oxygenated molecules such as ethanol and butanol burn more quickly than gasoline, leading to enhanced combustion stability and improved engine efficiency (Deng et al., 2013b, Fu et

al., 2014, Masum et al., 2013, Turner et al., 2011). CO emissions are typically reduced due to the greater oxidation resulting from the fuel oxygen content (Al-Hasan, 2003, He et al., 2003, Karavalakis et al., 2014, Varol et al., 2014, Yejian et al., 2007). Reduced combustion temperatures with oxygenated fuels reduce the NO_x emissions and EGT (Elfasakhany, 2014) and their oxygenated nature increases the rate of oxidation of PM and HC emissions (Chen et al., 2015, Goswami et al., 2015, Gu et al., 2012, Irimescu et al., 2015, Mattimaricq, 2012, Wang et al., 2014a, Zhang et al., 2015). Furthermore, (Wang et al., 2014c) observed that soot produced from the combustion of oxygenated fuels has lower activation energies than that produced by gasoline, resulting in increased oxidation rates in the exhaust. Some researchers have reported increased NO_x emissions with oxygenated fuels due to their increased fuel oxygen content (Bayraktar, 2005, Feng et al., 2013, Graham et al., 2008, Keskin et al., 2011, Masum et al., 2014) which is important to note. However, this may result from the air/fuel ratio in their engines not being changed from that of gasoline when the oxygenated fuel was used, resulting in an excess of oxygen in combustion and hence increased NO_x emissions.

On the other hand, despite the improved knock properties resulting from the higher heat of vaporization, the cold start performance can worsen because the fuel becomes harder to vaporize (Aleiferis et al., 2013). The higher heat of vaporization combined with the typically reduced vapour pressures and boiling points of oxygenated fuels in comparison to gasoline means that they have to be injected earlier in the engine cycle to form a homogenous mixture, reducing flexibility in engine calibration. Oxygenated fuels can absorb moisture which can lead to corrosion and fuel separation problems (Hu et al., 2012, Stone, 1999). Alcohols can also damage materials used in the fuel injection equipment and they may cause elastomer swelling and corrosion (Heywood, 1988, Robert Bosch GmbH, 2006).

Hydrous ethanol provides benefits over conventional anhydrous ethanol such as lower cost due to the simpler manufacturing process (final ethanol dehydration step is removed) and reduced NO_x emissions resulting from lower peak in-cylinder temperatures (its water content absorbs heat) (Masum et al., 2013). However, problems arise when the hydrous ethanol is blended into gasoline fuel because of the immiscibility of water and gasoline, limiting the amount of water that can be used in such mixtures (Stone et al., 2012).

1-butanol while not widely used in 1-butanol-gasoline blends has the potential to be used in the future with similar blend ratios as ethanol-gasoline blending; therefore, 1-butanol has been researched in this investigation (Fountain, 2012). This is because its energy content is higher than ethanol, butanol is less prone to water contamination and it is less corrosive than ethanol (Szwaja and Naber, 2010). Therefore, this will allow it to be distributed in the same infrastructure that is currently used for gasoline, significantly reducing the infrastructure costs as compared to ethanol (Szwaja and Naber, 2010). It must be noted however that 1-butanol has been observed to have poorer cold startability as compared to ethanol, because it is harder to ignite at cold conditions (20˚C) (Serras-Pereira et al., 2013), possibly limiting the blend ratio of 1-butanol in gasoline. Its production costs are also higher (Masum et al., 2013) providing a further drawback. Although 2-butanol (iso-butanol) has potential advantages over 1-butanol (higher octane number of 101 compared to 96 for 1-butanol, lower boiling point of 99.5˚C compared to 117.7˚C for 1-butanol resulting in better cold startability) (Liu et al., 2013), it was not investigated because of the greater availability of 1-butanol in the marketplace.

Ethanol is used on a wide scale only in its blended forms of up to 10%vol and in the near future this trend is likely to grow with ethanol-gasoline blends between 20-40%vol (Hamilton

et al., 2008, Stein et al., 2013, Wallner et al., 2013). This is being driven by a 10% minimum target for the use of alternative fuels in transportation in the EU legislated by Directive 2009/28/EC in 2009, and by the Renewable Fuel Standard in the Energy Independence and Security Act of 2007 in the USA (Daniel, 2012d, Directive 2009/28/EC, 2009, Splitter and Szybist, 2014). Therefore, ethanol fuel blending in gasoline has also been researched in this investigation. In order to improve the usefulness of the investigation, the blended form is tested which not only allows the effect of ethanol addition to gasoline on DISI engine combustion and emissions to be quantified; it also allows the precise effects of one of the most relevant ethanol-gasoline blends on DISI engine combustion and emissions to be quantified.

2.5 Regulated Engine-Out Emissions

2.5.1 PM Emissions

Solid particles created as a result of incomplete combustion are known as particulates which consist of chains of carbon particles, i.e. soot, onto which uncombusted or partially combusted hydrocarbons form deposits (Robert Bosch GmbH, 2006). According to (Zhang et al., 2014b), the nucleation mode particles mainly result from droplets formed by hydrocarbon condensation, as approximately measured by the HC emission, and the accumulation mode particles are mainly composed of carbonaceous agglomerates formed in local rich-fuel zones (Burtscher, 2005, Kittelson, 1998). Furthermore, there is a positive correlation between polycyclic aromatic hydrocarbon (PAHs) and accumulation mode particles (Zhang et al., 2014b).

The Euro VI (2014) emission legislation which has for the first time limited particulate number (PN) for DISI engines, in addition to the mass limit already imposed by Euro V

(2009), poses a significant challenge for engine researchers; thus, it is an important area of research (Hedge et al., 2011). The PN emissions are higher than those produced by a diesel engine with a particulate filter; therefore, this is one reason why the legislation has become stricter for DISI engines (Mathis et al., 2005, Wang, 2014b).

Due to the longer period of time they have been regulated for, PM mass emissions have become relatively well controlled in comparison to PN emissions. In addition to this, ultra-fine PM particles, in particular, have a negative impact on human health (Anderson et al., 2012b, Hull et al., 2005, United States Environmental Protection Agency, 2014). Therefore, there is a greater need to reduce PN which is why it is studied in detail in this investigation, rather than PM mass. This is despite the PN being less consistent than PM mass (Eastwood, 2008). The smallest particles are at the limit of detection of PM measurement instruments, causing the numbers of smaller particles recorded to vary more significantly than larger particles which are more easily detectable (Eastwood, 2008). These smaller sized particles are often the most numerous in the exhaust emission resulting in the more significant variation in PN (Eastwood, 2008).

PN formation is worse with homogeneous combustion (early fuel injection) as compared to stratified combustion (late fuel injection) due to less nuclei adsorption onto accumulation mode particles occurring, because a lower number of accumulation mode particles are produced in homogenous combustion as compared to stratified (Eastwood, 2008). This is a result of reduced piston wetting and improved mixture formation (Eastwood, 2008). For this reason, homogenous combustion has been studied in this investigation (start of injection (SOI) =280°bTDC) at medium to high engine loads (5.5-8.5 bar IMEP) where homogenous combustion would be used (Eastwood, 2008).

Overall, the regulations are dictating the current and future direction of engine development with growing emphasis being placed upon the reduction of PM mass and number based emissions from DISI engines (Delphi, 2012). PFI produces less PM than DI because there is typically more time for fuel-air mixing before combustion (Alger et al., 2000, Zhang et al., 2014b) and there is no wall wetting and fuel impingement onto the piston crown as there is with DI. Thus, the PN emissions of different vehicle types can be summarized as:

Diesel > DISI > Diesel + Particulate Filter > PFI

Particle formation in DISI engines can be classified into two stages. The first stage is the formation of the particles; the first condensed phase material arises from the fuel molecules via their oxidation and/or pyrolysis products which typically include various unsaturated hydrocarbons (Heywood, 1988). The condensation reactions of gas-phase species such as these result in the production of nucleation particles. The second stage of particle growth, which includes both surface growth and aggregation, is where the bulk of the solid-phase material is generated. This involves the bonding of gas-phase species to the surface of the particles and their incorporation into the particulate phase (Heywood, 1988). Gaseous particles also adsorb onto the particles in the engine exhaust (Heywood, 1988).

Overall, the formation mechanism of particulates in DISI engines is much the same as in Diesel engines in the sense that it is highly dependent on local fuel equivalence ratio and charge temperature (Piock et al., 2011). The greatest formation rates are thus typically found in areas of the combustion chamber with a high local fuel equivalence ratio (rich) and a low local charge temperature. However, it is important to note that lower charge temperatures can also decrease PM formation through reducing the numbers of primary carbon particles formed by the thermal pyrolysis and dehydrogenation reaction of fuel vapour/droplets (Zhang et al., 2014b), thus complicating PM behaviour. Oxidation of the particulates occurs post-

combustion in the expansion and exhaust strokes, and in the exhaust system of the engine, converting them to CO and CO_2 as well as less complex particles (Heywood, 1988, Piock et al., 2011).

EGR is generally considered to have a negative effect on engine particulates, however, not many research studies have been published investigating this issue (Alger et al., 2009a, Zhong et al., 2013). From the limited research available, it can be concluded that EGR reduces the need for fuel enrichment to reduce EGTs in turbocharged engines, causing PM mass and number to reduce significantly (Alger et al., 2010). However, much more research needs to be conducted into the effect EGR has on engine particulates.

2.5.2 NO_x and HC Emissions

Typically over 90% of the NO_x produced in combustion is NO, however, this is readily oxidize once it is released from the engine and it can go on to react with unburned non-methane hydrocarbons in the presence of ultraviolet light to form photochemical smog (Stone, 1999). Therefore, there is little benefit in measuring just NO or NO_2 output from an engine; rather it is more useful to measure NO_x. NO forms in the high temperature burned gas, where there is sufficient temperature for nitrogen in the air to oxidise, which typically occurs at temperatures above 1525˚C (Heywood, 1988, Nieman et al., 2012). Pure NO_2 is a toxic reddish-brown gas with strong odour which can cause irritation of mucous membranes when present in high concentrations, while some hydrocarbons are considered to be carcinogenic when people are exposed to them for a long time (Robert Bosch GmbH, 2006). In addition, some of their products produced when they are exposed to sunlight are also considered to be carcinogenic (Robert Bosch GmbH, 2006).

Emissions of NO_x and HC vary between different engines and are affected by ignition timing, load, EGR ratio, speed and air/fuel ratio (Stone, 1999). Regarding spark timing, typically advancing the spark timing will increase in-cylinder pressures and temperatures, increasing the formation of NO_x and increasing the oxidation of HCs in the combustion chamber, resulting in increased NO_x and decreased HC. Retarding the spark timing will typically reduce the in-cylinder pressures and temperatures, causing the NO_x emissions to decrease and the HC emissions to increase. Their real-life behaviour however, is more complicated than this simplification. More advanced spark timings will lead to poorer mixture preparation, which alone would lead to higher HC emissions. However, as the spark becomes more advanced, the time available for post-combustion oxidization is increased, which alone would lead to lower HC emissions. These factors interact with each other, which can sometimes lead to unexpected PM emission behaviour. Increasing the engine load will increase the in-cylinder pressure and temperatures, which will typically increase NO_x emissions and reduce HC emissions. As mentioned, EGR addition significantly reduces NO_x emissions; however, HC emissions are typically increased (Alger et al., 2009a, Davis and Borgnakke, 1982, Zhong et al., 2013).

Overall, HC emissions in SI engines originate from several sources. Firstly, unburned fuel-air escapes into the exhaust during the valve overlap period (Stone, 1999). Secondly, misfires or partial burns in which the mixture fails to ignite or the combustion was too slow or started too late, respectively, causes HC emissions (Heywood, 1988, Robert Bosch GmbH, 2006). Thirdly, absorption/desorption from oil films, combustion deposits and crevices occurs as the pressure is rising and falling within the engine cylinder (Heywood, 1988, Tomita et al., 1996). Fourthly, a quench layer of unburned and partially burned fuel is left at the combustion chamber wall when the flame is extinguished as it approaches it, which can be

released during the exhaust stroke (Tomita et al., 1996). Finally, poor mixture preparation, particularly during transients and cold start, leads to the partial oxidization of HCs in the engine cylinder, causing HC emissions (Stone, 1999).

In this investigation the NO_x emission from the engine was studied because as shown in Table 2-3, the legislation regarding NO_x has become stricter from 2009 (Euro V), making these emissions important to investigate to help further control them. Although the THC emission regulation has remained consistent since 2005 (Euro IV), they are still useful to study because of their relationship with the NO_x and nucleation mode particulate matter (PM) emissions (Zhang et al., 2014b). CO emissions are also harmful to human health. The CO molecule attaches itself to haemoglobin in the bloodstream, preventing oxygen from being transported by red blood cells, making it harder for the body to circulate oxygen to vital organs, resulting in nausea, headaches and other health problems. Despite this, CO emissions were not studied because their regulated numbers have been consistent from 2005 (Euro IV), thus, it was considered more useful to study other engine combustion and emission parameters.

2.5.3 CO_2 Emissions

CO_2 emissions are at the forefront of public perception due to their greenhouse gas effect and subsequent effect on global temperature and climate (Gov UK, 2011). The transportation sector as a whole is a significant contributor to global CO_2 emissions; therefore, there is a growing political drive to reduce CO_2 emissions from automobiles (Johnson, 2010, Zaccardi et al., 2009). While oxygenated fuels typically produce increased engine-out CO_2 emissions as compared to gasoline because of their reduced lower heating value (LHV) which increases fuel consumption, as discussed, they are typically produced using renewable methods. Therefore, net CO_2 output from the use of these fuels is reduced (Daniel, 2012c et al., Owen

and Coley, 1995, Parag and Raghavan, 2009, Turner et al., 2011). Improvements in fuel consumption also reduce CO_2 output from the transportation sector (Zaccardi et al., 2009). Therefore, oxygenated fuels and fuel consumption have been researched further in this investigation.

2.5.4 Legislation

The evolution of European Union emission legislation for DISI petrol cars with a mass of less than 1.305 kg is shown in Table 2-3.

Table 2-3   European Union emission legislation for DISI petrol cars (Delphi, 2012)

Tier	Date	Unit	CO	THC	NMHC	NOx	HC + NOx	PM	P (#/Km)
Euro I	1992		2.72	-	-	-	0.97	-	-
Euro II	1996		2.2	-	-	-	0.5	-	-
Euro III	2000		2.3	0.20	-	0.15	-	-	-
Euro IV	2005	mg/km	1.0	0.10	-	0.08	-	-	-
Euro V	2009		1.0	0.10	0.068	0.060	-	0.005	-
Euro VI	2014		1.0	0.10	0.068	0.060	-	0.005	6×10^{11}*

* 6×10^{12}/km within first three years from Euro 6 effective dates

The emissions limit themselves were defined firstly in 1970 (Directive (70/156/EC)) and they are tested over the New European Drive Cycle (NEDC); a synthetically generated test cycle consisting of phases of constant cruising speeds and constant rates of acceleration (Robert Bosch GmbH, 2005). In the near future, they will be tested over a Real Driving Emission (RDE) test cycle to more accurately measure the pollutant emissions by using real world driving conditions rather than a synthetically generated test cycle, which bears little relevance to real world driving conditions (European Council, 2016). US emission legislation is considered to be more stringent than the European emission legislation, with the Federal Test Procedure (FTP) drive cycle mirroring actual highway driving conditions which are harder to

specifically calibrate an engine for. This legislation is summarized in Table 2-4; it is applicable for vehicles up to 6,356 Kg (Robert Bosch GmbH, 2005).

Table 2-4   United States Federal emission legislation for Light Duty SI Vehicles <80,000 km (Delphi, 2012)

Emission	Unit	Tier I 1994	Tier II 2004
NMHC		160	65
NOx		250	90
CO	mg/km	2100	1050
PM (mass)		50	15
PM (number)	#/km	-	-

There is a certain degree of flexibility with the US legislation because each vehicle manufacturer must only ensure that the exhaust emissions for its total vehicle fleet do not exceed the specified average; not every vehicle from the fleet must meet the regulations (United States Environmental Protection Agency, 2010). Only a certain percentage of the manufacturer's fleet must comply with the legislation too, but the percentage is increasing year-on-year in order to reduce the emissions across the vehicle fleets of manufacturers (United States Environmental Protection Agency, 2010).

For both legislations, vehicles are randomly tested during their lifetime in order to ensure that their emissions have not become too degraded, thus adding an extra layer of difficulty for vehicle manufacturers (Robert Bosch GmbH, 2005).

2.5.4 TWCs

Despite the ability of TWCs to reduce the emissions from a gasoline vehicle significantly, particularly once it is activated (warmed-up), it is still important to reduce the emissions produced by the engine itself. This is because emissions increase significantly during cold-start when the catalyst is not at its optimum operating temperature, causing significant emissions to be produced by the vehicle (Frennet and Bastin, 1995). The NEDC begins from when the engine is started so if the emissions produced by the engine alone are not below a certain limit, the emissions produced during cold-start could potentially cause the vehicle to fail the emissions test (Isermann, 2014). In addition, when the engine undergoes acceleration, the air/fuel charge is typically enriched as well as during cold-start, meaning that the TWC conversion efficiency is reduced because it is not operating at its optimum stoichiometric condition (Alger and Mangold, 2009). Finally, there is a strong relationship between the nucleation mode particles and HC emission (Zhang et al., 2014b); therefore, it is still useful to study the HC emission to aid the study of PM emissions.

2.6 Summary

Overall, this literature review discussed the development of modern DISI technology, particularly in relation to fuel consumption improvement and emissions reduction. The major areas include discussion of the knocking phenomena, EGR and relevant emission regulations. Engine downsizing was introduced after which fuel economy improving and thus CO_2 reducing techniques of EGR (also used to reduce NO_x emissions), swirl and tumble intake airflows and compression ratio increase were discussed. SI fuels and emission regulations then follow due to their strong influence, particularly the latter, on the development of IC engines.

The main focus of the review is to provide a background to the fuel economy improving and thus CO_2 reducing techniques which are researched further in this investigation. Compression ratio increase helps to accomplish the objectives of engine researchers to increase engine efficiency and thus reduce fuel consumption, producing subsequent CO_2 emissions benefits. However, knock, which has been discussed in detail, is a limiting factor regarding the maximum compression ratio that can be achieved, limiting engine efficiency. Therefore, EGR is used to enable higher compression ratios to be achieved while reducing the engine NO_x emission output. Although the compression ratio of modern turbocharged SI engines is reduced compared to their equivalent NA engines (Su et al., 2014), in order to achieve a higher IMEP, this reduction can be reduced with EGR addition. Swirl and tumble intake airflows are used to improve fuel-air mixing in the combustion chamber for improved emissions, as well as increasing the combustion speed, to enable higher EGR levels and thus higher compression ratios to be used.

Spark ignition fuels were discussed in detail due to their significant effect on the engine emissions, with oxygenated fuels explored because of their potential to reduce net CO_2 output from the transportation sector, if produced by renewable means. The relevant emissions regulations have been discussed at length due to their significant influence on the development of IC engines and fuels, with the new Euro VI emission regulation, in particular, driving the reductions in PN emissions from DISI engines.

Ultimately, this literature review introduced the main motivation of this thesis which is to investigate the effect of the fuel economy improving and thus CO_2 emission reducing techniques of EGR (also used to reduce NO_x), swirl and tumble intake airflows, increased compression ratio, as well as the effect of oxygenated fuel components of 1-butanol and ethanol, on the combustion and emissions behaviour of a modern DISI engine.

Chapter 3

Experimental Setup and Techniques

The aim of this chapter is to present the experimental test facilities and the data acquisition systems and analysis methods used in this study.

3.1 Introduction

This chapter describes all of the test equipment used throughout this study. This includes the details of the single cylinder engine hardware and instrumentation, as well as the details of the emissions equipment. The engine control methodology, data acquisition systems and analysis methods are described in the following subsections.

The engine test facilities were created and developed by Jaguar Land Rover and the previous research students at the University in their PhD studies. During the investigation, the author was responsible for the development and maintenance of the single-cylinder thermal engine test facility. Developing the engine test cell facility involved improving the fuel and variable valve timing systems. Regarding maintenance of the facilities, this included changing minor components such as fuel pumps, water pumps, water heaters, etc., when they failed, and three engine rebuilds.

Overall, this chapter provides an overview of the current test facility. Further detailed descriptions can be found in (Wang, 2014b), (Daniel, 2012d), (Turner 2010) and (Luszcz, 2009).

3.2 Overview of Single-Cylinder Engine Test Cell

The schematic of the experimental test facility is shown in Figure 3-1.
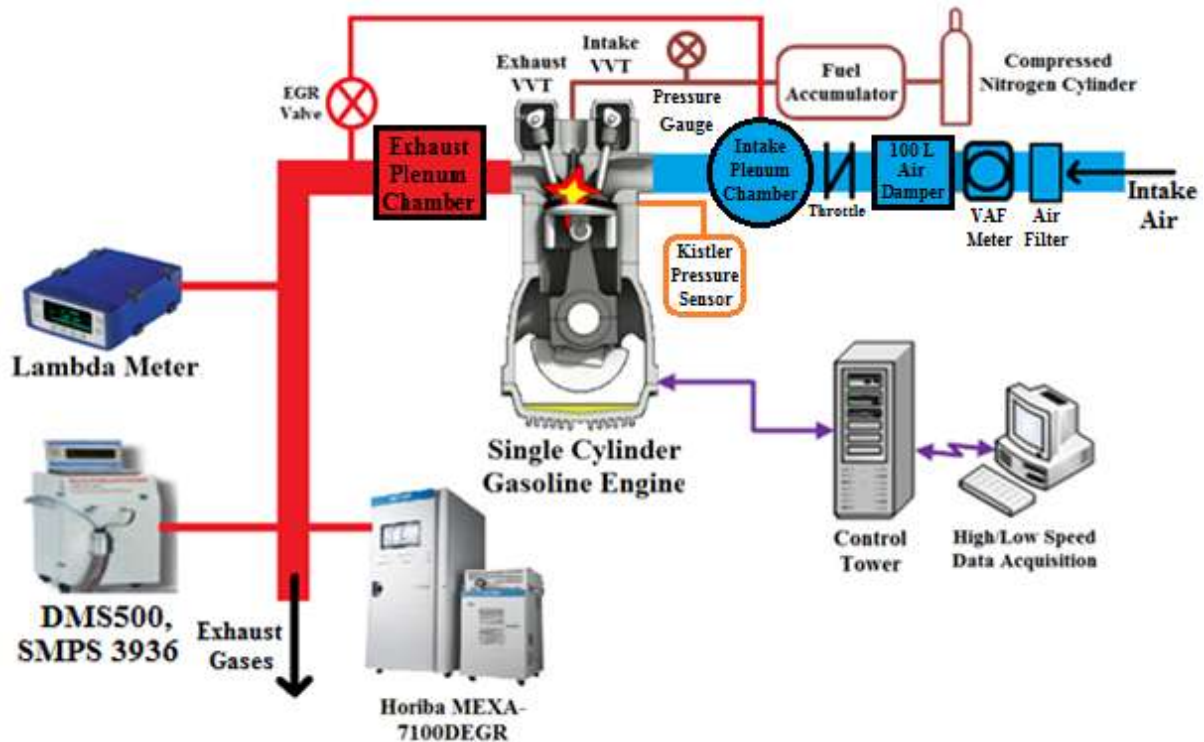
Figure 3-1   Schematic of single-cylinder engine test facility and instrumentation setup

The figure shows the 4-stroke single-cylinder spray-guided DISI engine used in this investigation. The cylinder head is a single-cylinder version of that used in the Jaguar AJ133 (2010) 5.0 litre V8 production engine. This was attached to a balancing unit based on a Ricardo Hydra engine which was redesigned by the Internal Combustion Engines (ICE) group at the University of Oxford. The engine cylinder head provides the combustion chamber with 4-valves and spray guided DI; both of which are found in modern DISI engines.

The modified single cylinder research engine was not designed to be very resistant to knock (high compression ratio of 11.5, large bore diameter of 90 mm). In addition, 95 RON gasoline was used throughout this research which is of a lower octane number than the 98

RON gasoline specified for the engine. Therefore, engine knock occurred at loads of 6.0 bar IMEP and above, which is somewhat lower than what can be expected with the state of the art aggressively downsized engines of modern cars on sale today. Furthermore, audible knock was observed to start occurring with 97 RON gasoline fuel at engine loads between 4.5 and 6.0 bar IMEP by previous research students using this research engine (Wang, 2014b, Daniel, 2012d). Therefore, the occurrence of knock at loads of 6.0 bar IMEP and above with 95 RON gasoline fuel is consistent with these previous investigations. This allowed the effect of EGR on knock to be studied at reduced loads to prevent any significant engine damage. The engine also features a variable valve timing (VVT) system which will be discussed in detail in a later section.

A full specification of the single-cylinder engine is shown in Table 3-1. The overall design of the engine provides it with an over-square configuration resulting in a high compression ratio and high swept volume, maximizing efficiency and output power.

Table 3-1   Experimental single-cylinder engine specification

Parameter	
Engine Type	4-Stroke, 4-Valve
Combustion System	Spray Guided DISI
Swept Volume	565.6 cc
Bore x Stroke	90 x 88.9 mm
Compression Ratio	10.7:1-11.5:1
Max. Torque @1500 rpm	44.2 Nm (~9.5 bar IMEP)

The balancing unit was attached to a test bed and the ancillary equipment used to operate the engine and to record the data was attached onto the engine and balancing unit. This will be discussed in detail in the following sections.

Before entering the engine, the intake air flow was filtered after which it passed through the volumetric airflow (VAF) meter, as shown in Figure 3-2, which recorded the rate of air flow through the engine. It then passed through a 100 litre damper tank which reduced the pressure fluctuations through the VAF after which it passed through the throttle and the intake plenum chamber; the chamber reduced the pressure fluctuations after the throttle. The air then went into the engine before mixing with and undergoing combustion with the fuel, after which the combustion products were ejected into the exhaust system. The exhaust gases passed through the exhaust plenum chamber which reduced the pressure fluctuations before being analysed by the Lambda meter to measure the air/fuel ratio. The gases were then analysed by the particulate and gaseous emission measurement systems, after which they were pumped out to the atmosphere via the engine laboratory ventilation system. An EGR line was connected just after the exhaust plenum chamber to the intake plenum chamber to achieve external EGR. To achieve swirl and tumble intake airflows in the engine, swirl and tumble inducing baffle plates were fitted between the intake runner and cylinder head. These systems are discussed in further detail in later sections.

3.2.1 Dynamometer and Electric Motor

In order to motor the engine, the crankshaft was attached to a dynamometer manufactured by Mawdsley's LTD. It used 450 volt electric power and it could maintain a constant speed or constant engine load with motoring or firing conditions. The speed was manually controlled by a dial in the engine control room and it was displayed on a digital indicator visible from the control room.

3.2.2 Intake and Exhaust System

As shown in Figure 3-2 and discussed, the 100 litre intake damper tank along with the intake and exhaust plenum chambers were used to reduce the pressure pulsations through the intake

and exhaust systems in order to stabilize the airflow through the engine. Based on the work of a previous student (Daniel, 2012d), a 100 litre intake damper was used in order to supply the engine with stable airflow at wide open throttle (WOT). Smaller plenums wee required just before the intake and just after the exhaust because the 100 litre intake damper already effectively reduced the pulsations in the intake and exhaust systems; they were required only to reduce the pulsations caused by the throttle and engine respectively.

3.2.3 Heating and Cooling Circuits

Heating and cooling circuits for the engine water and oil were incorporated into the engine test facility and are shown schematically in Figure 3-2. Each circuit was pumped and heated individually through water and oil pumps and heaters, respectively. In addition, a large water-water heat exchanger was used to transfer heat between the warm engine coolant and cold mains water and another smaller water-oil heat exchanger was used to transfer heat between the water and oil; both heat exchangers were manufactured by Bowman Ltd. Overall, the pumping, heating and heat exchange allowed the temperature of the water and oil circuits to be maintained within a reasonable range. During the experiments, the water and oil temperatures were maintained at $85^{\pm}5^{\circ}C$ and $95^{\pm}3^{\circ}C$ respectively, using a proportional integral differential (PID) controller. Once the temperature exceeded the set limit on the PID controller, it sent a signal which, via a relay, opened a solenoid valve, allowing cold mains water into the water-water heat exchanger to cool the engine coolant. This then cooled the engine oil through the second water-oil heat exchanger.
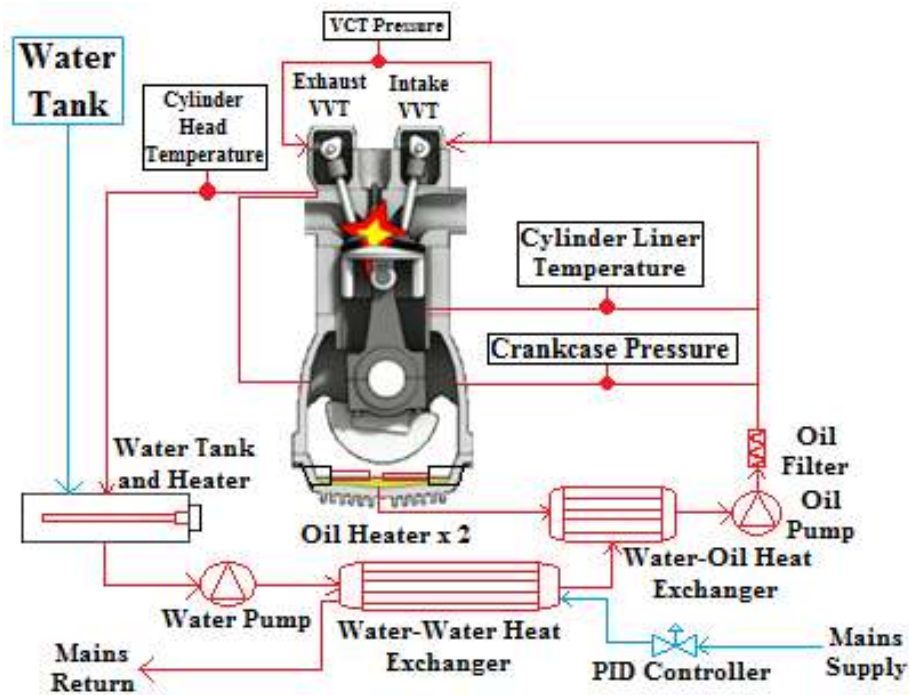
Figure 3-2   Schematic of water cooling and oil lubrication circuits

Tap water was used to cool the engine because the engine does not have any specialist cooling requirements. 10W40 oil was used to lubricate the engine, as recommended by Jaguar Land Rover. The water and oil levels were monitored and regularly topped up to ensure there was enough water and oil available to meet the cooling and lubricant requirements of the engine when motoring and firing. The oil was regularly replaced because EGR led to degradation of the oil due to an increased number of particulates condensing into the oil film on the combustion chamber walls.

3.2.4 Fuel Supply Systems

3.2.4.1 DI

The DI fuel system, as shown schematically in Figure 3-3, applied a constant pressure to the fuel through the use of a free piston accumulator and a compressed nitrogen bottle supplied by British Oxygen Company (BOC), which was controlled using a high pressure gas regulator manufactured by the company. The pressure (150 bar) supplied is more consistent

than that of a high pressure fuel pump. However, only 2 litres of fuel could be supplied to the accumulator with each charge, necessitating the engine to be stopped at regular intervals in order to refill the system.
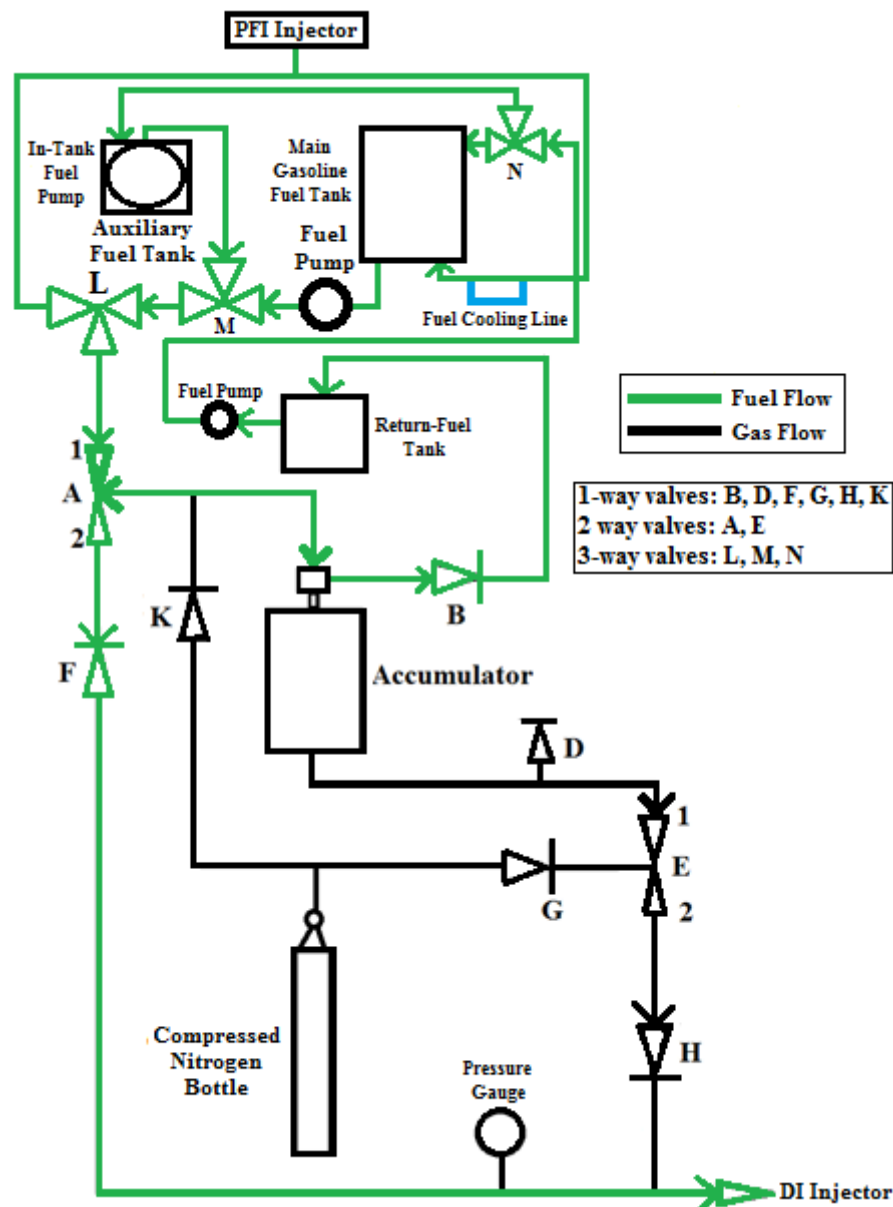
Figure 3-3   Schematic of fuel supply systems

The fuel required for the test was pumped using an electric out of tank pump from the main fuel tank in the test cell, through a three-way valve (L) directly into the accumulator. The three-way valve allowed the fuel to be pumped from the tank around the PFI system when it

was turned to the other position. A smaller auxiliary tank was used when a non-gasoline fuel was tested, which allowed the gasoline to be constantly stored in the main fuel tank, rather than having to be drained each time a non-gasoline fuel was used. The partially separate systems also allowed contamination between the fuels to be eliminated to ensure that the test data is reliable. The system operates via another three-way valve (M), so when the tank was used, the valve was turned to its other position to allow fuel to be pumped from the auxiliary fuel tank into the accumulator. Once the DI fuel system was charged, the pressurized fuel was transported to the DI injector using a variety of rigid and flexible tubing, and stainless steel compression fittings. The flow of fuel and nitrogen gas through the system was controlled using various manually operated valves. When refilling the system and changing fuels, the system was purged with nitrogen gas. If a non-gasoline fuel is used during the tests, the auxiliary fuel tank and the system were cleaned using a small amount of the non-gasoline fuel to ensure that there was no gasoline contamination in the non-gasoline fuel, when the fuel tank was subsequently filled with it. Similarly, at the end of the day, the system was cleaned with gasoline to avoid unnecessary damage to the injector and accumulator seals.

3.2.4.2 Port Fuel Injection (PFI)

A low pressure (3 bar) PFI system, also shown schematically in Figure 3-4, was used for the sole purpose of warming the engine prior to DI testing. As mentioned, the out of tank fuel pump was operated to pump fuel from the gasoline fuel tank and the three-way valve (L) was changed so that the fuel was pumped to the PFI injector. After the fuel exits the PFI injector, it passed through a water cooling line in order to avoid excessive heating of the fuel and excessive consequential vapour loss from the system, as shown in the figure.

3.2.5 DI Fuel Injector and Spark Plug Configuration

The combustion chamber of the engine has a flat top piston and a centrally mounted six-hole direct injector along with a side-mounted spark plug located close to the injector. Figure 3-4 shows the relative positions of the injector along with the injector spray plume.
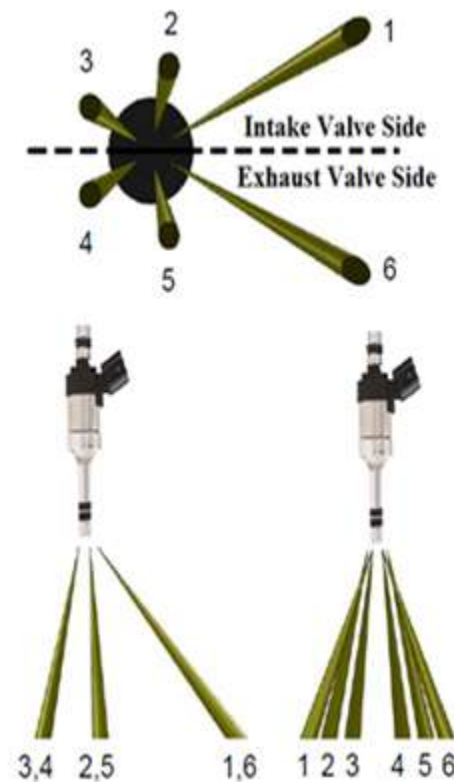
Figure 3-4   Relative positions of the direct injector along with the injector spray plume

The spark plug was located between fuel spray plumes 1 and 6, and it was inclined at an angle of 18° to the cylinder axis. As shown in the figure, the injector, which was manufactured by Bosch Ltd., had two symmetric groups of holes with three holes on each side of the injector, enabling the injector to deliver a hollow-cone spray.

Single-pulse injections were used throughout the experiments with an injection pulse width ranging from between ~1.5 and ~3ms for the load range of 5.5-8.5 bar IMEP studied. The injection event was triggered by a 12 volt DC electrical signal at the SOI of 280°bTDC used

throughout the experiments. More information about the SOI and other electrical engine control signals can be found in Section 3.3.

3.2.6 EGR

3.2.6.1 Hot EGR

A pipe with a valve was connected just after the exhaust plenum chamber to the intake plenum chamber in order to implement and control hot EGR in the engine, as shown in Figure 3-2. The Horiba MEXA-7100DEGR, discussed in detail in Section 3.5.2, had an in-built function which allowed a sample line to be connected to it, enabling the system to calculate the EGR addition (%) to the engine (accurate to ±0.02%). The sample line was connected to the intake and the CO_2 percentage was compared to the CO_2 percentage in the exhaust in order to calculate the EGR ratio using Equation 3-1.

$$EGR_{Ratio} = \frac{CO_{2(Intake)} - CO_{2(ambient)}}{CO_{2(Exhaust)} - CO_{2(ambient)}} \cdot 100(\%) \qquad (3\text{-}1)$$

The position of the EGR valve (±0.25% EGR accuracy) was then changed manually along with the throttle angle and injection pulse width to achieve the desired load and EGR addition. Although the intake manifold temperature was not controlled in the engine, the effects of the increased intake manifold temperature with increased EGR addition have been taken into account in the results. *(Please note that whenever EGR is discussed in this thesis, hot EGR is being referred to, unless stated otherwise).*

3.2.6.2 Cooled EGR

In order to achieve cooled EGR in the engine, the setup for the hot EGR was modified slightly to incorporate a 1.1 metre long heat exchanger to cool the EGR gases before they entered the engine, as shown in Figure 3-5. Air was blown over the heat exchanger to cool the EGR gases as they passed through and the overall length of the EGR line was increased

slightly in order to incorporate the heat exchanger. Although some water vapour was found to condense in the heat exchanger, it is believed that the vast majority did not condense. Thus, the water vapour content of the EGR gases was not significantly changed. The same procedure was followed as with the hot EGR to achieve the desired engine load and EGR addition.
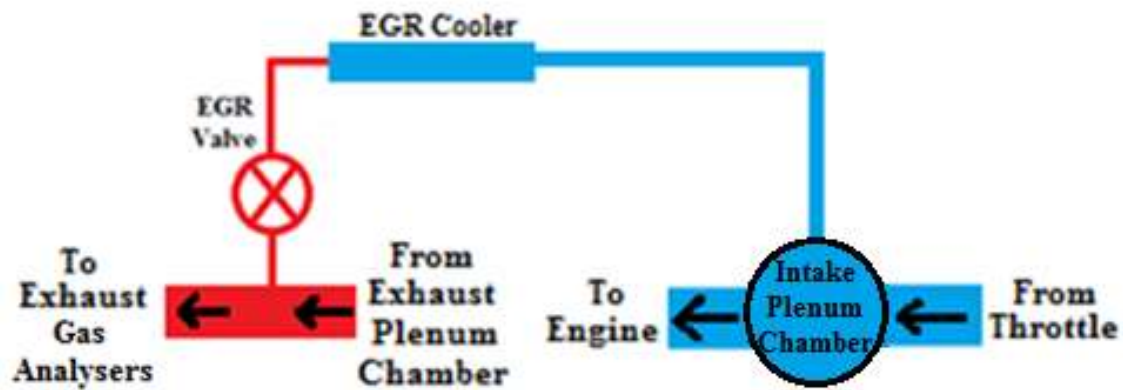
Figure 3-5   Cooled EGR schematic

3.2.6.3 Hot EGR after TWC

In order to simulate the effect of EGR after a TWC, a gas bottle supplied by BOC with a mixture of 86% nitrogen and 14% CO_2 was utilized. The mixture represents the composition of gases that would be present after a TWC assuming that 100% of the NO_x and CO from the engine has been converted to N_2 and CO_2 respectively, and assuming that all of the water vapour has been condensed and removed. It also assumes that all of the HCs and PM have been successfully oxidized in the exhaust system. This removed the effect of varying TWC exhaust gas conversion efficiencies which have been shown to vary the EGR ratio (Hoffmeyer et al., 2009, Lewis et al., 2014). This is due to changes in the CO conversion efficiency which affects the CO_2 percentage of the exhaust gas, affecting calculation of the EGR ratio (Equation 3-1).

Furthermore, it reduces the calorific value of the intake charge since energy cannot be extracted by oxidizing the HCs and PM in the engine cylinder and it reduces the heat capacity of the EGR gases because the water content of the EGR gases is removed. By using a simulated TWC, the back-pressure effect of a real TWC was eliminated allowing the effects of the post-TWC EGR gases on the engine combustion and emissions to be studied alone without the back-pressure effects. Fuel consumption would be expected to increase if the back-pressure effects were present because of increased pumping work.

The gas bottle was controlled using a regulator manufactured by BOC and a flow rate controller, after which a one-way valve manufactured by Swagelok was used to prevent any possible backflow into the gas bottle. The gas then passed through a 5 metre heated line maintained at temperatures between 75-200˚C, depending on the flow rate of gas through the line, to simulate the high temperature of the EGR gases after a TWC. Finally, the heated line was connected to the intake plenum on the engine to allow the EGR gases to mix sufficiently with the intake gases before they enter the engine. This setup is shown schematically in Figure 3-6.
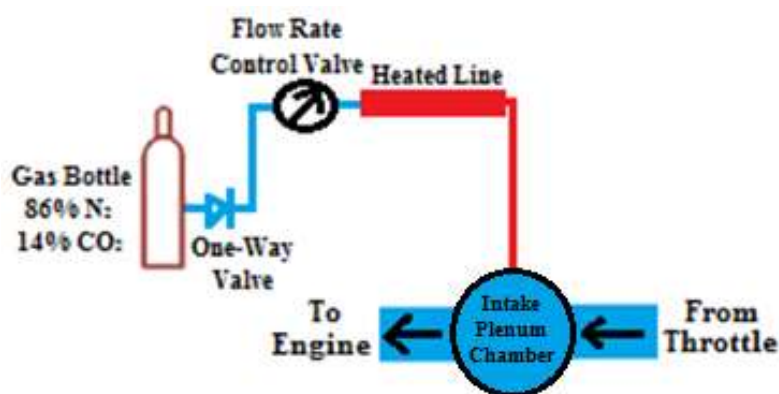
Figure 3-6   Hot EGR after TWC schematic

In order to achieve the desired engine load and EGR addition, the same procedure was followed as with the hot and cooled EGR. However, rather than the EGR valve being adjusted along with the throttle and injection pulse width, the flow rate controller was adjusted along with the throttle and injection pulse width and the temperature of the heated line was adjusted accordingly. Higher temperatures were used for higher flow rates and lower temperatures were used for lower flow rates, to achieve approximately the same temperature of heated gas for all flow rate conditions tested, as measured by the intake plenum temperature thermocouple. This was done to accurately reflect the similar EGTs that would be experienced when testing at a single engine load for the different EGR types in this investigation.

Although the EGT at a particular engine load will decrease with EGR addition, it is expected that the differences would become negligible after the TWC in a real vehicle. This is because sufficient heat transfer between the exhaust system and the atmosphere would be expected to occur by the time the exhaust gases passed through the TWC, cancelling out any relatively small EGT differences that would be otherwise observed at different EGR additions. Therefore, these differences have not been simulated in this investigation.

3.2.6.4 Cooled EGR after TWC

The same setup and procedure was used for the cooled EGR after TWC, except without the heated line, as shown in Figure 3-7.
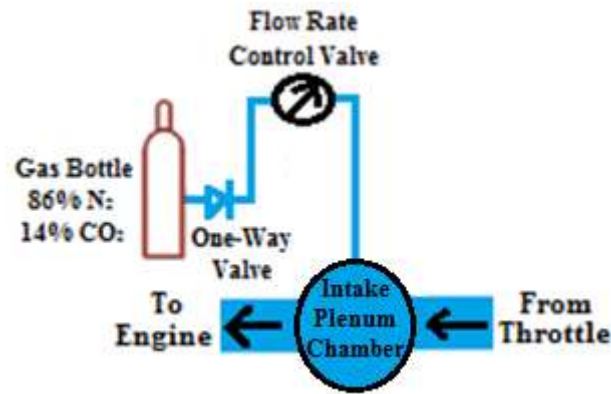
Figure 3-7   Cooled EGR after TWC schematic

3.2.7 Swirl and Tumble Intake Airflows

Baffle plates, as shown with drawings in Figures 3-9b and 3-9c, were installed on the engine between the intake runner and cylinder head in order to achieve swirl and high tumble airflow conditions, respectively, within the engine cylinder. The plates worked by blocking part of the intake flow into the engine to generate the swirl and high tumble. The swirl and tumble ratios were estimated using findings from other researchers, the results of which are presented in Section 3.2.7.1. As well as these two plates, another baffle plate shown in Figure 3-8a was made with the same profile as the intake runner, so that the intake geometry was the same for the reference low tumble condition as it was for the swirl and high tumble conditions. The tumble for this condition was generated by the vertical inclination of the intake runner alone.
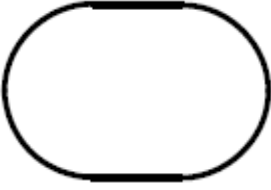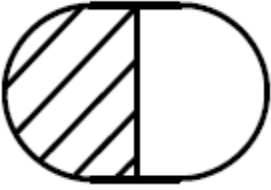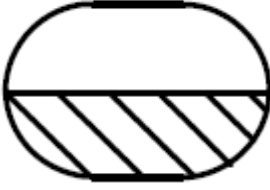
Low tumble baffle plate	Swirl baffle plate	High tumble baffle plate
(a)	**(b)**	**(c)**
	(hatched area indicates the baffle plate)	

Figure 3-8   **a)** Low tumble baffle plate, **b)** swirl baffle plate, **c)** high tumble baffle plate

3.2.7.1 Swirl and Tumble Ratio Estimation

For this investigation, the swirl and tumble ratios of the single-cylinder engine with the baffle plates fitted (Figure 3-8) were estimated based on data from previous investigations by other researchers. Several attempts were made to measure the ratios using PIV in a single-cylinder optical engine; however, they were unsuccessful due to technical difficulties which could not be overcome within the time available. Therefore, it became necessary to estimate the ratios rather than measure them.

Based on these findings of other researchers, the estimated swirl and tumble ratios of the baffle plates, as shown in Figure 3-8, have been estimated as shown in Table 3-2. A summary of the equipment and methods used by the other researchers to obtain their swirl/tumble ratios along with their findings has been provided in Table 3-3.

Table 3-2   Estimated swirl and tumble ratios for the three intake airflow conditions

Intake Airflow Condition	Swirl Ratio	Tumble Ratio
Low Tumble	0	0.7
Swirl	1.5	0.7
High Tumble	0	1.8

Table 3-3   Summary of other researchers findings for swirl and tumble ratios

Researcher	Engine Type	Cylinder Head Design	Number of Valves	Bore (mm)	Intake Runner Inclination Angle to horizontal (°)	Piston Shape	Engine Speed (rpm)	Swirl/Tumble Generation Method	Swirl/Tumble Measurement Method	Swirl Ratios	Tumble Ratios
AJ133 Engine	Single-cylinder	Pentroof	4	89	45	Flat Piston	1500	Baffle Plates	-	-	-
(Floch et al., 1995)	Single-cylinder	Pentroof	4	88	45	Flat Piston	-	Baffle Plates	Steady-flow test rig	0 (no baffle plate), 1.5 (swirl generating baffle plate)	0.7 (no baffle plate), 1.8 (tumble generating baffle plate)
(Teraji et al., 2009)	Single-cylinder	Pentroof	4	93	30	Flat Piston	1500	Baffle Plates	CFD (STAR-CD)	0 (no baffle plate), 1.5 (swirl generating baffle plate), 0 (tumble generating baffle plate)	1.5 (no baffle plate), 1.5 (swirl generating baffle plate), 2.1 (tumble generating baffle plate)
(Fujimoto and Tabata, 1993)	4-cylinder (modified to operate as single-cylinder)	Pentroof	4	78	n/a (only swirl ratios measured, and this only affects tumble ratio)	Flat Piston	-	Throttle plate in intake runner passage of one intake valve	Steady-flow test rig	0.4 (slightly closed plate)-3.8 (fully-closed)	-
(Li et al., 2001)	4-cylinder (modified to operate as single-cylinder)	Pentroof	4	80	n/a (only swirl ratios measured, and only this affects tumble ratio)	Flat Piston	1200	Blockage of intake port into one intake valve	PIV	2.30 (180˚bTDC$_{comb}$) - 1.90 (60˚bTDC$_{comb}$)	-

Overall, it can be seen that the swirl/tumble ratios of other researchers have been observed with equivalent or similar methods for generating the swirl and tumble intake airflows, as compared to those used in this investigation, and they have been observed with similar 4-valve pentroof combustion chamber designs. The results observed by other researchers are similar to one another across similar engine designs (pentroof combustion chamber), with different swirl/tumble generation methods and different intake runner inclinations to the horizontal, accounting for the differences in swirl/tumble ratios observed. Therefore, while not being 100% accurate, it is reasonable to expect that the swirl and tumble ratios in Table 3-2 will provide a good estimation of those used in this investigation.

Furthermore, tumble ratios have been shown to vary depending on what equipment is used to measure them (Kim et al., 2006). Therefore, it is believed that the estimation of the swirl and tumble ratios obtained will not affect the interpretation of the findings of this investigation more significantly than the use of different swirl/tumble measurement equipment. It is further believed that the relative differences in swirl and tumble ratios between the baffle plate designs have been accurately estimated, although the absolute magnitudes may differ slightly from the true values. Thus, the interpretation of the findings of this investigation will not be significantly affected.

3.2.8 Variable Compression Ratio

Although the single-cylinder engine had a geometric compression ratio of 11.5:1, the compression ratio could be modified by adjusting the number and size of metal inserts which are placed beneath the cylinder head. These acted to adjust the height of the cylinder head in relation to the piston BDC, allowing the compression ratio to be changed. The maximum compression ratio was however limited; beyond this limit the intake valves would have hit the piston crown. The real dynamic compression ratio of the engine could be adjusted by changing the valve timings; however, this was not pursued in this investigation. The compression ratio of the engine is thus calculated using Equation 3-2 (Heywood, 1988).

$$\text{Compression Ratio } (R_c) = \frac{V_d + V_c}{V_c} \qquad (3\text{-}2)$$

where V_d is the swept volume which remains constant and V_c is the clearance volume which is altered with the metal inserts. To achieve the desired compression ratio, the equation was solved for V_c which could then be related to the new size of the metal inserts (h) using Equation 3-3. This allowed the desired compression ratio to be achieved by inserting the metal inserts with the correct size.

$$V_c = \frac{\pi \cdot engine\ bore^2}{4} \cdot h \qquad (3\text{-}3)$$

3.3 Control Systems

The spark timing and injection pulse width along with the start of injection and coil charge duration were controlled using the engine timing control system (ETCS); a program written using LABVIEW and operated using a NI card (model 6602). This program was initially developed by the ICE group at the University of Oxford but subsequent modifications were made by a previous research student in the engine group (Luszcz, 2009). It allowed the engine parameters to be modified in real-time while the engine is running. A screenshot of the program front-panel is shown in Figure 3-9.
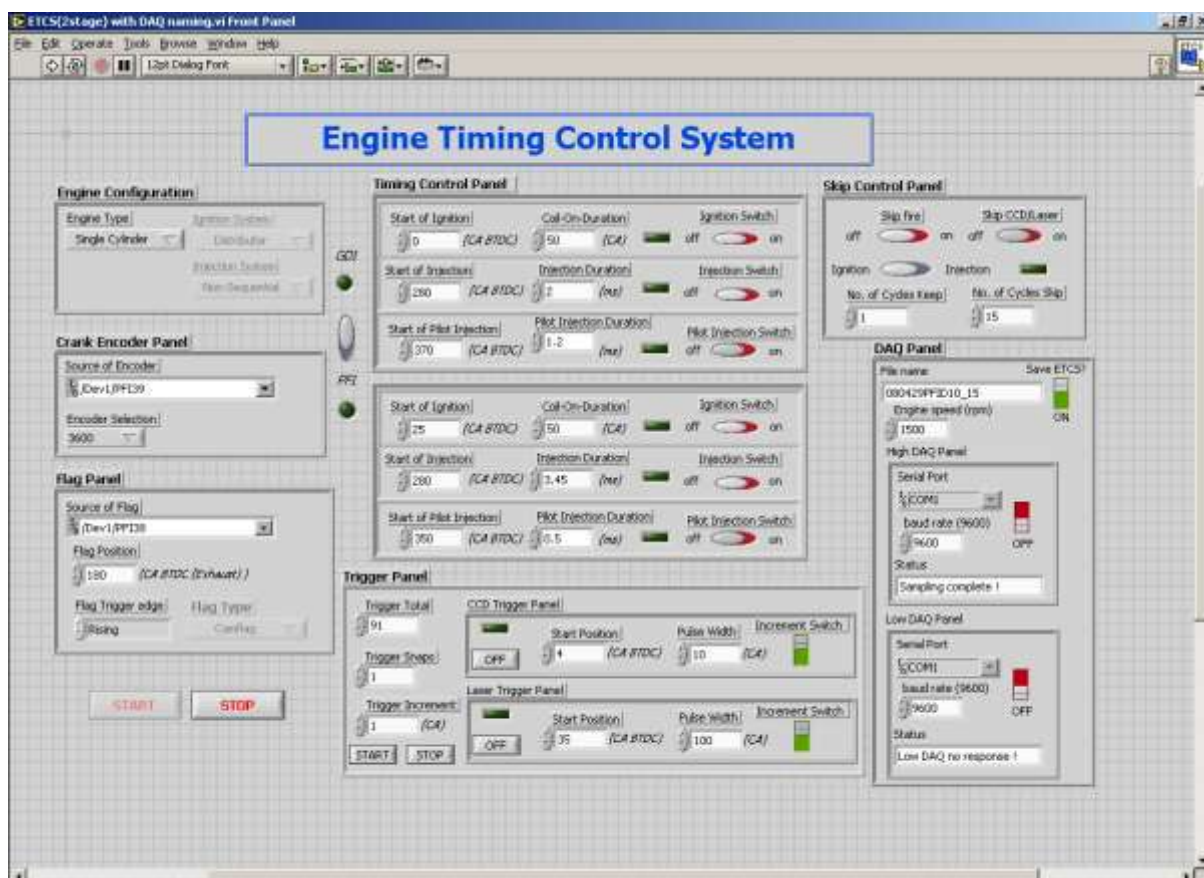
Figure 3-9   ETCS LabView program front-panel (Luszcz, 2009)

In order to achieve a particular engine load, fuel was injected and adjusted using the ETCS software and the airflow into the engine was controlled using a butterfly valve that was adjusted from the engine control room. The fuel and airflow were modified until the desired

engine load was achieved. When EGR was used, the EGR valve was also adjusted along with the injection pulse width and throttle position, as discussed, in order to achieve the desired engine load and EGR addition.

3.3.1 Crankshaft Encoder Setup

The crankshaft encoder was set up to correspond to the engine CAD in order to accurately control injection, ignition and the variable valve timings. This was achieved using a timing light which was attached to the ignition coil of the engine, enabling it to produce a stroboscopic light signal when the ignition coil was activated by the ETCS system at a specified ignition timing during low speed engine cranking. The light was shone onto the flywheel which had CAD markings; the reading achieved when the light came on was recorded and the encoder position was subsequently adjusted until the system was synchronized.

3.3.2 Variable Valve Timing System

The VVT system operated using crankcase oil pressure (3 bar) in order to control the positional offset of the intake and exhaust camshafts, relative to the position of the camshaft pulley ($\pm 25\ CAD$). In order to control the system, a LABVIEW program developed by a previous research student in the engine group (Luszcz, 2009) which controls the valve timing using a NI card (model 6202), was used. A screenshot of the program front-panel is shown in Figure 3-10. A Hall effect type sensor was used to detect the relative position of the camshaft and this position was controlled using hydraulic solenoids mounted in the cylinder head, which adjusted the oil pressure and thus changed the relative camshaft positions. The program constantly adjusted the oil pressure in order to maintain the cam timing within a range of $\pm 0.1\ CAD$.
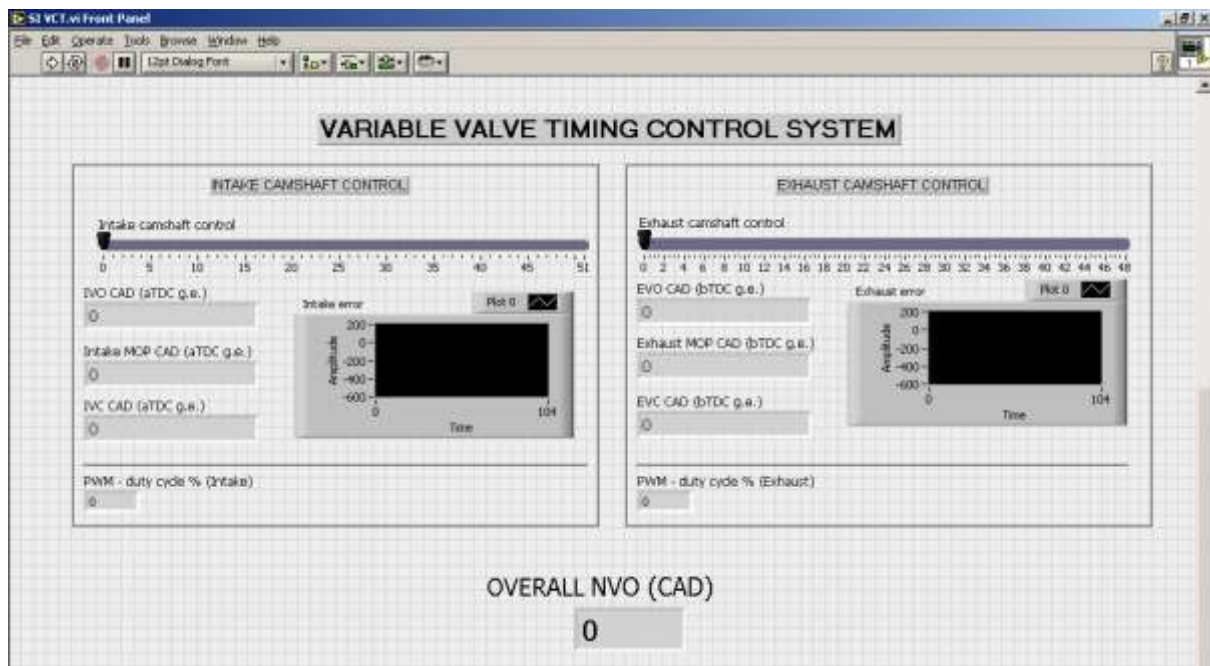
Figure 3-10   VVT LabView program front-panel (Luszcz, 2009)

Table 3-4 shows the geometry of the intake and exhaust camshafts and Figure 3-11 shows the intake and exhaust valve lift profiles along with that of a typical in-cylinder pressure trace. The camshaft itself had a high-lift profile typically used in SI engines and the valve timings were chosen in order to minimise the residual gas fraction to increase the effect that EGR has on the combustion and emissions. The engine was designed with an intake valve of a larger inner seat diameter and higher maximum lift than the exhaust valve, in order to improve VE.

Table 3-4   Single-cylinder engine camshaft geometry

Valve and Camshaft Geometry	
Intake Valve Lift	10 mm
Intake Valve Inner Seat Diameter	36 mm
Exhaust Valve Lift	9.3 mm
Exhaust Valve Inner Seat Diameter	33 mm
Intake Valve Duration	250 CAD
Exhaust Valve Duration	250 CAD
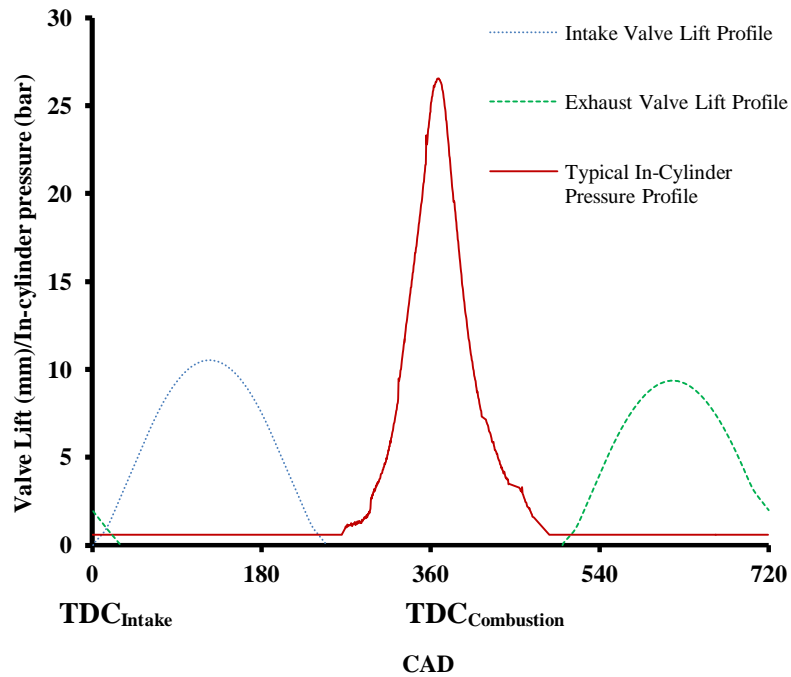
Figure 3-11   Intake and exhaust camshaft profiles

All of the signals sent from the control software to operate the engine as well as those produced by the sensors on the engine were sent to the control tower which consisted of the ETCS and VVT interface boxes which were used for the ETCS and VVT systems, respectively. Figure 3-12 summarizes the arrangement and flow for the various signals.
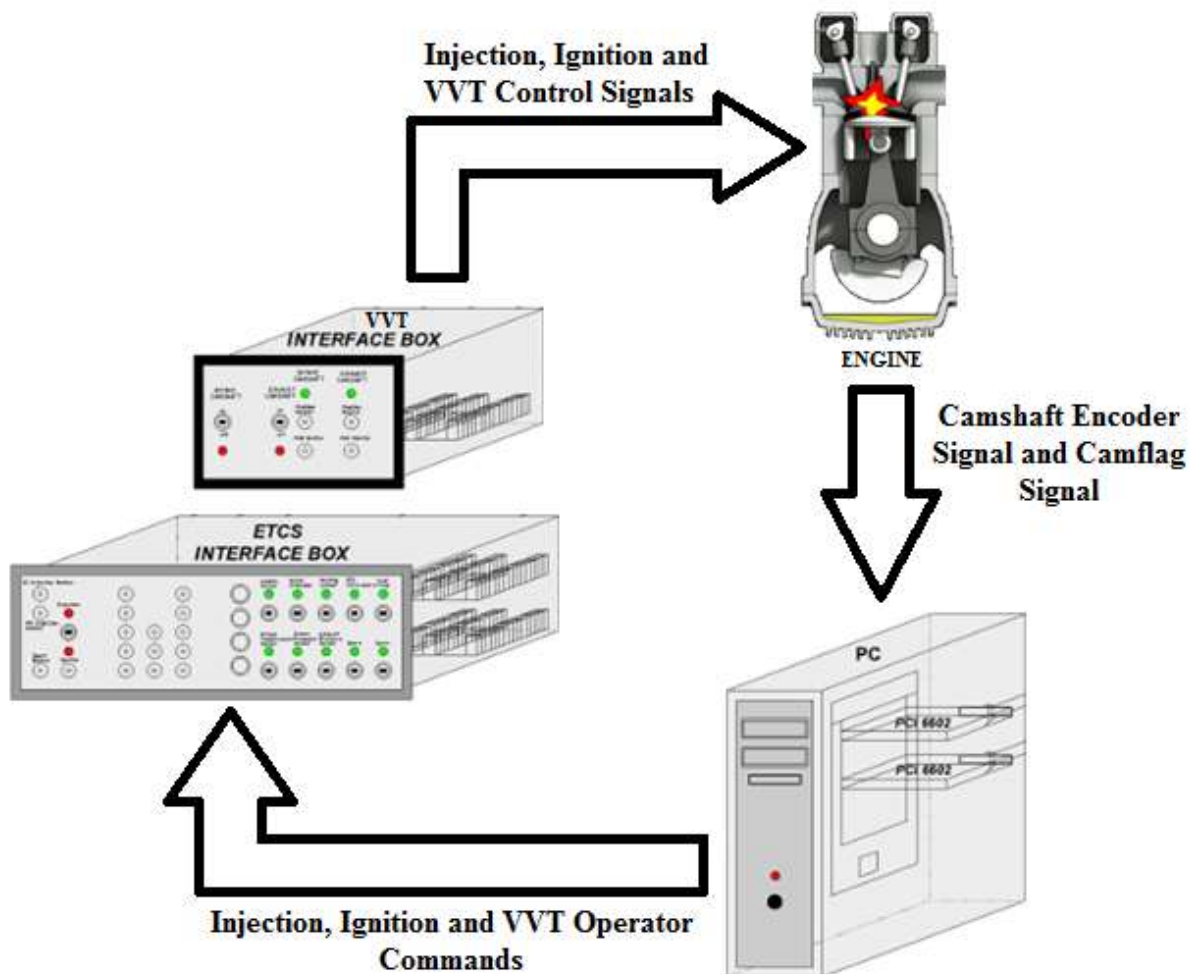
Figure 3-12   Engine ETCS and VVT control systems; their arrangement and signal flow

3.3.2.1 Variable Valve Timing Setup

Detailed instructions on how to set up the variable valve timing system can be found in (Wang, 2014b) and (Daniel, 2012d). These instructions were followed in order to set up the system on the engine after each rebuild.

3.4 Instrumentation

Various ancillary equipment was fitted onto the research engine and balancing unit in order to provide the measurements which were recorded and later analysed in this investigation. These mainly consisted of pressure, temperature and engine speed data, each of which is discussed further in the following sections.

3.4.1 Engine Speed and Torque

The engine was coupled via a universal joint to a DC dynamometer in order to maintain a constant speed of 1500 rpm ($\pm$1 rpm), regardless of the engine torque output. The speed was chosen because it represents a speed used frequently in emission test cycles and it is commonly used by researchers (Alger et al., 2009a, Heffel, 2003, Institution of Mechanical Engineers, 2013). This along with the medium-high engine loads (5.5-8.5 bar IMEP) studied mimics vehicle acceleration or driving on an incline, which is important to study because it is one of the worst conditions for fuel consumption and emission formation. A torque meter on the engine dynamometer was used to provide an instantaneous torque reading, which is useful in finding the MBT spark timings at a particular operating point.

3.4.2 Pressure and Temperature Measurements

In-cylinder pressure measurements in the engine were made using a Kistler 6041A water cooled piezoelectric pressure transducer along with a Kistler 5011B charge amplifier, which was used to amplify the signal from the transducer. The transducer itself was fitted at the side of the engine cylinder head between the intake and exhaust valves, to ensure that it had direct contact with the gases in the combustion chamber for accurate in-cylinder pressure measurement (Hountalas and Anestis, 1998). The electric charges induced by the piezoelectric material were amplified by the charge amplifier and then outputted as a modulated voltage. The pressure transducer was calibrated by Kistler using an oil weight bench machine in the range of 1 MPa/1 V to 10 MPa/10 V, and this calibration was then input into the charge amplifier as a tuning coefficient. Overall, the system was capable of absolute pressure measurements in the range of 0.08-10 MPa. Once the signals were amplified, they were sent to the data acquisition system.

In order to measure the intake and exhaust manifold pressures, EPT 3100 media isolated pressure transmitters manufactured by EuroSensor were used. K-type stainless steel thermocouples supplied by RS were used for the temperature measurements. The signals for these temperature sensors were sent to a TCK-4 thermocouple amplifier before being sampled by the NI data acquisition card.

3.4.3 VAF Meter

A Romet (model number: G25) VAF meter was used to measure the rate of airflow into the engine for fuel consumption calculations. The flow meter was designed to rotate one revolution for a fixed volume of air, allowing the airflow rate to be quantified. The meter itself was attached via a coupling to an encoder, with its speed recorded by the data acquisition system. In order to relate the frequency of the encoder to the volumetric airflow rate in the engine, a calibration was conducted at different throttle angles and thus different engine volumetric airflow rates. The airflow in the engine was measured using an orifice plate connected after the 100 litre intake damper and before the throttle, which created a unit pressure difference for a unit flow across it. This pressure difference was measured using an inclined u-tube manometer and the reading was used to calculate the actual flow rate in the engine using Equation 3-4.

$$Q\ (l/s) = C_d \cdot \sqrt{\frac{2\Delta P}{\rho}} \cdot \frac{A_2}{\sqrt{1-(\frac{A_2}{A_1})^2}} \quad \text{(3-4) (Eastop and McConkey, 1993)}$$

C_d is a dimensionless number representing the orifice plate discharge coefficient and $\frac{A_2}{A_1}$ is the ratio of the orifice flow plate areas. C_d can be obtained by dividing the actual flow rate with the theoretical flow rate. This actual flow rate was calculated at a known orifice flow rate calibration where a 4 kPa pressure drop is equivalent to an actual flow rate of 21 litres/second. The theoretical flow rate in this case was calculated using Equation 3-4 by

assuming that C_d is 1. The moisture pressure was not taken into account when calculating the air density, limiting the accuracy of this method. Along with the u-tube monometer readings, the frequency of the encoder was recorded, therefore allowing a correlation between the two to be calculated. The calibration equation was then input into the low speed data acquisition (LSDAQ) software, which is discussed further in Section 3.6.2, in order to calculate the volumetric airflow rate at any given engine condition. The u-tube manometer and encoder frequency readings were repeated three times at each throttle position in order to improve the accuracy of the calculation.

Figure 3-13 shows the calibration between the calculated and actual airflow rates. It is clear that the calibration achieved is good. However, even with a R^2 value of 0.9966, there is an average percentage error of 1.6% between the calculated and actual airflow rates. This was obtained by individually calculating the percentage error for each of the data points on Figure 3-13, and then taking the mean average of these. The error is largely due to the limited resolution of the u-tube manometer device and the limited unit pressure difference produced across the orifice plate.
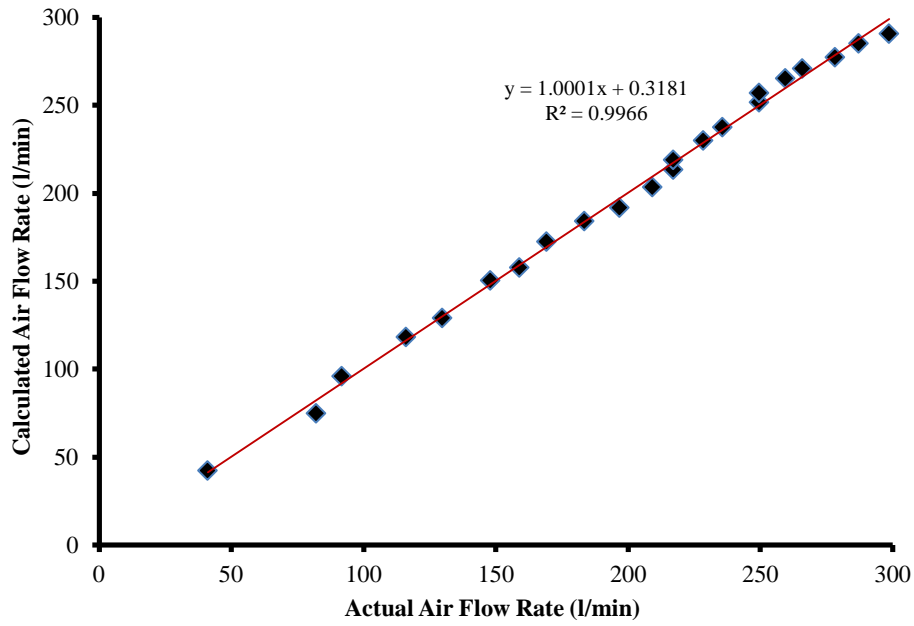
Figure 3-13   Calibration results of the VAF Meter

The minimum and maximum VAF rates measured in this study were 200 and 300 l/min respectively, which is within the calibration range shown in Figure 3-13. The maximum airflow rate in the engine if the VE was 80% would be 339 l/min according to Equation 3-5.

$$VAF = \frac{rpm}{2} \cdot Cylinder\ Volume \cdot VE = \frac{1500}{2} \cdot 0.5656 \cdot 0.8 = 339\ l/min \quad (3\text{-}5)$$

Therefore, the maximum airflow rate used in the experiment of 300 l/min at an engine load of 8.5 bar is approximately correct, considering the engine can reach a maximum load of approximately 9.5 bar.

3.4.4 Lambda Meter

For all of the tests in the engine, the dynamic Lambda value was measured using a ETAS LA4 Lambda meter and a Bosch heated wideband oxygen sensor. Fuel-specific curves were used in the Lambda meter to interpret the dynamic (actual) AFR using the oxygen content in the exhaust. Before a new fuel is tested in the engine, its hydrogen-to-carbon (H/C) and oxygen-to-carbon (O/C) ratios were input into the system along with its stoichiometric

air/fuel ratio. This was then used by the Lambda meter to characterise the fuel curves to calculate the dynamic AFR. As discussed, in order to achieve a specific engine load, the throttle and injector pulse width were modified along with the EGR valve, if EGR was used. Not only was the target load achieved using this procedure but the target Lambda value too. Overall, this system was open loop meaning that the injection pulse width required regular manual modifications to ensure Lambda remains within target.

3.5 Emissions Measurement

In this study the legislated European and United States emissions of PM, NO_x and HC were measured. The devices used to measure these emissions are described in the following sub-sections.

3.5.1 Particulate Emissions

The PM emissions were sampled 0.3m from the exhaust valve, downstream of the exhaust plenum, and they were measured using two devices; firstly the differential mobility spectrometer (DMS) 500 manufactured by Cambustion Ltd. and secondly the scanning mobility particle sizer (SMPS) 3936, manufactured by TSi. Through experience, the DMS500 provided more consistent readings, resulting from the equipment being newer. However, due to limited equipment availability, the SMPS 3936 was used in these experiments too.

In order to improve the consistency of the PN data, particles smaller than 10 nm which are detectable by the PM measurement equipment used in this investigation were removed from the range of particles studied. The particles have been characterized in this investigation by their diameter in order to distinguish between ultra-fine particles and fine particles, since the ultra-fine particles are the most significant contribution to PN and they are the most harmful to human health (Anderson et al., 2012b, Hull et al., 2005).

In this investigation, the nucleation mode particles have been classified as those within the 10-30 nm range and the accumulation mode particles have been classified as those within the 30-500 nm range for data from the DMS 500. For the results from the SMPS 3936, the accumulation mode particle range was 30-300 nm, due to the lower maximum particle size it can measure. This is based on the PM data recorded which can be seen to form two distinct peaks within the stated ranges. (Zhang et al., 2014b) also classified nucleation mode particles as those below 30 nm and accumulation mode particles as those above 30 nm in their SI engine investigation using gasoline fuel along with butanol and ethanol splash blends.

It must be noted that the separation between the two modes is ill-defined (Kittleson, 1998) and that in this investigation; the PM accumulation mode was shifted towards a smaller size for the data collected using the SMPS 3936, because of the use of the thermodenuder, as will be explained in a later section. It must also be noted that with the DMS 500 when no thermodenuder was used and with the SMPS 3936 despite the use of the thermodenuder, some nucleation mode particles still remained in the accumulation mode peak. This is because they were adsorbed onto the accumulation mode particles. Also, despite the use of the thermodenuder with the SMPS 3936, a nucleation mode particle peak was still observed. Therefore, this method of PM mode separation has its limitations.

3.5.1.1 DMS 500

The DMS 500 classified particles according to their size by separating them in a parallel differential electrical mobility analyser, as shown in Figure 3-14.
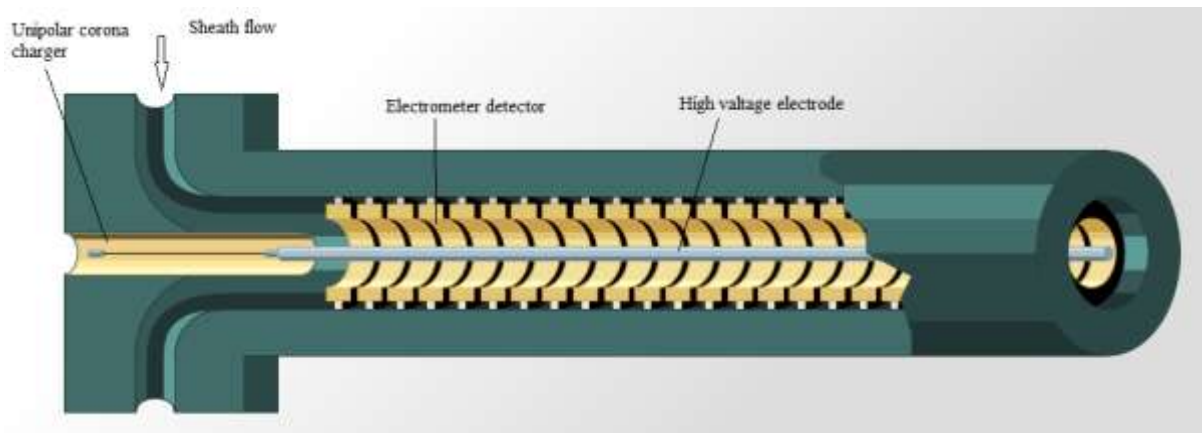
Figure 3-14 Cambustion DMS 500 analyser operating principle

Firstly, the particulates were pumped from the exhaust into the two stage dilution system built into the instrument, as shown in Figure 3-15. The sample line from the exhaust to the dilution system was maintained at 150˚C in order to avoid condensation of the particulates. The particulates were then diluted in the primary dilution stage at a fixed dilution ratio of 5:1 for gasoline engine measurement, in which the mass flow rate is controlled by HEPA filtered compressed air. A rotating disc was then used to perform the secondary high ratio dilution with a dilution ratio of 16:1 used for this investigation; the system allowed a maximum secondary dilution ratio of 500:1. This resulted in an overall dilution ratio of 45.2:1. The choice of dilution ratios ensured that a good signal to noise ratio was maintained while extending instrument cleaning intervals, as recommended by the manufacturer (Cambustion, 2011). Samples were collected at a rate of 1 Hz for approximately 2 minutes for each reading to improve the consistency of the data collected.
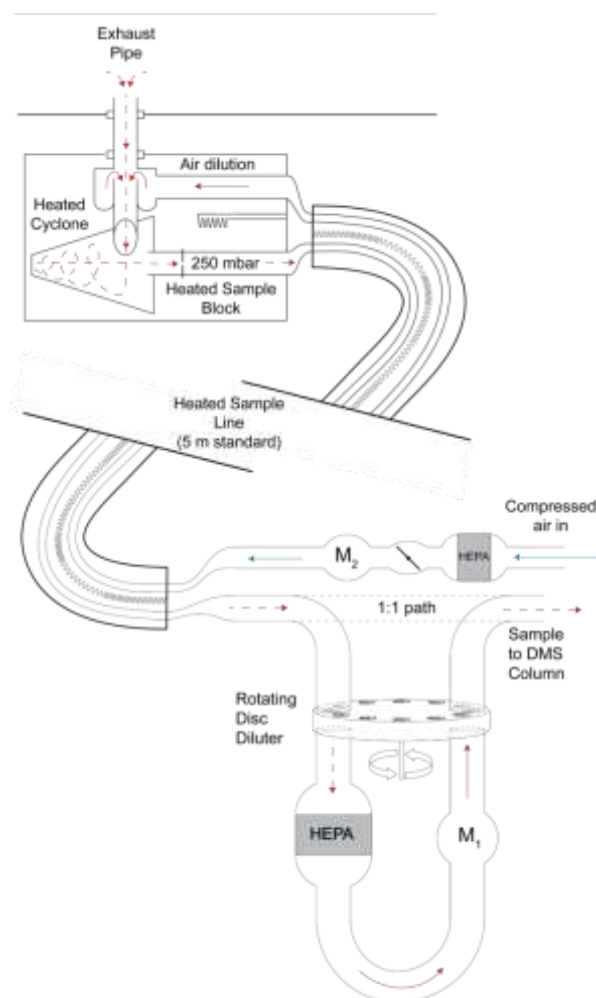
Figure 3-15   Schematic of the DMS 500 two-stage dilution system

Once the particles were diluted, they were passed through a unipolar corona charger. This charged the particles with a positive electric charge which was proportional to the particle size. The filtered sheath flow then pumped the charged particles into the particle classifier. The high voltage electrode as shown in Figure 3-14 then attracted the positively charged particles towards the electrometer detector. The distance travelled by the particles along the classifier was proportional to their size and inversely proportional to their mass. The classifier which consisted of 22 electrometer detectors measured the charge quantity and distance travelled by the particles, thus allowing the particle size, mass and number data to be quantified. Finally, the Cambustion software recorded the particulate measurements.

3.5.1.2 SMPS 3936

The SMPS 3936 system was comprised of three different units. Firstly, a TSi rotating disk thermodiluter (model 379020A) maintained at 150˚C was used to dilute the exhaust sample before it was pumped through a Topas TDD 590 thermodenuder at a temperature of 400˚C, to remove most of the volatile nucleation mode particles in order to make it easier to distinguish the nucleation and accumulation mode particles from one another. PM emissions from DISI engines are mostly composed of volatile particles; they are fundamentally different from those produced by diesel engines. Volatilities not only exist in the nucleation mode, but they are also adsorbed onto accumulation mode particles. This makes it difficult to measure the PM size distribution accurately. Therefore, the use of the thermodenuder device enabled the particle size and number distribution to be accurately measured (Wang, 2014b).

Secondly, the particles were processed in the electrostatic classifier (model 3080) which had a differential mobility analyser (model 3081) attached to it, in order to separate the particles according to size. Thirdly, the particles were counted in the condensing particle counter (model 3775). The settings inputted into the SMPS system for this study are summarized in Table 3-5. The overall dilution ratio used in this study for the SMPS is 45.72:1, based on the work of a previous research student in the engine group (Daniel, 2012d).

Table 3-5   SMPS 3936 system settings

SMPS 3936 System Settings	
Sample Flow Rate (l/min)	1
Sheath Flow Rate (l/min)	10
Scan Up Time (s)	90
Retrace Time (s)	30
Minimum Particle Diameter (nm)	7.23
Maximum Particle Diameter (nm)	294.3

In addition to making it easier to distinguish the nucleation and accumulation mode particles from one another, the use of the thermodenuder also resulted in a significant PN reduction and the PM distributions being shifted towards a smaller size. As discussed, both of these were clearer at higher engine loads where there was more soot formation. This is due to the non-adsorbed nucleation mode particles and those nucleation mode particles adsorbed onto accumulation mode particles, respectively for the nucleation and accumulation mode particles, being partially removed by the thermodenuder. This was a compromise that the author and the previous research student (Wang, 2014b) made in order to improve the ability to distinguish between the nucleation and accumulation modes, as mentioned. Overall, what is most important is the relative change between different engine conditions rather than absolute numbers, since these can vary significantly between different engines (Wang, 2014b).

3.5.2 Gaseous Emissions

The gaseous emissions were sampled 0.3 metres from the exhaust valve on the opposite side to the PM sampling point, downstream of the exhaust plenum, before being pumped through a pre-filter and heated line, both of which were maintained at 190°C to avoid condensation of the emissions. They were then subsequently analysed by the Horiba MEXA-7100DEGR. The specification of the system is shown in Table 3-6.

Table 3-6   Horiba MEXA-7100DEGR specification

Horiba MEXA-7100DEGR Specification	
	Dry CLD
NO$_x$ Analyser	(min. ppm=0-10, max. ppm = 0-10,000)
	Zero gas = N$_2$, span gas = NO/NO$_2$
	Hot-wet FID
HC Analyser	(min. ppm=0-10, max. ppm = 0-50,000)
	Zero gas = N$_2$/air, span gas = C$_3$H$_8$
	NDIR (dry)
CO Analyser	(min. ppm=0-100, max. ppm = 0-12%)
	Zero gas = N$_2$, span gas = CO/N$_2$
	NDIR (dry)
CO$_2$ Analyser	(min. ppm=0-5000, max. ppm = 0-20%)
	Zero gas = N$_2$, span gas = CO/N$_2$
Accuracy	±1%

Nitrogen oxides in the Horiba system were measured using a dry chemiluminescence detector (CLD) and total hydrocarbons, HC, were analysed using a hot-wet flame ionization detector (FID) (Robert Bosch GmbH, 2006). Prior to the NO$_x$ being analysed, the NO$_2$ was converted into NO to enable it to be measured in the CLD. Once in the CLD, ozone was used to produce a reaction with the NO, and as a result a photon was emitted. This produced a current which was converted to a voltage output which was a function of the NO and thus NO$_x$ concentration in the sample. For HC analysis, the sample gas was pumped into a nozzle charged with a high voltage, after which it was analysed using a hydrogen flame. In the high temperature hydrogen flame, some of the hydrocarbon molecules were ionized, resulting in a flow of current between the positively charged nozzle and a collector. The current was then converted into a voltage output which was a function of the HCs in the sample. The voltage outputs created by the respected CLD and FID detectors were used to calculate the relative concentration of NO$_x$ and HCs in the exhaust sample.

Oxides of carbon (CO and CO_2) were measured using a non-dispersive infra-red (NDIR) detector. The device measured the change in light intensity as an infra-red beam was passed through the sample gas chamber. Oxides of carbon absorb infra-red light so the change in light intensity could be used to calculate the relative concentrations of CO and CO_2 in the sample gas.

Prior to each test, the Horiba was heated to its pre-set temperatures and the device was calibrated using zero calibration gases. The test points were typically recorded one after another during which the system continuously measured the gaseous emissions. When the engine was stopped, the system was purged with compressed air to avoid build-up of condensates in the system, which could have affected future measurements.

3.6 Data Acquisition and Processing

High speed crank-angle resolved engine data was recorded using a NI card (model 6251) and the low speed, time resolved engine data was also recorded using a NI card (model 6602). This is explained in detail in the following sections.

3.6.1 High Speed Data Acquisition

In order to acquire detailed in-cylinder pressure data with a good resolution, the in-cylinder pressure data was recorded at high speed with a resolution of 0.5 CAD for 300 consecutive cycles, using the high speed data acquisition (HSDAQ) program written in LabView by a previous research student in the engine group (Luszcz, 2009). The screenshot of the front panel of the program is shown in Figure 3-16. With an engine speed of 1500 rpm, this equates to data being collected every 80 ms (12.5 Hz). In order to ensure the correct CAD was recorded for the in-cylinder pressure data, the intake pressure was also recorded and the two were "pegged" to each other, as described in Section 3.6.4. An average was taken for

these data over 300 engine cycles to reduce the effect of small fluctuations in the measurements on the data. The stability of the VVT system was measured by recording the intake and exhaust cam position data from their respected sensors.
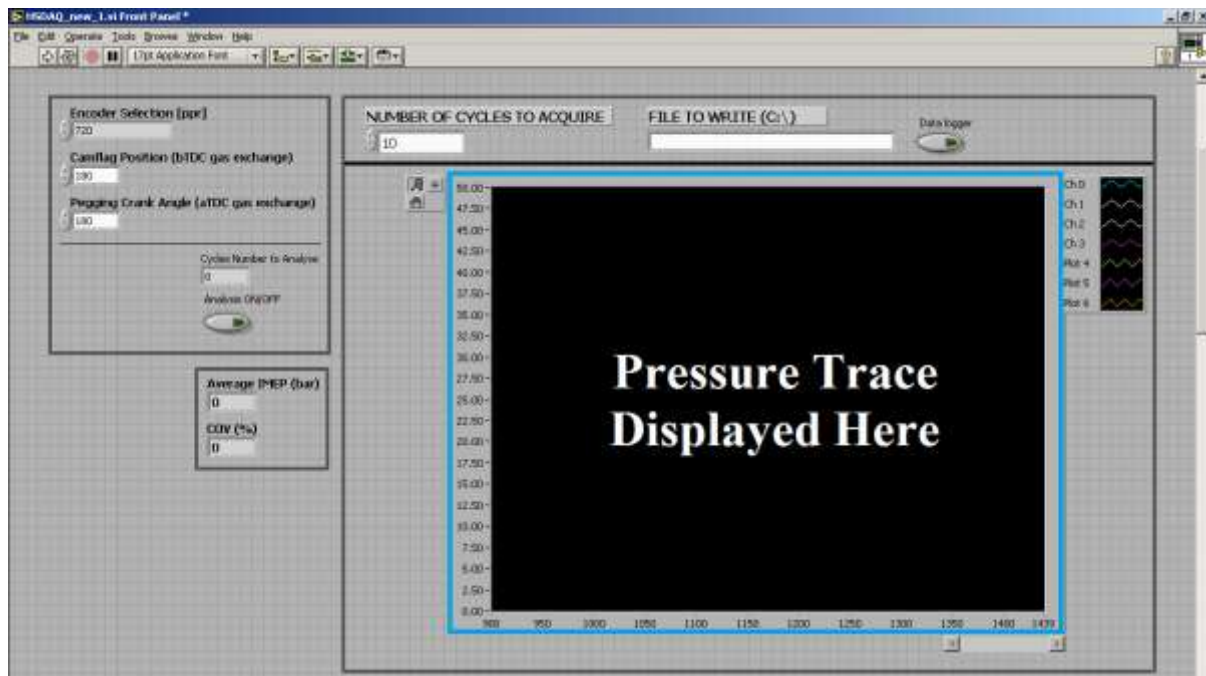
Figure 3-16 HSDAQ LabView program front-panel (Luszcz, 2009)

3.6.2 Low Speed Data Acquisition

Due to the lower variation in the remaining engine data such as the engine temperatures (intake, exhaust, cylinder wall, coolant, oil), ambient conditions (pressure, temperature), VAF rate, throttle position, Lambda and the gaseous emissions data (NO_x, HC), the data was collected on a time resolved basis rather than a crank resolved basis. As with the high speed data, an average was taken for these data, with an average taken over 200 samples. The data was acquired using the LSDAQ program, again written in LabView by a previous research student (Luszcz, 2009). The screenshot of the front-panel of the program is shown in Figure 3-17.
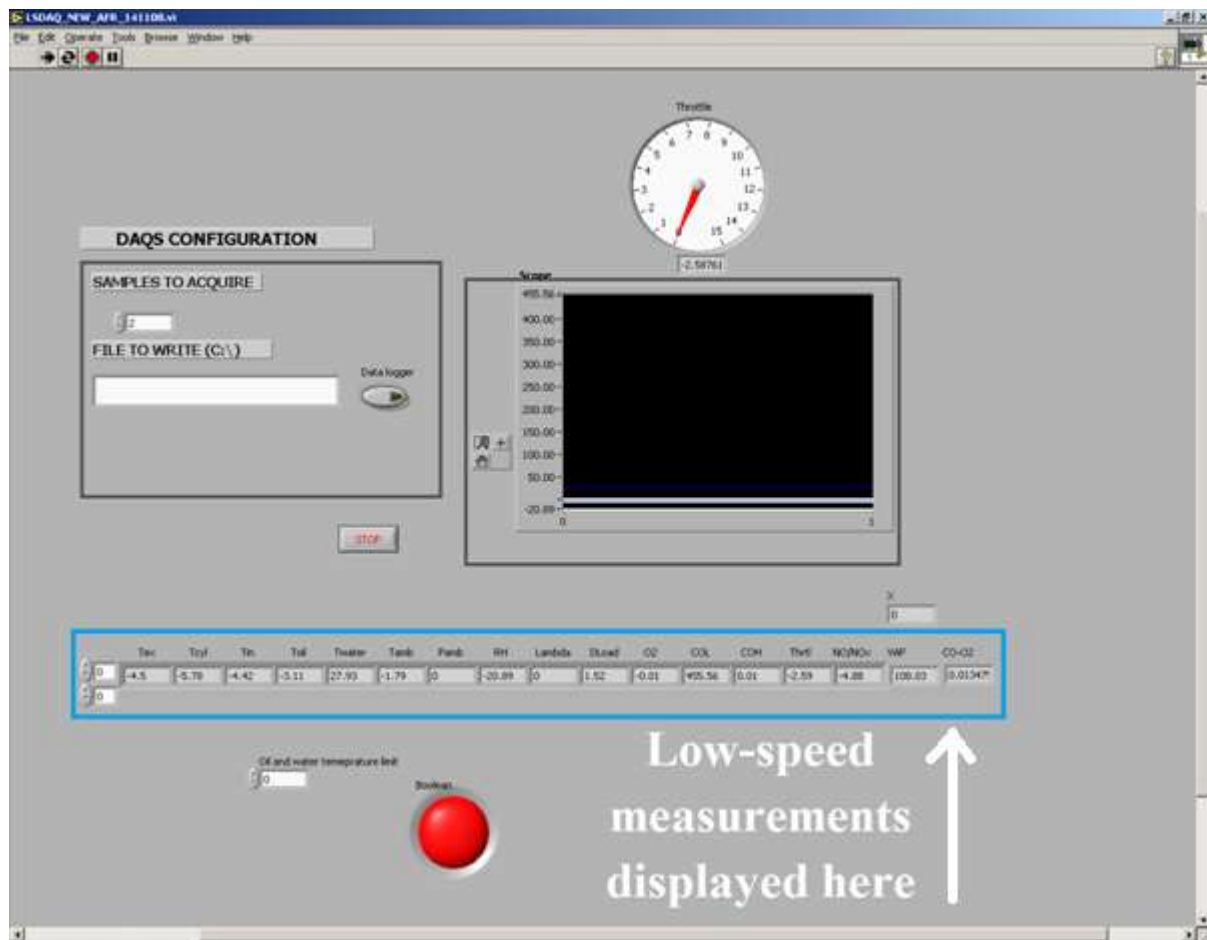
Figure 3-17   LSDAQ LabView program front-panel (Luszcz, 2009)

3.6.3 Initial Data Processing

A custom MatLab script written by the ICE group at the University of Oxford and developed by previous research students at the University was used to analyse the data from the high and low speed data acquisition systems. The method described by Stone (Stone, 1999) was used to calculate the net IMEP from each engine cycle, and this was averaged across 300 consecutive cycles.

3.6.4 In-cylinder Pressure Interpretation

As mentioned, the intake pressure data was collected along with the in-cylinder pressure data in order to ensure the correct CAD was recorded for the in-cylinder pressure data. The two were "pegged" to one another at the same CAD, (BDC$_{intake}$), where the two pressures were

equal, to ensure that the correct CAD was recorded for the in-cylinder pressure data. Overall, this helped to overcome the effects of drift which would otherwise have made the piezoelectric pressure transducer used in these experiments unsuitable (PCB Piezeotronics, 2015). A smoothing function was programmed into the MatLab script in order to reduce the fluctuations in the recorded pressure trace, to make it simpler to analyse.

3.6.5 In-cylinder Gas Temperature Calculation

PM emissions are strongly dependent on charge temperature as are NO_x and HC emissions. Therefore, a Ricardo WAVE model was created to simulate the in-cylinder conditions recorded in the experiments, in order to calculate the average in-cylinder temperatures. The model was then calibrated and verified using five cases for each, to ensure the model was accurate for the engine conditions tested in this investigation. This is described in the following sections.

3.6.5.1 Ricardo WAVE Combustion Model

Figure 3-18 shows the Ricardo WAVE model used in this investigation.
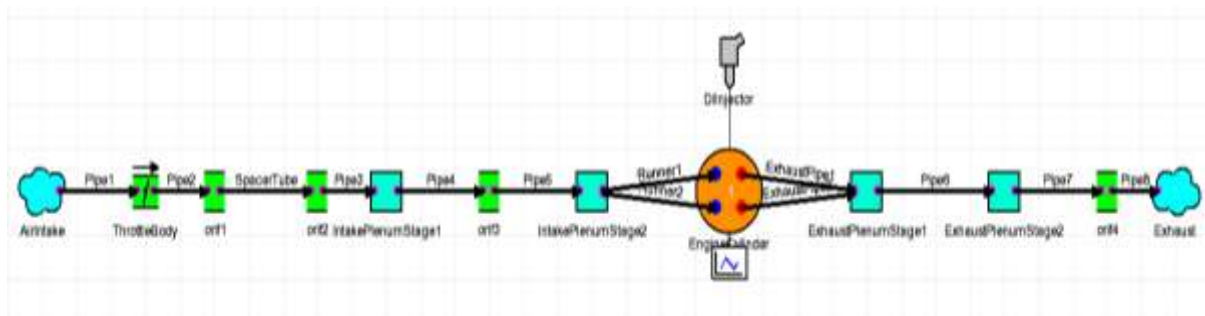
Figure 3-18   Ricardo WAVE simulation model

Ricardo WAVE is a one-dimensional engine and gas dynamics simulation tool created by Ricardo PLC, and it is widely used in engine research and development by Universities and the automotive industry. In order to simplify the analysis, the software uses the ideal gas law combined with a prediction of trapped residuals and fuel vaporization behaviour, in order to

estimate the average in-cylinder gas temperature. This is much simpler than detailed chemical kinetics, reducing the computational requirements and calculation times significantly. Therefore, while the average in-cylinder temperature data in this investigation does not represent actual measurements, it does provide some insight into the global average gas temperatures. The fuel properties of indolene were used to simulate the combustion of gasoline in order to further simplify the analysis. When simulating the combustion of the fuel blends used in this investigation, the known properties were inputted but some unknown properties such as viscosity-temperature behaviour were taken from indolene. A primary combustion sub-model based on the recorded MFB profile was used along with a SI Wiebe combustion sub-model, which required the input of MFB50 and MFB10-90, in order to simulate the in-cylinder temperature conditions.

In order to produce the model, the following steps were taken:

1. Intake and exhaust systems and components were measured

2. Engine geometry such as the bore, stroke, valve diameters and cam profiles were measured

3. The information was then used to construct the Ricardo WAVE model geometry

4. The model self-check function was used to ensure correct matching of inlet and outlet geometries between the components in the model, to ensure it could be solved

After the geometry had been produced, the other parameters were input into the software after which it was calibrated and verified, as described in the following sections.

3.6.5.2 Ricardo WAVE Combustion Model Calibration

Five test points were used to calibrate the Ricardo WAVE model and the procedure shown in Figure 3-19 was followed in order to perform the calibration.
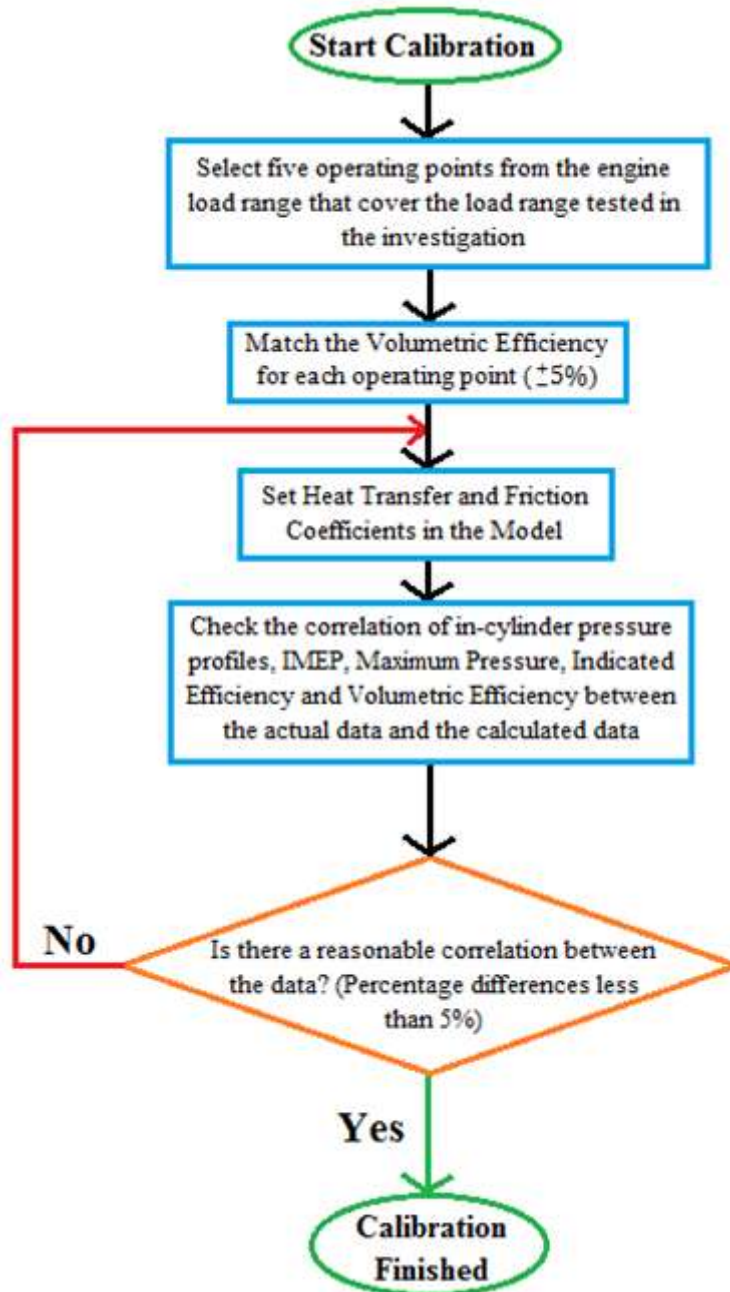
Figure 3-19 Ricardo WAVE model calibration procedure

The valve timings used for the model calibration were IVO=16°bTDC and EVC=36°aTDC, and the IMEPs for the give cases are shown in Table 3-7.

Table 3-7   Test cases for Ricardo WAVE model calibration

	IMEP (bar)
Case 1	3.63
Case 2	4.86
Case 3	6.19
Case 4	7.43
Case 5	8.68

The actual and calculated in-cylinder pressure data is shown in Figures 3-20a, 3-20b, 3-20c, 3-20d and 3-20e for the five respected cases. Overall, there is a good agreement between the data, showing that the model has been calibrated well.

Fig. 3-21a: In-cylinder Pressure (case 1)

Fig. 3-21b: In-cylinder Pressure (case 2)

Fig. 3-21c: In-cylinder Pressure (case 3)

Fig. 3-21d: In-cylinder Pressure (case 4)

Fig. 3-21e: In-cylinder Pressure (case 5)
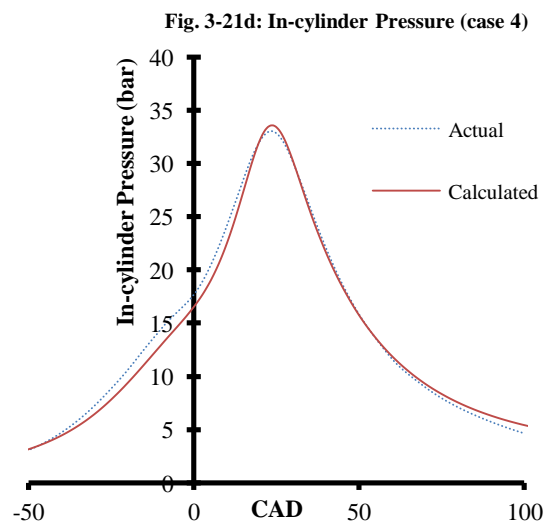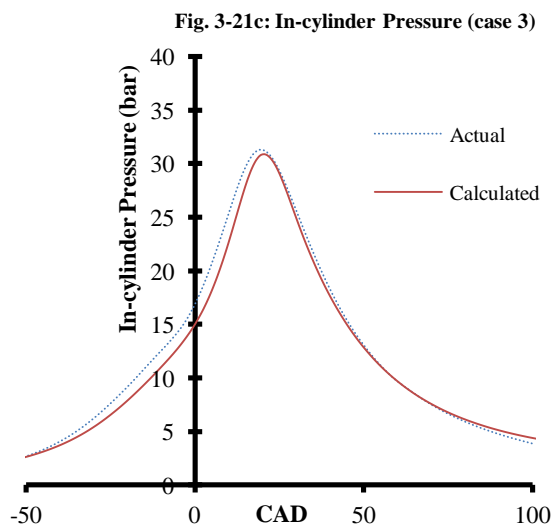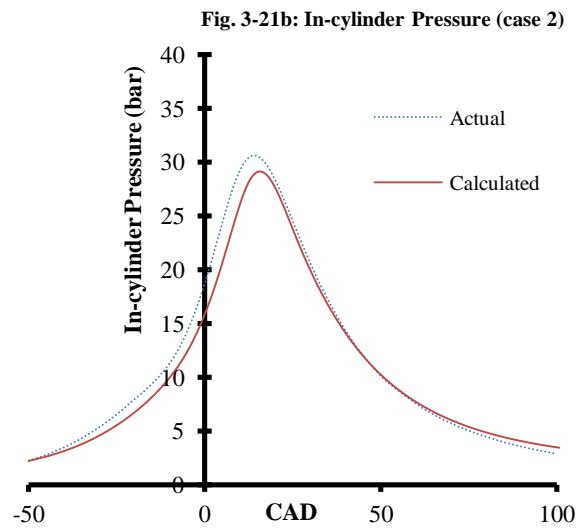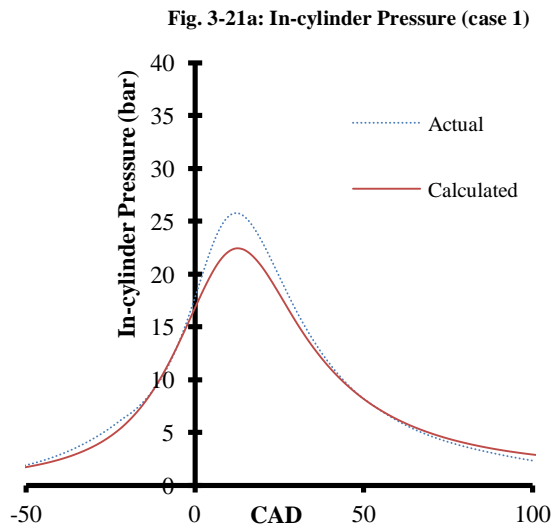
Figure 3-20 In-cylinder pressure versus CAD data comparisons for Ricardo WAVE model calibration: **a)** case 1, **b)** case 2, **c)** case 3, **d)** case 4 and **e)** case 5

The actual and calculated IMEP, P_{max}, indicated efficiency and VE for the five cases are respectively shown in Figures 3-21a, 3-21b, 3-21c and 3-21d.

Fig. 3-22b: IMEP (bar)

Fig. 3-22b: P_{max} (bar)
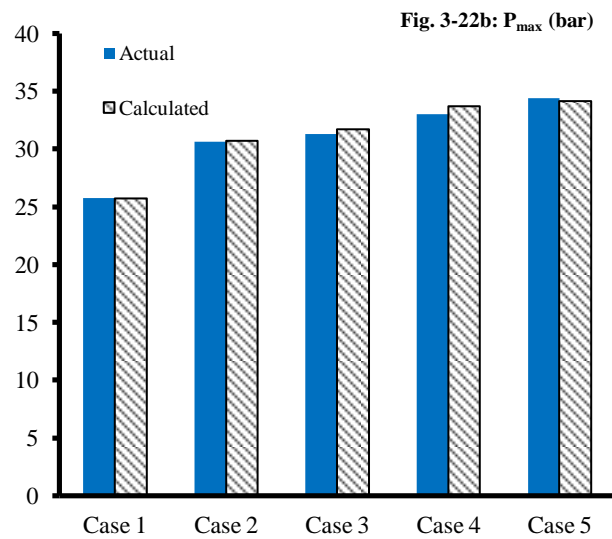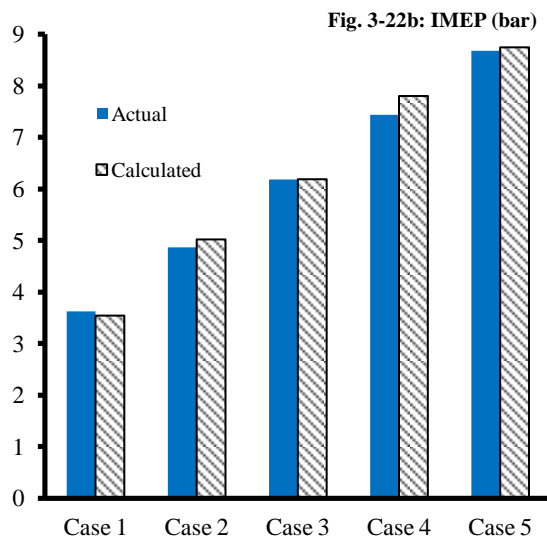
Figure 3-21 Engine data comparison for Ricardo WAVE model calibration: **a)** IMEP (bar), **b)** P_{max} (bar), **c)** indicated efficiency and **d)** VE

The percentage difference for these parameters is shown respectively in Figures 3-22a, 3-22b, 3-22c and 3-22d for IMEP, P_{max}, indicated efficiency and VE. As with the in-cylinder pressure data, there is good agreement, showing that the model has been calibrated well. The confidence intervals have been calculated and analyzed for the parameters above; these show that the random error in the data was very low (less than 0.1% in most cases). Therefore, random error is not thought to have significantly contributed to the differences observed between the actual and calculated data, and because it is so small, it has not been displayed with confidence intervals on the figures.
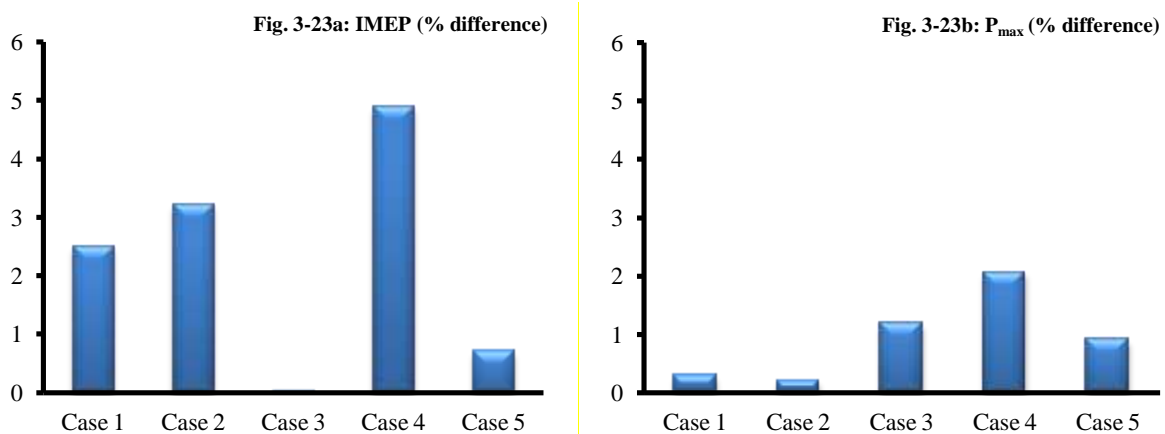
Figure 3-22   Engine data percentage difference comparison for Ricardo WAVE model calibration: **a)** IMEP, **b)** P_{max}, **c)** indicated efficiency and **d)** VE

Overall, the VEs have all been calibrated to within 5% of each other at all of the engine loads, and the other parameters correlate well with each other. Therefore, the calibration steps described in Figure 3-19 have been completed.

3.6.5.3 Ricardo WAVE Combustion Model Verification

Five further test points were used to verify the Ricardo WAVE model. The valve timings used were IVO=6˚aTDC and EVC=61˚aTDC, and the IMEPs for the cases are shown in Table 3-7.

Table 3-8   Test cases for Ricardo WAVE model verification

	IMEP (bar)
Case 1	3.74
Case 2	5.16
Case 3	6.47
Case 4	7.87
Case 5	8.90

The actual and calculated in-cylinder pressure data is shown in Figures 3-23a, 3-23b, 3-23c, 3-23d and 3-23e for the five respected cases. Overall, there is a good agreement between the data, providing sufficient verification for the model.

Fig. 3-24a: In-cylinder Pressure (case 1)
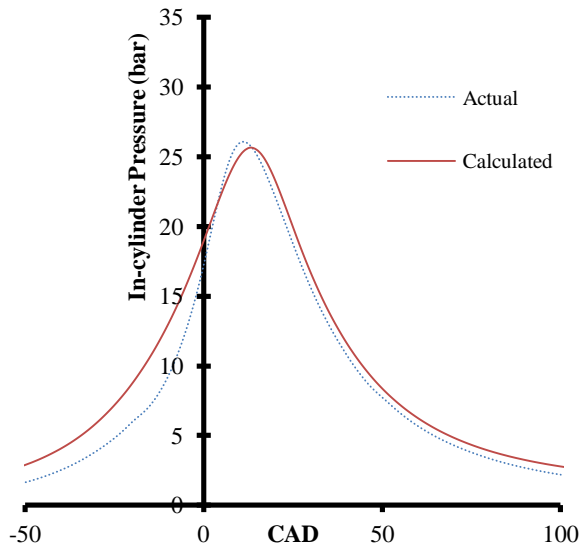
Fig. 3-24b: In-cylinder Pressure (case 2)
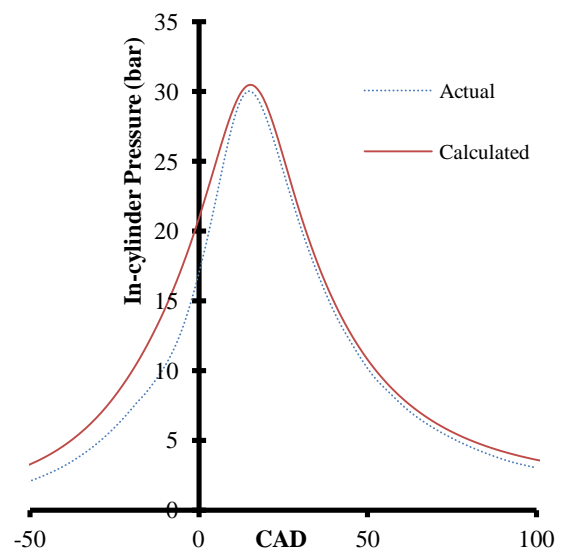
Fig. 3-24c: In-cylinder Pressure (case 3)
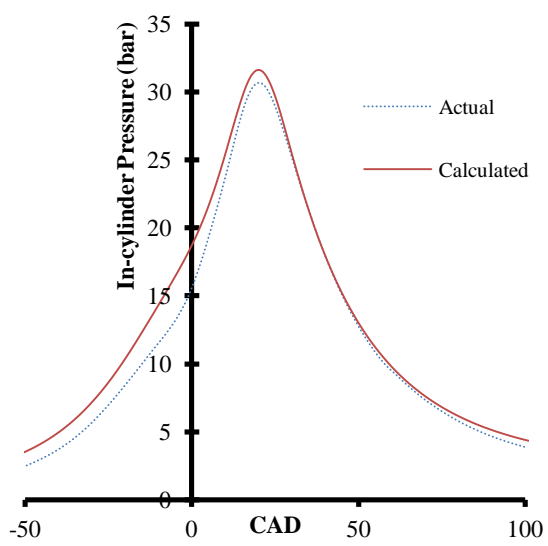
Fig. 3-24d: In-cylinder Pressure (case 4)
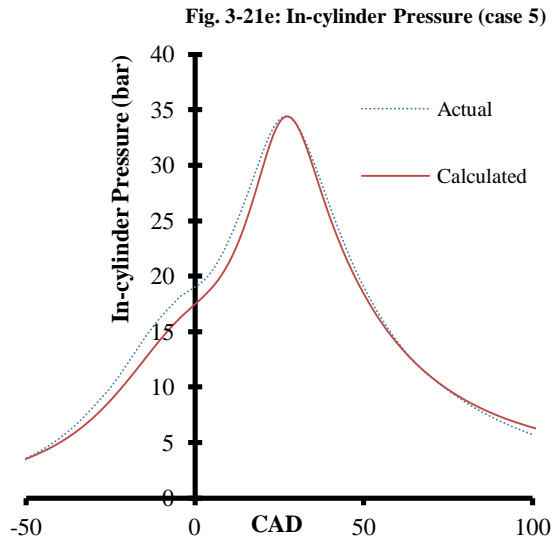
Fig. 3-24e: In-cylinder Pressure (case 5)
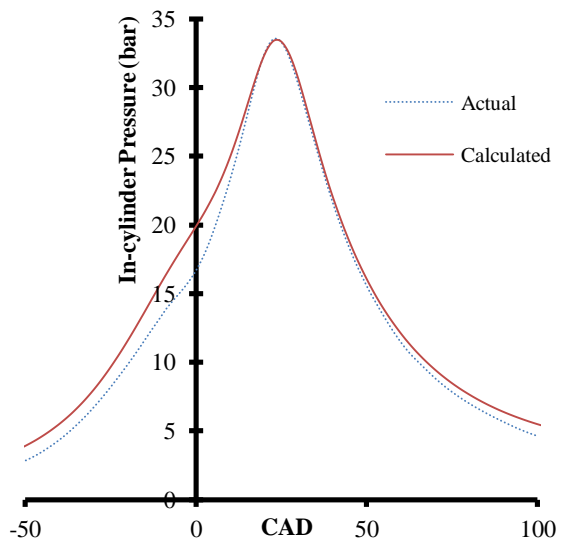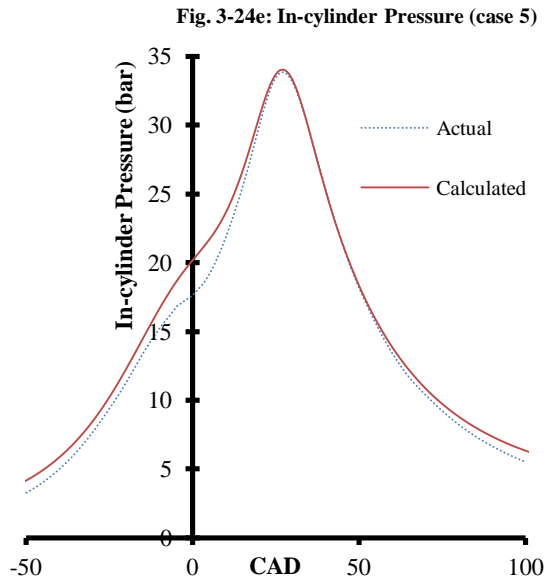
Figure 3-23   In-cylinder pressure versus CAD data comparisons for Ricardo WAVE model verification: **a)** case 1, **b)** case 2, **c)** case 3, **d)** case 4 and **e)** case 5

The actual and calculated IMEP, P_{max}, indicated efficiency and VE for the five cases are respectively shown in Figures 3-24a, 3-24b, 3-24c and 3-24d.
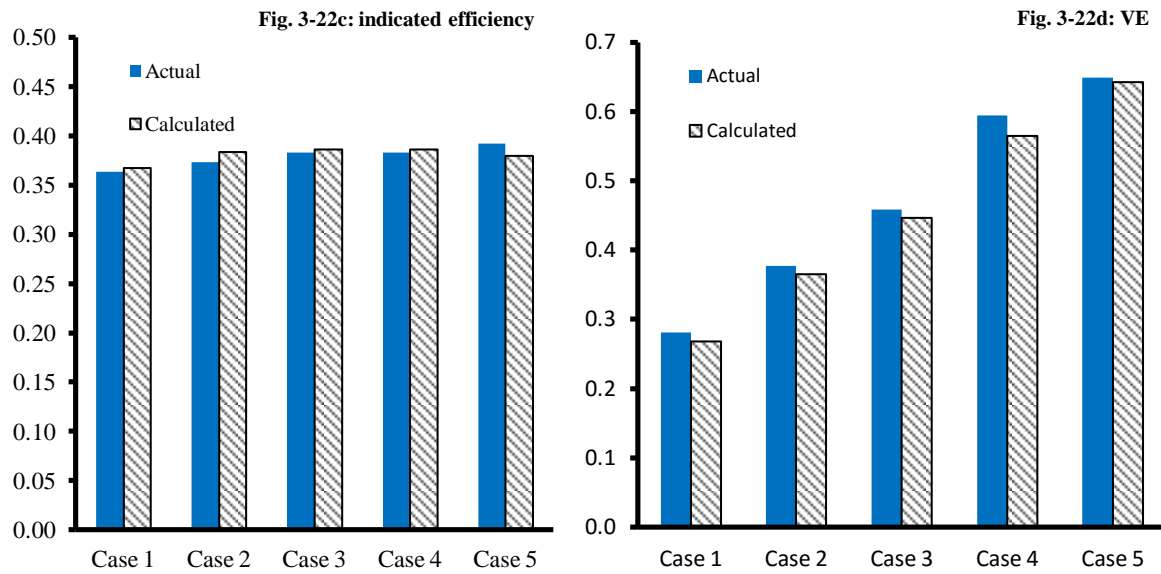

Fig. 3-25a: IMEP (bar)

Fig. 3-25b: P_{max} (bar)
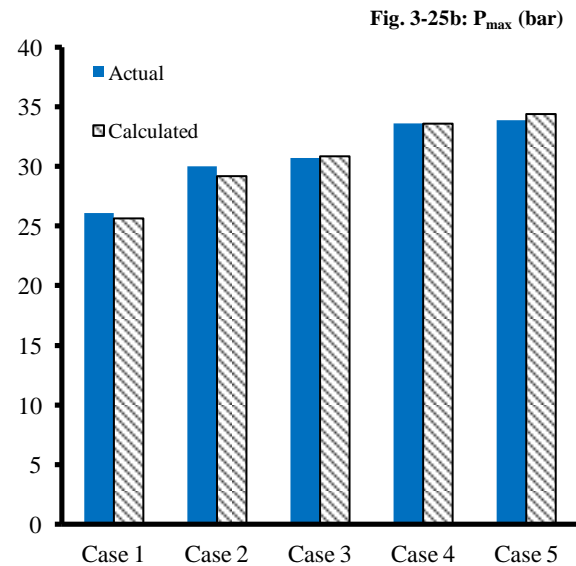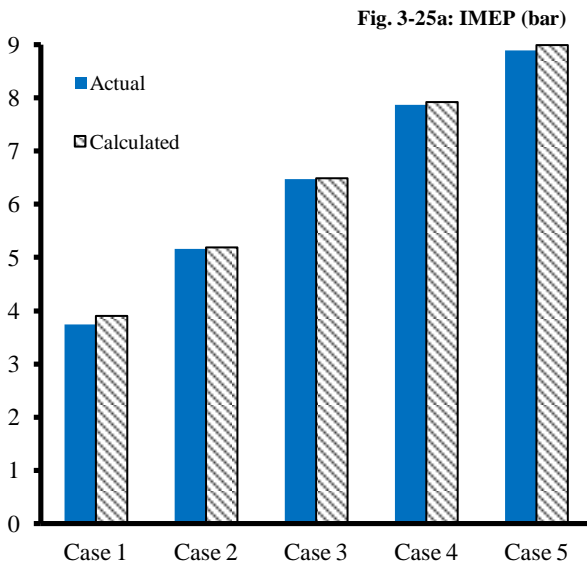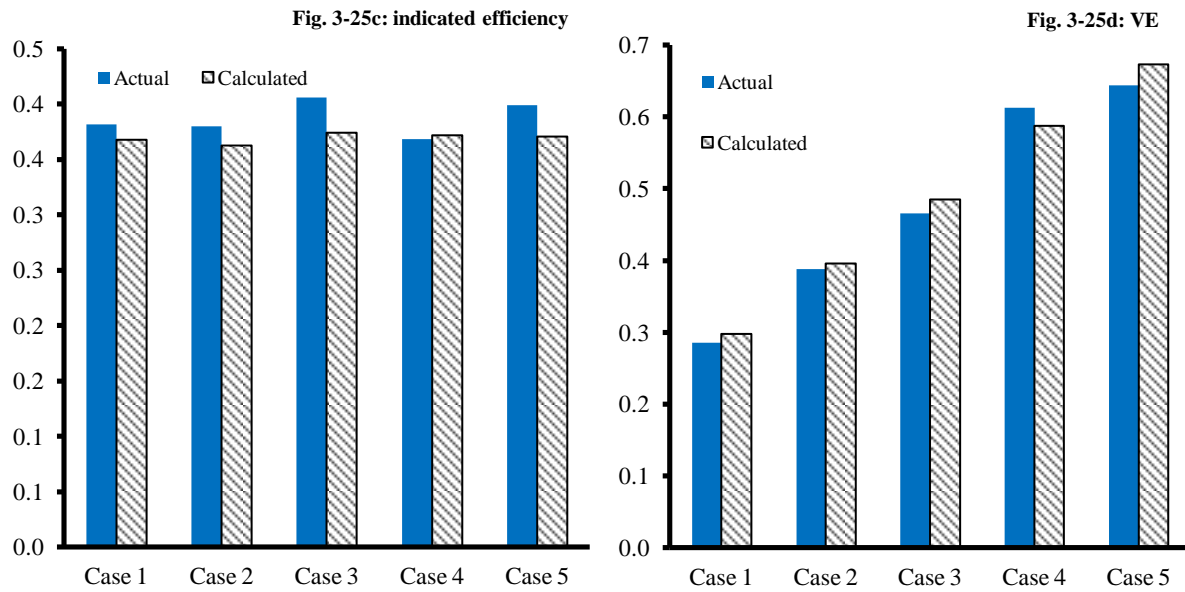
Figure 3-24 Engine data comparison for Ricardo WAVE model verification: **a)** IMEP (bar), **b)** P_{max} (bar), **c)** indicated efficiency and **d)** VE

The percentage difference for these parameters is shown respectively in Figures 3-25a, 3-25b, 3-25c and 3-25d for IMEP, P_{max}, indicated efficiency and VE. As with the in-cylinder pressure data, there is good agreement, showing that the model has been sufficiently verified. However, there is an exception with cases 3 and 5 having a percentage difference larger than 5% for between the actual and calculated indicated efficiencies. Despite this, the difference was still below 10% and the other parameters had a percentage difference less than 5%. Therefore, it is believed that the model has been sufficiently verified.

Again, the confidence intervals have been calculated and analyzed for the parameters above. As with the calibration results, random error was found to be less than 0.1% in most cases. Therefore, random error is not thought to have significantly contributed to the differences observed between the actual and calculated data, and because it is so small, it has not been displayed with confidence intervals on the figures.
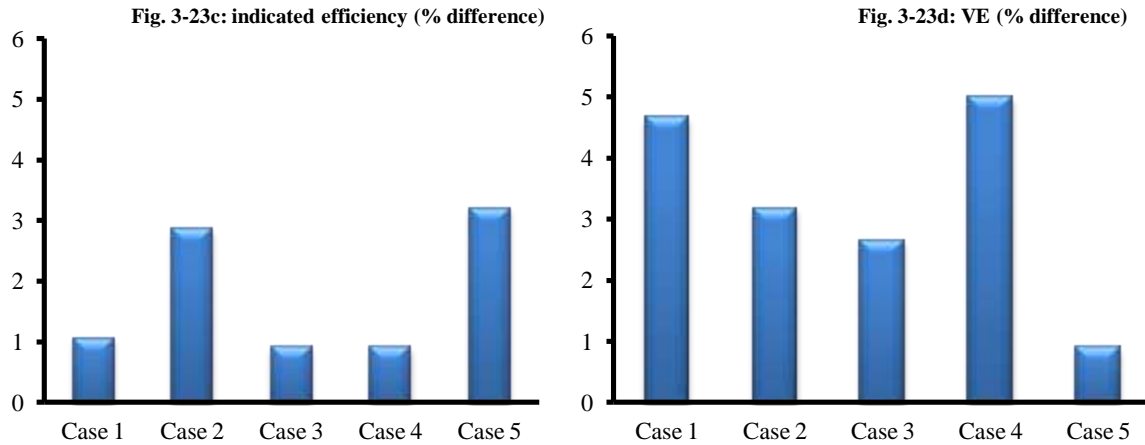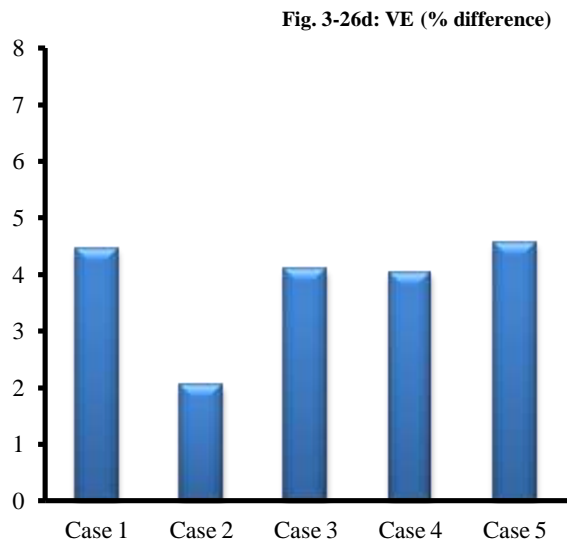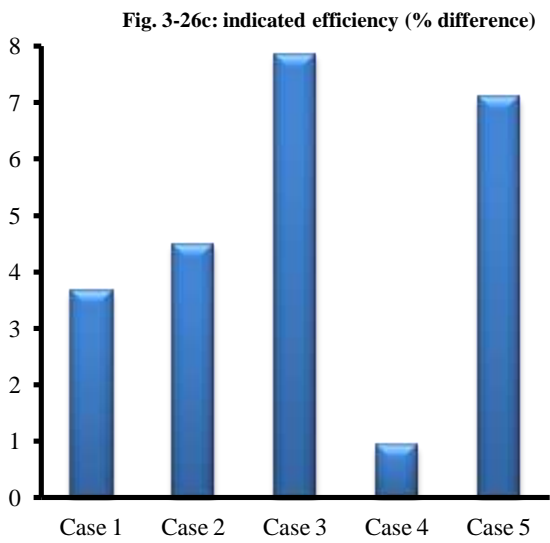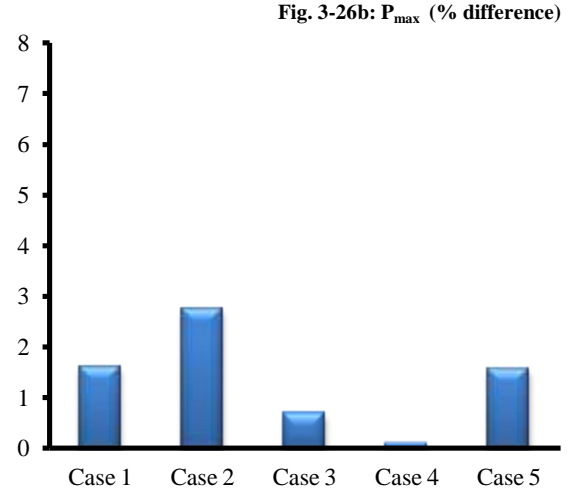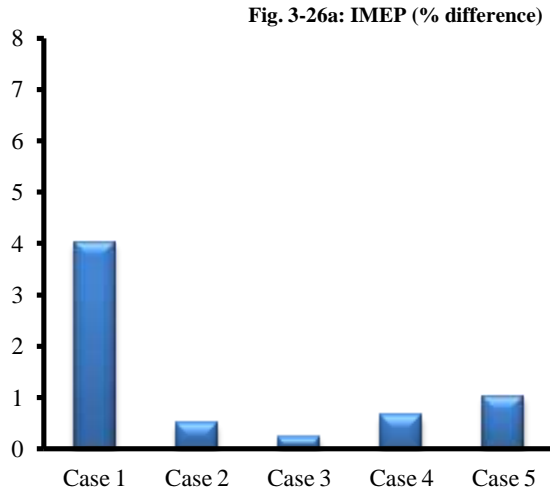
Figure 3-25 Engine data percentage difference comparison for Ricardo WAVE model verification: **a)** IMEP, **b)** P_{max}, **c)** indicated efficiency and **d)** VE

Overall, the VEs have all been verified to within 5% of each other at all of the engine loads, and the other parameters correlate well with each other, therefore, the model has been sufficiently verified for the load conditions (5.5-8.5 bar IMEP) used in this investigation. This will enable it to be used to accurately calculate the average in-cylinder temperatures for the recorded measurements in this investigation. Furthermore, the ability to change the intake air temperature has been utilized in the study of EGR, particularly with hot and cooled EGR, in order to incorporate the effect of the intake air temperature on the average in-cylinder temperatures. Despite the model being accurate, the author acknowledges that more work

could be done in order to improve the accuracy of the modelling, such as creating and developing a detailed 3D engine model.

3.6.6 Heat Release Analysis

The net heat release rate (dQ/dθ) was calculated from the in-cylinder pressure data in order to calculate MFB, using Equation 3-6 (Stone, 1999).

$$\frac{dQ}{d\theta} = \frac{\gamma}{\gamma-1} P \frac{dV}{d\theta} + \frac{1}{\gamma-1} V \frac{dP}{d\theta} + \frac{dQ_w}{d\theta} \qquad (3\text{-}6)$$

where γ (heat capacity ratio) is the ratio of specific heats which is approximated for different parts of the engine cycle, (dV/dθ) is the rate of change of in-cylinder volume with respect to CAD, (dP/dθ) is the rate of change of in-cylinder pressure with respect to CAD and (dQ$_w$/dθ) is the cumulative net heat release rate. The heat release rate was then integrated in order to obtain the MFB, as shown in Equation 3-7 (Stone, 1999).

$$MFB = \frac{\int_{\theta_s}^{\theta_i} \frac{dQ}{d\theta} d\theta}{\int_{\theta_s}^{\theta_e} \frac{dQ}{d\theta} d\theta} \qquad (3\text{-}7)$$

The numerator of the equation is the integral of the net heat release rate between a specified intake crank angle before the combustion process (i.e. CAD at MFB0) and the crank angle of interest (e.g. CAD at MFB50), and the numerator of the equation is the integral of the net heat release rate across the complete combustion window (i.e. between the CAD at MFB0 and MFB100). Key parameters were then obtained from the MFB curve; mainly the MFB50 along with MFB10-90, which are important in the interpretation of the combustion data.

3.6.7 Thermal (Indicated) Efficiency

In order to calculate the indicated efficiency (η) for this study, Equation 3-8 was used (Cengel and Boles, 2007).

$$\eta = \frac{\dot{W}_{net}}{LHV \cdot \dot{m}_{net}} \qquad (3\text{-}8)$$

where $\dot{W}_{net}$ is the net work output from the engine, LHV is the lower heating value of the fuel (assumes that all water from the combustion remains as vapour) and $\dot{m}_{net}$ is the net mass flow rate of fuel into the combustion chamber.

3.6.8 Fuel Consumption

The gravimetric net indicated specific fuel consumption (ISFC$_{net}$) was calculated using the aforementioned VAF readings (converted into a mass flow rate, $\dot{m}_{air}$) and the Lambda value (λ), using Equation 3-9.

$$ISFC = \frac{\dot{m}_{air} \cdot Air/Fuel\ ratio_{stoichiometric} \cdot \lambda}{P_i} \qquad (3\text{-}9)$$

where Air/Fuel ratio$_{stoichiometric}$ is the stoichiometric air/fuel ratio and P_i is the indicated power. The intake temperature was also used to calculate the air density in order to improve the accuracy of the VAF rate reading (converted into $\dot{m}_{air}$), before it was used to calculate the fuel consumption.

3.6.9 Knock Analysis

A MatLab script was developed by the author in order to remove the unwanted noise from the pressure trace, to calculate the knocking amplitude. The script read the pressure data and applied a Butterworth 2nd order type filter to isolate the frequency range of 4-12 kHz, which ensured that the first and second harmonic knocking frequencies from the engine remained after the low and high frequency engine generated signal noise had been removed. It then calculated the knocking amplitude from the amplitude of the filtered pressure trace. This provided the knocking amplitudes from the pressure data, which allowed the KLMBT spark timing to be quantified for each engine condition. The KLMBT was defined as the most

advanced spark timing in which 97% or less of the knock amplitudes were below 2 bar. The maximum acceptable knock amplitude of 2 bar was chosen based on the work of (Mittal et al., 2007). If the maximum brake torque (MBT) was reached before the KLMBT spark timing, then this spark timing was defined as the KLMBT; an asterisk has been added to denote that the spark timing was not knock limited. Using this method of finding the KLMBT spark timing resulted in a variation margin of up to 10% for lower load (5.5 bar IMEP) and 5% for higher load (7.0 and 8.5 bar IMEP) conditions when the spark-timing was adjusted at each testing point for the engine tests in Chapters 4 and 5 of this thesis. It is believed that this should not affect interpretation of the data because the difference made by the margin in load can be neglected.

All of the results in this investigation are reported at the KLMBT spark timings, or at the MBT spark timing if the knock limit was not reached, because these are the optimum engine operating points in order to achieve best fuel consumption and engine power (Zhu et al., 2007). The engine of a vehicle will always be calibrated at the KLMBT/MBT (or at a set spark retard from the KLMBT/MBT) for steady state warm running, if emissions are not a concern, because customers typically purchase a vehicle based on its rated fuel consumption and output power. Therefore, the author considered them to be the most appropriate operating points at which to record the data, in order to maximize the impact of this research.

The HSDAQ LabView program discussed in Section 3.6.1 was later modified by the author, as shown in Figure 3-26, to implement on-line filtering of the pressure trace, in order to quickly identify the KLMBT spark timing before the engine data was recorded. This enabled the tests in Chapter 6 of this thesis to be completed in a significantly shorter time than the method described in the previous paragraph. It also enabled the discussed load variation to be eliminated.
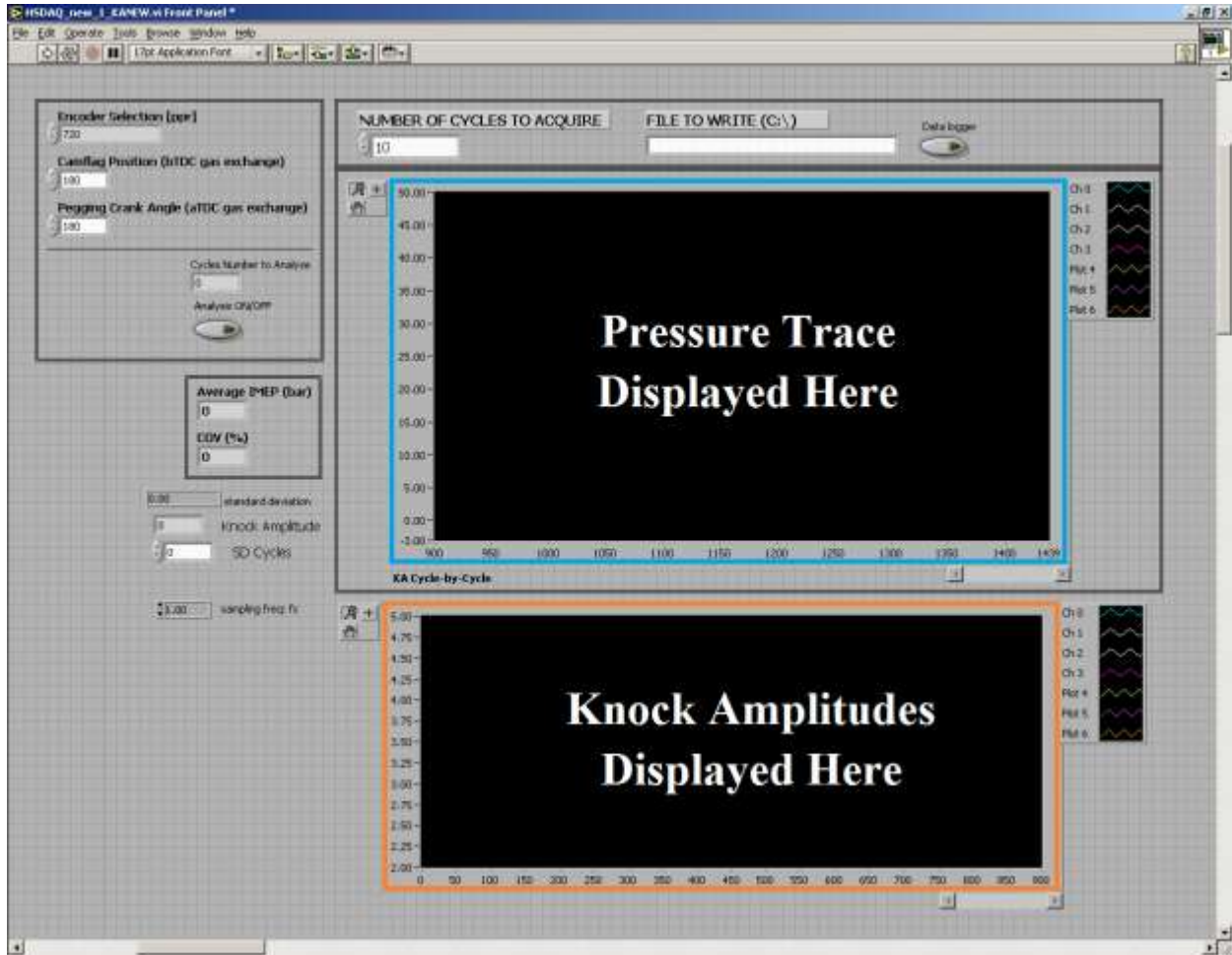
Figure 3-26   Modified HSDAQ LabView program displaying the on-line knock amplitudes

3.6.10 Gravimetric Gaseous Emissions Analysis

In order to calculate the indicated specific emissions (g/kWh) for this study, Equation 3-10 was used (Heywood, 1988).

$$is_{Emission} = \rho_{Emission} \cdot Emission_{ppm} \cdot \frac{\dot{V}_{exhaust}}{P_i} \qquad (3\text{-}10)$$

where $\rho_{emission}$ represents the density of the gaseous emission, $Emission_{ppm}$ is the reading of the emission from the Horiba system which was recorded by the data acquisition system, $\dot{V}_{exhaust}$ is the volumetric flow rate of the exhaust stream and P_i is the indicated power.

The molar mass of the exhaust stream was calculated based on the fraction of each component (NO_x, HC, CO, CO_2, N_2) and it was subsequently used to calculate the density of the emission ($\rho_{emission}$) using Equation 3-11.

$$\rho_{Emission} = P \cdot \frac{M_{Emission}}{R \cdot T} \qquad (3\text{-}11)$$

where $M_{Emission}$ represents the molar mass of the emission (e.g. NO), P and T are the exhaust stream pressure and temperature, respectively, and R is the gas constant. The calculation was conducted separately for the NO_x and HC emissions to provide the data presented in the thesis.

3.6.11 Confidence Intervals

For the data presented in this thesis, the averaged data from the 3 readings for each measurement was plotted along with the 95% confidence intervals, where appropriate, in order to enable the significant effects on the data to be identified. The confidence intervals were calculated using Equation 3-12.

$$CI = \bar{x} \overset{+}{_{-}} Z_{\alpha/2} \cdot \frac{\sigma}{\sqrt{n}} \quad (3\text{-}12)$$

where CI = confidence interval, $\bar{x}$ = mean, $Z_{\alpha/2}$ = factor based on the desired confidence interval of 95%, which is 1.96, σ = standard deviation and n = sample size.

These confidence intervals only address the random errors that occur in the measurements; system errors are not included. However, these are discussed further in the following section.

3.7 Analysis of the Uncertainties in the Recorded Data

For a detailed analysis of the analysis of the uncertainties in the data recorded for this thesis, please refer to **Appendix A1**.

3.8 Fuel Properties

The properties of the fuels used in this investigation are shown in Table 3-9. Both gasoline and ethanol were supplied by Shell Global Solutions, UK. The 1-butanol and heptane were supplied by Fisher Scientific UK Ltd at a purity of 99.5%.

Table 3-9   Test Fuel Properties

	ULG95	1-Butanol	Ethanol	Bu20	E20
Chemical Formula	C_2-C_{14}	$C_4H_{10}O$	C_2H_6O	C_2-C_{14}	C_2-C_{14}
H/C Ratio	1.922	2.5	3	2.038	2.084
O/C Ratio	0.021	0.25	0.5	0.067	0.093
Gravimetric oxygen content (%)	2.36	21.6	34.78	6.21	8.84
Density @ 20˚C (kg/m^3)	743.9	811	790.9	757.3	753.3
RON	95	98	106	-	102[1,2]
Stoichiometric air–fuel ratio	14.15	11.2	8.95	13.71	13.78
LHV (MJ/kg)	42.22	32.71	26.9[3]	39.73	37.76
Heat of Vaporization $\Delta_{vap}H$ (25˚C) (KJ/mol)	~37.3[4]	52.0[5]	42.3[6]	34.6	34.6
Initial boiling point (˚C)	34.6	118	78.4	-	-

[1] (Anderson et al., 2012a)
[2] (Foong et al., 2014)
[3] Measured at the University of Birmingham.
[4] (Balabin et al., 2007)
[5] (National Institute of Standards and Technology, 2011a)
[6] (National Institute of Standards and Technology, 2011b)

Overall, the properties of the gasoline used represent the majority of gasoline fuel sold in Europe and America, making it suitable for this investigation. Although a commercial gasoline fuel was used for part of this investigation (first part of Chapter 4), it matched the RON and ethanol content of the ULG95 fuel used in the remainder of the investigation, so it is assumed that the fuel specification did not vary significantly from the one shown in the table. Oxygenate content is thought to have varied, however, based on the results observed and this is discussed further in a later section. The gravimetric content (GC) analysis of the fuel is shown in Table 3-10.

Table 3-10   Gasoline GC Analysis

Component	% volume
Paraffin	43.9
Olefin	11.7
Naphthene	6.2
Naphthene,	1.6
Polynaphthene	<0.1
Aromatics	26.9
Saturated C11+Hydrocarbons	2.0
Oxygen Compounds	7.7
Saturated Hydrocarbons	50.1
Unsaturated Hydrocarbons	13.3

3.9 Experimental Test Procedures

Before any experimental data was collected for the engine tests, a baseline test was conducted to ensure that the data recorded from the engine was approximately the same as a previously recorded accurate baseline. If there was a significant variation between the two then the cause was identified and resolved before the baseline test was repeated. The procedure was repeated until the engine results on a particular day conformed to the previously determined baseline conditions. Before recording data, the engine cylinder block was warmed to 95˚C as measured by a thermocouple embedded 5 mm inside the block, to ensure consistent knock behaviour. Once the engine was recording reliable data, the test point was conducted and it was repeated several times until 3 consistent sets of data were recorded, in order to ensure that the data recorded was an accurate representation of the engine combustion and emissions and to reduce the impact of day-to-day fluctuations on the results. This was then repeated to collect all of the test points, which were required on a particular day.

3.10 Summary

Overall, this chapter has described the experimental test facilities used in this work. All of the tests were conducted in a 4-stroke spray-guided DISI single-cylinder thermal engine. The engine is typical of modern, while not state of the art, gasoline DISI engines. Finally, the data collection and analysis procedures were discussed.

Although the author benefitted from the engine setup created and developed by the various previous research students at the University, several important improvements were made in order to further develop and improve the setup. Firstly, the connection of the gasoline fuel line directly to the fuel tank along with the incorporation of a three-way valve in the PFI fuel line, in order to fill the DI accumulator directly from the gasoline fuel tank, improved safety in the engine test cell and made fuel refilling easier. Secondly, the connection of the fuel tank, previously used to fill up the DI system, to the main gasoline fuel tank, allowed residue fuel from the DI system to be easily pumped out of the tank. This greatly minimized fuel vapours from entering the atmosphere when the DI system was subsequently purged into the tank. Thirdly, the creation of separate fuel tank for non-gasoline fuels made it easier to prevent contamination of the gasoline and non-gasoline fuels. Finally, interference between signal lines for the VVT system and water temperature control system were eliminated. Previously when the mains water control valve was triggered open to cool the engine, the VVT control system was sometimes affected, causing the valve timings to reset, meaning measurements had to be repeated regularly. These modifications are in addition to three engine rebuilds, VAF meter calibrations and ongoing work to maintain the engine test facility.

Chapter 4

The Effect of EGR and its Type on Engine Combustion and Emissions

The aim of this chapter is to provide details of the combustion and emissions characteristics of a DISI engine operated with EGR addition at different engine loads of 5.5, 7.0 and 8.5 bar IMEP, and with different EGR types of hot EGR, cooled EGR, hot EGR after TWC and cooled EGR after TWC at a single engine load of 7.0 bar IMEP.

4.1 Introduction

The main combustion parameters investigated in this chapter are the KLMBT spark timing, in-cylinder pressure, calculated average in-cylinder temperature, MFB, fuel consumption and EGT. PM, NO_x and HC are the main emission parameters investigated.

There is an ever growing demand for reduction of NO_x emissions from engines and for improvements in fuel economy, as emissions regulations become stricter and CO_2 emissions are at the forefront of public perception. One way to achieve these demands is to use external EGR in engines to suppress the temperature rise in the combustion chamber, reducing NO_x emissions and allowing the KLMBT spark timing to be advanced, as well as enabling the throttle to be more opened, providing significant fuel economy benefits. Furthermore the Euro VI emissions regulations which limit PN for the first time have increased interest in the effect of EGR addition on engine particulates, with the potential of EGR coming under question because it has been shown to have a negative effect on particulates (Gill et al., 2011, Ma et al., 2014).

Overall, the author recognizes that the Euro VI emissions regulations have led many to question the potential of EGR, noting that it is generally considered to increase engine

particulates. Thus, this is an area that has been researched further in this chapter. There is also a lack of work regarding the effect of different types of EGR (hot EGR, cooled EGR, hot EGR after TWC, and cooled EGR after TWC) on engine combustion and gaseous emissions, on the same engine at the same load condition, thus, this was also investigated further in this chapter.

4.2 Experimental Procedure

The experimental test procedure outlined in Section 3.9 of this thesis was followed in order to conduct the engine tests, to collect the data presented and discussed in this chapter. Relative air-fuel ratio λ was maintained at 1 during the experiments and a COV_{IMEP} of 5% was not exceeded. Valve timings were set at IVO=16˚bTDC, EVC=36˚aTDC. KLMBT spark timings and a fixed geometric compression ratio of 11.5 were used. In order to achieve EGR in the engine, and in order to achieve the desired engine load and EGR condition, the equipment setup and test procedure outlined in Section 3.2.6.1 was followed for the hot EGR condition, and those outlined in Sections 3.2.6.2, 3.2.6.3 and 3.2.6.4 were followed for the cooled EGR, hot EGR after TWC and cooled EGR after TWC conditions, respectively.

The load range of 5.5-8.5 bar IMEP was chosen to study in the first part of this chapter because it represents the medium-high load range of this engine where EGR should be of most benefit to reduce engine knock, thus making the results more useful. In addition, the use of DI in the engine is most relevant to this load range for knock suppression; at lower loads the reduced in-cylinder pressure prior to ignition resulting from the charge cooling is not necessary and it reduces indicated efficiency. Furthermore, in a real engine, a DI fuel pump will consume more energy than a PFI fuel pump. Therefore, there must be a fuel consumption benefit of using DI; i.e. charge cooling, in order to compensate for the additional energy the DI pump would consume. The load of 7.0 bar IMEP was chosen to study in the second part of

this chapter because allowed a reasonable, while not a high EGR addition of 14% to be achieved. A higher engine load would have meant that the throttle would have needed to be more opened, thus reducing the maximum level of EGR that would have been achieved. One load was chosen to study so that an in-depth understanding could be formed, which would not have been possible if multiple loads were studied with the multiple EGR types.

The spark was swept for all engine loads and all EGR types in order to find the KLMBT spark timing using the technique outlined in Section 3.6.9, or by using the torque calculated from the engine data if the MBT was reached before the knock limit. A mixture of pump and research grade gasoline was used in this research with the properties outlined in Section 3.8. The pump grade gasoline was used in the experiments for the first part of this chapter and the research grade gasoline was used in the experiments for the second part of this chapter. The pump grade gasoline specification did not differ significantly from the research grade gasoline specification; the RON and ethanol content were the same. Therefore, it is believed that the use of both gasoline types did not significantly affect the interpretation of the results. Oxygenate content is thought to have varied, however, based on the results observed and this is discussed further in a later section. The DMS 500 was used to measure the PM emission and the Horiba MEXA-7100DEGR was used to measure the gaseous emissions of NO_x and HC. PM was not measured in the second part of this chapter because of limited equipment availability.

The test matrix provided in Table 4-1 was carried out in order to investigate the effect of hot EGR at different engine loads on the engine combustion and emissions. **The results and discussion of these tests can also be found in (Lattimore, 2016a).**

Table 4-1   Experiment test matrix (EGR addition & engine load)

EGR Addition (%) / IMEP (bar)	0	2	3	4	8	12	13
5.5	1		2	3	4	5	
7.0	6		7	8	9		
8.5	10	11	12				

The test matrix provided in Table 4-2 was carried out in order to investigate the effect of different EGR types on the engine combustion and gaseous emissions at the single load of 7.0 bar IMEP.

Table 4-2   Experiment test matrix (EGR addition & EGR type)

EGR Addition (%) / EGR Type	0	7	10	14
Hot EGR	1	2		3
Cooled EGR		4	5	
Hot EGR after TWC		6		7
Cooled EGR after TWC		8		9

4.3 Results and Discussion

4.3.1 Hot EGR Effect on Combustion and Emissions in a DISI Engine

4.3.1.1 KLMBT Spark Timing

The KLMBT spark timings for the tested engine conditions are presented in Table 4-3. EGR enabled the spark to be advanced significantly, through the suppression of temperature rises in the end-zone. It can be seen in Figures 4-2a, 4-2b and 4-2c that EGR addition led to calculated average in-cylinder temperature reductions even with spark advances for the engine loads tested. However, the spark advances did enable the combustion temperature reducing effect of EGR to be mitigated, as can be most clearly seen in Figure 4-2b for the engine load of 7.0 bar IMEP. It must be noted that knocking could have been avoided if the compression ratio was fully optimized for the fuel used. However, this was not pursued in

order to investigate the effect of the parameter changes on engine knock limit and the consequent combustion and emissions at this limit.

For the load of 5.5 bar IMEP, the spark timings were not knock limited due to the low combustion pressure and temperature as shown in Figures 4-1a and 4-2a respectively, allowing them to be advanced by 12 CAD to maintain their optimum MBT phase across the 0 to 8% EGR range. However, the laminar flame speed reducing effects of EGR (Rhodes and Keck, 1985) resulted in the combustion phasing becoming retarded from the optimum with further EGR additions of 12 and 13% (Figure 4-3a), despite the further 6 CAD spark advance that was implemented.

The spark timings at the other engine loads however were knock-limited so they could only be advanced by 8 and 4 CAD respectively for the engine loads of 7.0 and 8.5 bar IMEP. EGR was limited to 3% for the engine load of 8.5 bar IMEP because the throttle valve was more open (~15° throttle angle) compared to the other engine loads where the throttle valve was more closed (~7° at 7.0 bar IMEP, ~5° at 5.5 bar IMEP), which increased the intake manifold pressure and subsequently reduced the pressure difference between the exhaust and the intake. This meant that the EGR gas flow rate in the EGR line was reduced, which reduced the EGR ratio compared to the other engine loads. The relatively small throttle angles resulted from the oversized throttle; it was designed for a 3.0 litre engine, meaning that it did not need to be opened fully in order to achieve the maximum engine load, as the case would have been with a smaller throttle valve. Despite the limited EGR that was achieved at the highest considered load, it was still important to study this engine load to quantify what improvements could be made with the limited EGR available. This condition is used to represent the high-end load of this engine. The highest load of ~9.5 bar IMEP which can be

achieved with this engine was not pursued because no EGR addition can be achieved at this condition, because the engine is operating at WOT.

It is anticipated that the KLMBT spark timing advances would have been greater for the engine loads of 7.0 and 8.5 bar IMEP if the intake manifold temperature increases resulting from the EGR addition could have been eliminated. This is because the lower intake temperature would have decreased the engine knock tendency. For 5.5 bar IMEP, the flame would be expected to travel slower in the cooler fuel-air mixture resulting from the cooler intake manifold, thus necessitating greater MBT spark timing advances to attempt to maintain the optimum combustion phasing.

Table 4-3   KLMBT spark timings (˚bTDC) (* = not knock limited) (EGR addition & engine load)

EGR Addition (%) IMEP (bar)	0	2	3	4	8	12	13
5.5	27*			33*	39*	45*	45*
7.0	14			14	18	22	
8.5	10	12	14				

4.3.1.2   In-cylinder Pressures and Temperatures

The in-cylinder pressures for the engine load of 5.5 bar IMEP are presented in Figure 4-1a. They show that in-cylinder pressure reduced as the EGR addition increased. This is because the EGR gases had a higher heat capacity than fresh air and the flame travelled at a slower speed (Rhodes and Keck, 1985), reducing the temperature and subsequent pressure rises in the combustion chamber, causing the overall in-cylinder pressures to reduce. In addition, there was up to a 10% load variation at the lower engine loads when the spark-timing was adjusted at each testing point, as discussed, accounting for some of the observed in-cylinder

pressure reduction as EGR was increased; IMEP reduced by 0.15 bar across the EGR range at the engine load of 5.5 bar IMEP.

The in-cylinder pressures for the load of 7.0 bar IMEP in Figure 4-1b show a different behaviour to those at 5.5 bar IMEP, with slight increases observed, despite similar ratios of EGR being achieved. This occurred because the spark timings for the engine load of 5.5 bar IMEP were not knock limited, however, at 7.0 bar IMEP they were. Therefore, the spark timings at 5.5 bar IMEP could always be advanced to attempt to continue delivering their optimum MFB50 phase of 8-10°aTDC, which resulted in the optimum in-cylinder pressure and temperature at the 0% EGR condition (optimum balance between compression and expansion work produced on the piston). With the EGR addition, the combustion became slower, and this could not be compensated for by advancing the MFB50. This meant that the EGR addition resulted in the overall combustion pressures being reduced. The spark timing at 7.0 bar IMEP however, being knock limited, could always be advanced towards its optimum MFB50 phasing with EGR addition, causing the in-cylinder pressure to be maintained and even increased slightly. Despite this, it appears that the average in-cylinder temperature could not be maintained causing it to reduce across the EGR range as shown in Figure 4-2b.

Similar in-cylinder pressure behaviour was observed at the engine load of 8.5 bar IMEP in Figure 4-1c along with similar in-cylinder temperature decreases across the EGR range as shown in Figure 4-2c. Therefore, it is again concluded, as with 7.0 bar IMEP, that although the KLMBT spark timings advances (towards their optimum MFB50 phasing) were not sufficient to maintain or increase the average in-cylinder temperature, they were sufficient to increase the in-cylinder pressures. Thus, EGR addition appears to reduce the calculated average in-cylinder temperature more than it reduces in-cylinder pressures.

At 5.5 bar IMEP, the in-cylinder pressure increases would likely have been reduced, due to the lower intake temperatures, if the intake manifold temperature increases could have been eliminated. It would be anticipated that the in-cylinder pressure increases would have been greater for the engine loads of 7.0 and 8.5 bar IMEP if the intake manifold temperature increases resulting from the EGR addition could have been eliminated. This is because the KLMBT spark timing advances would have been greater, as discussed.

Fig. 4-1a: In-cylinder Pressure (5.5 bar)

Fig. 4-1b: In-cylinder Pressure (7.0 bar)
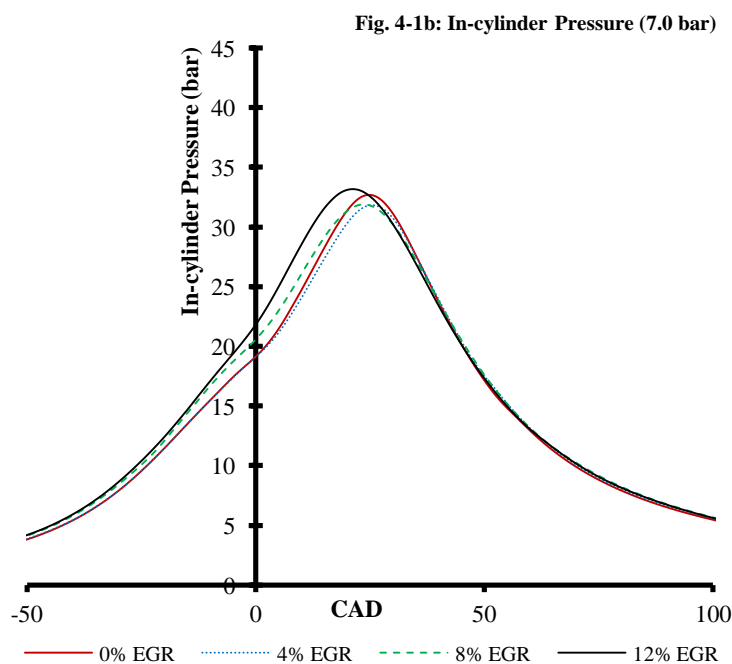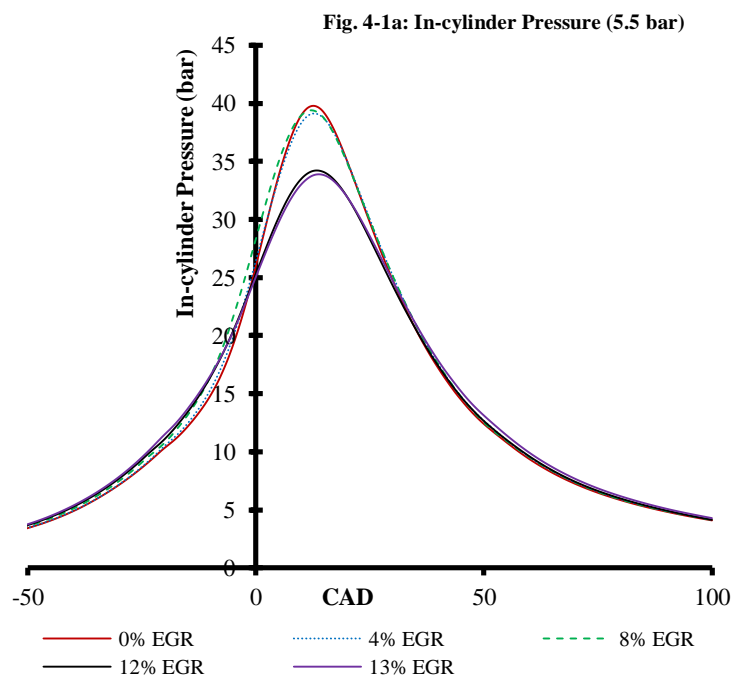
Figure 4-1 In-cylinder pressures versus CAD at KLMBT spark timings for **a)** 5.5 bar IMEP, **b)** 7.0 bar IMEP and **c)** 8.5 bar IMEP

The calculated average in-cylinder temperatures decreased across the EGR range for the three tested engine loads of 5.5, 7.0 and 8.5 bar IMEP, as shown in Figures 4-2a, 4-2b and 4-2c. As explained, despite the in-cylinder pressures increasing across the EGR range for the engine loads of 7.0 and 8.5 bar IMEP, the calculated average in-cylinder temperatures decreased, as they did at 5.5 bar IMEP (where in-cylinder pressure decreased across the EGR range), due to the temperature suppression effect of the EGR gases, resulting from their higher heat capacity as compared to that of fresh air.

At 5.5 bar IMEP, it would be expected that the in-cylinder temperature decreases would have been greater if the intake manifold temperature increases could have been eliminated, due to the lower intake gas temperature. However, for the engine loads of 7.0 and 8.5 bar IMEP it is believed that the increased intake manifold temperatures resulting from the EGR addition were compensated for by the less optimized combustion phasing resulting from the

consequent reduced KLMBT spark timing advance, compared to the maximum spark advance possible. This was a result of those higher intake manifold temperatures; lower temperatures would have enabled a greater spark advance before significant levels of knock occurred. The gas temperature during the intake stroke would have been reduced slightly, if the intake manifold temperature increases could have been eliminated. However, it is thought that the improved KLMBT spark timing would have quickly compensated for the decrease by the time temperatures reached the beginning of the range reported (500˚C), due to the combustion happening in a smaller volume; thus, the effect would have been minimal.

Fig. 4-2a: In-cylinder Temperature (5.5 bar)

Fig. 4-2b: In-cylinder Temperature (7.0 bar)

Fig. 4-2c: In-cylinder Temperature (8.5 bar)

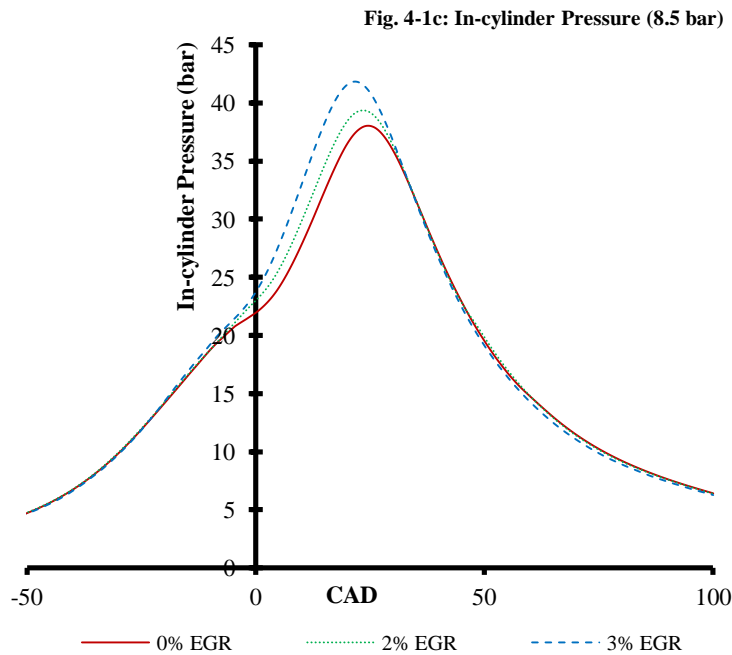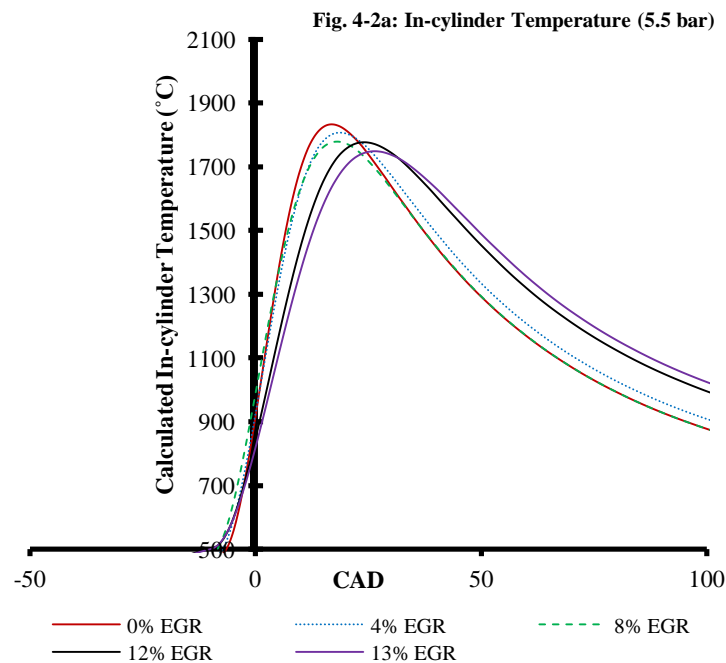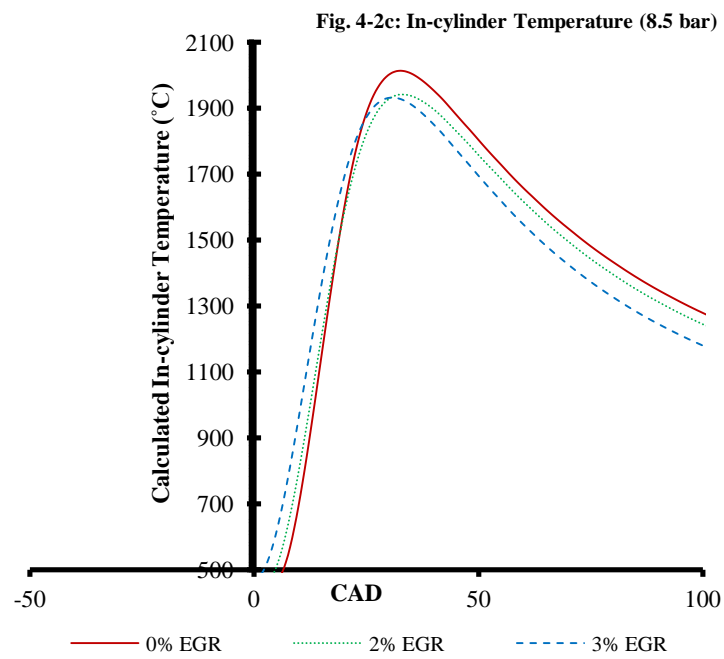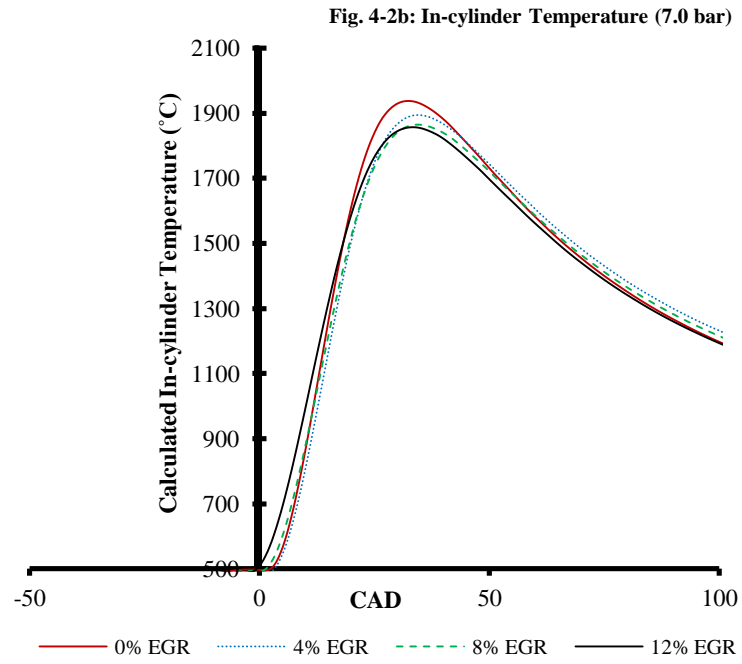**Figure 4-2**   Calculated average in-cylinder temperatures versus CAD at KLMBT spark timings for **a)** 5.5 bar IMEP, **b)** 7.0 bar IMEP and **c)** 8.5 bar IMEP

4.3.1.3 MFB

From Figure 4-3a it can be seen that the MFB profile for the engine load of 5.5 bar IMEP became smoother and elongated with EGR addition, as the laminar flame speed was reduced by the EGR addition (Rhodes and Keck, 1985), increasing the combustion duration. This decreased the rate at which the fuel was burned, resulting in the observed behaviour. This is reflected in the calculated average in-cylinder temperature data discussed in the previous section which showed that the overall combustion temperatures reduced with EGR addition, not only at 5.5 bar IMEP, but at the other engine loads too. If the compression ratio was optimised for the fuel used, the combustion phasing would have been optimised for each test point. Therefore, it would be expected that the combustion of gasoline would have been quicker at the knock limited spark timings due to higher in-cylinder turbulence at the time of ignition.

The MFB for the load of 7.0 bar IMEP, as shown in Figure 4-3b, followed the same trend as that for 5.5 bar IMEP between the EGR ratios of 0 and 4%; the profile became smoother and elongated, as the combustion duration was increased. However, the MFB profile for the EGR ratio of 8% became more like that observed at 0% EGR, and the combustion duration became slightly longer. Despite this, the differences between the MFB data at the EGR additions of 4 and 8% are likely due to experimental uncertainties. The KLMBT spark timing was advanced by 4 CAD between the EGR ratios of 8 and 12% resulting in the combustion beginning earlier, allowing a more advanced MFB profile to be achieved as compared to that observed at 0 and 8% EGR addition. However, the profile became more elongated because the slower flame speed reduced the rate at which the fuel was burned. These results suggest that the KLMBT spark timing advance achieved with EGR addition at 7.0 bar IMEP was more able to overcome the reduced laminar flame speed caused by the EGR addition, but at 5.5 bar IMEP, the spark advance was less able to overcome it. Overall, the gradients were much more

consistent for 7.0 bar IMEP (Figure 4-3b) as compared to 5.5 bar IMEP (Figure 4-3a) because of this.

The MFB data in Figure 4-3c for the load of 8.5 bar IMEP showed a similar trend to the data at 7.0 bar IMEP after the initial EGR addition and spark advance. However, as the spark was advanced further with more EGR addition, the MFB profile became significantly advanced suggesting that the increased spark advance at 3% EGR was better able to overcome the combustion slowing effects of the EGR gases than was the case with the spark advance achieved at 2% EGR.

Taking the MFB data for the three engine loads into consideration, the KLMBT spark advances achieved with EGR addition could overcome the resulting slower flame speeds in some cases, but in other cases, the advances were not sufficient, causing the MFB profiles to become smoother and more elongated. This may be further related to the observed improvements in fuel economy and the reduction in EGT, along with the engine emissions; all of which will be discussed further in the following sections. Overall, these relationships should be studied further to find an optimized MFB for gasoline combustion.

For 5.5 bar IMEP, the MFB profile would be expected to become more elongated if the intake manifold temperature increases resulting from the EGR addition could have been eliminated, due to the slower flame speed in the cooler fuel-air charge. This would be expected to occur at the other engine loads too, but much less significantly, because the temperature decreases with the cooler intake gases would be expected to be quickly cancelled out by the effect of the greater KLMBT spark timing advances, as discussed. Furthermore, the MFB profile for 5.5 bar IMEP between the EGR ratios of 0 and 8% would not become more advanced or retarded, because the optimum combustion phasing would be expected to

be maintained. However, it would still be expected to become retarded at the EGR additions of 12 and 13%. It would be anticipated that the MFB profile advances would have been greater for the engine loads of 7.0 and 8.5 bar IMEP. This is because the KLMBT spark timing advances would have been greater, as discussed.

Fig. 4-3a: MFB (5.5 bar)

Fig. 4-3b: MFB (7.0 bar)

Fig. 4-3c: MFB (8.5 bar)
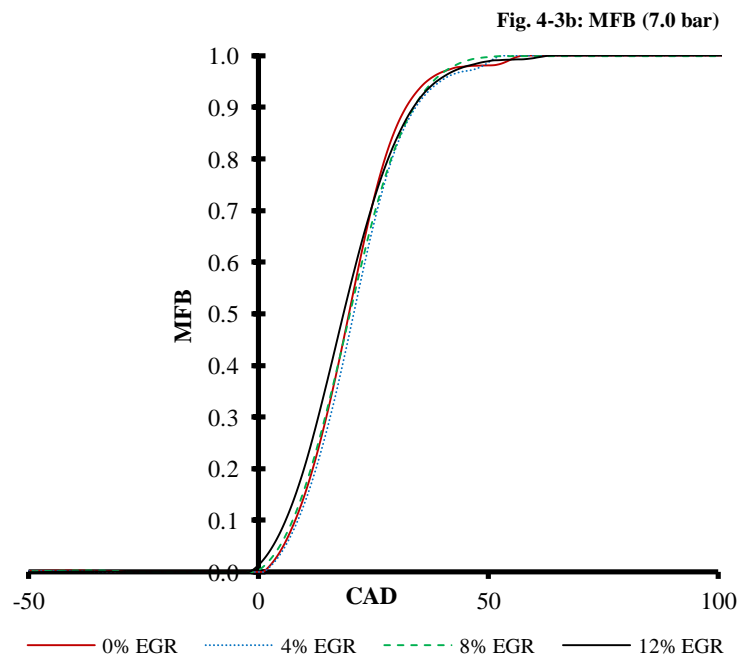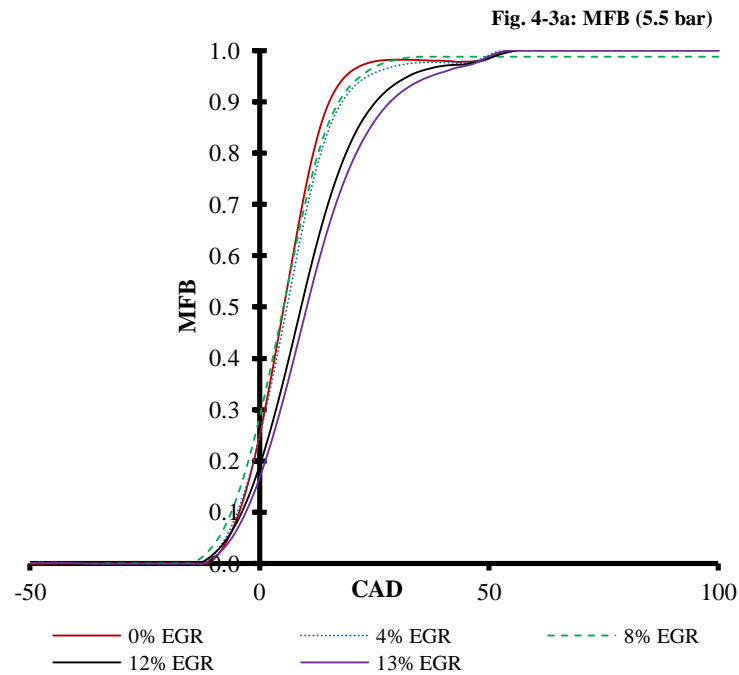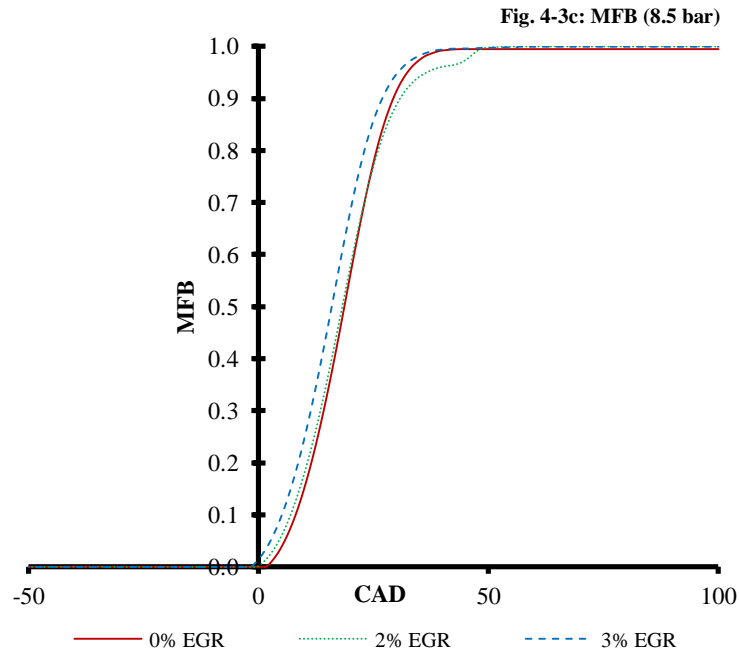
Figure 4-3   MFB versus CAD at KLMBT spark timings for **a)** 5.5 bar IMEP, **b)** 7.0 bar IMEP and **c)** 8.5 bar IMEP

4.3.1.4 Fuel Consumption

Gravimetric $ISFC_{net}$ at the KLMBT spark timings for the three engine load conditions at the different EGR ratios tested is shown in Figure 4-4. There is a clear trend of decreasing fuel consumption as the EGR addition was increased because, as explained previously, the KLMBT could be advanced significantly, as the increasing EGR addition suppressed temperature rises in the end-zone of the combustion chamber, inhibiting knock that would otherwise have been produced. This allowed the MFB50 phasing of the engine to be advanced towards its optimum phase for the engine loads of 7.0 and 8.5 bar IMEP, increasing the engine efficiency and consequently reducing the fuel consumption (de O. Carvalho et al., 2012). This occurred because more of the combustion process occurred at a lower in-cylinder volume and thus, it generated higher combustion pressures. This improved the rate of combustion and it increased the expansion of the combustion products into useful energy.

109

Also, because the gas from EGR takes a part of the intake air volume, the throttle valve had to be opened more to provide the same amount of fresh air as in the non-EGR case, or in other words, the same amount of oxygen for combustion. This reduced the pumping losses across the EGR range and thus the fuel consumption at all engine loads; PMEP reduced from 0.45 to 0.38 bar for the load of 5.5 bar IMEP, 0.33 to 0.25 bar for the load of 7.0 bar IMEP, and 0.24 to 0.22 bar for the load of 8.5 bar IMEP, across their respected EGR ranges. For the loads of 5.5, 7.0, and 8.5 bar IMEP, the fuel consumption reduced by 2.2, 4.1 and 1.0% respectively across the EGR range. Furthermore, the reduced combustion temperatures with EGR addition improved thermal efficiency (Ratnak et al., 2015, Siokos et al., 2015), contributing to the fuel economy improvements observed.

The rate of fuel consumption decrease at 5.5 bar reduced at the higher EGR ratios because the spark timings were not knock limited for this relatively low load. Thus, between 0 and 8% EGR addition, the spark timing was at its optimum phase, and it became retarded slightly from its optimum phase as the EGR addition was increased to 12 and 13%. This left little opportunity for fuel consumption improvement through pumping loss reduction. Furthermore, because the MFB50 became later at 12 and 13% EGR addition (Figure 4-3a), the rate of fuel consumption decrease was reduced at these conditions. It is proposed that the increased rate of fuel consumption decrease observed at the engine load of 7.0 bar IMEP when the EGR ratio was increased from 8 to 12% occurred because the in-cylinder pressure increased significantly in comparison to that observed with the previous EGR increase from 4 to 8% (Figure 4-1b). This was possibly due to the earlier start of heat release (Figure 4-3b). The in-cylinder pressure at 8.5 bar IMEP only increased slightly between the EGR ratios of 0 and 2%, despite the EGR addition and consequent spark advance, leading to the relatively small improvement in fuel economy (Figure 4-4). However, the in-cylinder pressures

increased significantly as the EGR addition was increased further to 3%, leading to the significant improvement in fuel economy observed.

For the load of 5.5 bar IMEP, the fuel consumption improvements would have worsened if the intake manifold temperature increases could have been eliminated, because the combustion duration would have increased, as discussed, meaning that the conversion efficiency of the pressure and heat from the combustion would have reduced. Fuel consumption improvements for the loads of 7.0 and 8.5 bar IMEP would have been greater, due to the greater KLMBT spark timing advances that would be expected. This effect would be expected to overcome the slightly increased combustion duration that would also be expected at these engine loads.

Despite the fuel consumption reduction observed and discussed, it must be noted that the VAF had an average error of 1.6%; therefore, the reduction of 1.0% observed across the EGR range at the engine load of 8.5 bar IMEP is limited, because it could have resulted from this error. The reductions observed for 5.5 and 7.0 bar IMEP are however above 1.6%, thus, they are not limited. The error mainly resulted from the limited resolution of the u-tube manometer device used to calibrate the air flow meter. Despite the resolution being 1 mm, it still remained a limiting factor in achieving better calibration between the VAF and u-tube manometer reading, thus limiting the VAF accuracy. The error also resulted from the orifice flow plate used to calibrate the flow meter.
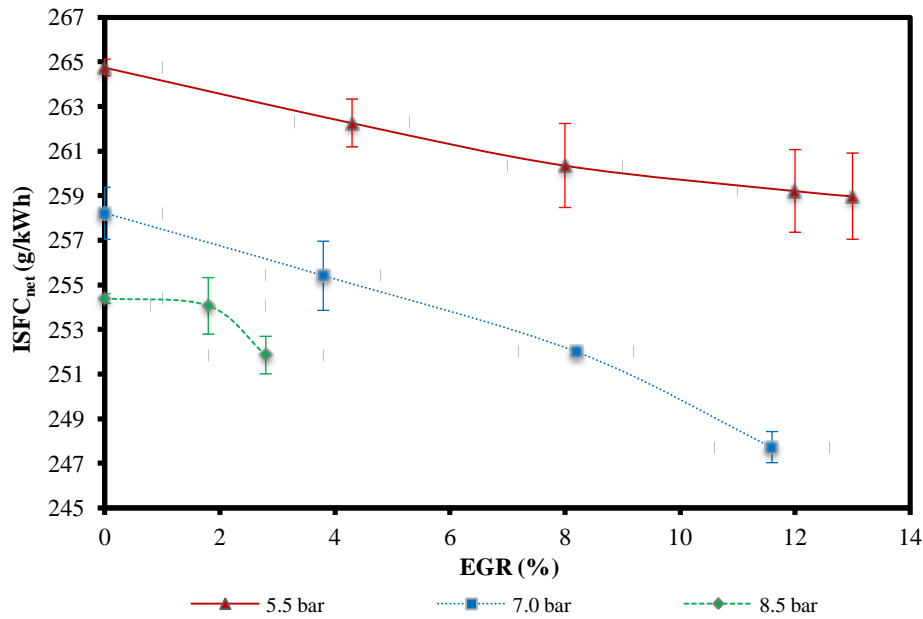
Figure 4-4 Gravimetric ISFC$_{net}$ versus EGR ratio at KLMBT spark timings

4.3.1.5 EGT

The EGT decreased significantly across the EGR range for the three tested engine loads, as shown in Figure 4-5. Overall, it decreased by 21.9, 32.7, and 7.6°C for the loads of 5.5, 7.0 and 8.5 bar IMEP, respectively. As previously discussed, the calculated average in-cylinder temperatures significantly reduced with EGR addition for the engine load of 5.5 and 8.5 bar IMEP, and they reduced less significantly for the engine load of 7.0 bar IMEP, contributing to some of the reductions in EGT across the EGR range. However, it is thought that the main contribution to the reduced EGTs was the advanced combustion phasing enabled by the EGR addition. It is proposed that this led to a more efficient conversion of the pressure and heat from the combustion into piston work, causing the gases to cool more in the engine cylinder before they were ejected into the exhaust. With the combustion starting earlier as the EGR addition was increased, this effect became greater, causing the EGTs to reduce across the EGR range. For turbocharged engines with EGR, this effect is very useful for protecting the turbocharger turbine.

The temperature decrease is lower for 5.5 bar IMEP compared to 7.0 bar IMEP despite the maximum level of EGR increasing. This is because the conversion efficiency of the pressure and heat from the combustion into piston work could not be improved due to the combustion already being at its optimum phasing. Furthermore, the optimum combustion phasing could not be maintained at 12 and 13% EGR addition, as discussed, resulting in the EGTs not decreasing further at these conditions. The EGT at 7.0 bar IMEP increased slightly by 6°C at the EGR ratio of 4%, whereas one would expect it to have decreased. Another slight increase was observed between the EGR ratios of 0 and 2% at 8.5 bar IMEP. Despite these observed increases, they are not considered to be significant; therefore, they will not be commented on further.

For the load of 5.5 bar IMEP, the EGT decreases would have likely reduced if the intake manifold temperature increase could have been eliminated, due to the aforementioned reduced conversion efficiency of the pressure and heat from the combustion, due to an expected increased combustion duration. The EGT decreases would likely have been greater for the engine loads of 7.0 and 8.5 bar IMEP, due to an increased conversion efficiency of the pressure and heat from the combustion, resulting from the greater KLMBT spark timing advances that would be expected. This effect would be expected to overcome the slightly increased combustion duration that would also be expected at these engine loads.
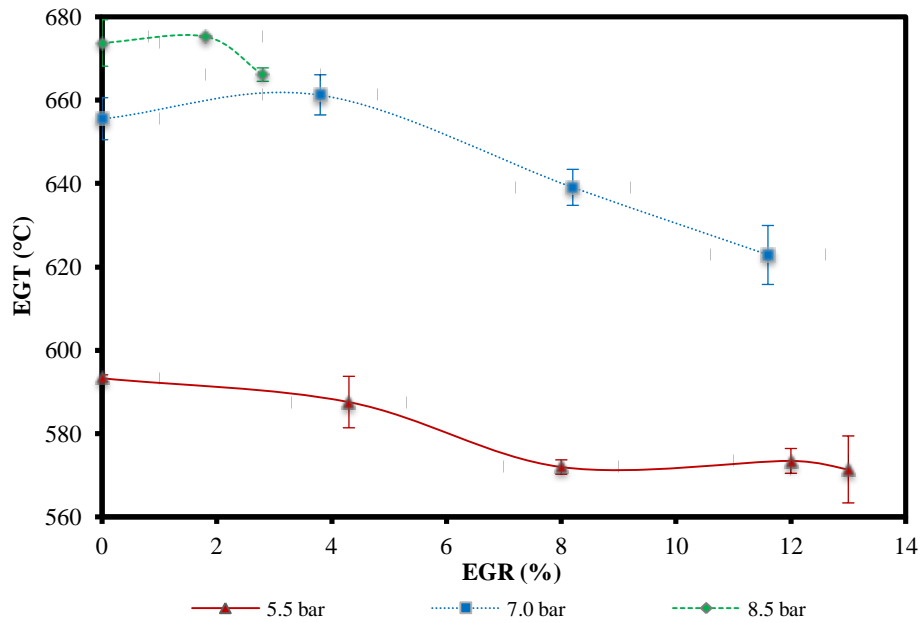
Figure 4-5   EGT versus EGR ratio at KLMBT spark timings

4.3.1.6 PM Emissions

The nucleation mode of the PM emissions decreased and the accumulation mode increased as EGR ratio was increased from 0 to 12% for the engine load of 5.5 bar IMEP, as shown in Figure 4-6a. The two modes could be distinguished from one another because they formed two distinct peaks; the nucleation mode peak is comprised of the smaller particles on the left-hand side of the plot (10-30 nm) (Figure 4-6a) and the accumulation mode peak is comprised of the larger particles on the right-hand side of the plot (30-500 nm). According to (Zhang et al., 2014b) the nucleation mode particles mainly result from droplets formed by hydrocarbon condensation and the accumulation mode particles are mainly composed of carbonaceous agglomerates formed in local rich-fuel zones (Burtscher, 2005, Kittelson, 1998).

At the engine load of 5.5 bar IMEP, the increase in EGR suppressed the temperature rise in the combustion chamber, reducing the oxidation rate of soot particles, leading to the increased accumulation mode particles observed between 0 and 12% EGR addition. This appears to have been more significant than the decreases in primary carbon particles formed

by the thermal pyrolysis and dehydrogenation reaction of fuel vapour/droplets, which would have occurred with the reduced in-cylinder temperatures (Zhang et al., 2014b). It is proposed that the observed reductions in nucleation mode particles occurred because they were adsorbed onto the increasing amounts of soot accumulation particles. Thus, as the soot accumulation mode particles increased across the EGR range, the numbers of nucleation mode particles decreased. In addition to the reduced oxidation rate of soot particles across the EGR range caused by the reduced combustion temperatures, it is proposed that the spark timing advances reduced the time available for fuel-air mixing. This led to poorer mixture preparation and thus more pockets of high local equivalence ratio which could not burn completely contributing to the higher numbers of soot accumulation mode particles observed across the EGR range. The EGT decreases across the EGR range also contributed to the accumulation mode PM increases observed.

Increases in nucleation and accumulation mode particles were observed across the EGR range for 7.0 bar IMEP as shown in Figure 4-6b. However, the increase in the nucleation mode was not consistent, therefore, it will not be commented upon further. It is thought that the calculated average in-cylinder temperature decreases led to the accumulation mode PM increases. Again, this appears to have been more significant than the decreases in primary carbon particle formation (Zhang et al., 2014b). In addition, due to the spark timing advances achieved, it is proposed that the mixture preparation would have been poorer, contributing further to the increased soot accumulation mode particles observed across the EGR range. This is reflected in the MFB data (Figure 4-3b) which shows that the MFB50 was advanced significantly at the EGR ratio of 12% when compared to the MFB at 0% EGR. Again, the EGT decreases across the EGR range also contributed to the accumulation mode PM increases observed.

The observed behaviour at 5.5 and 7.0 bar IMEP was not observed at 8.5 bar IMEP in Figure 4-6c, despite the calculated average combustion temperature decreasing (Figure 4-2c). At 8.5 bar IMEP, there was no significant change in the nucleation and accumulation mode particles observed. This is due to the low EGR addition achieved at this engine load.

Overall, the contribution of nucleation mode particles became weaker as the engine loads were increased. This agrees with the reduced HC emission observed as the engine load was increased (Figure 4-8); the HC emission is mainly composed of the volatile particulate fraction included in the nucleation mode (Costagliola et al., 2013). Thus, this explains the strong relationship between the HC emission and nucleation mode particles observed in the data. The accumulation mode particles increased with engine load due to the higher rate of soot production and growth at higher temperatures in the combustion chamber (Zhang et al., 2014b). In addition, as the load is increased, more fuel is injected which results in more locally rich areas in the combustion chamber, further increasing soot formation (Wang, 2014b). (Wang et al., 2014c) observed the activation energies and temperatures required to oxidise soot increased with engine load, further explaining the increased accumulation mode particles as the engine load was increased. Furthermore, there is increased fuel impingement at higher loads resulting from the longer injection pulse width and increased fuel mass injected, resulting in yet more increases in soot formation (Wang, 2014b).

The PM behaviour at 5.5 and 7.0 bar IMEP is different from that observed by (Alger et al., 2010) and (Hedge et al., 2011) where significant soot reductions across the EGR range was reported, with soot levels being represented by the accumulation mode. It is likely however that because the engines in their investigations were turbocharged, the EGR addition reduced the need to enrich the fuel charge for the purpose of reducing turbocharger inlet temperatures, consequently reducing their soot emission. Clearly there are complex behaviours regarding

the formation of PM emissions in engines which need to be investigated in detail on a fundamental level.

It is proposed that the decrease in accumulation mode particles at 5.5 bar IMEP as the EGR addition was increased to 13% occurred because the spark timing (Table 4-3) was not advanced as compared to that at 12% EGR addition. This means that while the mixture preparation was equivalent, the combustion duration was increased (Figure 4-3a), providing more time for the particles to oxidize in the hot flames. Additionally, there is a decrease in the accumulation mode particles for the load of 7.0 bar IMEP at 4% EGR addition (Figure 4-6b). It is believed that the increased exhaust temperatures (Figure 4-5) increased the rate of post-combustion oxidation of the accumulation mode particles, resulting in the observed decrease. Such behaviour is reasonable to expect considering soot accumulation mode particles from a DISI engine can be effectively oxidised between 400-600°C (Wang et al., 2014c).

If the intake manifold temperature increases could have been eliminated, the accumulation mode particles would have been increased more significantly at 5.5 bar IMEP. This is due to the expected increased MBT spark timing advances further worsening mixture preparation, and the more significant in-cylinder temperature decreases further reducing the oxidation rate of the particulates. Nucleation mode particles would consequently be reduced because they would be adsorbed onto the greater number of accumulation mode particles. At 7.0 bar IMEP, it would be expected that the accumulation mode particles would be increased too, resulting, again, in nucleation mode particle decreases, due to poorer mixture preparation resulting from the greater KLMBT spark timing advances. At 8.5 bar IMEP, it is expected that there would be no significant effect of the lower intake manifold temperature on the PM behaviour, due to the low 3% EGR addition achieved.

Fig. 4-6a: PM (5.5 bar)

Legend: 0% EGR, 4% EGR, 8% EGR, 12% EGR, 13% EGR

Fig. 4-6b: PM (7.0 bar)

Legend: 0% EGR, 4% EGR, 8% EGR, 12% EGR
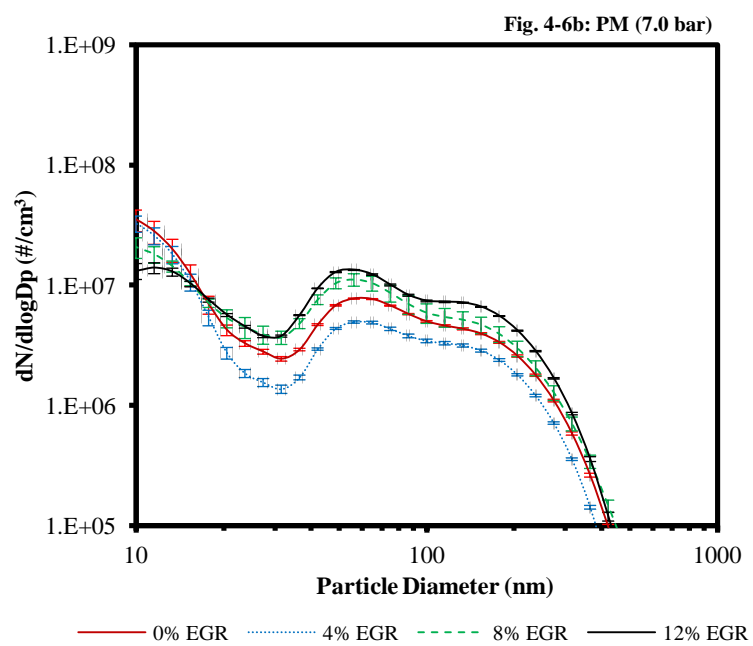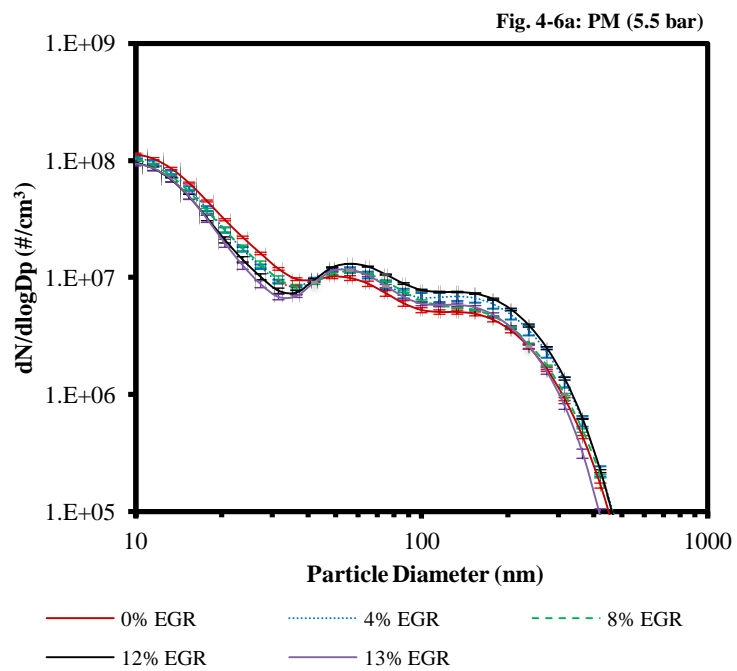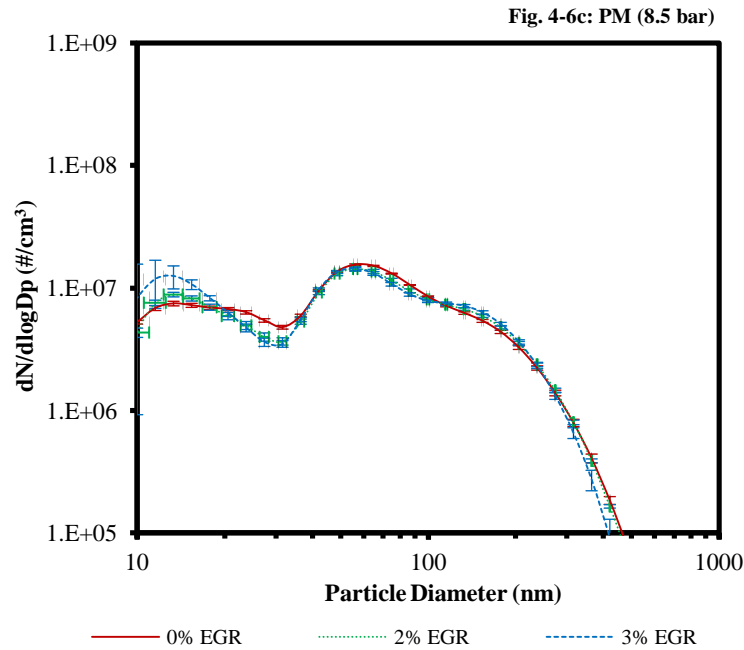
Figure 4-6 PN emissions versus particle diameter at KLMBT spark timings at **a)** 5.5 bar IMEP, **b)** 7.0 bar IMEP and **c)** 8.5 bar IMEP

4.3.1.6 Gaseous Emissions (NO$_x$ and HC)

The NO$_x$ emission at the KLMBT spark timings for the three engine load conditions at the tested EGR ratios is presented in Figure 4-7. The NO$_x$ emission increased significantly as the engine load was increased due to the higher calculated average in-cylinder temperatures which increased the formation of NO$_x$ in the hot flames. There is a clear trend of the NO$_x$ decreasing as the EGR percentage was increased. EGR reduced the calculated average in-cylinder temperatures (Figures 4-2a, 4-2b and 4-2c) for the three engine loads tested, resulting in the NO$_x$ reductions observed. The overall reduction for the loads of 5.5, 7.0 and 8.5 bar IMEP are 64.3, 50.9 and 12.2%, respectively, showing the significant potential EGR has on NO$_x$ emission reduction.

The rate of decrease of the NO$_x$ emission with EGR addition became greater as the engine load was increased; however, the NO$_x$ decrease in terms of percent, over the achievable EGR range for the respective loads, reduced as the engine load was increased. The rate of decrease

became greater as the engine load was increased because EGR addition was more effective at reducing the average in-cylinder temperature as the engine load was increased. This can be seen in Figures 4-2a, 4-2b and 4-2c, with similar calculated average in-cylinder temperature reductions achieved for the three engine loads tested, despite the maximum EGR addition reducing as the engine load was increased. It is thought that the greater mass of EGR gases as the engine load was increased; at equivalent EGR additions in terms of percent, due to the greater mass of intake air, caused the in-cylinder temperature to be suppressed more significantly, resulting in the observed behaviour. It is thought that the NO_x decrease in terms of percent reduced as the engine load was increased, because of the reduced maximum EGR addition that could be achieved.

At 5.5 bar IMEP, the NO_x emission would have been reduced more significantly if the intake manifold temperature increases could have been eliminated, due to the lower expected combustion temperatures. At 7.0 and 8.5 bar IMEP, there would be no significant change expected because, as discussed, the peak of the calculated average in-cylinder temperatures would not have changed significantly. Again, it is thought that the improved KLMBT spark timing would have quickly compensated for the decreased intake gas temperature by the time temperatures reached the beginning of the range reported (500°C). Thus, the effect on the NO_x emission which occurs at temperatures much higher than 500°C would not have been significant.
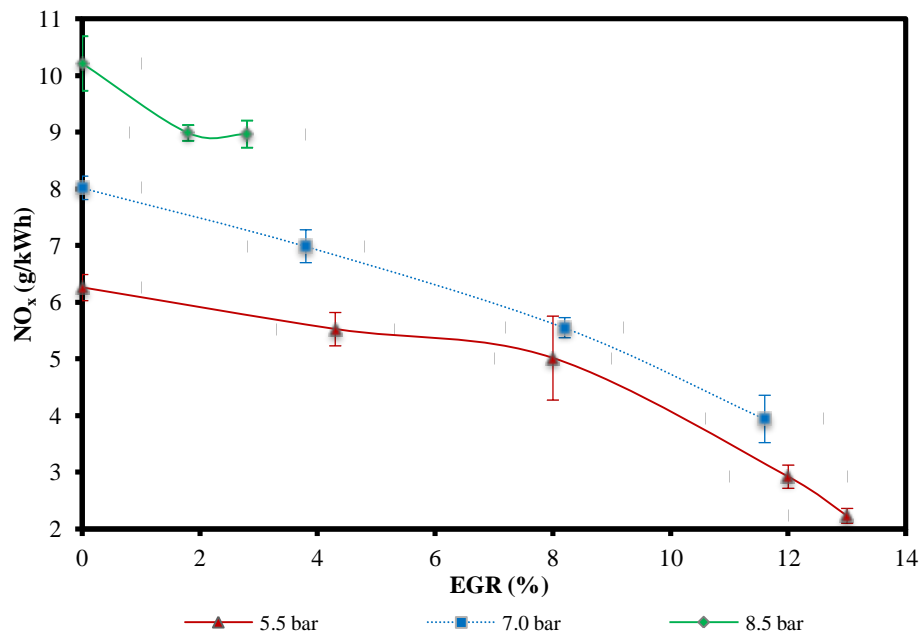
Figure 4-7   NO$_x$ emissions versus EGR ratio at KLMBT spark timings

The HC emission data for the three tested engine loads across their respective EGR ranges is shown in Figure 4-8. At 0% EGR, lower HCs were observed as the engine load was increased because the calculated average in-cylinder temperatures were higher which increased the oxidation rate of the HCs, reducing the numbers observed. The reduced calculated average in-cylinder (Figures 4-2a-c) and exhaust (Figure 4-5) gas temperatures across the EGR range for the three tested engine loads resulted in the HC emission increases observed across the ranges for the respective loads. They increased by 48.3, 19.0 and 6.8% across the EGR range for the engine loads of 5.5, 7.0 and 8.5 bar IMEP, respectively. It is proposed that the reduced in-cylinder temperatures increased the thickness of the quench layers covering the combustion chamber surface and slowed down and reduced the evaporation of impinged fuel, resulting in the HC emission increase. The reduced exhaust temperatures reduced the oxidation rate of HCs contributing to the increases observed. Some researchers have observed similar overall HC increases with EGR addition (Alger et al., 2009a, Diana et al., 1996, Takaki et al., 2014, Zhang et al., 2014b), but others have observed unchanged HC (Grandin et al., 1998, Kumano and Yamaoka, 2014, Song et al., 2014).

The reduced time available for the fuel-air mixture preparation due to the KLMBT spark advances across the EGR range will have resulted in poorer charge preparation, leading to more pockets of a high local equivalence ratio, also contributing to the HC emission increases observed. The same reasoning can also help explain why the HC emissions reduced as the engine load was increased and the spark timing became more retarded.

There was a small but significant reduction in the rate of HC emission increase at 8% EGR for 5.5 bar IMEP. This is mirrored by the slight decrease in the rate of reduction in NO_x emissions at the same condition (Figure 4-7). It is believed that the relatively smaller change in the MFB profile (Figure 4-3a) between the EGR ratios of 4 and 8%, as compared to that observed between the EGR ratios of 0 and 4%, led to a smaller reduction in the ROHR, resulting in this behaviour. The HC emission decreased slightly for 5.5 bar IMEP between the EGR additions of 12 and 13%. Although a decrease was observed it is not considered to be significant, as can be seen from the confidence intervals on the figure. Therefore, it will not be commented on further.

If the intake manifold temperature increases could have been eliminated, it is expected that the HC emission reduction at 5.5 bar IMEP would have been increased, due to the higher EGTs which could be expected in such a case. At 7.0 and 8.5 bar IMEP, the effect of the lower EGTs would be expected to be cancelled out by the increased post-combustion time provided by the greater KLMBT spark timing advance. Thus, it is not thought that the intake manifold temperature increases with EGR additon had a significant effect on the HC emission at these engine loads.

Despite the increases in HCs observed across the EGR range for the three engine loads tested, it would be expected that a traditional TWC would be able to handle these increases to maintain the vehicle-out HC emissions at non-EGR levels. This is based on the work of

(Hoffmeyer et al., 2009) who found that HCs are almost completely reduced by the catalyst, even as the EGR rate is increased, due to an increased conversion efficiency of the catalyst. However, more research would be required to confirm whether it can be achieved in this engine.
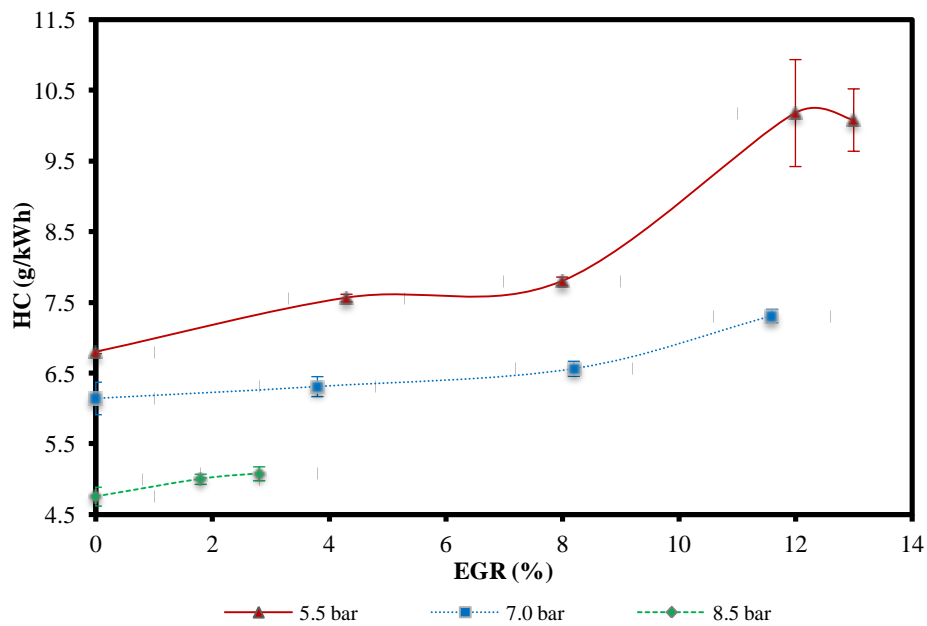

Figure 4-8   HC emissions versus EGR ratio at KLMBT spark timings

4.3.2 Effect of Different EGR Types on Combustion and Gaseous Emissions in a DISI Engine

4.3.2.1 KLMBT Spark Timing

The KLMBT spark timings, as shown in Table 4-4, could be advanced significantly with EGR addition for all the EGR types tested. They were advanced by 10, 10, 12 and 14 CAD for the hot EGR, cooled EGR, hot EGR after TWC and cooled EGR after TWC EGR types, respectively. The EGR addition enabled the spark to be advanced significantly, through the suppression of temperature rises in the end-zone. The KLMBT spark timing was most advanced for the cooled EGR after TWC condition across the EGR range because the removal of NO from the EGR gases reduced the knocking tendency of the engine (Kawabata et al., 1999) and the cooler EGR gases reduced the temperature in the end-zone of the combustion chamber. These reasons also explain the greater KLMBT spark timing advances for hot EGR after TWC and cooled EGR, respectively, as compared to the hot EGR condition.

Despite this, KLMBT spark timing advances would likely have been greater if intake manifold temperature increases resulting from the EGR addition could have been eliminated, due to the reduced end-zone temperatures. It must be noted that knocking could have been avoided if the compression ratio was fully optimized for the fuel used, as mentioned previously.

The EGR addition could only be increased to 10% for the cooled EGR condition because of the pressure loss in the EGR heat exchanger. This means that a pump would be required to achieve higher levels of EGR or a more efficient heat changer in terms of cooling power vs. pressure loss would be required. A pump would reduce any fuel consumption benefits of the cooled EGR system, therefore reducing any advantages it may have over the hot EGR

system. Despite the pressure loss in the heated line for the hot EGR after TWC condition, this could be compensated for by increasing the gas flow rate of the compressed gas bottle, allowing the high EGR addition to be achieved.

Table 4-4   KLMBT spark timings (˚bTDC) (EGR addition & EGR type)

EGR Addition (%) / EGR Type	0	7	10	14
Hot EGR	14	18		24
Cooled EGR		20	24	
HE after TWC		20		26
CE after TWC		20		28

4.3.2.2 In-cylinder Pressures and Temperatures

The in-cylinder pressures for the four EGR types at the KLMBT spark timings, as shown in Figures 4-9a, 4-9b, 4-9c and 4-9d, generally increased with EGR addition and the subsequent spark advances which could be achieved, and the maximum in-cylinder pressure became slightly earlier due to the more advanced spark timings. This was because the KLMBT spark timing advances resulted in the heat being released from the fuel at an earlier CAD, enabling higher in-cylinder pressures to be achieved before the downwards piston motion caused the in-cylinder pressure to decrease again. However, the maximum in-cylinder pressure remained approximately the same across the EGR range for hot EGR (Figure 4-9a), with the peak pressure becoming less advanced than with the other EGR types. This was due to the lower spark advance achieved at equivalent EGR ratios (Table 4-4) and the resulting retardation of the MFB50 across the EGR range (Figure 4-12).

Greater in-cylinder pressure increases would have been likely if the intake manifold temperature increases, resulting from the EGR addition, could have been eliminated. This is because it would likely have led to greater KLMBT spark timing advances, as discussed.

Fig. 4-9a: In-cylinder pressure (hot EGR)

Fig. 4-9b: In-cylinder Pressure (cooled EGR)

Fig. 4-9c: In-cylinder Pressure (Hot EGR after TWC)

Fig. 4-9d: In-cylinder Pressure (Cooled EGR after TWC)
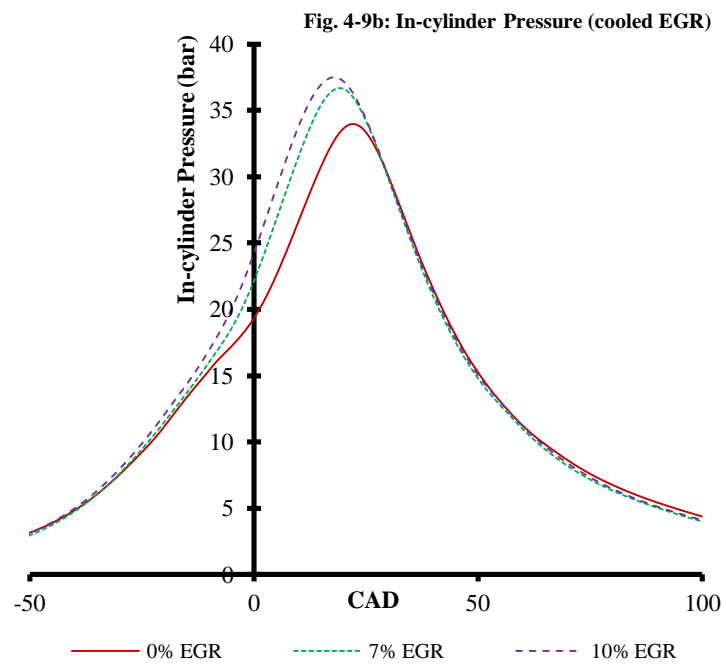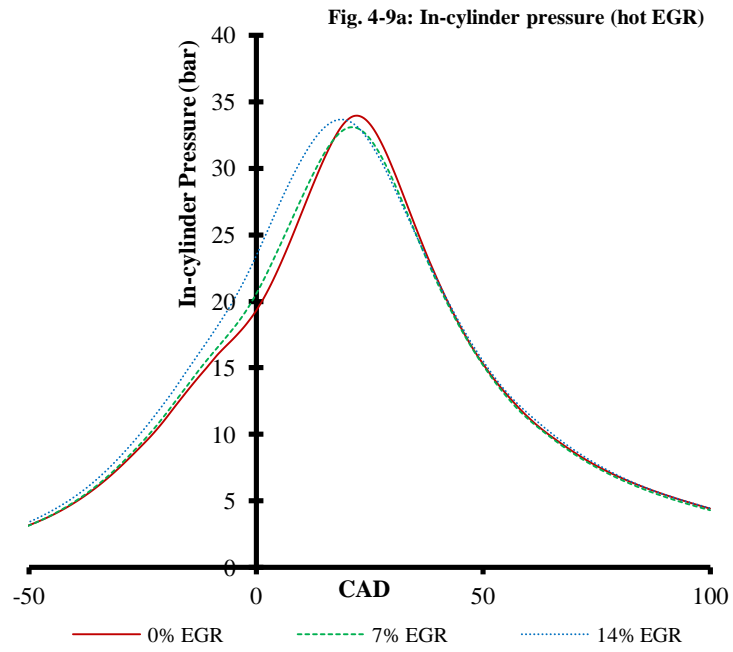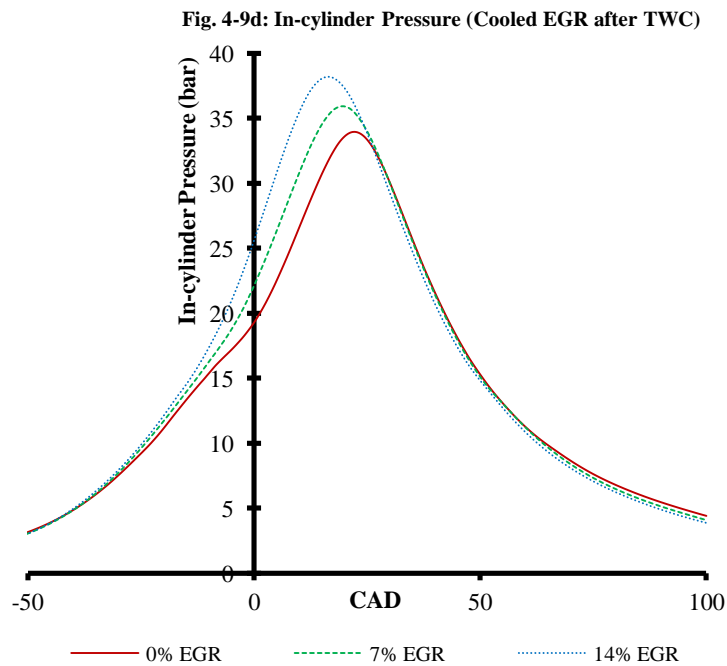
Figure 4-9   In-cylinder pressures versus CAD at KLMBT spark timings for **a)** hot EGR, **b)** cooled EGR, **c)** hot EGR after TWC and **d)** cooled EGR after TWC

The calculated average in-cylinder temperatures, as shown in Figures 4-10a, 4-10b, 4-10c and 4-10d at the KLMBT spark timings, decreased across the EGR range for the different EGR types due to the temperature suppression effect of the EGR gases. The temperatures decreases across the EGR range were greater for the cooled EGR and cooled EGR after TWC EGR

127

types as compared to the hot EGR and hot EGR after TWC EGR types due to their lower intake plenum temperatures in comparison (Figure 4-18).

It is believed that the increased intake manifold temperatures resulting from the EGR addition were compensated for by the less optimized combustion phasing resulting from the consequently reduced KLMBT spark timing advance (Table 4-4), compared to the maximum spark advance possible, as explained previously. It is thought that the improved KLMBT spark timing would have quickly compensated for the intake gas temperature decrease by the time temperatures reached the beginning of the range reported (500˚C); thus, the effect would have been minimal.

Fig. 4-10a: In-cylinder Temperature (hot EGR)

Fig. 4-10b: In-cylinder Temperature (cooled EGR)

Fig. 4-10c: In-cylinder Temperature (hot EGR after TWC)

Fig. 4-10d: In-cylinder Temperature (cooled EGR after TWC)
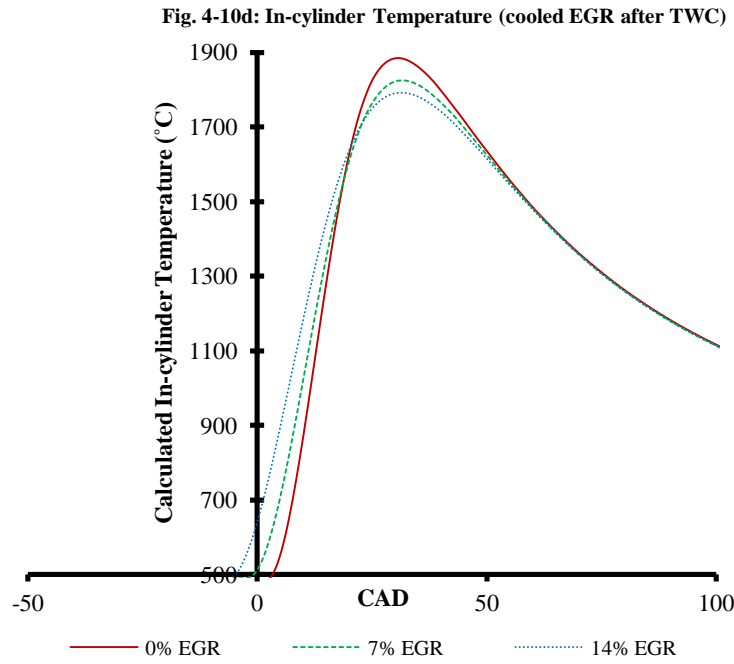
Figure 4-10 Calculated average in-cylinder temperatures versus CAD at KLMBT spark timings for **a)** hot EGR, **b)** cooled EGR, **c)** hot EGR after TWC and **d)** cooled EGR after TWC

4.3.2.3 MFB

The MFB profiles at the KLMBT spark timings, as shown in Figures 4-11a, 4-11b, 4-11c and 4-11d for the four EGR types, started earlier and became elongated as the EGR ratio was increased, due to the spark timing becoming more advanced and due to the laminar flame speed reducing effects of the EGR gases, respectively (Rhodes and Keck, 1985). The MFB profile for the cooled EGR condition (Figure 4-11b) was approximately the same at the EGR ratios of 7 and 10%. This is because the rate of spark advance between 7 and 10% EGR was 1.33 CAD/EGR (%), which was higher than the 0.86 CAD/EGR (%) rate of spark advance achieved between the EGR ratios of 0 and 7%. This allowed the MFB profile to be maintained with little change between 7 and 10% EGR addition whereas between 0 and 7% EGR addition, the less significant spark advance caused the MFB profile to become more elongated, producing the observed behaviour. For a quantitative analysis of the combustion

speed, the MFB50 and MFB10-90 have been calculated from the MFB profiles (please see next section).

Again, KLMBT spark timing advances would likely have been greater if intake manifold temperature increases, resulting from the EGR addition, could have been eliminated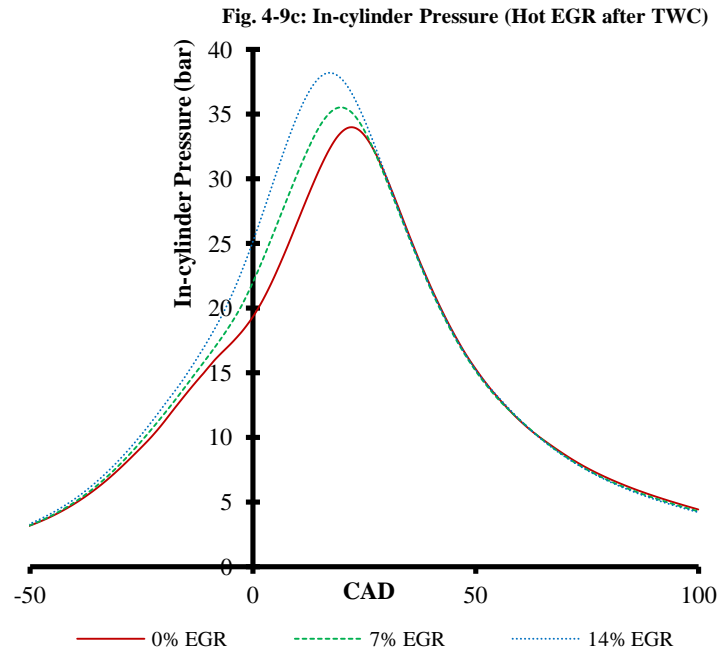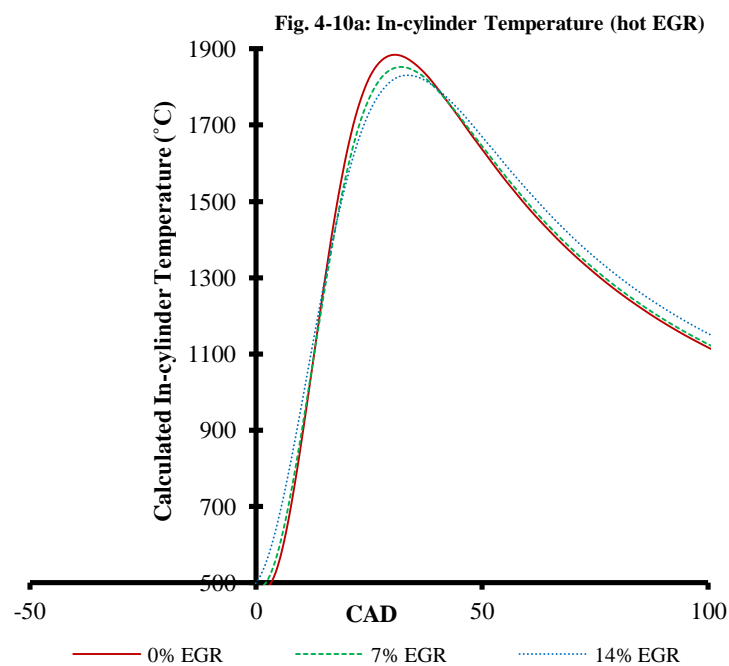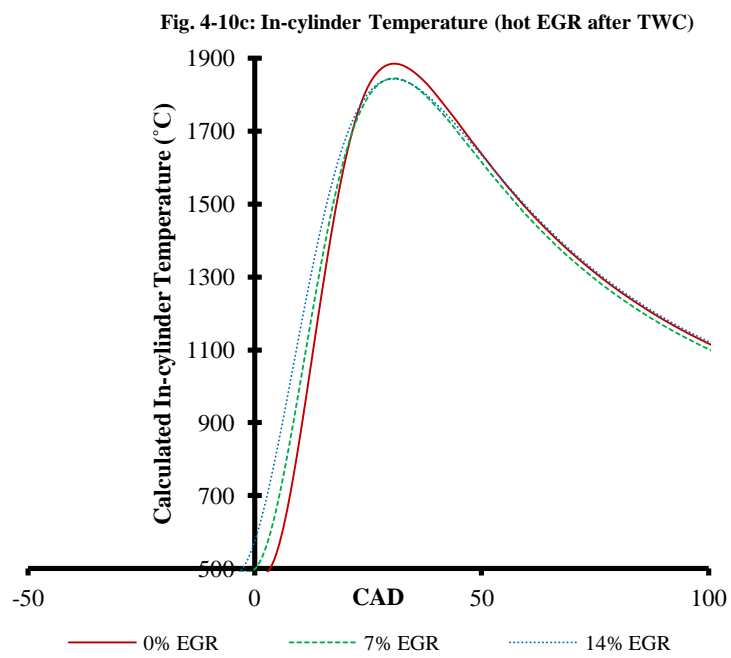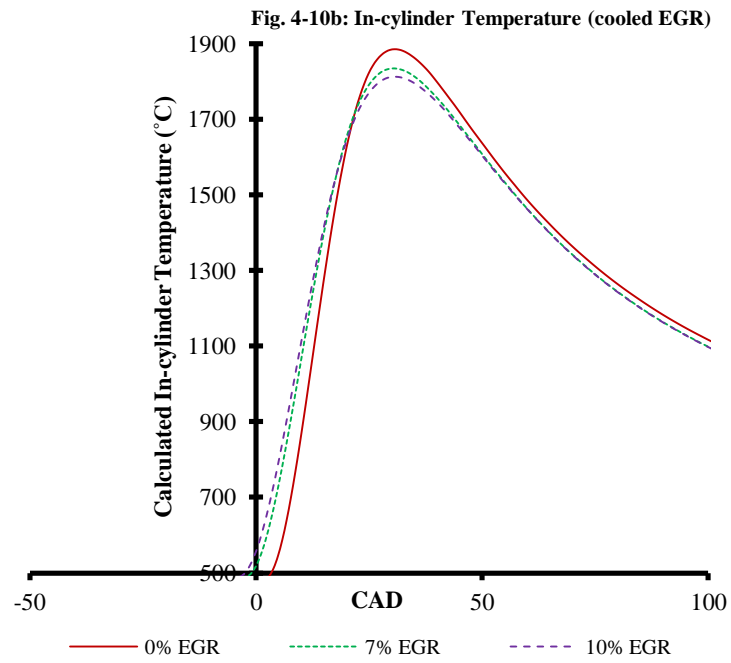; thus, the MFB profiles would likely have been advanced slightly in comparison to those in Figures 4-11a-d. The profile would also become slightly more elongated because the laminar flame speed would be reduced in the cooler fuel-air charge.

Fig. 4-11a: MFB (hot EGR)

Fig. 4-11b: MFB (cooled EGR)

Fig. 4-11c: MFB (hot EGR after TWC)

132

Fig. 4-11d: MFB (cooled EGR after TWC)

| 0% EGR | 7% EGR | 14% EGR |
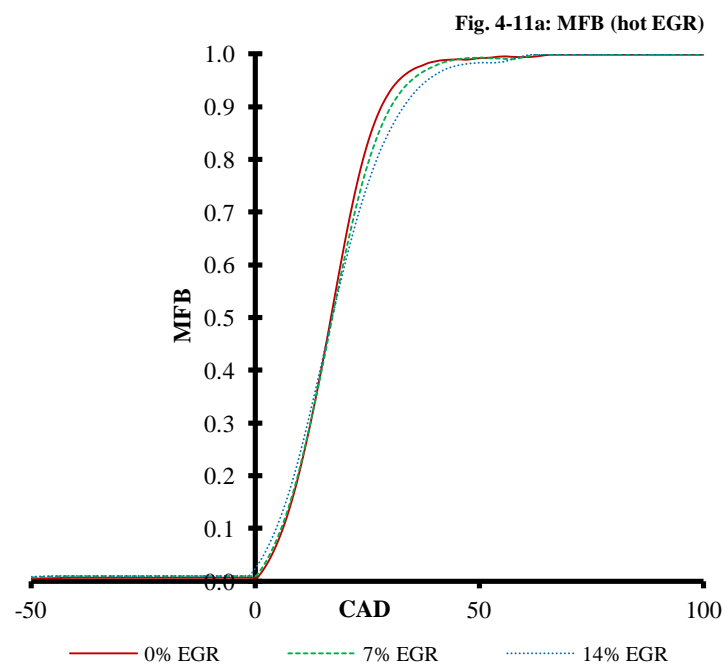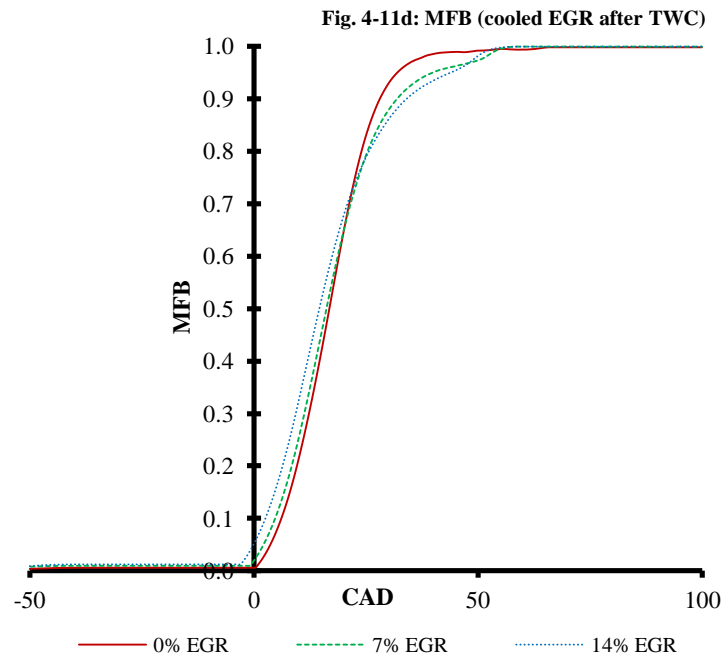
Figure 4-11   MFB versus CAD at KLMBT spark timings for **a)** hot EGR, **b)** cooled EGR, **c)** hot EGR after TWC and **d)** cooled EGR after TWC
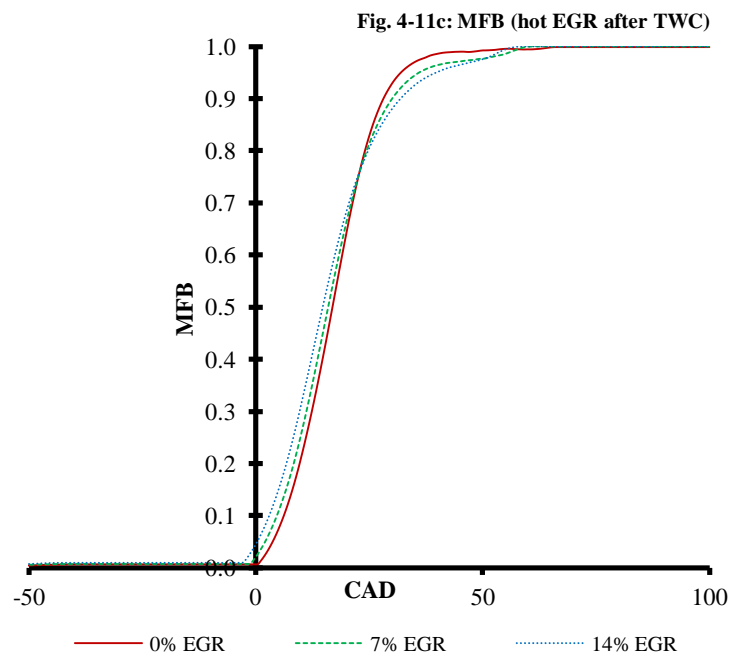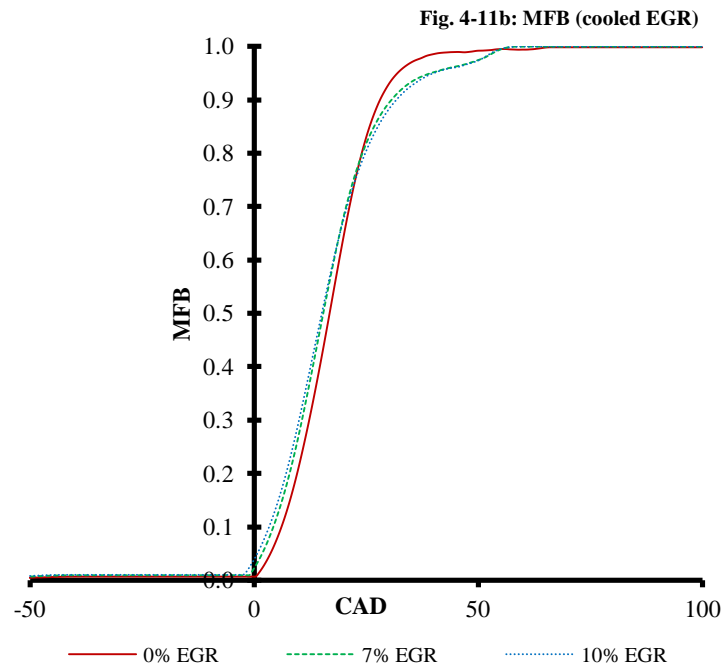
4.3.2.4 MFB50 and MFB10-90

The MFB50 at the KLMBT spark timings became earlier across the EGR range for the three conditions of cooled EGR, hot EGR after TWC and cooled EGR after TWC as shown in Figure 4-12. This is because, as discussed, the KLMBT spark timings (Table 4-4) could be advanced significantly with the EGR addition. However, for the hot EGR condition, the MFB50 became later. It seems therefore that the KLMBT spark timing advance achieved was not sufficient to overcome the laminar flame speed slowing effects of the EGR addition, whereas for the other EGR types, it was. This is because the spark timing advance was less significant for the hot EGR condition as compared to the other EGR conditions, because it did not benefit from the cooled EGR gas or from the removed NO; the other three EGR types benefited from at least one of these things. Therefore, the lesser spark advance was not able to overcome the combustion slowing effects of the EGR gases, but the greater spark advances achieved with the other EGR types were sufficient to overcome them.

Despite the same KLMBT spark timings being achieved for the cooled EGR, hot EGR after TWC and cooled EGR after TWC at 7% EGR addition, the MFB50 data is not the same. It is proposed that this is due to the different intake plenum temperatures (Figure 4-18) which meant that the fuel-air charges were of different temperatures before combustion, resulting in a variation in flame speeds and thus slightly different MFB50 data, despite the same spark timings.

Again, KLMBT spark timing advances would likely have been greater if intake manifold temperature increases, resulting from the EGR addition, could have been eliminated. Thus, the MFB50 would likely have been slightly advanced in comparison.
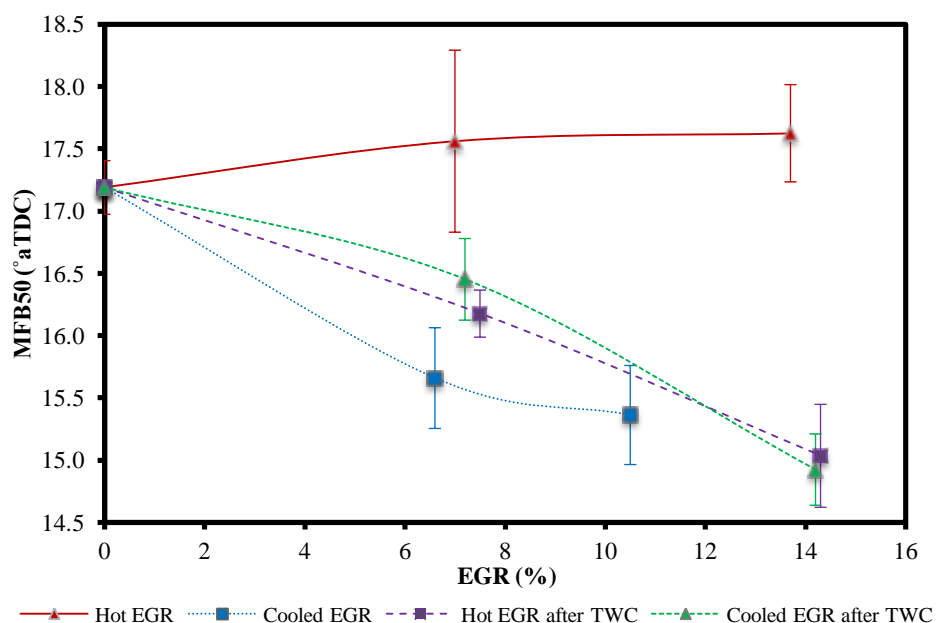
Figure 4-12   MFB50 versus EGR ratio at KLMBT spark timings

The combustion duration (MFB10-90) at the KLMBT spark timings, as shown in Figure 4-13, increased significantly for all of the EGR types across the EGR range because of the aforementioned laminar flame speed reducing effects of the EGR gases (Rhodes and Keck, 1985). The cooled EGR and cooled EGR after TWC EGR types were more significantly affected than the hot EGR and hot EGR after TWC EGR types. It is proposed that this is

because the flame travelled at a slower speed in the cooler fuel-air charge. The cases with the simulated TWC were more greatly affected then their corresponding hot and cooled conditions respectively. It is proposed that this was because of the slightly reduced intake plenum temperatures (Figure 4-18) for the TWC conditions as compared to their corresponding hot and cooled conditions. This is thought to have reduced the laminar flame speed which increased the combustion duration for these in respect to their corresponding non-TWC conditions.

As explained, if the intake manifold temperature increases could have been eliminated, it is believed that the flame would travel more slowly in the resulting cooler fuel-air charge, increasing the combustion duration slightly. If the compression ratio was optimised for the fuel used, the combustion phasing would have been optimised for each test point, therefore, it would be expected that the combustion at all of the conditions tested would have been quicker due to higher in-cylinder turbulence at the time of ignition.
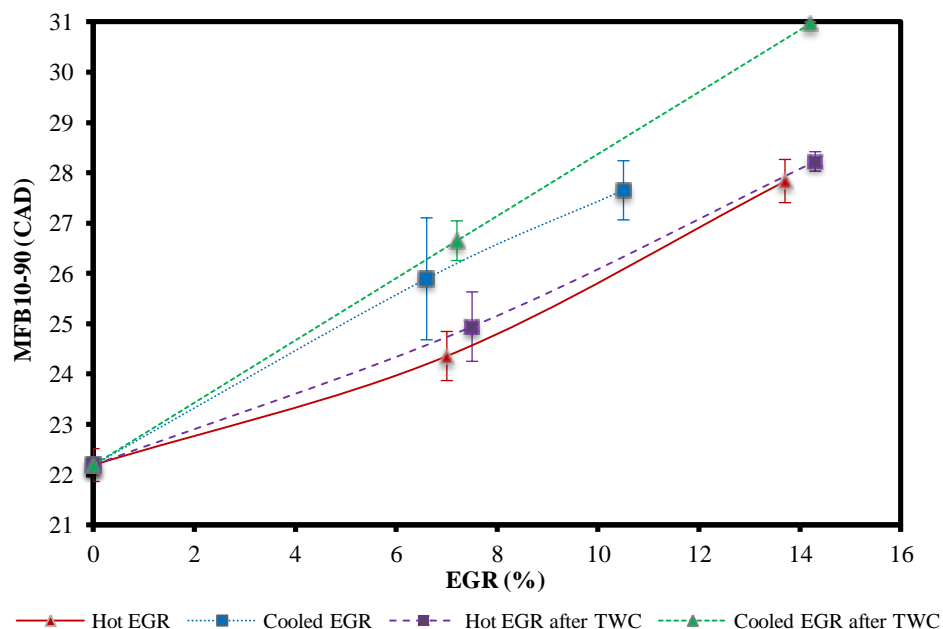
Figure 4-13   MFB10-90 versus EGR ratio at KLMBT spark timings

4.3.2.5 Fuel Consumption

Gravimetric $ISFC_{net}$ at the KLMBT spark timings decreased for all EGR types as shown in Figure 4-14. The fuel consumption reductions were due to MFB50 advances for the cooled EGR, hot EGR after TWC and cooled EGR after TWC EGR types, along with pumping loss reductions and thermal efficiency improvements (reduced in-cylinder temperatures), as explained in the first part of Chapter 4. It must be noted that if the hot and cooled EGR after TWC EGR types had used a real TWC rather than a simulated TWC then their fuel consumption would have been higher across the EGR range due to the increased back-pressure resulting from a real TWC increasing the pumping losses.

Overall, the fuel consumption decreased by 1.8, 3.8, 1.6 and 2.9%, respectively, across the EGR range, for the hot EGR, cooled EGR, hot EGR after TWC and cooled EGR after TWC EGR types. Despite these fuel consumption reductions observed, it must be noted that the VAF had an average error of 1.6%, as discussed, therefore, the reduction of 1.6% observed across the EGR range for the hot EGR after TWC condition is limited, because it could have resulted from this error. The reductions for the other EGR types are however not considered to be limited. Again, KLMBT spark timing advances would likely have been greater if intake manifold temperature increases, resulting from the EGR addition, could have been eliminated. Thus, the fuel consumption improvements would likely have been greater.

The fuel consumption reduction was greatest for the cooled EGR condition despite the limited EGR that could be achieved, because its MFB50 (Figure 4-12) was further advanced by the EGR addition and consequent spark advances than that of the other EGR types. In addition, its combustion duration (Figure 4-13) did not increase as significantly as that of the cooled EGR after TWC EGR type, improving the conversion efficiency of heat and pressure into piston work through improved combustion phasing. The next greatest fuel consumption

reduction achieved was for cooled EGR after TWC. This is because the KLMBT spark timing advance (Table 4-4) was the greatest, therefore allowing the MFB50 to be advanced closer to its optimum phase (Figure 4-12). Fuel consumption reductions were achieved with hot EGR despite its MFB50 becoming retarded with EGR addition (Figure 4-12). This is because its PMEP was significantly reduced across the EGR range (Figure 4-15) and it reduced in-cylinder temperatures significantly (Figure 4-10a) which improved thermal efficiency.

The hot EGR after TWC EGR type achieved fuel consumption improvements of lesser magnitude than the cooled EGR and cooled EGR after TWC conditions because its KLMBT spark timing could not be advanced as much, meaning its MFB50 (Figure 4-12) was more retarded than those of the cooled EGR and cooled EGR after TWC EGR types. At 7% EGR, its MFB50 was more advanced than that of the cooled EGR after TWC EGR type (Figure 4-12) and its PMEP was lower (Figure 4-15), but its fuel consumption was still higher. It is proposed that this was due to the higher peak of the calculated average in-cylinder temperature (1844˚C) compared to that of the cooled EGR after TWC EGR type (1823˚C), as shown in Figures 4-10c and 4-10d, respectively. It is thought that this increased heat transfer to the combustion chamber walls, reducing the thermal efficiency, thus causing the fuel consumption to be higher.

Hot EGR had lower fuel consumption at the maximum EGR addition of 14% than the hot EGR after TWC EGR type. Despite this observation, it is not considered to be significant considering it is within the margin of error, as indicated by the relevant confidence intervals (Figure 4-14). For the cooled EGR and cooled EGR after TWC EGR types, the fuel consumption reduction became less significant as the EGR addition was increased from 7% to its maximum, as compared to that achieved as the EGR addition was increased from 0 to

7%. This observation is also not considered to be significant because it is within the margins of error, as indicated on the figure.

If the intake plenum temperature increases (Figure 4-18) could have been eliminated, it is believed that the fuel consumption improvements would have been greater, especially for hot EGR, due to the greater KLMBT spark timing advances and thus more optimized MFB50 that would be expected.
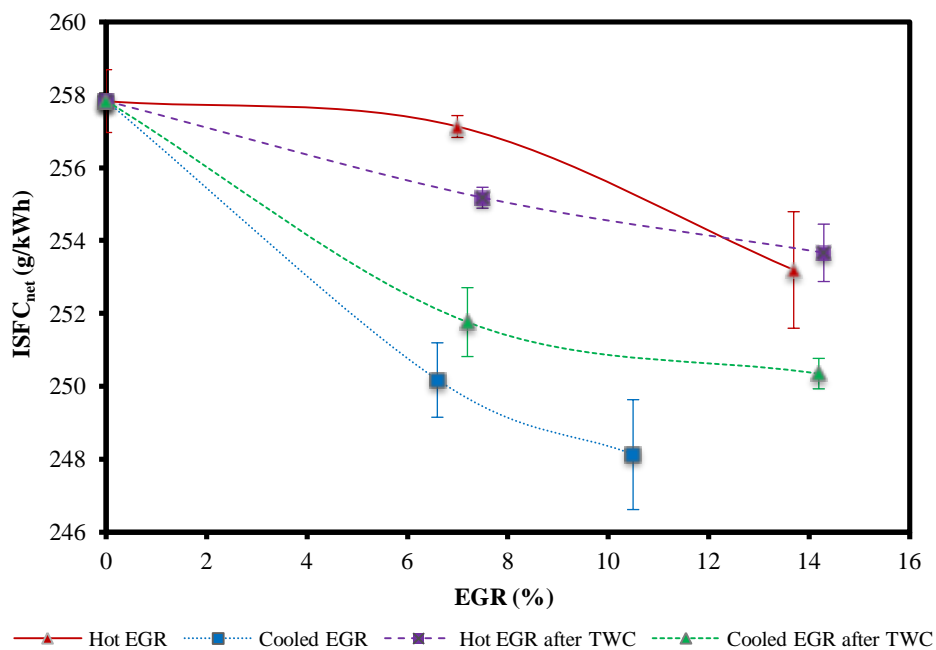
Figure 4-14   Gravimetric ISFC$_{net}$ versus EGR ratio at KLMBT spark timings

4.3.2.6 PMEP

The PMEP at the KLMBT spark timings, as shown in Figure 4-15, decreased for all of the EGR types across the EGR range, because as mentioned, the throttle valve had to be opened more to provide the same amount of fresh air as in the non-EGR case, or in other words, the same amount of oxygen for combustion.

It is proposed that the greatest reduction across the EGR range was achieved with the hot EGR condition because the intake plenum temperature increased the most (Figure 4-18). This

caused the intake air to become less dense meaning that the throttle had to be more opened in order to maintain a stoichiometric mixture than it did with the other EGR types, thus causing the pumping losses to reduce more significantly. For hot and cooled EGR, the reduction was greatest as the EGR was increased from 7% to its maximum, whereas the greatest reduction for hot and cooled EGR after TWC occurred as the EGR was increased from 0 to 7%. It is thought that the more significant increase in intake plenum temperature (Figure 4-18) for hot EGR, as the EGR addition was increased from 7 to 14%, meant that the throttle had to be opened more than when the EGR addition was increased from 0 to 7%, resulting in the observed behaviour. The observed behaviour for the cooled EGR condition is within the margin of error as indicated by the confidence intervals; therefore, it is not considered to be significant.

Pumping work was greater for the cooled EGR after TWC EGR type than the hot EGR after TWC EGR type. It is proposed that this is due to its lower intake plenum temperature (Figure 4-18). This meant that the intake air was denser so the throttle had to be opened less to allow the same amount of fresh air into the combustion chamber as with the hot EGR after TWC EGR type, thus increasing the pumping work in comparison. It must be noted that if the hot and cooled EGR after TWC EGR types had used a real TWC rather than a simulated TWC, their PMEP would have been greater across the EGR range due to the increased back-pressure resulting from a real TWC increasing the pumping losses.

The PMEP reduction would likely have been less significant if intake manifold temperature increases, resulting from the EGR addition, could have been eliminated. This is because the intake air would have become denser, necessitating the throttle to be more closed to allow the same amount of fresh air into the combustion chamber, thus increasing the pumping work.
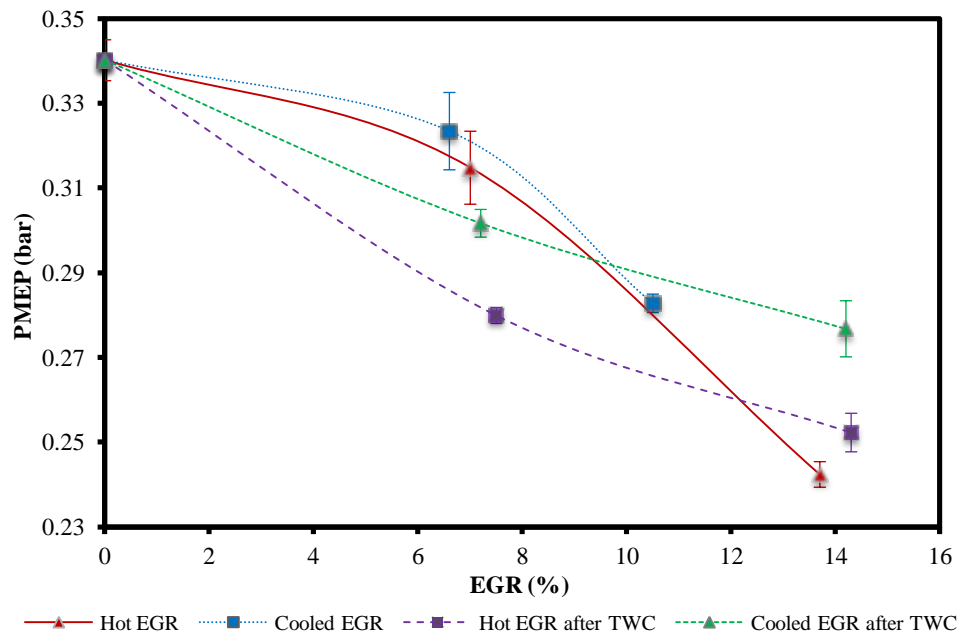
Figure 4-15   PMEP versus EGR ratio at KLMBT spark timings

4.3.2.7 EGT

The EGT at the KLMBT spark timings decreased significantly for all of the EGR types across the EGR range, as shown in Figure 4-16. Overall, it decreased by 40.4, 41.6, 46.9 and 52.1°C for the EGR types of hot EGR, cooled EGR, hot EGR after TWC and cooled EGR after TWC, respectively. This is because the KLMBT spark timing advances (Table 4-4) resulted in the pressure and heat from combustion being more efficiently converted into piston work, as discussed.

The temperatures reduced for hot EGR despite its MFB50 becoming later. It is proposed that the earlier KLMBT spark timing (Table 4-4) resulted in the energy from the fuel being released earlier. This resulted in energy being more efficiently converted from the combustion in piston work, despite the slightly later MFB50 (Figure 4-12) and the longer combustion duration (Figure 4-13) across the EGR range, resulting in reduced EGTs across the EGR range.

At 10% EGR addition, the greatest reductions were observed for cooled EGR. It is thought that this is because its MFB50 (Figure 4-12) was the most advanced at 10% EGR addition, meaning that the pressure and heat from the combustion was more efficiently converted into piston work. This caused the EGT to decrease more than with the other EGR types which had a later MFB50 at 10% EGR addition. Cooled EGR after TWC then hot EGR after TWC had the next greatest rate of reduction across their tested EGR ranges. Again, this can be explained by the more advanced MFB50 for the cooled EGR after TWC EGR type as compared to the hot EGR after TWC EGR type (Figure 4-12).

Again, KLMBT spark timing advances would likely have been greater if intake manifold temperature increases, resulting from the EGR addition, could have been eliminated. This would have likely resulted in greater EGTs decreases across the EGR range, as discussed previously.
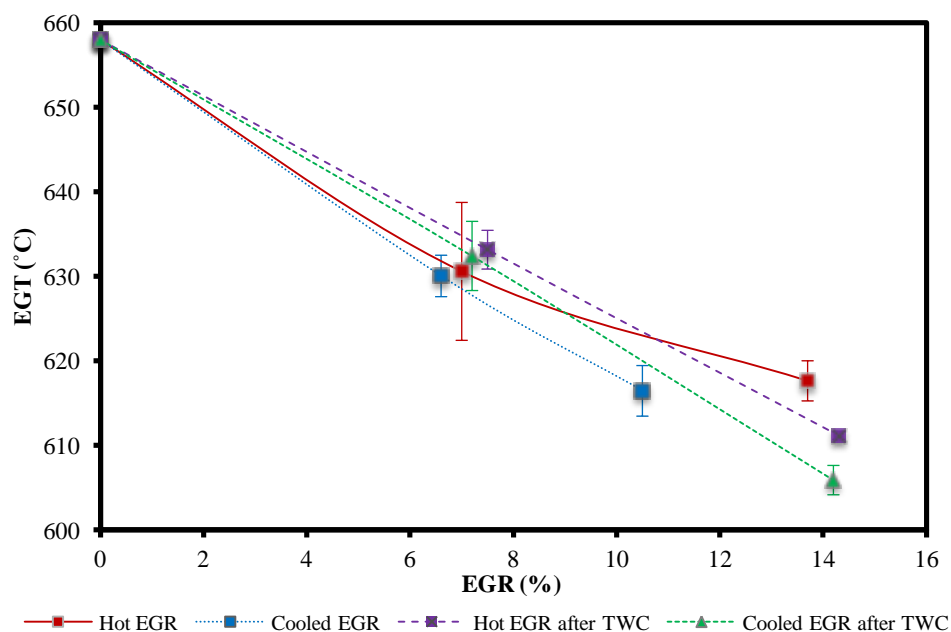
Figure 4-16   EGT versus EGR ratio at KLMBT spark timings

4.3.2.8   COV_{IMEP}

The COV_{IMEP} at the KLMBT spark timings increased significantly across the EGR range for all of the EGR types, as shown in Figure 4-17. It is proposed that this is because the combustion speed was reduced across the EGR range (Figure 4-13) which meant that the flame was more affected by the airflow in the combustion chamber, thus increasing the COV_{IMEP} observed. As can be seen from the confidence intervals indicated on the figures, the differences between the different EGR types could have resulted from experimental error, therefore, they will not be commented upon further.

As discussed, it is believed that the combustion duration would have been slightly increased if the intake manifold temperature increases could have been eliminated. This would be expected to increase the COV_{IMEP} slightly because the flame would be more affected by the airflow in the combustion chamber.
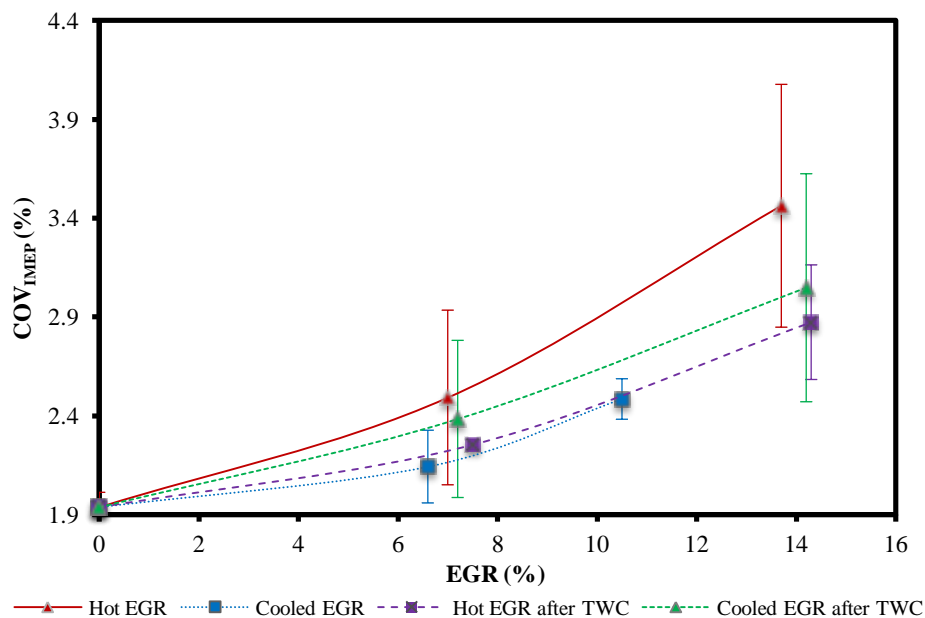
Figure 4-17 COV_{IMEP} versus EGR ratio at KLMBT spark timings

4.3.2.9 Intake Plenum Temperature

The intake plenum temperature at the KLMBT spark timings, as shown in Figure 4-18, increased significantly across the EGR range for all of the EGR types. This was expected for the hot EGR and hot EGR after TWC EGR types but it was less expected for the cooled EGR and cooled EGR after TWC EGR types. It is proposed that the cooled EGR gases were not as cold as the engine fresh intake air, therefore causing the intake plenum temperatures to increase. The intake temperatures are still lower for the cooled EGR types as compared to the hot EGR types, as is to be expected. Any further relative differences between the different EGR types are not considered to be significant as can be seen from the confidence intervals displayed on the figure.
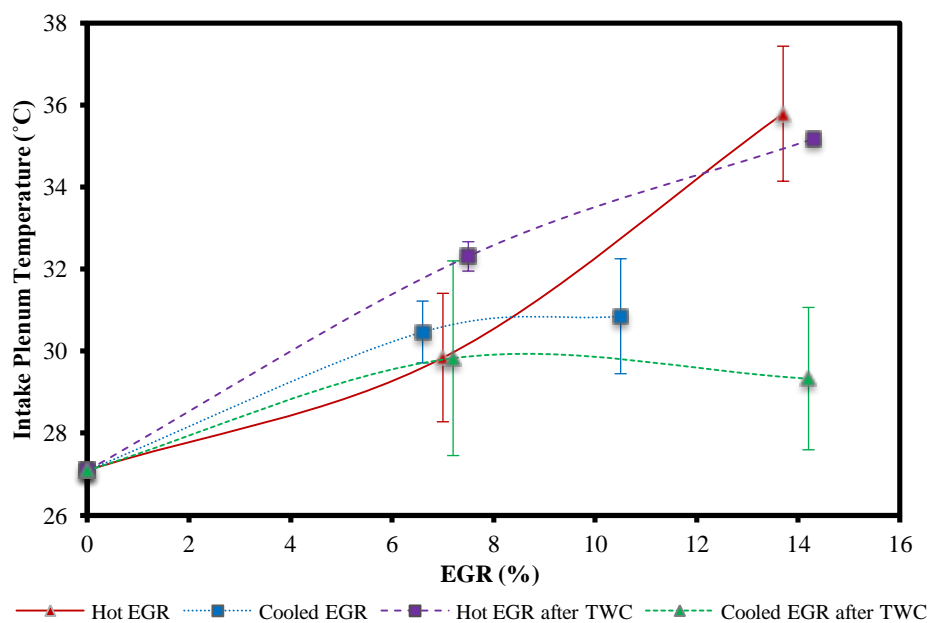
Figure 4-18   Intake plenum temperature versus EGR ratio at KLMBT spark timings

4.3.2.10 Gaseous Emissions (NO$_x$ and HC)

The NO$_x$ emission at the KLMBT spark timings, as shown in Figure 4-19, decreased significantly by 50.5, 31.3, 43.7 and 45.3% across the EGR range for the hot EGR, cooled EGR, hot EGR after TWC and cooled EGR after TWC EGR types, respectively. It is proposed that the reduced calculated average in-cylinder temperatures across the EGR range (Figures 4-10a-d) resulted in a reduced oxidation rate of in-cylinder nitrogen gas in the hot flames, resulting in the observed behaviour.

The reduction was greatest for hot EGR, similar for hot and cooled EGR after TWC, and it was the least for cooled EGR. It is thought that this is because the MFB50 (Figure 4-12) became later for hot EGR across the EGR range. The MFB50 for cooled and hot EGR after TWC were similar across the EGR range therefore explaining why their NO$_x$ emission was similar, while the MFB50 was the most advanced for the cooled EGR condition, resulting in the highest NO$_x$ emission across the EGR range. With an advanced MFB50, the fuel-air mixture burns at an earlier point in the engine cycle where the in-cylinder turbulence is stronger, causing the combustion to proceed more quickly. It is thought that this resulted in higher local temperatures which resulted in the differences in NO$_x$ emissions between the different EGR types across the EGR range. While there were differences in the peaks of the calculated average in-cylinder temperatures for the different EGR types (Figure 4-10a-d), it is thought that the differences in MFB50 and their subsequent effects on local in-cylinder temperatures were more significant regarding the NO$_x$ behaviour. This is because the average temperature differences were relatively small (~40°C at maximum EGR additions).

As discussed, it is not believed that the intake manifold temperature increases with EGR addition had a significant effect on the peak calculated average in-cylinder temperatures.

Therefore, it is not thought that the NO_x emission was significantly affected by the intake manifold temperature increases.
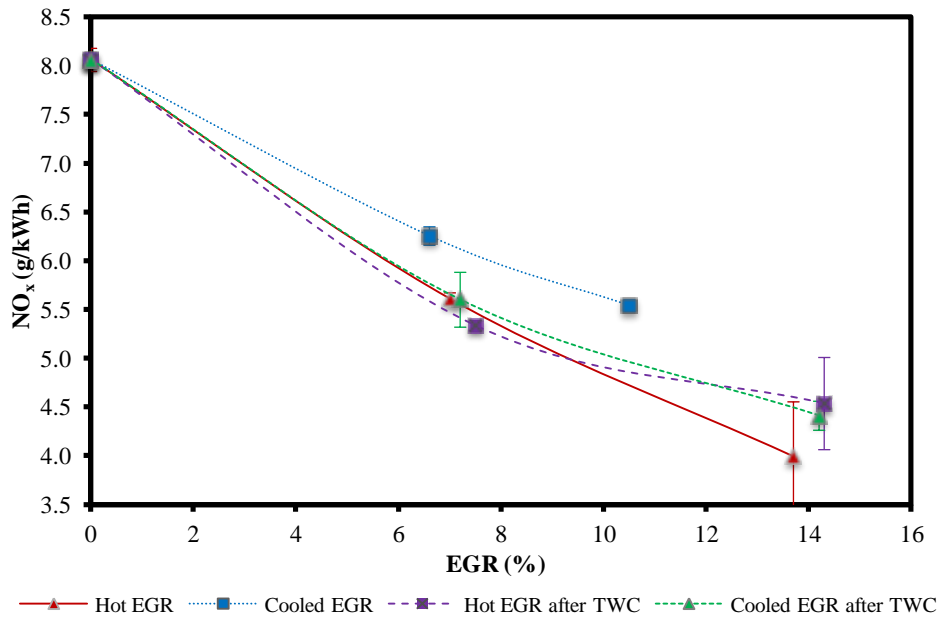
Figure 4-19 NO_x emissions versus EGR ratio at KLMBT spark timings

The HC emission at the KLMBT spark timings significantly increased across the EGR range for all of the EGR types tested, as shown in Figure 4-20. It was increased by 14.7, 11.0, 12.9 and 10.1% for the four respected EGR types of hot EGR, cooled EGR, hot EGR after TWC and cooled EGR after TWC. It is thought that the in-cylinder temperature (Figures 4-10a-d) and EGT decreases across the EGR range (Figure 4-16) reduced the oxidation of HCs for all of the EGR types in the engine cylinder and exhaust, respectively, leading to the HC increases across the EGR range. Also, the increased combustion duration (Figure 4-13) reduced the time available for post-combustion oxidization of HCs for all of the EGR types, contributing to their increases across the EGR range.

The increase was greatest for hot EGR, followed by hot EGR after TWC, then cooled EGR, then cooled EGR after TWC. It is proposed that the later MFB50 for hot EGR and hot EGR after TWC across the EGR range (Figure 4-12) reduced the time for post-combustion

oxidation, causing their HC emission to increase the most. Although the MFB50 for the cooled EGR condition was more advanced than that of the hot and cooled EGR after TWC conditions, its HC emission across its EGR range of 0 to 10% was similar to that of the hot EGR after TWC condition and higher than that of the cooled EGR after TWC condition within the same 0 to 10% EGR range. This is because it introduced additional HCs into the combustion chamber while the hot and cooled EGR after TWC conditions did not, because the simulated EGR gas was taken from the gas bottle. Therefore, the additional HCs reduced the oxidation of the HCs in the combustion chamber producing the higher than expected HC emission. With a real TWC, most but not all of the HCs would have been removed from the EGR gas, resulting in a similar effect, although its significance would be reduced. It is proposed that the longer combustion duration for the cooled EGR after TWC condition as compared to the hot EGR after TWC condition (Figure 4-13) resulted in an improvement in HC oxidization because of the slower flame, reducing the emission in comparison.

As discussed in the first part of this chapter, it is not believed that the intake manifold temperature increases had a significant effect on the HC emissions observed. Again, despite the increases in HCs observed across the EGR range for the four EGR types tested, it would be expected that a traditional TWC would be able to handle this increase to maintain the vehicle-out HC emissions at non-EGR levels.
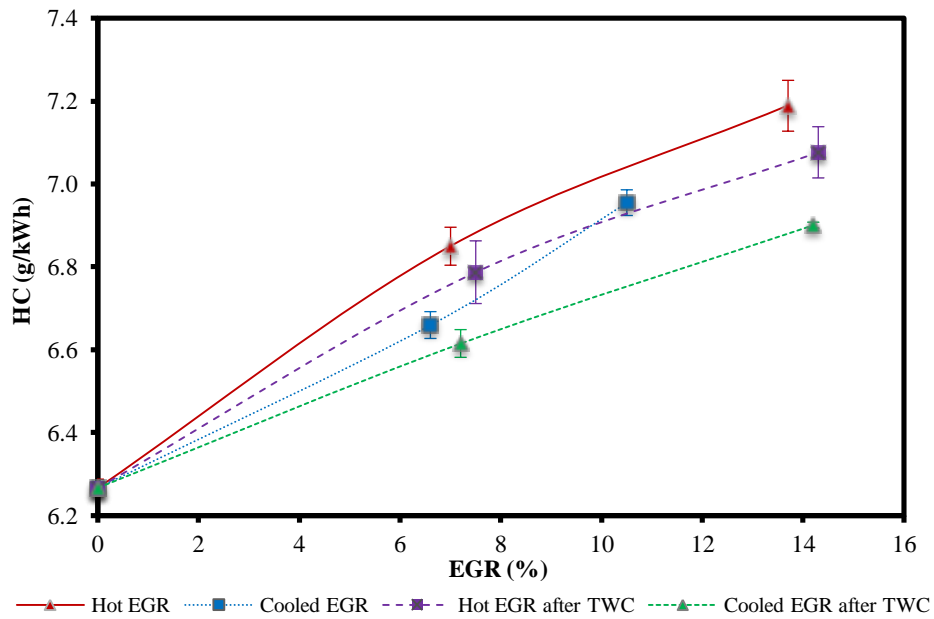
Figure 4-20   HC emissions versus EGR ratio at KLMBT spark timings

4.4 Data Continuity

For a detailed analysis regarding the continuity of the data between the first and second parts

of this chapter, please refer to **Appendix B1**.

4.5 Conclusions

The effect of hot EGR on the combustion and emissions of a single cylinder DISI research engine was investigated in this chapter and the following conclusions have been made.

1. KLMBT spark timing was advanced significantly by 18, 8, and 4 CAD for the three respective engine loads of 5.5, 7.0 and 8.5 bar IMEP, due to EGR suppressing the temperature rises in the end-zone of the combustion chamber.

2. Fuel consumption was reduced by 2.2, 4.1, and 1.0% for the three respective engine loads with EGR addition, because the pumping work was reduced for all engine loads and the KLMBT could be advanced towards its optimum phasing for the engine loads of 7.0 and 8.5 bar IMEP.

3. EGR addition increased the accumulation mode particles and reduced the nucleation mode particles for the loads of 5.5 bar IMEP (from 0 to 12% EGR addition) and 7.0 bar IMEP, because of the combustion temperature suppression effect of the EGR, and subsequent nuclei adsorption by the increased numbers of accumulation mode particles. However, the nucleation mode particle reduction for 7.0 bar IMEP was not significant and the accumulation mode particles reduced as the EGR was increased from 12 to 13% for the load of 5.5 bar IMEP. In addition, there was not a significant change in nucleation and accumulation mode particles for the load of 8.5 bar IMEP because of the low 3% maximum level of EGR achieved.

These main findings from this section are also summarized in Table 4-5.

Table 4-5   Results summary (EGR addition & engine load) (<mark>highlighted</mark>=improvement, <u>underlined</u>=worsening)

Result Summary / Engine Load (bar)	KLMBT	ISFC$_{net}$	EGT	PM Nucleation	PM Accumulation	NO$_x$	HC
5.5	18 CAD	2.2%	21.9°C	Reduction	<u>Increase</u>	64.3%	<u>48.3%</u>
7.0	8 CAD	4.1%	32.7°C	Reduction	<u>Increase</u>	50.9%	<u>19.0%</u>
8.5	4 CAD	1.0%	7.6°C	No sig. change	No sig. change	12.2%	<u>6.8%</u>

The effect of different EGR types of hot EGR, cooled EGR, HE after TWC and CE after TWC on the combustion and gaseous emissions of a single cylinder DISI research engine was also investigated in this chapter and the following conclusions have been made.

4. KLMBT spark timing was advanced significantly by 10, 10, 12 and 14 CAD, respectively, for the four EGR types, due to EGR suppressing the temperature rises in the combustion chamber end-zone; cooler EGR gases and the removal the NO from the EGR gases accounted for the differences between the different EGR types.

5. Fuel consumption was reduced by 1.8, 3.8, 1.6 and 2.9% for the four respective EGR types, because pumping losses were reduced for all EGR types and the MFB50 could be advanced towards its optimum phasing for most EGR types.

6. The NO$_x$ emission was reduced significantly by 50.5, 31.3, 43.7 and 45.3% across the EGR range for the four respective EGR types, due to the temperature suppression effect of the EGR gases. MFB50 combustion phasing differences resulting from the different KLMBT spark timing advances achieved accounted for the differences between the different EGR types.

7. Overall, if fuel consumption is the priority than the cooled EGR type is the best EGR type, while if emission reduction (NO$_x$ and HC) is the priority than cooled EGR after TWC is the best EGR type.

The main findings from this section are also summarized in Table 4-6.

Table 4-6   Results summary (EGR addition & EGR type) (highlighted=improvement, underlined=worsening)

Result Summary ⟍ EGR Type	KLMBT	ISFC$_{net}$	EGT	NO$_x$	HC
Hot EGR	10 CAD	1.8%	40.4°C	50.5%	14.7%
Cooled EGR	10 CAD	3.8%	41.6°C	31.3%	11.0%
HE after TWC	12 CAD	1.6%	46.9°C	43.7%	12.9%
CE after TWC	14 CAD	2.9%	52.1°C	45.3%	10.1%

Chapter 5

The Effect of Intake Airflow and Hot EGR on Engine Combustion and PM Emissions

The aim of this chapter is to provide details of the combustion and PM emissions characteristics of a DISI engine operated with swirl and tumble intake airflows, and with EGR addition, at a single engine load of 7.0 bar IMEP.

5.1 Introduction

The main combustion parameters investigated in this chapter are KLMBT spark timing, in-cylinder pressure, calculated average in-cylinder temperature, MFB, fuel consumption and exhaust temperature. PM is the emission parameter investigated.

There is an ever growing demand for reduction of PM emissions from engines, as emission regulations become stricter, particularly with the Euro VI regulation which has limited both particulate mass and size for the first time in DISI engines. It is well known that swirl and tumble have a significant effect on air-fuel mixture formation as well as on the combustion and emissions of IC engines. However, what is not well known is the effect they have on the formation of particulates in DISI engines, and what effect combining swirl and tumble with EGR has on the combustion and PM emissions. EGR suppresses the temperature rise in the combustion chamber, reducing NO_x emissions and allowing the KLMBT spark timing to be advanced, as well as enabling the throttle to be more opened, providing significant fuel economy benefits. However, swirl and tumble affect the speed of the combustion, which affects the laminar speed slowing effect of the EGR gases. Therefore, it is important to understand the influence of swirl and tumble, combined with EGR, on combustion and PM emissions. The Euro VI emissions regulation has increased interest in the role of EGR

addition on engine particulates, with the potential of EGR coming under question because of it has been observed to have a negative effect on particulates (Gill et al., 2011, Ma et al., 2014). Therefore, it is an important area to study.

Overall, the author recognizes an opportunity to extend the research of swirl and tumble in DISI engines further by investigating the effect of swirl and tumble, and EGR addition on PM emissions in this chapter. By doing this, it is hoped that the effect can be quantified in order to inform the engine design process in terms of the selection of swirl and tumble ratios, and the possible incorporation of a swirl/tumble valve into DISI engines to help achieve these at specific engine speeds and loads. The author also recognizes that the Euro VI emissions regulation has led many to question the potential of EGR, considering it is generally considered to increase engine particulates. Thus, this is another area researched further in this chapter.

5.2 Experimental Procedure

The experimental test procedure outlined in Section 3.9 of this thesis was followed in order to conduct the engine tests in the single-cylinder engine to collect the data presented and discussed in this chapter. Relative air-fuel ratio λ was maintained at 1 during the experiments and a COV_{IMEP} of 5% was not exceeded. Valve timings were set at IVO=16˚bTDC and EVC=36˚aTDC. KLMBT spark timings and a fixed geometric compression ratio of 11.5 were used. The baffle plates as shown and discussed in Section 3.2.7 were used to create the swirl and high tumble intake airflows in the engine, in addition to what is already produced by the relevant engine geometry, such as the design of the intake runner. As well as these two plates, another baffle plate was made with the same profile as the intake runner, so that a reference low tumble condition could be tested with the same intake geometry as the swirl

and high tumble conditions. The estimated swirl/tumble ratios for the three baffle plates are provided in Table 3-2. In order to achieve hot EGR in the engine, and in order to achieve the desired engine load and EGR addition, the equipment setup and test procedure outlined in Section 3.2.6.1 was followed.

The load of 7.0 bar IMEP was chosen to study because it represents a medium-high load in this engine, and while it produces knock, the knock produced is of a lower magnitude than that at higher engine loads, allowing swirl and tumble to be studied without causing any significant engine damage. It also allowed a reasonable, while not a high EGR addition of 14% to be achieved. A higher engine load would have meant that the throttle would have needed to be more opened, thus reducing the maximum level of EGR that could have been achieved. One load was chosen to study so that an in-depth understanding could be formed, which would not be possible if multiple loads were studied with the different intake airflows. The spark was swept for each intake airflow condition and EGR ratio in order to find the KLMBT spark timing using the MatLab script pressure trace analysis technique outlined in Section 3.6.9. A research grade gasoline was used to obtain the results in this chapter with the properties outlined in Section 3.8. The SMPS 3936 was used to obtain the PM emission results in this chapter. Gaseous emissions were not measured in this chapter because it is believed that the literature sufficiently covers this area.

The test matrix provided in Table 5-1 was carried out in order to investigate the intake airflow and EGR effect on engine combustion and PM emissions at the single engine load of 7.0 bar IMEP.

Table 5-1   Experiment test matrix (intake airflow & EGR addition)

EGR Addition (%) Intake Air-Flow	0	4	7	8	10	11
Low Tumble	1	2		3		4
Swirl	5	6		7		8
High Tumble	9	10	11			

5.3 Results and Discussion

5.3.1 KLMBT Spark Timings

From the KLMBT spark timings, as shown in Table 5-2 for the different intake airflow conditions, it can be seen that the spark was retarded for the swirl and high tumble conditions, as compared to the low tumble condition; the high tumble condition being the most retarded. Overall, the increased turbulence produced in the swirl and high tumble conditions (CID was reduced by ~1 CAD with greater reductions observed with EGR addition) as compared to the baseline low tumble condition meant that the spark timing had to be retarded in order for the turbulence and thus combustion speed to decay in order to avoid knock. Although the additional turbulence was allowed to dissipate somewhat by retarding the spark timing, it is still believed to have improved mixture formation more significantly than spark retardation alone would have done, which will be explored further in the emissions section.

From the MFB data (Figure 5-3a) it can be seen that the combustion duration was longer for the swirl condition than it was for the low tumble condition (MFB was ~24.0 CAD for the swirl condition and it was ~22.5 CAD for the low tumble condition, at 0% EGR addition). Therefore, it is thought that this provided more time for the temperature to rise in the end-zone of the combustion chamber, producing auto-ignition, resulting in the retarded KLMBT

spark timing for the swirl condition. It must be noted that knocking could have been avoided if the compression ratio was fully optimized for the fuel used, as discussed previously.

For the high tumble condition, it is proposed that the velocity of the intake air was increased significantly, causing the fuel-air mixture to burn much more quickly (MFB10-90 was ~21.0 CAD, compared to ~22.5 and ~24.0 CAD for the low tumble and swirl conditions, respectively, at 0% EGR addition). It is believed that this increased the amount of heat radiated to the fuel-air mixture in the end-zone of the combustion chamber which caused knock to be initiated at an earlier spark timing than for the other two intake airflow conditions, necessitating the KLMBT spark timing to be retarded in comparison. It is proposed that this effect was more significant than the faster flame speed, which does not appear to have been fast enough to consume the auto-ignition site before it auto-ignited. This evident relationship between flame speed and knock tendency should be investigated further to find the optimum flame speed for minimum knock.

The end-zone temperatures were reduced (allowing the calculated average in-cylinder temperatures to be maintained or their reductions minimized (Figures 5-2b, 5-2c and 5-2d)) by the combustion slowing effects of the EGR addition (Rhodes and Keck, 1985). This allowed the spark timing to be advanced to an earlier point in the engine cycle where the in-cylinder turbulence was stronger, cancelling out the effect EGR had on the laminar flame speed, preventing engine knock that otherwise would have occurred.

At the high tumble condition with 0% EGR addition, the combustion was faster than with the other two intake airflow conditions, as mentioned. This meant that good KLMBT spark timing improvements could be made with EGR addition. Although EGR addition will have allowed the KLMBT spark timing to be advanced at the low tumble and swirl conditions too,

it is proposed that the effect was greater with the high tumble condition. This is because its KLMBT spark timings started further away from the optimal condition which meant that greater (or equal) improvements in the KLMBT spark timing could be made at equivalent EGR additions.

KLMBT spark timing advances would have been greater if the intake manifold temperature increases resulting from the EGR addition could have been eliminated, as discussed previously.

Table 5-2   KLMBT spark timings (°bTDC) (intake airflow & EGR addition)

EGR Addition (%) Intake Air-Flow	0	4	7	8	11
Low Tumble	16	20		24	26
Swirl	8	10		12	14
High Tumble	-2	2	6		

5.3.2 In-cylinder Pressure and Temperature

The in-cylinder pressure data at 0% EGR addition presented in Figure 5-1a shows that the in-cylinder pressure significantly decreased with the swirl and high tumble conditions, as compared to the low tumble condition. This was due to the significant spark retard required (Table 5-2), causing more energy to be released from the fuel during the expansion stroke, once the in-cylinder pressure was already reducing. Therefore, this energy did not contribute to the in-cylinder pressure increases, resulting in the in-cylinder pressure decreases observed.

The in-cylinder pressures across the EGR ranges, as presented in Figures 5-1b, 5-1c and 5-1d, for the low tumble, swirl and high tumble conditions, respectively, generally increased across the EGR range. The reason for the increases observed are the advances in the KLMBT spark

timing achieved with the EGR addition, releasing more of the energy from the fuel at an earlier point in the engine cycle where it could contribute to the in-cylinder pressure increases. However, for the maximum EGR addition of 11% at the low tumble and swirl conditions, the in-cylinder pressure reduced. This is because the KLMBT spark timing advance achieved with EGR addition was not sufficient at these conditions to overcome the combusiton slowing effects of the additional EGR gases (Rhodes and Keck, 1985).

In-cylinder pressure increases with EGR addition will likely have been greater if the intake manifold temperature increases could have been eliminated, due to the greater KLMBT spark timing advances that would be expected.

Fig. 5-1a: In-cylinder Pressure (three airflow conditions)
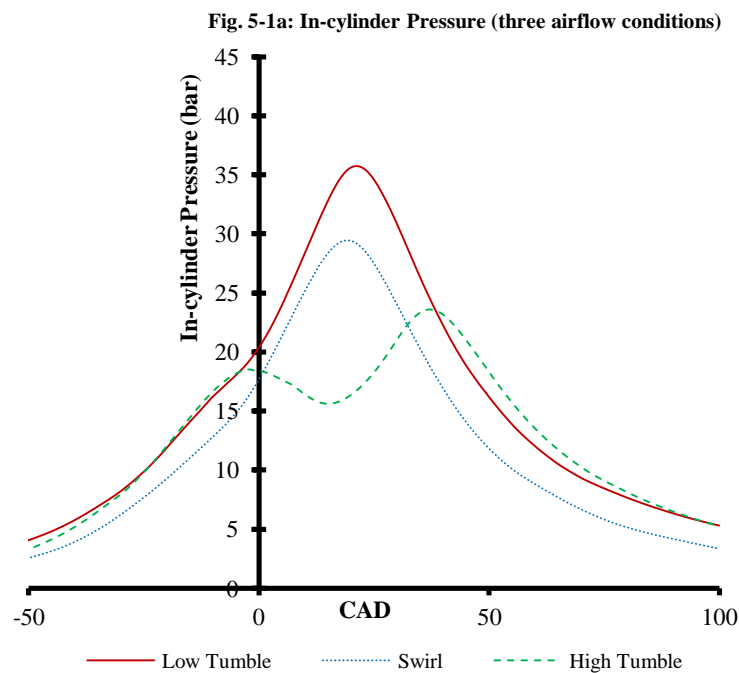
Fig. 5-1b: In-cylinder Pressure (low tumble)

—— 0% EGR	········ 4% EGR
- - - 8% EGR	- - - 11% EGR

Fig. 5-1c: In-cylinder Pressure (swirl)

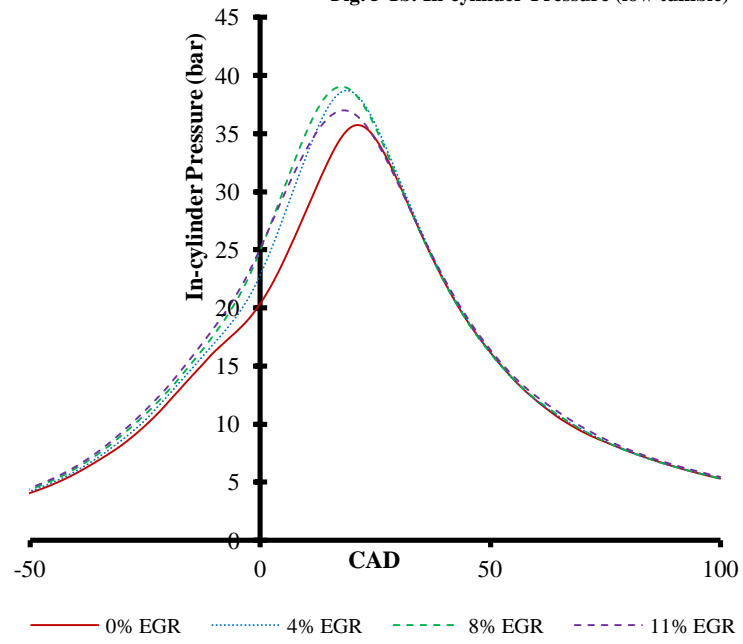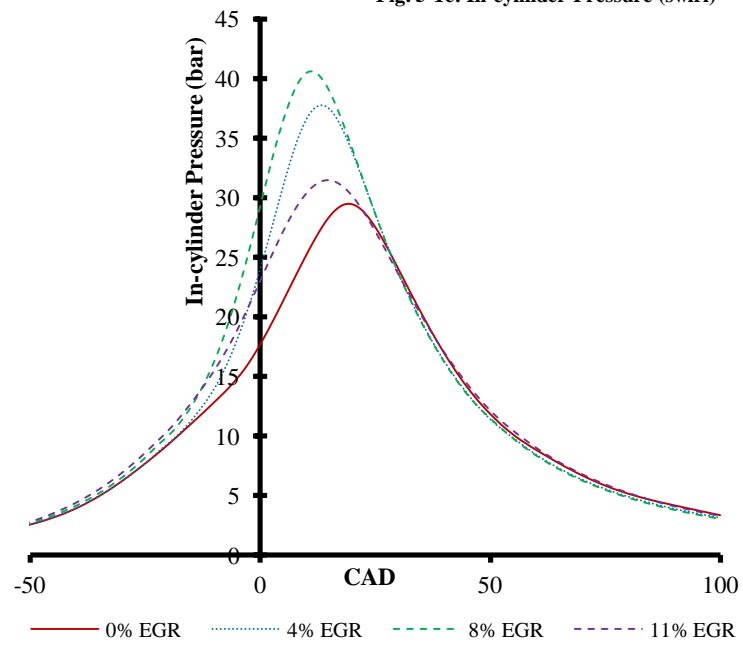|	
—— 0% EGR	········ 4% EGR
- - - 8% EGR	- - - 11% EGR

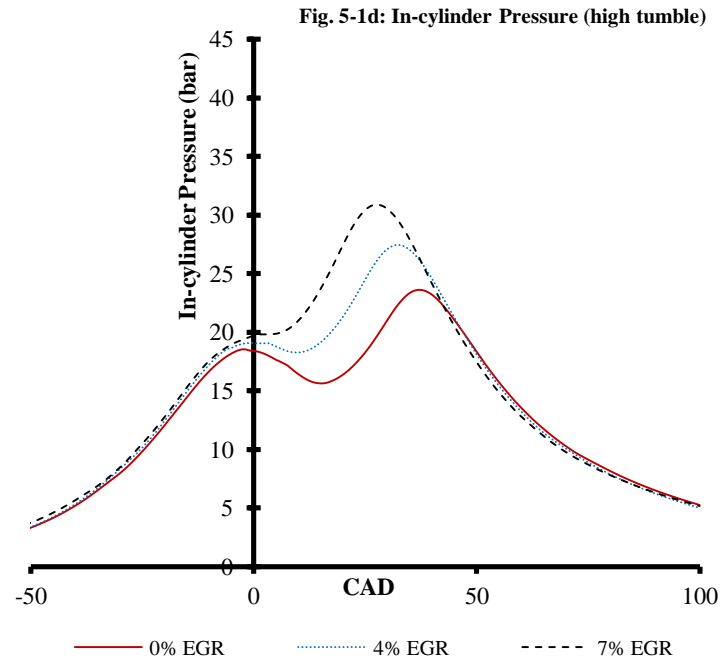Fig. 5-1d: In-cylinder Pressure (high tumble)

Figure 5-1   In-cylinder pressure verses CAD at KLMBT spark timings for **a)** the three intake airflow conditions at 0% EGR, **b)** low tumble, **c)** swirl, **d)** high tumble

The calculated average in-cylinder temperature profile at 0% EGR, as presented in Figure 5-2a, was approximately the same for the swirl condition as it was for the low tumble condition, although it was slightly retarded in comparison. The KLMBT spark timing had to be retarded for the swirl condition as compared to the low tumble condition (Table 5-2), resulting in the observed behaviour. For the high tumble condition, the calculated average in-cylinder temperature significantly increased compared to the other two intake airflow conditions, due to the faster combustion, as discussed previously. This significantly increased the rate that heat was released from the fuel, resulting in the increased calculated average in-cylinder temperature. The calculated average in-cylinder temperature profile for the high tumble condition was also retarded in comparison, because of its KLMBT spark timing retard (Table 5-2).

There was no significant change in the magnitude of the calculated average in-cylinder temperatures across the EGR range for the low and high tumble conditions as shown in

Figures 5-2b and 5-2d. As discussed, the EGR addition allowed the KLMBT spark timing to be advanced through suppression of end-zone temperatures, which appears to have overcome the combustion temperature reducing effects of the EGR gases. They have a higher heat capacity than the fresh air they replaced in the engine cylinder thus without advancing the spark timing, the calculated average in-cylinder temperatures would have decreased. However, the spark advance allowed them to be maintained across the EGR range by releasing the heat earlier from the fuel. At 4 and 8% EGR addition for the low tumble intake airflow it appears that the KLMBT spark timing advance was sufficient to increase the calculated average in-cylinder temperatures causing the increases observed at these conditions. For the swirl condition, as shown in Figure 5-2c, the KLMBT spark timing advances were not sufficient to maintain the calculated average in-cylinder temperatures, thus resulting in the decreases observed across the EGR range.

It is believed that the increased intake manifold temperatures resulting from the EGR addition were compensated for by the less optimized combustion phasing resulting from the consequently reduced KLMBT spark timing advance (Table 5-2), compared to the maximum spark advance possible, as discussed in the first part of Chapter 4. Thus, it is thought the two effects of increased intake manifold temperature and reduced subsequent KLMBT spark timing advances cancelled one another out, meaning there was no overall effect on the peak of the calculated average in-cylinder temperatures.

Fig. 5-2a: In-cylinder Temperature (three airflow conditions)

Low Tumble   Swirl   High Tumble

Fig. 5-2b: In-cylinder Temperature (low tumble)

0% EGR   4% EGR   8% EGR   11% EGR
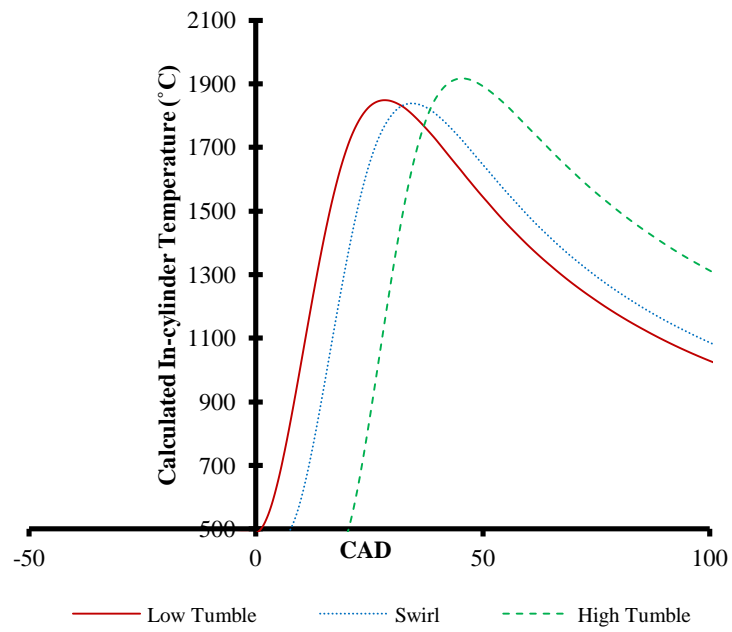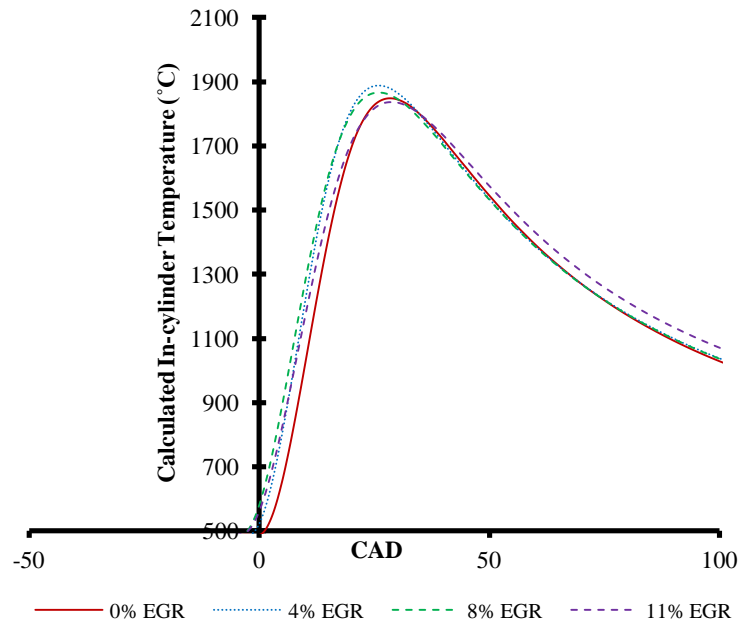
161

Fig. 5-2c: In-cylinder Temperature (swirl)

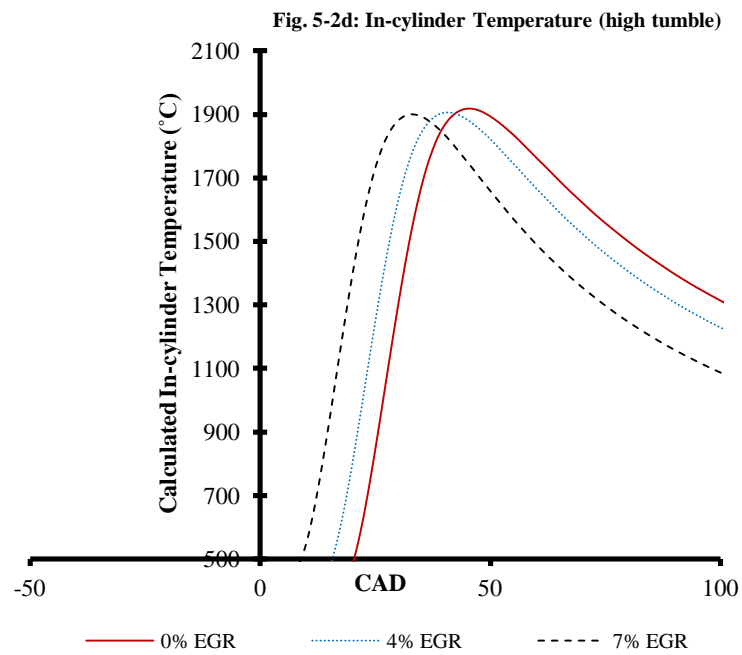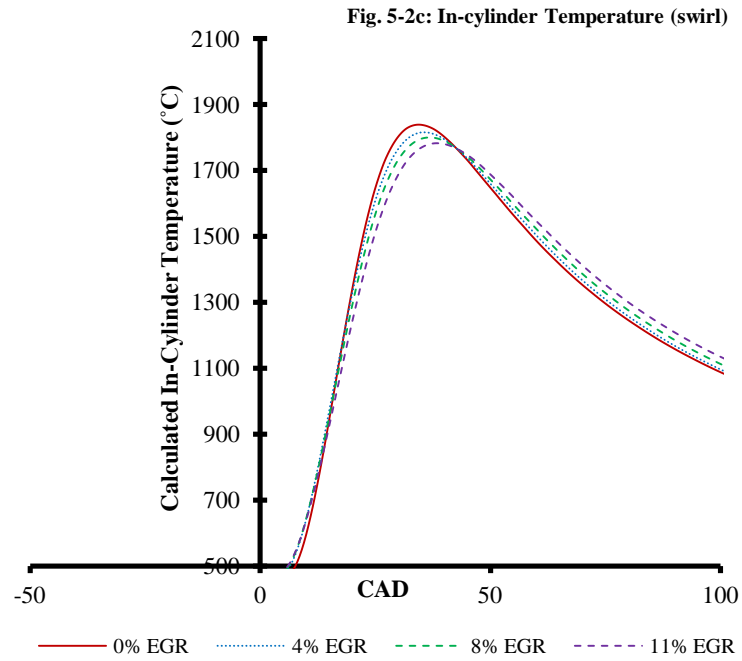Fig. 5-2d: In-cylinder Temperature (high tumble)

Figure 5-2   Calculated average in-cylinder temperature verses CAD at KLMBT spark timings for **a)** the three intake airflow conditions at 0% EGR, **b)** low tumble, **c)** swirl, **d)** high tumble

5.3.3 MFB

The low tumble and swirl intake airflow conditions had similar MFB profiles, as shown in Figure 5-3a at 0% EGR addition, despite the retarded spark timing for the swirl condition as compared to the low tumble condition. The swirl condition increased the speed of the initial flame propagation compared to the low tumble condition by approximately 1 CAD, causing the MFB50s at 0% EGR to be very similar. (Nagayama et al., 1977) also observed a similar effect. However, the later stage of combustion appears to have been longer for the swirl condition. This is most likely due to the breakdown of the swirl flow into weak general in-cylinder turbulence. The high tumble condition in comparison had a significantly retarded MFB profile compared to the low tumble and swirl conditions, despite its initial flame propagation also being quicker. This was due to its retarded KLMBT spark timing (Table 5-2). Unlike the swirl condition, it does not appear to suffer from the longer late stage of combustion.

The MFB data, presented in Figures 5-3b, 5-3c and 5-3d for the three respected intake airflow conditions of low tumble, swirl and high tumble, shows that the MFB profile generally became advanced with EGR addition. This is because the KLMBT spark timing could be advanced (Table 5-2), as explained in the first part of Chapter 4. It can be seen in Figure 5-3b for the low tumble condition that 11% EGR addition resulted in a significantly increased combustion duration. Therefore, it appears that the KLMBT spark advance achieved was not sufficient to overcome the combustion slowing effects of the additional EGR, at this condition. A similar effect occurred with the swirl intake airflow condition, but rather than increasing the overall combustion duration, it produced a significantly slower earlier stage of combustion than observed at lower EGR additions and a similar overall combustion duration.

Therefore, the additional EGR appears to have had a significant effect on this early stage of combustion, while not affecting the overall combustion duration.

Again, KLMBT spark timing advances would likely have been greater if intake manifold temperature increases, resulting from the EGR addition, could have been eliminated. Thus, the MFB profiles would likely have been advanced slightly in comparison to those shown in Fig. 5-3b-d. In addition, it is expected that the flame would spread slightly more slowly in the cooler charge, thus, the MFB profile would become slightly more elongated. If the compression ratio was optimised for the fuel used, the combustion phasing would have been optimised for each test point, therefore, it would be expected that the combustion of gasoline would have been quicker due to higher in-cylinder turbulence at the time of ignition.
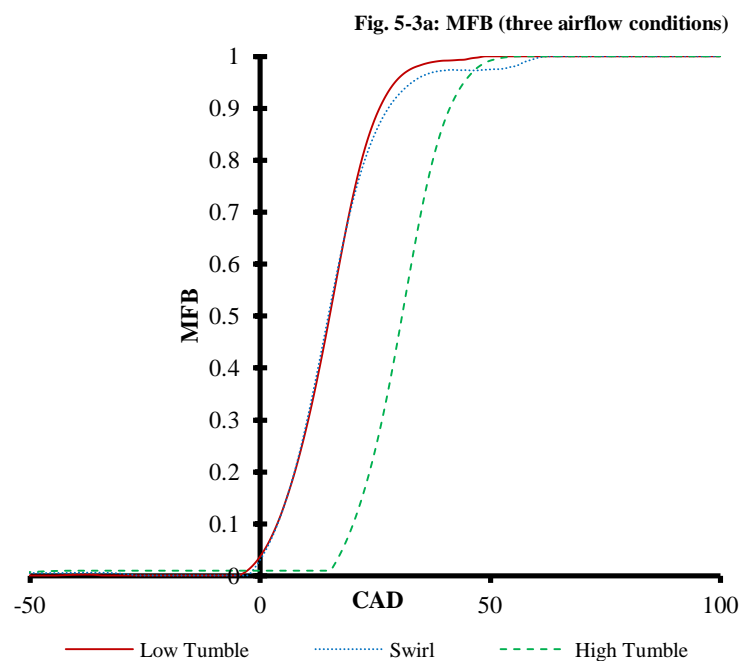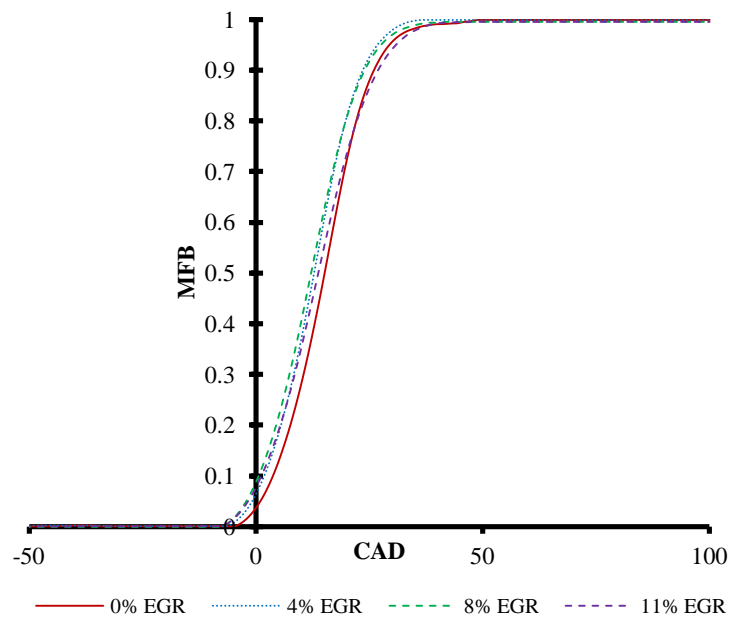

Fig. 5-3a: MFB (three airflow conditions)
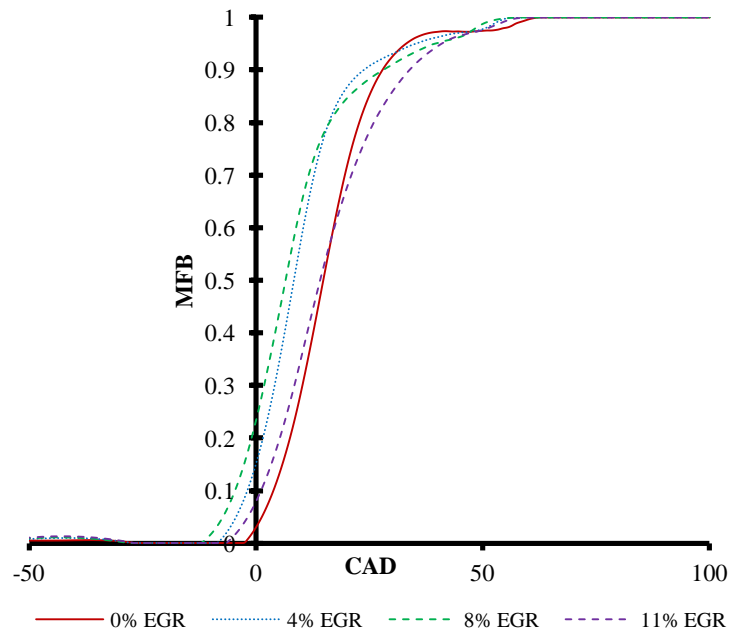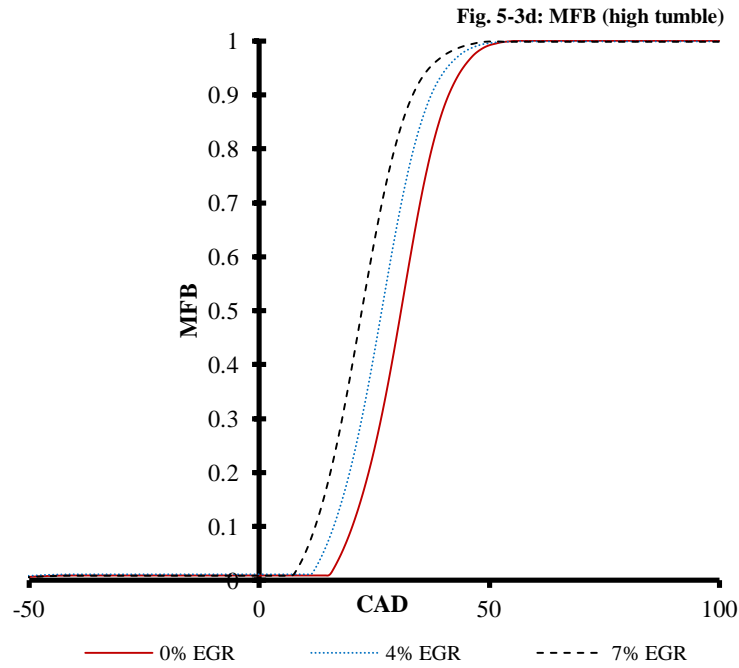
Fig. 5-3b: MFB (low tumble)

0% EGR   4% EGR   8% EGR   11% EGR

Fig. 5-3c: MFB (swirl)

0% EGR   4% EGR   8% EGR   11% EGR

Figure 5-3 MFB verses CAD at KLMBT spark timings for **a)** the three intake airflow conditions at 0% EGR, **b)** low tumble, **c)** swirl, **d)** high tumble

5.3.4 Fuel Consumption

Gravimetric ISFC$_{net}$ increased significantly for the swirl and high tumble conditions, as shown in Figure 5-4; it was increased by 6.4 and 15.5%, respectively, as compared to the low tumble condition. This is because the combustion duration was increased for the swirl condition (Figure 5-3a), and the KLMBT spark timing retard caused the MFB50 (Figure 5-3a) to be retarded from its optimum 8-10˚aTDC phasing for the high tumble condition (de O. Carvalho et al., 2012). Thus, it is thought that these resulted in a reduced conversion efficiency of the pressure and heat from the combustion into piston work, resulting in the fuel consumption increases. The MFB50 retard for the high tumble condition was more significant than the combustion duration increase for the swirl condition, explaining why its fuel consumption was higher in comparison. Although the baffle plates for the swirl and high tumble conditions did partially block the intake runner which alone would have increased fuel consumption through increased pumping losses, the greater throttle angle required to

burn the additional injected fuel required for the swirl and high tumble conditions effectively compensated for this; pumping work was only increased by 0.01 bar for the swirl condition and it was decreased by 0.06 bar for the high tumble condition.

The fuel consumption generally decreased across the EGR range by 2.4, 3.9 and 10.2% for the three engine conditions of low tumble, swirl and high tumble respectively. This is because the KLMBT spark timings could be advanced towards their optimum phasing with the EGR addition (de O. Carvalho et al., 2012). PMEP reductions (from 0.36 to 0.28 bar for the low tumble condition, 0.37 to 0.30 bar for the swirl condition, and 0.29 to 0.27 bar for the high tumble condition), and the reduced combustion temperatures which improved thermal efficiency (Ratnak et al., 2015, Siokos et al., 2015) also contributed to the fuel consumption improvements. All of these were explained previously in the first part of Chapter 4. The VAF had an average error of 1.6%, as discussed in the previous chapter; therefore, the fuel consumption decreases observed are not limited.

The fuel consumption increased slightly with 11% EGR addition at the low tumble condition because the rate of KLMBT spark timing advance was reduced, when compared with the advances achieved with other increases in EGR addition. The KLMBT spark timing was only advanced by 2 CAD compared to 4 CAD with previous EGR additions, so the MFB50 became retarded as the KLMBT spark advance achieved was not sufficient to overcome the laminar flame speed slowing effects of the additional EGR (Rhodes and Keck, 2012). This caused its MFB50 to become retarded away from the optimum 8-10°aTDC phasing (Figure 5-3b), increasing its fuel consumption.

Again, KLMBT spark timing advances would likely have been greater if intake manifold temperature increases, resulting from the EGR addition, could have been eliminated; thus, the fuel consumption improvements would likely have been greater.
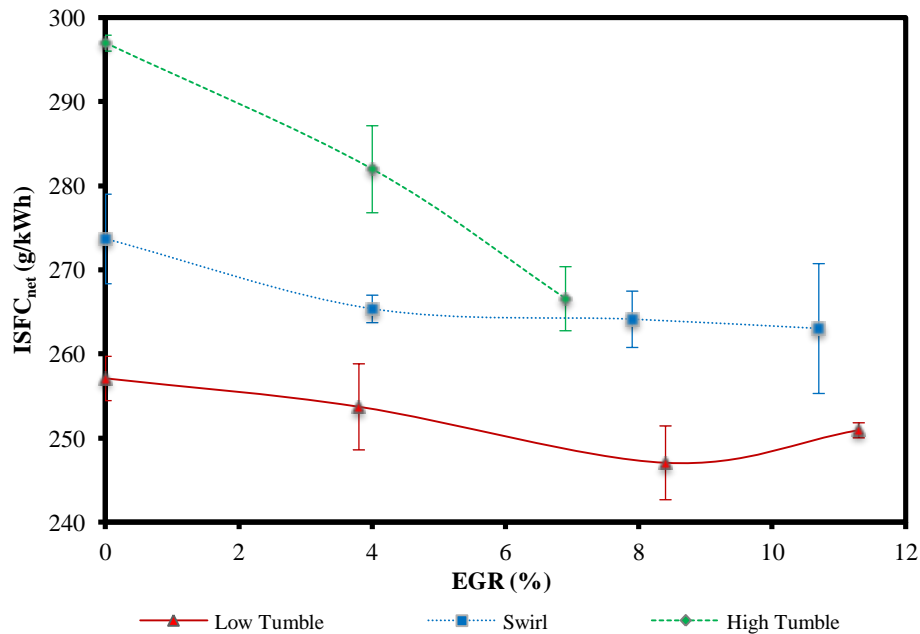
Figure 5-4   Gravimetric ISFC$_{net}$ versus EGR ratio at KLMBT spark timings

5.3.5 EGT

From Figure 5-5 it can be seen that the EGT increased significantly by 16.0 and 68.2°C at 0% EGR addition, respectively, for the swirl and high tumble conditions, as compared to the low tumble condition. It is proposed that the longer combustion duration for the swirl condition at 0% EGR addition (~24.0 CAD) as compared to the low tumble condition (~22.5 CAD), resulted in the pressure and heat from the combustion being less efficiently converted into piston work. This caused the gas temperature to become higher in the expansion and exhaust strokes, resulting in the EGT increase observed. It is proposed that the significantly later MFB50 for the high tumble condition at 0% EGR resulted in the same effect, producing the observed behaviour. The greater MFB50 retardation for the high tumble condition as

compared to the other two intake airflow conditions (Figure 5-3a) was more significant than the increased combustion duration for the swirl condition as compared to the low tumble condition. Therefore, this resulted in the more significant increase in EGT.

As to be expected, the EGT decreased with EGR addition for all of the intake airflow conditions, because the MFB50 was more advanced (Figures 5-3b, 5-3c and 5-3d), as explained in the first part of Chapter 4.

Again, KLMBT spark timing advances would likely have been greater if intake manifold temperature increases, resulting from the EGR addition, could have been eliminated. This would likely have resulted in greater improvements in EGTs across the EGR range, as explained in the first part of Chapter 4.
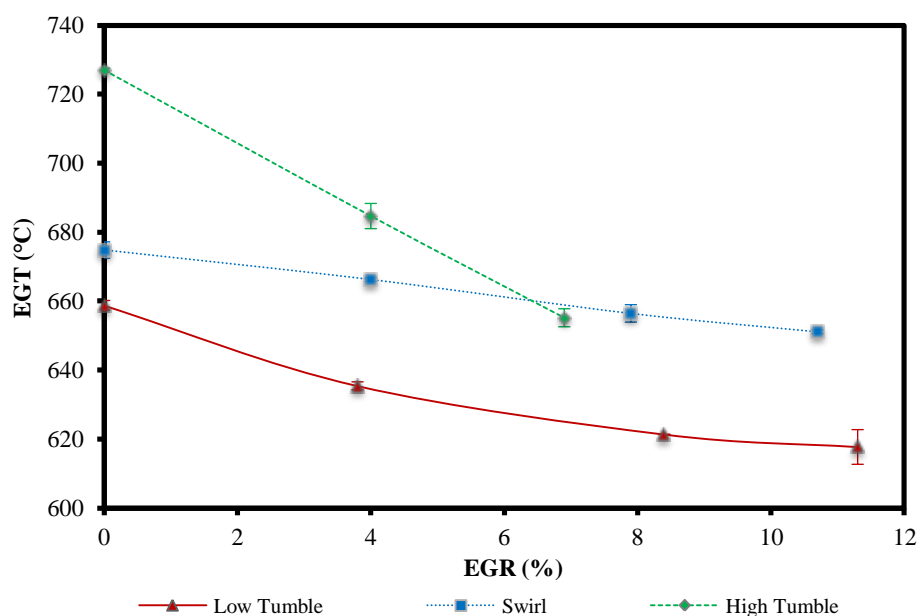

**Figure 5-5**   EGT versus EGR ratio at KLMBT spark timings

5.3.6 PM Emissions

5.3.6.1 Intake Airflow Effect on PN Emission

The nucleation mode particles, identified as the smaller diameter particles forming the peak on the left-hand side of the plot (10-30 nm) shown in Figure 5-6a, decreased significantly with the swirl and high tumble conditions, as compared to the low tumble condition. The soot accumulation particles, identified as the larger diameter particles forming the peak on the right-hand side of the plot (30-300 nm), decreased too for the swirl condition, while they remained approximately the same for the high tumble condition, as compared to the low tumble condition. These significant changes have been confirmed by analysing the 95% confidence intervals, which could not be displayed in the figures because the figures themselves would have become unclear.

It is proposed that the significant reduction in nucleation and accumulation particles observed with the swirl condition was a result of not just the improved air-fuel mixture preparation due to the KLMBT spark timing retard required (Table 5-2), but more importantly the increased turbulence resulting from the swirl airflow. This provided more time for mixture preparation as compared to the low tumble condition and it increased the rate at which the fuel and air mixed, respectively. It is thought that this reduced the number of pockets of a high local equivalence ratio meaning that the particulates oxidized more fully in the combustion, resulting in the behaviour observed. The calculated average in-cylinder temperature profiles for the swirl condition as compared to the low tumble condition (Figure 5-2a), at 0% EGR addition, were similar with similar peaks; therefore, combustion temperature is not thought to have caused the observed behaviour.

It is proposed that the significantly higher calculated average in-cylinder temperature for the high tumble condition at 0% EGR addition (Figure 5-2a) resulted in the substantial reduction of nucleation mode particles observed, along with the increased time available for air-fuel mixture preparation resulting from the spark retard and the improved mixture formation resulting from the high tumble airflow. However, the later MFB combustion phasing (Figure 5-3a) is thought to have reduced the time available for post-combustion oxidization, resulting in similar numbers of accumulation mode particles as compared to the low tumble condition. Overall, swirl had the greatest benefit regarding PN emissions, which means it has potential to be used to reduce PN emissions to ensure compliance with the Euro VI emission regulations.

Fig. 5-6a: PM (three airflow conditions)

Fig. 5-6b: PM (low tumble)

Fig. 5-6c: PM (swirl)
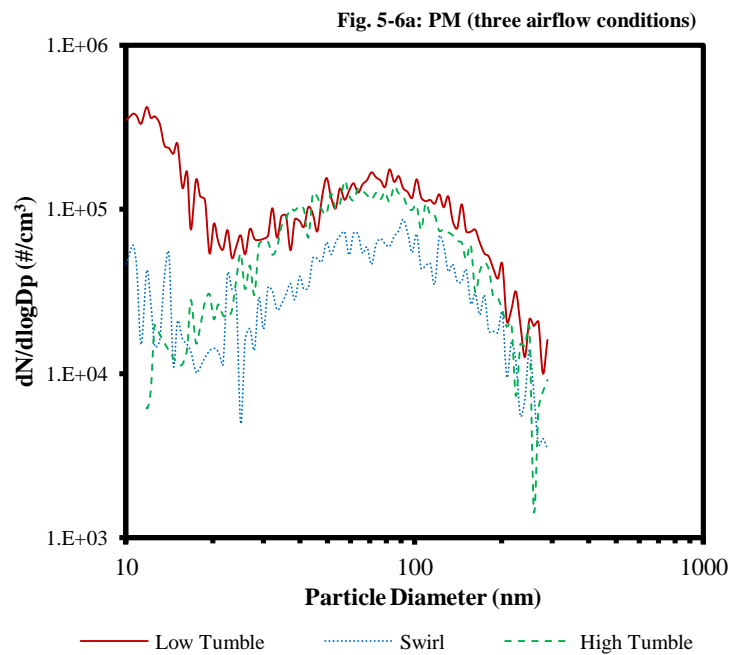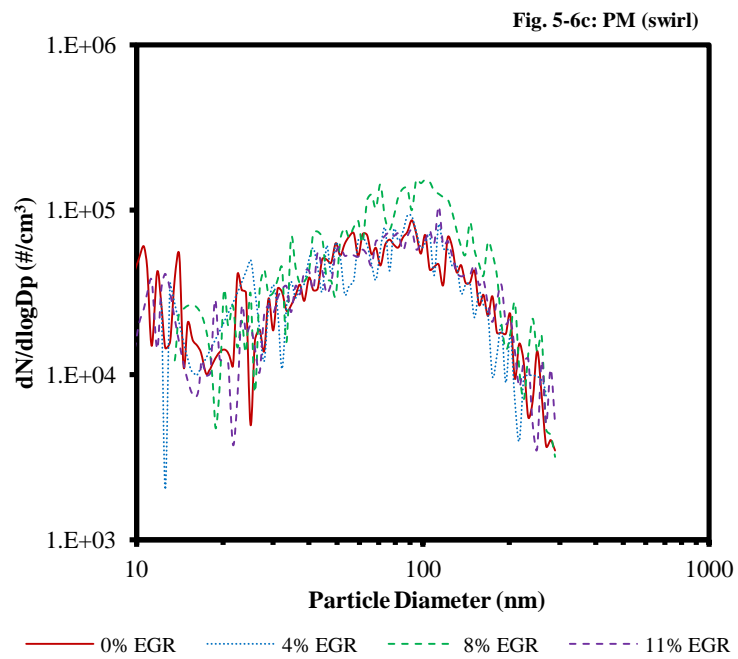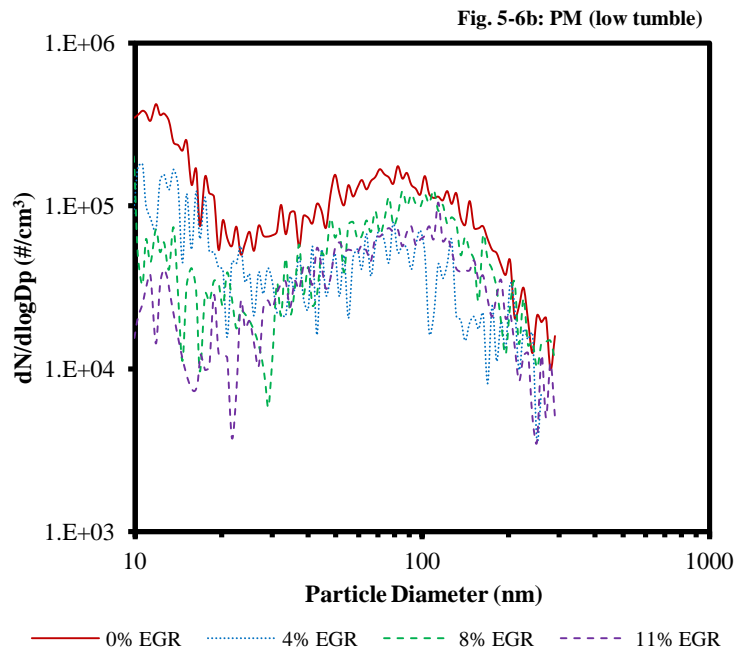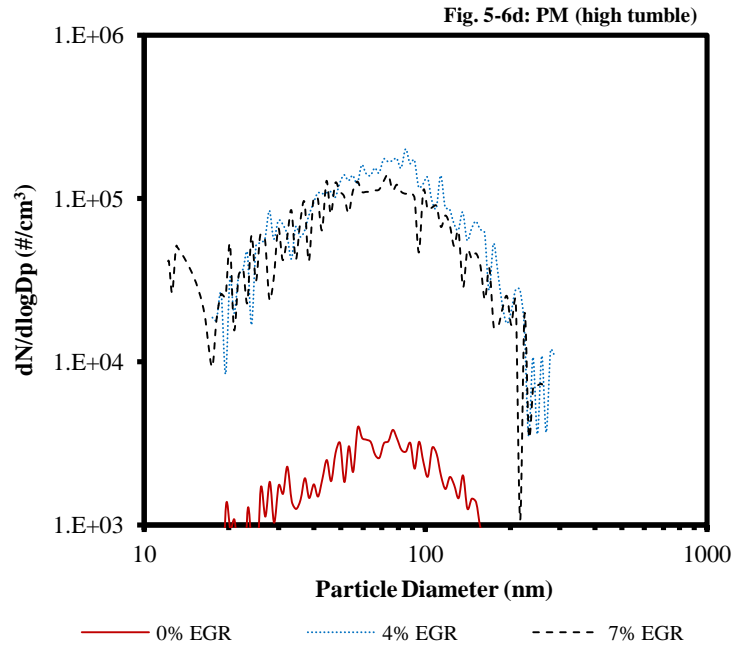
Figure 5-6   PN emissions versus particle diameter at KLMBT spark timings for **a)** the three intake airflow conditions at 0% EGR, **b)** low tumble, **c)** swirl, **d)** high tumble

5.3.6.2 EGR Effect on PN Emission

The PN emissions for the low tumble, swirl and high tumble intake airflow conditions across the EGR range are shown in Figures 5-6b, 5-6c and 5-6d, respectively. For the low tumble condition, there was a significant decrease of nucleation and accumulation mode particles across the EGR range. The significance of this and other PN changes discussed have been confirmed by analysing the 95% confidence intervals, which could not be displayed in the figures because the figures themselves would have become unclear. It is proposed that the increased post-combustion oxidization time resulted in the observed behaviour. It is thought that this was more significant than the reduced time available for fuel-air mixing and thus poorer mixture preparation with the KLMBT spark advances. The peak calculated average in-cylinder temperature across the EGR range when comparing 0 and 11% EGR addition (Figure 5-2b) remained approximately the same so it is not thought that this had an effect.

For the swirl condition, the PN did not change significantly across the EGR range, although the accumulation mode particles did significantly increase as the EGR addition was increased from 4 to 8%. It is proposed that the reduced calculated average in-cylinder temperatures across the EGR range (Figure 5-2c) and the poorer air-fuel mixture preparation due to the KLMBT spark timing advances (Table 5-2) across the range cancelled out the effect of the increased post-combustion oxidization time and the effect of decreased primary carbon particle formation with the reduced in-cylinder temperatures (Zhang et al., 2014b). This caused the PN to remain approximately the same across the range, when comparing those observed at 0 and 11% EGR addition.

The PM for the high tumble intake airflow condition did not change significantly across the EGR range. Despite the KLMBT spark timing being advanced as the EGR addition was increased (Table 5-2), providing less time for fuel-air mixing, it is proposed that the improved post-combustion oxidization time was sufficient to maintain the particles at similar levels with the EGR addition.

For the swirl condition, as mentioned, the accumulation mode particles increased significantly as the EGR addition was increased from 4 to 8%. It is proposed that this was caused by the increased calculated average in-cylinder temperatures (Figure 5-2c) which increased primary carbon particle formation by the thermal pyrolysis and dehydrogenation reaction of fuel vapour/droplets (Zhang et al., 2014b). As the EGR addition was further increased to 11%, the calculated average in-cylinder temperature decreased (Figure 5-2c), which resulted in the PM reducing due to the decreased primary particle formation.

If the intake manifold temperature increases with EGR addition could have been eliminated, then it is expected that the PM emissions would have been reduced for the low tumble

condition due to an increased post-combustion oxidization time resulting from the expected KLMBT spark timing improvements (Daniel et al., 2012e). However, the reduced fuel-air mixing time could cancel out some of these improvements. This behaviour would also be expected with the swirl and high tumble conditions, because similar behaviour was observed in the experimental data when the KLMBT spark timing was advanced.

Overall, these results agree with the research of (Alger et al., 2010) and (Hedge et al., 2011) who observed PN reductions with EGR addition, although it must be noted that their results were both from a turbocharged engine; the varying enrichment of the fuel-air charge will have significantly affected their results.

5.4 Data Continuity

For a detailed analysis regarding the continuity of the data between this chapter and Chapter 4, please refer to **Appendix B2**.

5.5 Conclusions

The effect of swirl and tumble intake airflows and hot EGR on the combustion and PM emissions of the single-cylinder DISI research engine was investigated in this chapter and the following conclusions have been made.

1. Swirl and high tumble significantly increased the fuel consumption with respect to the low tumble condition by 6.4 and 15.5% respectively, but EGR addition minimized these increases. The fuel consumption increase was 4.8 and 6.2%, respectively, at the maximum EGR additions for swirl and high tumble conditions, compared to that observed at the maximum EGR addition for the low tumble condition.

2. At 0% EGR addition, swirl significantly reduced the nucleation and accumulation mode particles, with the high tumble intake airflow condition only significantly reducing the

nucleation mode particles. It is thought that the KLMBT spark timing retard required with the swirl and high tumble intake airflow conditions increased the mixture preparation time, resulting in the observed behaviour. Also, the additional turbulence produced by the airflows improved mixture formation, reducing the number of pockets of a high local equivalence ratio, resulting in the reduced particle numbers. A reduced post-combustion oxidization time prevented the high tumble condition from reducing the accumulation mode particles.

3. The PN emission was decreased significantly with EGR addition for the low tumble condition, due to an increased post-combustion oxidization time, while there was no significant change for the swirl and high tumble conditions. This is mainly because poorer fuel-air mixture preparation caused by KLMBT spark timing advances cancelled out the benefit produced by the increased post-combustion oxidization time.

The main findings from this chapter are also summarized in Table 5-3.

Table 5-3   Results summary (intake airflow & EGR addition) (<mark>highlighted</mark>=improvement, <u>underlined</u>=worsening)

Result Summary / Intake Airflow/EGR Condition	KLMBT	ISFC$_{net}$	EGT	PM	
				Nucleation	**Accumulation**
Swirl (compared to reference condition at 0% EGR addition)	<u>8 CAD</u>	<u>6.4%</u>	<u>16.0°C</u>	<mark>Reduction</mark>	<mark>Reduction</mark>
High tumble (compared to reference condition at 0% EGR addition)	<u>18 CAD</u>	<u>15.5%</u>	<u>68.2°C</u>	<mark>Reduction</mark>	No sig. change
Low tumble [max. EGR] (compared to 0% EGR)	<mark>10 CAD</mark>	<mark>2.4%</mark>	<mark>41.1°C</mark>	<mark>Reduction</mark>	<mark>Reduction</mark>
Swirl [max. EGR] (compared to 0% EGR)	<mark>6 CAD</mark>	<mark>3.9%</mark>	<mark>23.7°C</mark>	No sig. change	No sig. change
High tumble [max. EGR] (compared to 0% EGR)	<mark>8 CAD</mark>	<mark>10.2%</mark>	<mark>71.8°C</mark>	No sig. change	No sig. change

Chapter 6

The Effect of Compression Ratio, Fuel and EGR on Engine Combustion and Emissions

The aim of this chapter is to provide details of the combustion and emissions characteristics of a DISI engine operated at different compression ratios with different fuels (8.5 bar IMEP), and at different compression ratios with EGR addition (7.0 bar IMEP).

6.1 Introduction

The main combustion parameters investigated in this chapter are KLMBT spark timing, in-cylinder pressure, calculated average in-cylinder temperature, MFB, fuel consumption and exhaust temperature. PM, NO_x and HC are the main emission parameters investigated.

There is an ever growing demand for reduction of PM, NO_x and HC from engines as emissions regulations become stricter, as well as the growing demand to reduce net CO_2 emissions from the transportation sector, which is at the forefront of public perception. One way to achieve these demands is to increase compression ratio; this improves thermal efficiency causing fuel consumption and thus CO_2 output to reduce. Another way is to use renewable oxygenated fuels in engines to increase the oxidation of particulates in the combustion chamber to reduce their numbers, as well as potentially reducing NO_x and HC emissions. In addition, biomass is converted to make the renewable oxygenated fuel, which reduces transportation's net CO_2 output (Wang et al., 2013). Furthermore, the Euro VI emissions regulations which for the first time limit the PN from DISI engines have increased interest in the effect of oxygenated fuels on engine particulates. They have the potential to significantly reduce particulate emissions having health benefits, particularly for people

living in urban areas (Anderson et al., 2012b, United States Environmental Protection Agency, 2014). The regulations have also increased interest in the effect of EGR addition on engine particulates, with the potential of EGR coming under question because of it has been observed to have a negative effect on them (Gill et al., 2011, Ma et al., 2014).

Overall, despite the amount of research that has been conducted into 1-butanol-gasoline and ethanol-gasoline blended fuels, there appears to be lack of agreement in terms of the effect these fuel blends on the combustion and emissions of gasoline engines. In addition, little work has been conducted regarding the effect of these fuel blends on the combustion and emissions of DISI engines, especially regarding the effect of 1-butanol-gasoline blends on PM emissions. This is because the majority of the research conducted has been on PFI engines with ethanol-gasoline fuel blends. Finally, 1-butanol-gasoline and ethanol-gasoline fuel blends have not been studied well with each other along with a reference of gasoline fuel at different compression ratios. Therefore, the research in this chapter has been conducted to provide deeper knowledge about the effect of 1-butanol-gasoline and ethanol-gasoline blended fuels on the combustion and emissions of DISI engines.

In addition, despite the amount of work that has been conducted into compression ratio and EGR separately, little work has been conducted studying their combined effect on engine combustion and PM emissions. Especially, it is important to know the combined effect of these two fuel consumption (and NO_x in the case of EGR) improving techniques on engine particulates because of the limitations that the Euro VI emissions regulation has on these. Therefore, these areas have also been investigated further in this chapter.

6.2 Experimental Procedure

The experimental test procedure outlined in Section 3.9 of this thesis was followed in order to conduct the engine tests on the single-cylinder engine to collect the data presented and discussed in this chapter. Relative air-fuel ratio λ was maintained at 1 during the experiments and a COV_{IMEP} of 5% was not exceeded. Valve timings were set at IVO=16°bTDC and EVC=36°aTDC. KLMBT spark timings were used and the geometric compression ratio was varied between 10.7 and 11.5 in the experiments. To change the compression ratio in the engine the procedure outlined in Section 3.2.8 was followed. When using the non-gasoline fuel splash blends the procedure discussed in Section 3.2.4.1 was followed to prevent contamination between the fuels. In order to achieve hot EGR, and in order to achieve the desired engine load and EGR addition, the equipment setup and experimental test procedure outlined in Section 3.2.6.1 was followed.

The load of 8.5 bar IMEP was chosen to study for the investigation of the compression ratio and fuel effect on engine combustion and emissions because it represents one of the worst conditions for knock in this engine, as well as being an engine load that is highly relevant for both NA and turbocharged DISI engines, increasing the usefulness of the data produced. The load of 7.0 bar IMEP was chosen to study for the investigation of the compression ratio and EGR effect on engine combustion and PM emissions because it represents a medium-high load in this engine where knock is present, and it allowed a reasonable, while not a high EGR addition of 14% to be achieved. A higher engine load would mean that the throttle would have needed to be more opened thus reducing the maximum level of EGR that could have been achieved. One load was chosen to study for both parts of the investigation so that an in-depth understanding could be formed; this would not be possible if multiple loads were studied.

The spark was swept for all compression ratios, fuels and EGR additions in order to find the KLMBT spark timing using the LabView on-line pressure trace analysis technique outlined in Section 3.6.9. This allowed the KLMBT spark timing to be found much more quickly than the MatLab post-experiment processing method. This is because it enabled the KLMBT spark timings to be found while the engine was operating, thus allowing the measurements at the KLMBT spark timings to be recorded alone, saving significant amounts of time. The SMPS 3936 was used to measure the PM emission for both parts of this chapter and the Horiba MEXA-7100DEGR was used to measure the NO_x and HC gaseous emissions for the first part of this chapter. Gaseous emissions were not measured in the second part of this chapter because it is believed that the literature sufficiently covers this area, and the EGT data was omitted for the same reason.

A research grade gasoline was used in this research. This was used in addition to 1-butanol and ethanol for the results in the first part of this chapter. All of the fuel properties as well as those of the two tested fuel blends of Bu20 and E20 are outlined in Section 3.8. The ULG95 was used in its supplied form, while the 1-butanol and ethanol fuels were mixed with the ULG95 fuel to form the Bu20 and E20 fuel splash blends with each containing 20%vol 1-butanol and 20%vol ethanol respectively. The ULG95 fuel was supplied with 5%vol ethanol pre-mixed in it, so the 20%vol 1-butanol blend and ULG95 fuel also had 5%vol ethanol in them too, while the E20 blend had no ethanol in addition to the 20%vol. In total the Bu20 blend had 20%vol 1-butanol with 5%vol ethanol, the E20 blend had 20%vol ethanol and the ULG95 fuel had 5%vol ethanol.

The test matrix provided in Table 6-1 was carried out in order to investigate the compression ratio and fuel effect on engine combustion and emissions at the single engine load of 8.5 bar IMEP. **The results and discussion of these tests can also be found in (Lattimore, 2016b).**

Table 6-1   Experiment test matrix (compression ratio & fuel)

Compression Ratio / Fuel	10.7	10.9	11.2	11.5
Bu20	1	2	3	4
E20	5	6	7	8
ULG95	9	10	11	12

For the investigation of the compression ratio and EGR effect on engine combustion and PM emissions at the single engine load of 7.0 bar IMEP, the test matrix provided in Table 6-2 was carried out.

Table 6-2   Experiment test matrix (compression ratio & EGR addition)

Compression Ratio / EGR Addition (%)	10.7	10.9	11.2	11.5
0	1	2	3	4
7	5	6	7	8
14	9	10	11	12

6.3 Results and Discussion

6.3.1 Investigation of Compression Ratio and Fuel Effect on Combustion and Emissions

6.3.1.1 KLMBT Spark Timing

From the KLMBT spark timings shown in Table 6-3, it can be seen that in the case of gasoline, an increase in the compression ratio had no significant effect on KLMBT. The same trend was also observed for the butanol blend (similar octane rating as gasoline) and even for the ethanol blend, despite the high octane rating of ethanol. This is because at the engine load of 8.5 bar IMEP, the engine was very prone to knock, even in the case of alcohols, due to the high low temperature reactivity of alcohols (He et al., 2015) and the higher amount of fuel

being injected into the combustion chamber (i.e. ethanol has a lower calorific value than butanol and gasoline). Thus, despite the compression ratio changing, no change in the KLMBT spark timing could be realized. It must be noted that knocking could have been avoided if the compression ratio was fully optimized for the fuels used. However, this was not pursued in order to investigate the effect of the parameter changes on engine knock limit and the consequent combustion and emission parameters at this limit.

It can also be seen that more advanced KLMBT spark timings could be achieved with Bu20 and E20 as compared to ULG95, with the most advanced spark timings being achieved with Bu20. This is due to their higher octane numbers and the superior charge cooling effect of alcohols compared to gasoline. Despite ethanol having a higher octane number than 1-butanol and an increased cooling effect (in terms of mass), more advanced KLMBT spark timings could be achieved with Bu20. It is believed that the 5%vol ethanol content in the Bu20 blend (20%vol 1-butanol with 5%vol ethanol) was sufficient to compensate for the reduced charge cooling effect and for the lower octane number of 1-butanol as compared to ethanol. It is also thought that the higher chemical reactivity (He et al., 2015), faster laminar flame speeds (Figure 6-5) and shorter fuel injection duration (less fuel quantity is required for the same engine output power due to the higher heating value compared to ethanol) for the 1-butanol blend with respect to the ethanol blend meant that the end-zone auto-ignition sites were consumed before they had an opportunity to auto-ignite. Thus, these factors contributed to the KLMBT spark timing advances.

Overall, it is believed that E20 would perform better over a larger compression ratio range than Bu20; particularly at compression ratios higher than 11.5, due to its higher octane number and increased cooling effect. Thus, the small compression ratio range is a limitation of this experiment.

Table 6-3   KLMBT spark timings (˚bTDC) (compression ratio & fuel)

Compression Ratio / Fuel	10.7	10.9	11.2	11.5
Bu20	14	14	14	14
E20	12	12	12	12
ULG95	10	10	10	10

6.3.1.2 In-cylinder Pressures and Temperatures

The in-cylinder pressure traces for the two fuels blends of Bu20 and E20 along with that for the ULG95 reference fuel are shown in Figures 6-1a, 6-1b and 6-1c, respectively. It is clear that as the compression ratio was increased, the maximum in-cylinder pressure increased, for the two fuel blends and the reference fuel tested. This is because the more compact combustion chamber achieved through the compression ratio increase, reduced the heat losses to the surroundings, resulting in the in-cylinder pressure increases. The in-cylinder pressures were highest for Bu20, followed by E20, then ULG95. This is due to the more advanced KLMBT spark timings (Table 6-3) which could be achieved with Bu20 and E20 as compared to those achieved with ULG95, with the most advanced spark timings being achieved for Bu20. This resulted in heat being released from the fuel at an earlier CAD, enabling higher in-cylinder pressures to be achieved before the downwards piston motion caused the in-cylinder pressure to decrease again.
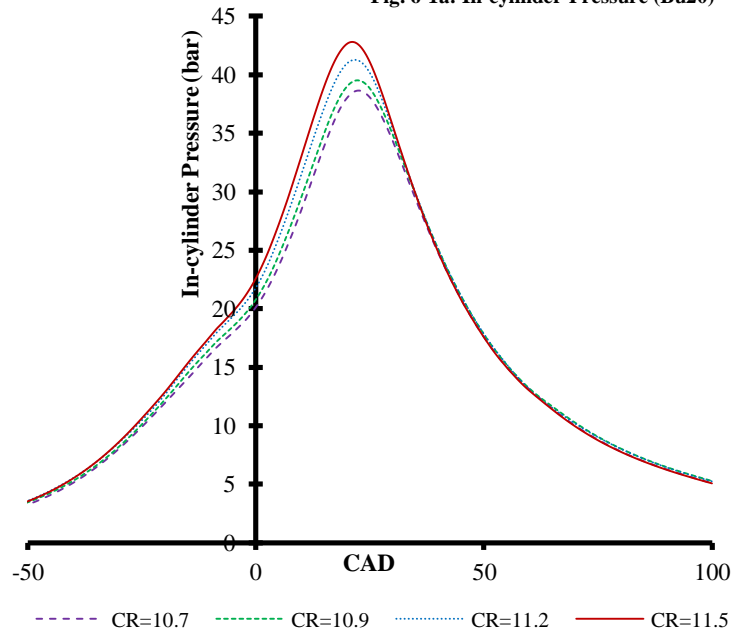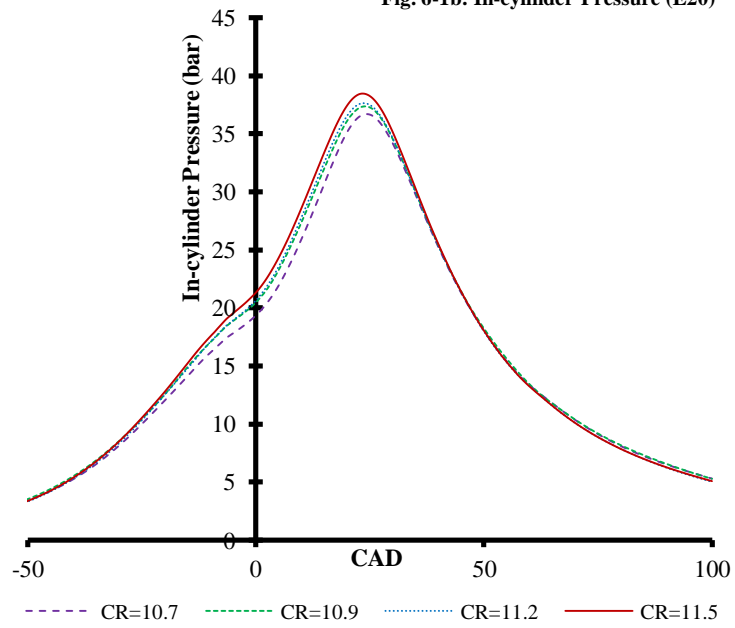
Fig. 6-1a: In-cylinder Pressure (Bu20)

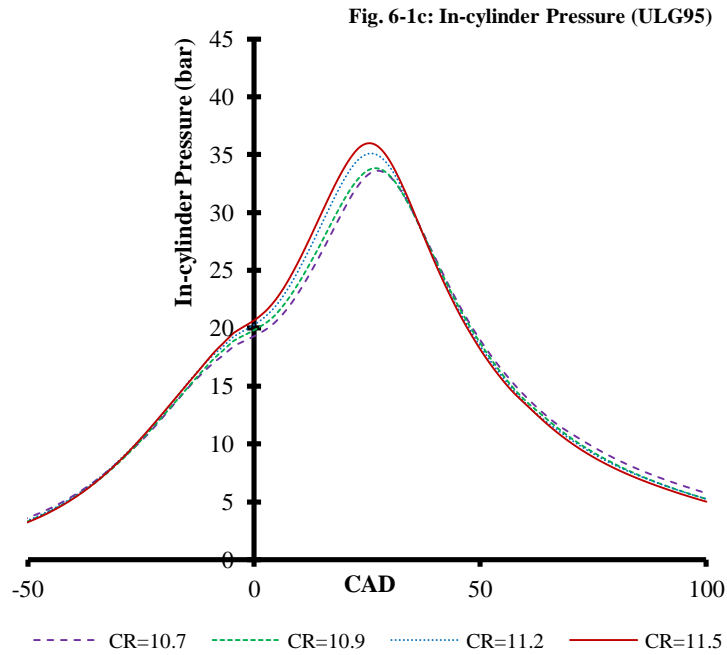Fig. 6-1b: In-cylinder Pressure (E20)

Fig. 6-1c: In-cylinder Pressure (ULG95)

Legend: CR=10.7, CR=10.9, CR=11.2, CR=11.5

Figure 6-1   In-cylinder pressure versus CAD for **a)** Bu20, **b)** E20 and **c)** ULG95 at KLMBT spark timings

Figures 6-2a, 6-2b and 6-2c show the calculated average in-cylinder temperatures for the two fuel blends of Bu20 and E20 and for the reference fuel of ULG95, respectively. Overall, the calculated average in-cylinder temperature increased as the compression ratio was increased. This is because of the aforementioned more compact combustion chamber achieved with the compression ratio increase reducing heat losses to the surroundings. The calculated average in-cylinder temperatures were highest for ULG95, with Bu20 and E20 having lower but similar calculated average in-cylinder temperatures across the compression ratio range. It is proposed that this is due to the higher heat of vaporization of 1-butanol and ethanol as compared to ULG95 (Table 3-9). This meant that more energy was required to vaporize these fuels, causing the average in-cylinder temperatures to reduce. The reduced fuel calorific values of Bu20 and E20 compared to ULG95 also contributed to the lower average in-cylinder temperatures (longer injection pulse was required).

185

Fig. 6-2a: In-cylinder Temperature (Bu20)

CAD

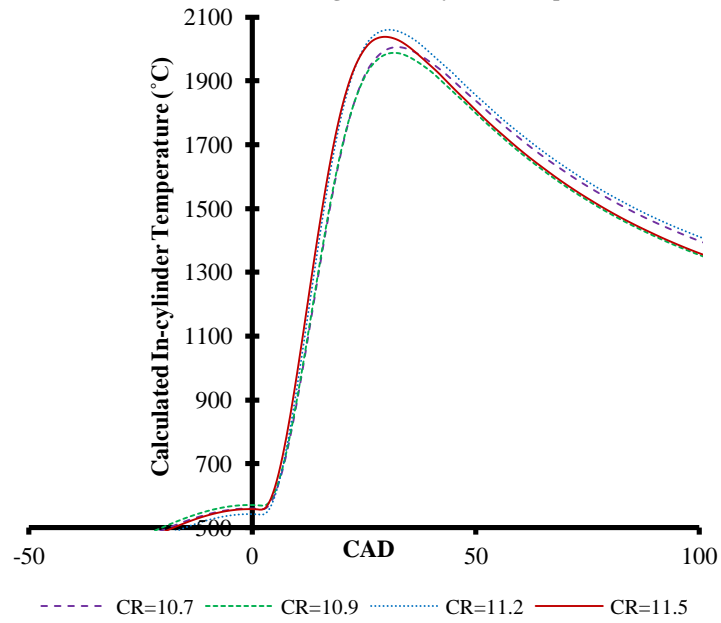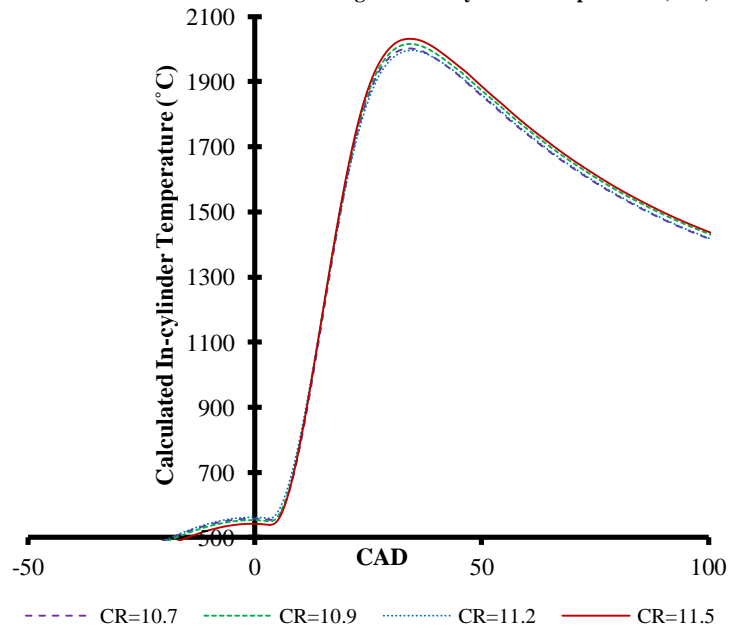- - - - CR=10.7   - - - - CR=10.9   .... CR=11.2   —— CR=11.5

Fig. 6-2b: In-cylinder Temperature (E20)

CAD

- - - - CR=10.7   - - - - CR=10.9   .... CR=11.2   —— CR=11.5

186

Fig. 6-2c: In-cylinder Temperature (ULG95)

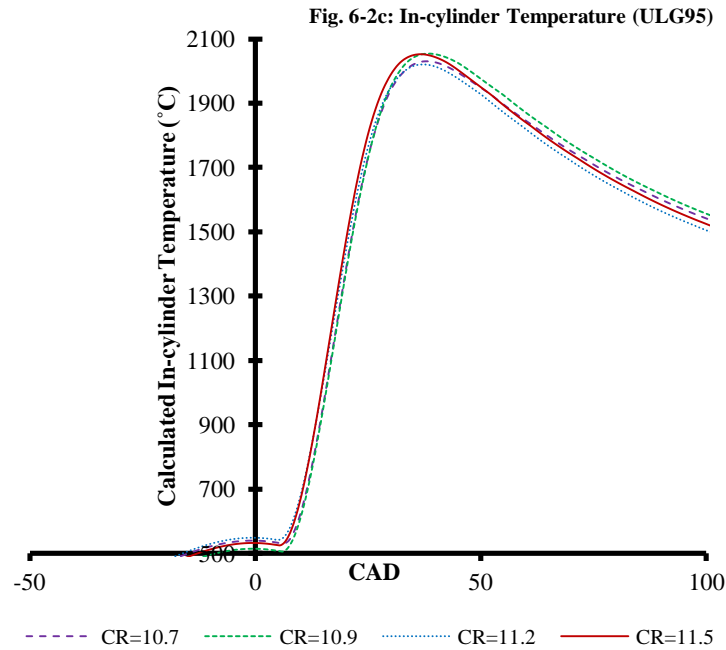CR=10.7   CR=10.9   CR=11.2   CR=11.5

Figure 6-2   Calculated average in-cylinder temperature versus CAD at KLMBT spark timings for **a)** Bu20, **b)** E20 and **c)** ULG95

6.3.1.3 MFB

The MFB profiles for the two tested fuel blends of Bu20 and E20, and the reference fuel of ULG95 are shown in Figures 6-3a, 6-3b and 6-3c, respectively. For E20, there are no significant differences between the profiles at the different compression ratios while Bu20 and ULG95 show a slightly advanced combustion as the compression ratio was increased. It is proposed that the more highly compressed fuel-air mixtures at the higher compression ratio burned more quickly than the less highly compressed mixtures at the lower compression ratios, causing the combustion to proceed more quickly. Despite this, it appears that the last stage of combustion (less than 10% of the fuel mass remaining) was faster at lower compression ratios for all three fuels. For a quantitative analysis of the combustion speed, the MFB50 and MFB10-90 have been calculated from the MFB profiles (please see next section).
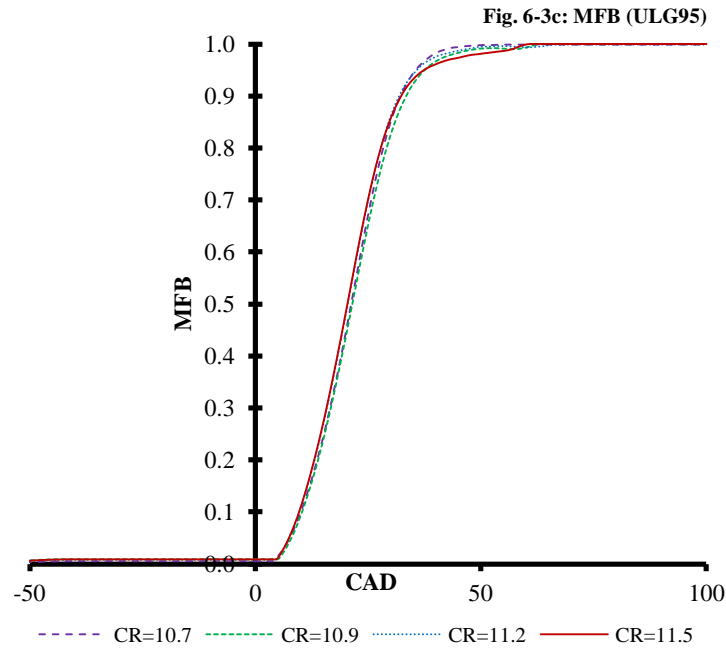
Fig. 6-3a: MFB (Bu20)

Fig. 6-3b: MFB (E20)
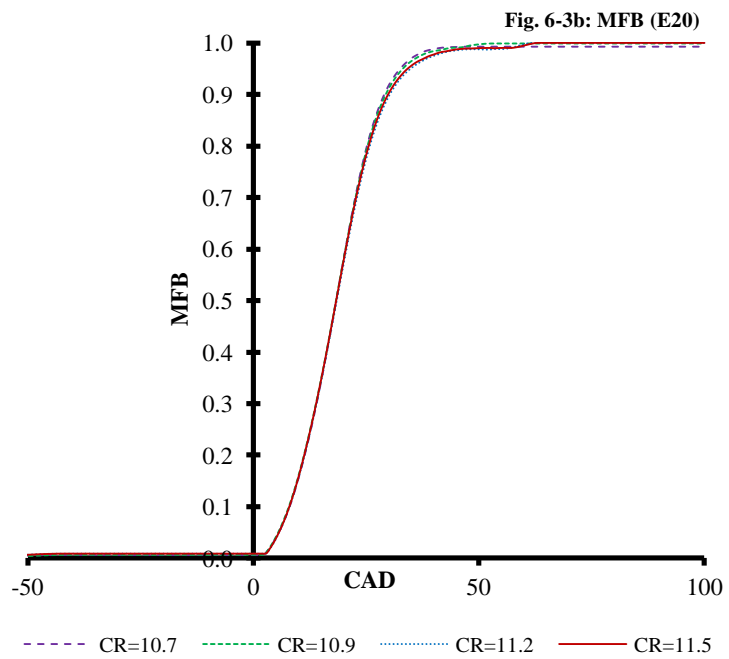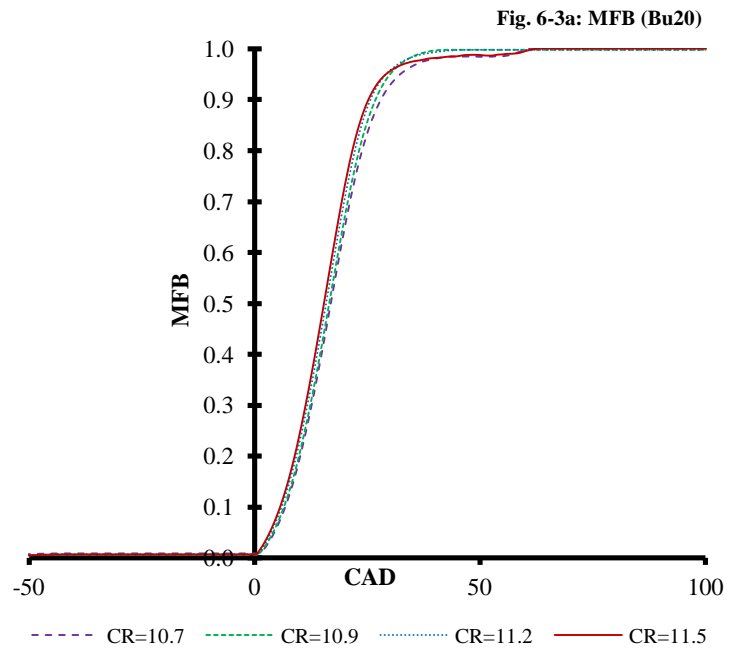
Figure 6-3 MFB versus CAD at KLMBT spark timings for **a)** Bu20, **b)** E20 and **c)** ULG95

6.3.1.4 MFB50 and MFB10-90

Figure 6-4 shows the MFB50 data for the two tested fuel blends of Bu20 and E20, and the tested reference fuel of ULG95, across the compression ratio range. As discussed and explained previously, the KLMBT spark timings were most advanced for Bu20, with E20 second and ULG95 third, thus leading to the most advanced MFB50 of Bu20 across the compression ratio range, followed by E20 and ULG95. The MFB50 remained almost constant across the compression ratio range for E20; this is reflected in the MFB profile for E20 (Figure 6-3b). It is thought that experimental error resulted in the observed trend, as indicated by the confidence intervals. However, for the other two fuels of Bu20 and ULG95, there was a significant reduction in the MFB50 across the compression ratio range. Again, it is proposed that the more highly compressed fuel-air mixtures at the higher compression ratio burned more quickly than the less highly compressed mixtures at the lower compression ratios, causing the combustion to proceed more quickly, thus resulting in the MFB50 becoming advanced.
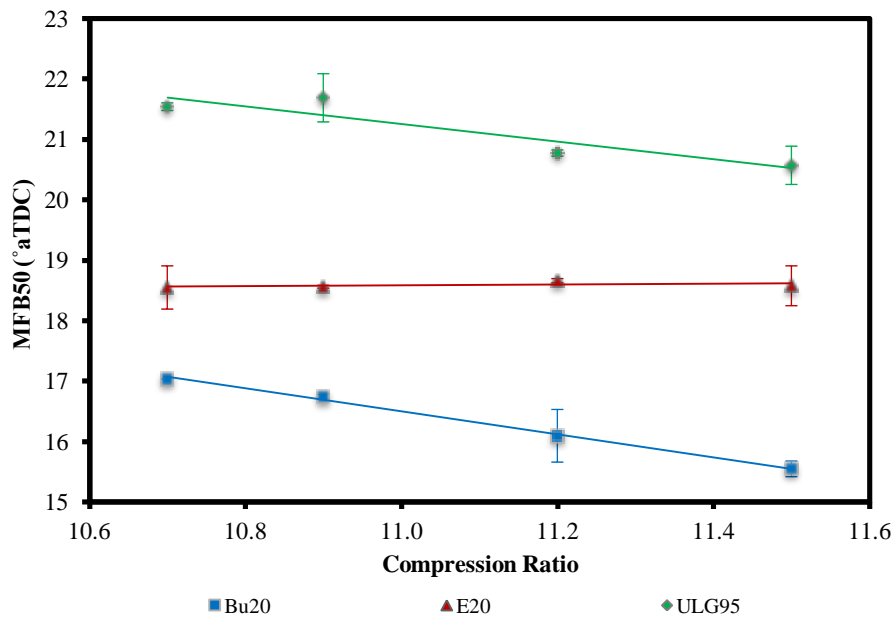
Figure 6-4   MFB50 versus compression ratio at KLMBT spark timings

Figure 6-5 shows the combustion duration (MFB10-90) data for the two tested fuel blends of Bu20 and E20, and the tested reference fuel of ULG95, across the compression ratio range. 1-butanol and ethanol addition to gasoline reduced the combustion duration of the fuel; it is proposed that 1-butanol and ethanol increased the laminar flame speed, due to the oxygen in their molecules. The higher chemical reactivity of 1-butanol as compared to ethanol and the shorter injection duration of Bu20 with respect to E20 explain its shorter combustion duration in comparison. The shorter combustion duration of Bu20 and E20 as compared to ULG95 is also due to enhanced in-cylinder turbulence (Stone, 1999) during their combustion which results from their advanced spark timings. Furthermore, as a result of their advanced spark timings, the combustion occurs in a smaller volume which increases the in-cylinder temperature that further promotes combustion. It has to be also noted that the combustion duration of Bu20 reduced significantly across the compression ratio range; this continues the trend in Figure 6-4 which shows that the first half of the combustion process also proceeded more quickly across the range.

If the compression ratio was fully optimised for each fuel tested, the combustion phasing would have been optimised for each fuel. Therefore, it would be expected that the combustion of each fuel, particularly that of ULG95, would have been quicker due to higher in-cylinder turbulence at the time of ignition.
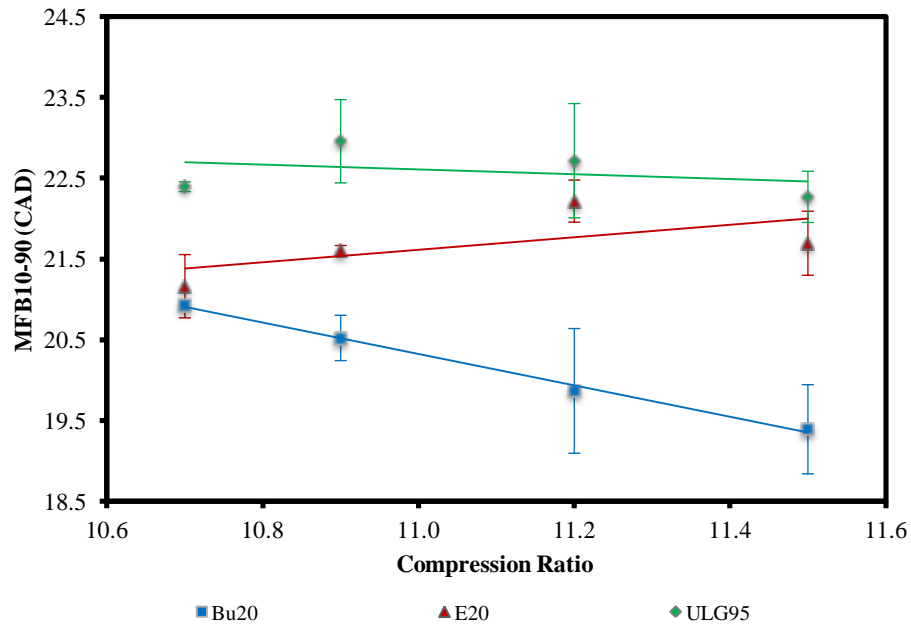

Figure 6-5   MFB10-90 versus compression ratio at KLMBT spark timings

6.3.1.5 Indicated Efficiency

The indicated efficiency for the two tested fuel blends of Bu20 and E20, and the tested reference fuel of ULG95, across the compression ratio range, is shown in Figure 6-6. They increased by 1.3, 1.3 and 1.1% for Bu20, E20 and ULG95, respectively. This compares to a maximum theoretical thermal efficiency increase of 1.8% which can be obtained from Equation 6-1 by assuming γ=1.4 and solving for the minimum and maximum respected compression ratios of 10.7 and 11.5.

$$\eta = 1 - \frac{1}{r^{\gamma-1}} \text{ (6-1)}$$

Therefore, the thermal efficiency increase observed is realistic. It is well known that the volumetric fuel consumption of oxygenated fuels and their low percentage blends in gasoline is significantly higher than that of gasoline due to their lower calorific value. Therefore, this is why the indicated efficiency rather than the volumetric fuel consumption has been analysed in this section.

As the compression ratio is increased, indicated (thermal) efficiency increases, thus producing the observed behaviour. Bu20 had the highest indicated efficiency, followed by E20 then ULG95, due to their respected KLMBT spark timings (Table 6-3) and their respected combustion durations (Figure 6-5). The more advanced the spark timing and the faster the combustion, the more efficiently the fuel was converted into engine power, thus resulting in the indicated efficiency increases observed. Their higher indicated efficiencies also resulted from their lower combustion temperatures (Figures 6-2a, 6-2b and 6-2c) which reduced the heat loss through the combustion chamber walls.

It should be noted that the compression ratio of this engine is not optimised. Within the compression ratio range tested, the knock limit was reached before the optimal MFB50 phasing was achieved (Figure 6-4). If the fuels were tested across a range of lower compression ratios, it is expected that knock may not occur even at WOT. Thus, at the tested engine load of 8.5 bar IMEP, the engine efficiency may be improved for the fuels tested because the combustion phasing will be optimized and there will be a higher in-cylinder turbulence at the time of ignition. This would be expected to reduce the combustion duration and thus improve thermal efficiency further. However, it is important to note that there is a trade-off because thermal efficiency would be reduced at lower compression ratios. It must also be noted that because the injected fuel mass is increased with the Bu20 and E20 fuel blends as compared to ULG95, a fuel pump in a real engine would consume more power

which would reduce the indicated efficiency in comparison to that observed in this investigation.
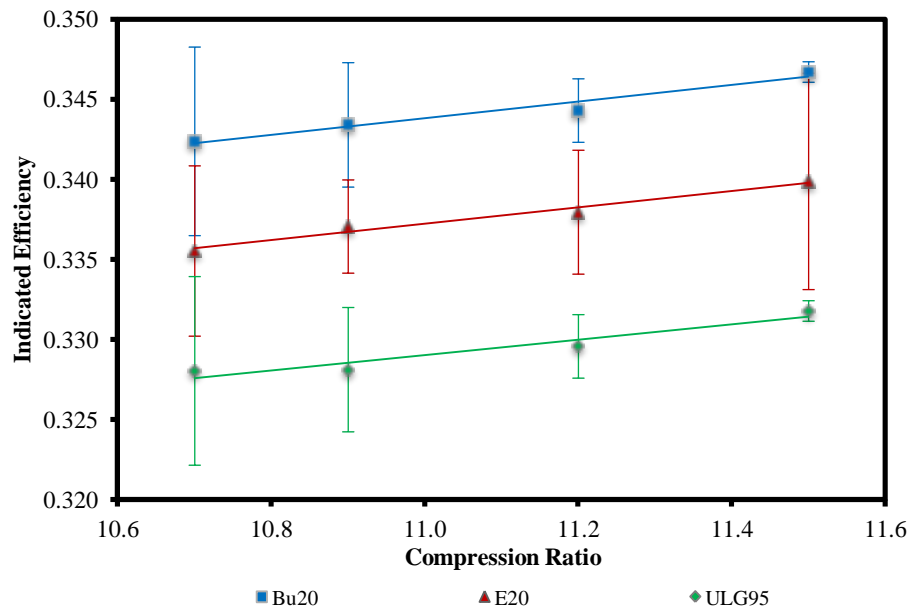

Figure 6-6   Indicated efficiency versus compression ratio at KLMBT spark timings

6.3.1.6 EGT

Figure 6-7 shows the EGTs for the two tested fuel blends of Bu20 and E20, and the tested reference fuel of ULG95 across the compression ratio range. It is clear to see that there is general small decrease in EGTs across the compression ratio range. It is proposed that as the compression ratio was increased and the MFB50 became advanced, the pressure and heat was more efficiently converted into piston work leading to the EGT decreases across the compression ratio range. (Kramer et al., 2000) also observed EGT reductions as compression ratio was increased.

The results also show that ULG95 had the highest EGT for all compression ratios, followed by E20, then Bu20. It is proposed that the more advanced MFB50 of Bu20 as compared to ULG95 and E20 (Figure 6-4) resulted in more efficient conversion of the pressure and heat into work on the piston, resulting in the reduced EGTs in comparison. The MFB50 phasing

was more advanced for E20 than ULG95 for all compression ratios (Figure 6-4) leading to lower EGTs in comparison. The lower calculated average in-cylinder temperatures for the Bu20 and E20 fuel blends due to their higher heat of vaporization as compared to ULG95, will have also contributed to their lower EGTs.
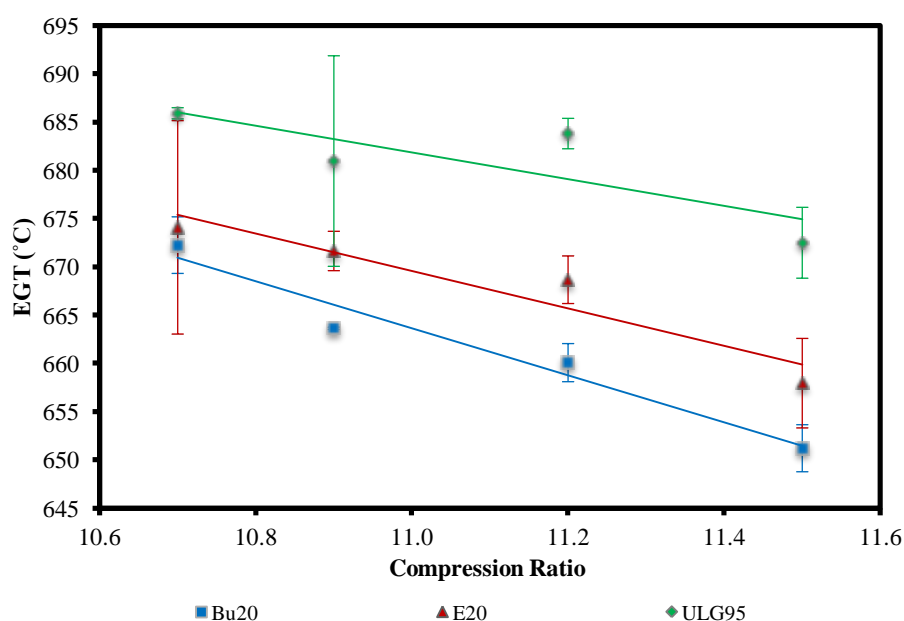

Figure 6-7   EGT versus compression ratio at KLMBT spark timings

6.3.1.7 PM Emissions

6.3.1.7.1 Compression Ratio effect on PN Emission

The PN emissions for the two tested fuel blends of Bu20 and E20, along with the tested reference fuel of ULG95 are shown in Figures 6-8a, 6-8b and 6-8c, respectively. It is clear to see from Figure 6-8a that the compression ratio increase reduced the smaller nucleation mode particles on the left-hand side of the plot (10-30 nm) for the Bu20 blend. It is proposed the observed reduction was due to the increased calculated average in-cylinder temperatures across the compression ratio range which increased the oxidation of the particles in the combustion chamber. The KLMBT spark timing was unchanged across the compression ratio
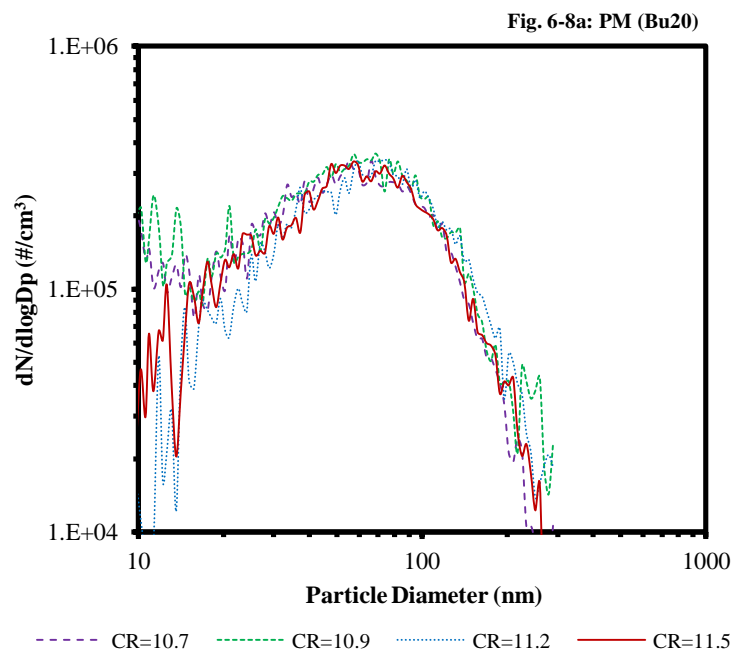
range, therefore, mixture preparation was not considered to have had an effect on the observed behaviour. Although the in-cylinder temperature increases would have increased primary carbon particle formation by the thermal pyrolysis and dehydrogenation reaction of fuel vapour/droplets (Zhang et al., 2014b), the increased oxidation of the particles also resulting from the in-cylinder temperature increases was clearly the stronger effect.

E20 showed a similar trend to Bu20 but it was much weaker; the nucleation mode particles decreased as the compression ratio was increased. Again, it is proposed that the higher calculated average in-cylinder temperatures (Figure 6-2b) increased the rate of oxidation of these particles in the combustion chamber, leading to the observed trend. For both Bu20 and E20, no significant changes in accumulation mode particle numbers on the right hand side of the plot (30-300 nm) were observed. It is believed that the increased oxidization of particles resulting from the increased calculated average in-cylinder temperatures across the compression ratio range was cancelled out by increased rate of particle formation caused by the increased primary carbon particle formation (Zhang et al., 2014b), also resulting from the increased in-cylinder temperatures.

The data for ULG95 shows a completely uni-modal distribution with no significant nucleation mode particles being recorded. As the compression ratio was increased, the formation of accumulation mode particles increased. It is proposed that the accumulation mode particles increased across the compression ration range for ULG95 because the increased calculated average in-cylinder temperatures increased primary carbon particle formation (Zhang et al., 2014b), as with E20. This appears to have overcome the effect of increased particle oxidization resulting from the higher calculated average in-cylinder temperatures. Again, the KLMBT spark timing was unchanged across the compression ratio range, thus mixture preparation is not thought to have had an effect on the observations.

For the two tested fuel blends Bu20 and E20, along with the tested reference fuel ULG95, it is proposed that significant nuclei adsorption of nucleation mode particles onto the accumulation mode particles occurred and this along with the thermodenuder, which removed many of the nucleation particles before they could be measured, led to the mostly uni-modal behaviour observed.

Overall, the effect of compression ratio increase on PM emissions is not significant when the 95% confidence intervals are taken into consideration, due to the compression ratio increase being relatively small. The 95% confidence intervals themselves could not be displayed on the figures because they would have become unclear.

Fig. 6-8a: PM (Bu20)

Fig. 6-8b: PM (E20)

CR=10.7   CR=10.9   CR=11.2   CR=11.5

Fig. 6-9c: PM (ULG95)

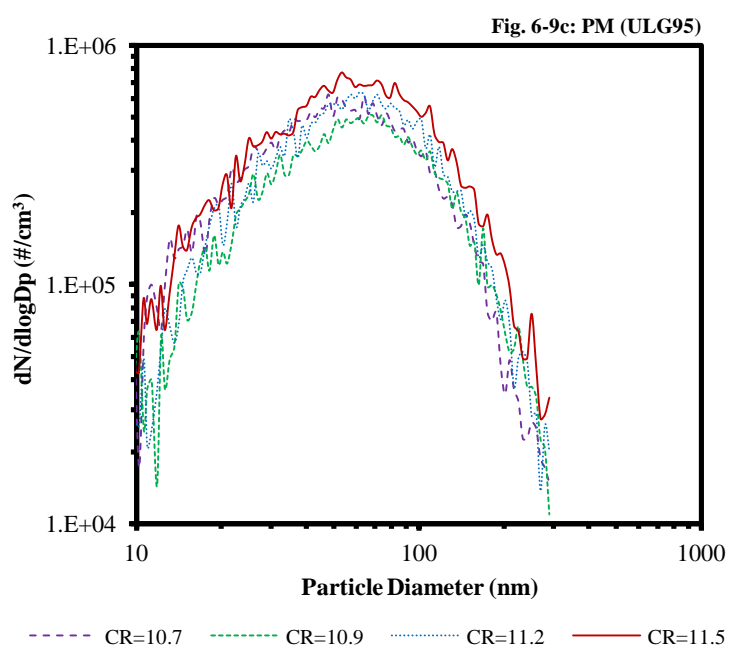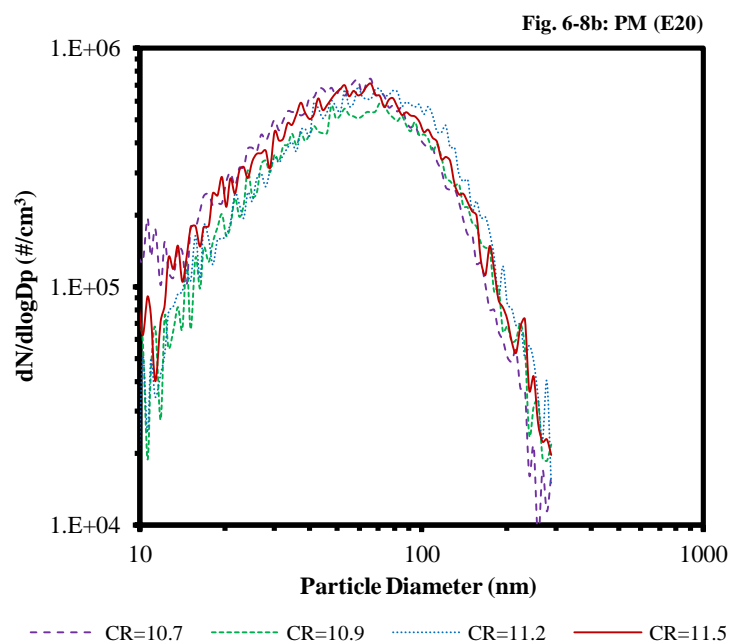CR=10.7   CR=10.9   CR=11.2   CR=11.5

Figure 6-8   PN emissions versus particle diameter at KLMBT spark timings for **a)** Bu20, **b)** E20 and **c)** ULG95

6.3.1.7.2 Fuel Effect on PN Emission

Comparing the behaviours of the different fuels in Figures 6-8a, 6-8b and 6-8c, 1-butanol significantly reduced the PN when added to the gasoline fuel, whereas ethanol had little or no effect. It is proposed that the significantly earlier MFB50 phasing (Figure 6-4) and shorter combustion duration of Bu20 (Figure 6-5), as compared to the other two fuels, provided more time for oxidation of the particulates after the combustion process, leading to the significant PN reduction. This appears to have overcome effect of the advanced KLMBT spark timing (Table 6-3), which would have reduced the fuel-air mixing time, as well as the effect of the reduced calculated average in-cylinder temperatures (Figure 6-2a). These would have resulted in more pockets of a high local equivalence ratio and a reduced oxidation rate in the combustion chamber, respectively, which alone would have led to an increase in accumulation mode particles.

Also, it is important to note that reduced calculated average in-cylinder temperatures will have also reduced the soot formation rate through reducing the formation of primary carbon particles (Zhang et al., 2014b), thus contributing to the reductions observed. In addition, it is thought that because the gasoline already had 5%vol ethanol content, the increase in ethanol content to 20%vol made little difference to the PN behaviour of E20. Furthermore, E20 may not have reduced PM because of increased piston/wall wetting resulting from the increased injection duration required to maintain the same engine load, due to its reduced calorific value. The calorific value of Bu20 is higher so this effect was not as significant as with E20. Overall, there is no significant effect of fuel type on the particles average size with all distributions peaking at around 60 nm.

(Gu et al., 2012, He et al., 2010, Karavalakis et al., 2013, Niass et al., 2012, Zhang et al., 2014b) also reported that 1-butanol addition to gasoline fuel reduced the PN concentration, and (Bielaczyc et al., 2014, Catapano et al., 2013, Catapano et al., 2014, Costagliola et al., 2013, Di Iorio et al., 2011, Ojapah et al., 2014, Storey et al., 2010, Vuk and Vander Griend, 2013) also observed the same for ethanol addition to gasoline fuel.

There are further reasons as to why the accumulation mode particles decreased with 1-butanol addition to gasoline fuel. There is a positive correlation between the accumulation mode particles and the polycyclic aromatic hydrocarbons (PAHs); the addition of alcohol to gasoline reduces the aromatic content of the fuel, thus it also caused the accumulation mode particles to decrease (De Abrantes et al., 2009, Zhang et al., 2014b). Furthermore, the oxygen content in the fuel blend leads to a lower formation rate of soot and also to a higher oxidation rate of soot (Zhang et al., 2014b). Biofuels tend to have a lower droplet velocity and relatively low mean droplet diameter, which reduces piston impingement resulting in higher combustion efficiency (Figure 6-6) and lower accumulation mode particle formation (Tian et al., 2010). Furthermore, biofuels burn at higher pressures (Figures 6-1a and 6-1b) which help to promote pyrolysis, reducing solid carbonaceous emissions (Daniel, 2012d).

Lastly, Bu20 had a noticeably higher number of nucleation mode particles than the other two fuels tested. It is thought that this was due to the lower soot accumulation mode particles observed, which meant less adsorption of the nucleation mode particles onto the accumulation mode particle surfaces occurred, leading to higher numbers being observed.

Overall, the effect of 1-butanol addition to gasoline on PM emissions is significant when the 95% confidence intervals are taken into consideration, while ethanol addition to gasoline has no significant effect at the blend ratio tested.

6.3.1.8 Gaseous Emissions (NO$_x$ and HC)

Figure 6-9 presents the NO$_x$ emission data for the two tested fuel blends and tested reference fuel. Overall, there is a significant increase in NO$_x$ emissions across the compression ratio range; they increased by 17.9% for Bu20, 21.7% for E20 and 23.5% for ULG95. These increases occurred because of the aforementioned increase in calculated average in-cylinder temperatures across the compression ratio range, which caused more NO$_x$ to be formed. It is also clear that ULG95 had the highest NO$_x$ emission, followed by Bu20 then E20. It is proposed that the lower calculated average combustion temperatures of Bu20 (Figure 6-2a) and E20 (Figure 6-2b) reduced the formation of NO$_x$ emissions in comparison to ULG95.

Despite the calculated average in-cylinder temperatures being similar for Bu20 and E20 across the compression ratio change and ethanol having a higher oxygen to carbon ratio than 1-butanol, Bu20 produced more NO$_x$ emissions than E20. It is proposed that the earlier MFB50 of Bu20 as compared to E20 (Figure 6-4) resulted in the observed behaviour. With an advanced MFB50, the fuel-air mixture burns at an earlier point in the engine cycle where the in-cylinder turbulence is stronger, causing the combustion to proceed more quickly. It is thought that this resulted in higher local temperatures which resulted in the increased NO$_x$ emissions for Bu20. Furthermore, the NO$_x$ emissions can also be attributed to the H/C ratio. E20 had the highest H/C ratio, followed by Bu20 then ULG95. As reported by (Harrington and Shishu, 1973), the NO$_x$ emission has an inverse relationship to H/C. The combustion of fuels with a higher H/C ratio tends to have a lower adiabatic flame temperature because water has a higher specific heat capacity than CO_2 (Harrington and Shishu, 1973, Daniel et al., 2011), thus further explaining why the NO$_x$ emission formation was lower for E20 as compared to Bu20.
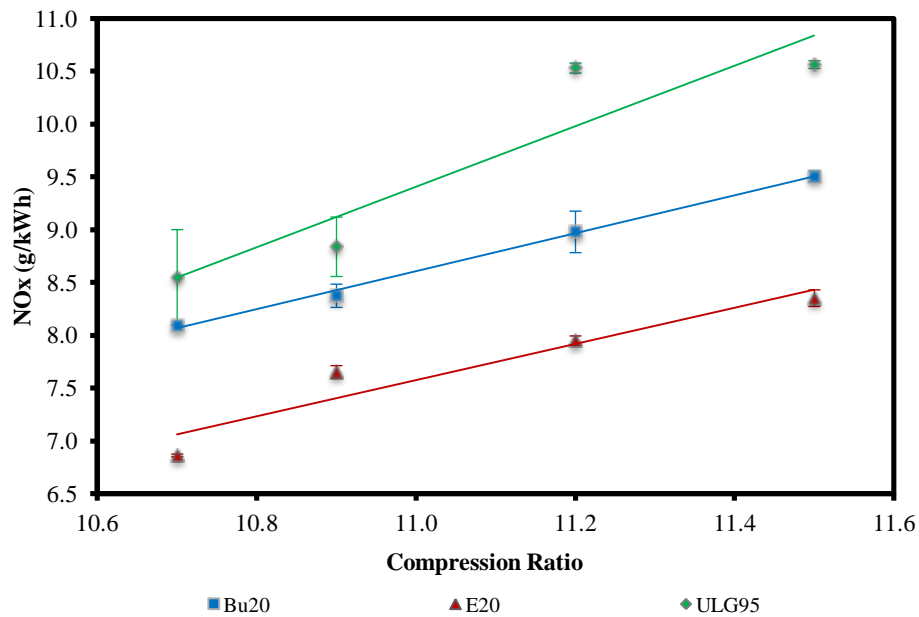
Figure 6-9   NO$_x$ emissions versus compression ratio at KLMBT spark timings

Figure 6-10 presents the HC emissions data for the two tested fuel blends and the tested reference fuel. It is clear to see that the HC emissions increased significantly across the compression ratio range; they increased by 20.9% for Bu20, 20.8% for E20 and 26.2% for ULG95. It is believed that the increased surface to volume ratio of the combustion chamber and the higher relative influence of the crevice volume as compared to the whole volume of the combustion chamber resulted in the observed HC emission increases (Kramer et al., 2000, Maji et al., 2001).

The HC emissions were lower for Bu20 and E20 as compared to ULG95 because their oxygen content was higher, which promoted the oxidation of HC in the combustion chamber. This appears to have overcome the reduced fuel-air mixing time caused by the more advanced KLMBT spark timings and the reduced combustion temperatures, which alone would have caused the HC emissions to increase. Ethanol has a higher oxygen to carbon ratio than 1-butanol, thus, there was a higher HC oxidation rate with E20 as compared to Bu20, leading to lower HC emissions in comparison. Also, the KLMBT spark timing was more

advanced for the Bu20 fuel blend in comparison to E20, resulting in poorer mixture preparation and thus higher HC emissions. Despite the differences observed in the HC (and NO$_x$) emission between the different fuels, this would be expected to diminish in a vehicle when a TWC is used, due to their high conversion efficiencies.

It must be noted that these HC emissions are uncorrected; the sensitivity of the FID analyser to oxygenated compounds has not been taken into account. Research has shown that FID analysers have reduced sensitivity to oxygenated fuels (Cheng et al., 1998, Wallner and Miers, 2008), suggesting that the HC emissions for Bu20 and E20 are higher than those observed in these results, necessitating detailed HC emission speciation for reliable analysis. The ULG95 fuel also contains oxygenated components (5%vol ethanol content) so its HC emissions are likely to be higher too.
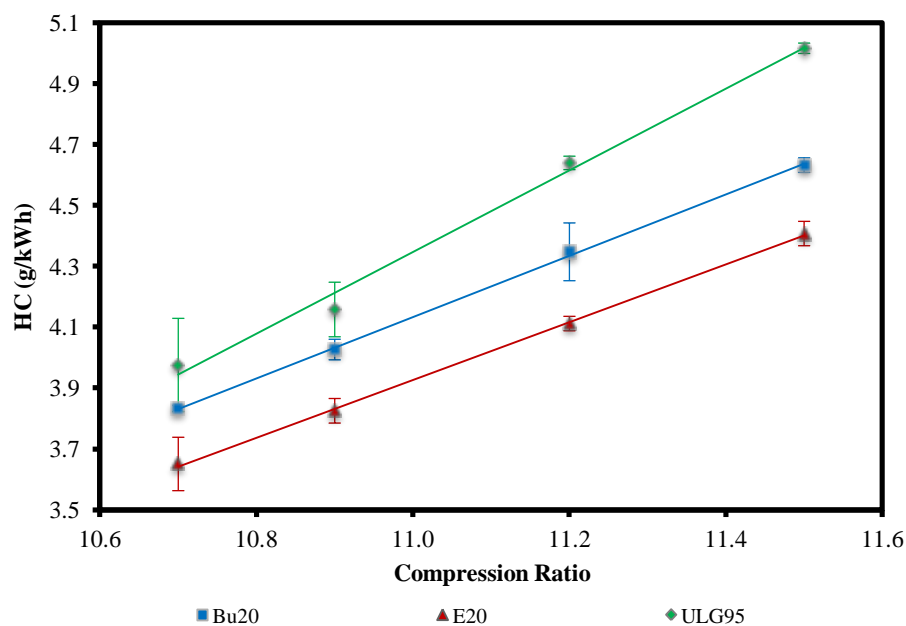

Figure 6-10   HC emissions versus compression ratio at KLMBT spark timings

6.3.1.9 Big Picture

Figure 6-11 shows the overall effect of compression ratio and fuel on the gaseous emissions, indicated efficiency and total PN. It is clear to see that for ULG95, the gaseous emissions of NO_x and HC increased with increased compression ratio, along with the indicated efficiency and total PN. However, when 1-butanol and ethanol are blended into the ULG95 fuel, the gaseous emissions of NO_x and HC are reduced, along with total PN, and the indicated efficiency is increased. Ethanol is most effective to reduce the gaseous emissions (NO_x and HC) of the ULG95 fuel and 1-butanol is most effective to reduce the total PN emission.
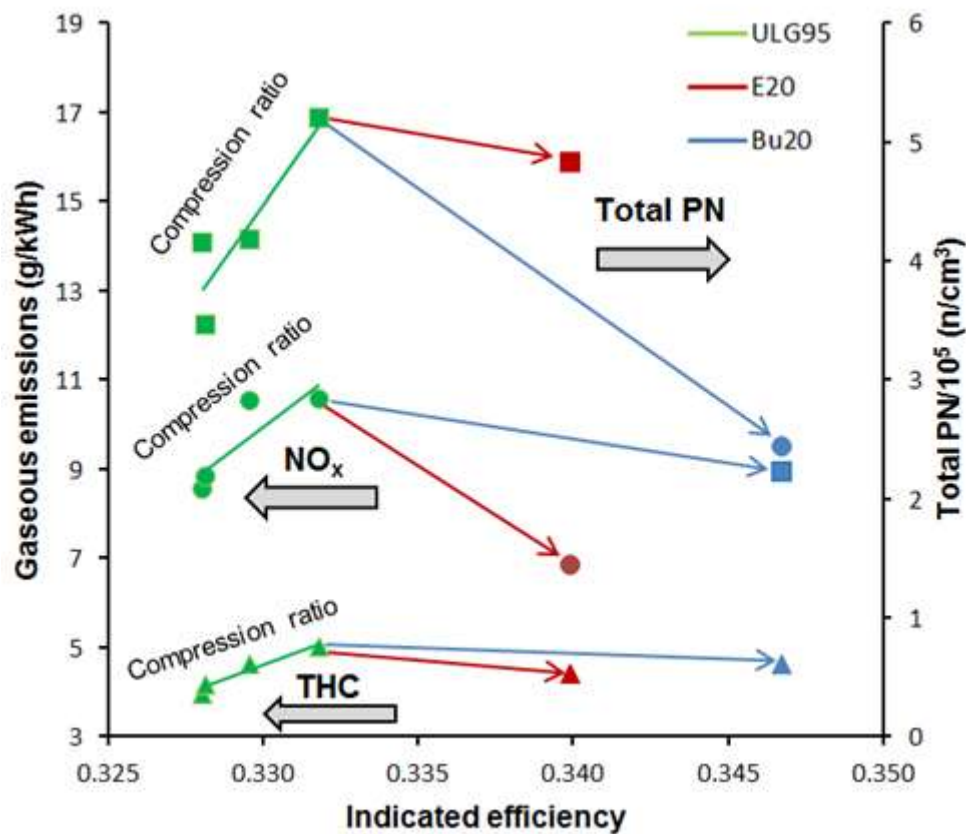

Figure 6-11   Overall effect of compression ratio and fuel on gaseous emissions, indicated efficiency and total PN (integrated across 10-289 nm range) at KLMBT spark timings

6.3.2 Investigation of the Compression Ratio and Hot EGR Effect on Combustion and PM Emissions

6.3.2.1 KLMBT Spark Timing

The KLMBT spark timings for the three EGR conditions are shown in Table 6-4. As the compression ratio was increased, the KLMBT spark timing was retarded because the fuel-air mixture was more compressed at TDC. This increased the pressure and temperature in the combustion chamber, leading to increases in the end-zone temperatures, which would have resulted in engine knock had the spark timing not been retarded. The research engine began to knock at a load of 6.0 bar IMEP, thus, the compression ratio increase made the engine more prone to knock at the tested load of 7.0 bar IMEP, resulting in the spark retard required.

The KLMBT spark timing was advanced as the EGR addition was increased because the temperatures in the end-zone of the combustion chamber were suppressed by the EGR gases. Despite this, KLMBT spark timing advances would likely have been greater if intake manifold temperature increases, resulting from the EGR addition, could have been eliminated. The overall effect of the compression ratio increase and EGR addition was to advance the spark timing by 2 CAD, due to the knock suppression ability of the EGR gases.

The 4 CAD retard in KLMBT spark timing at 7% EGR addition as the compression ratio was increased from 11.2 to 11.5, larger than the 2 CAD spark retard required with the other compression ratio increases, is not considered to be significant. Therefore, it will not be commented upon further.

Table 6-4   KLMBT spark timings (˚bTDC) (compression ratio & EGR addition)

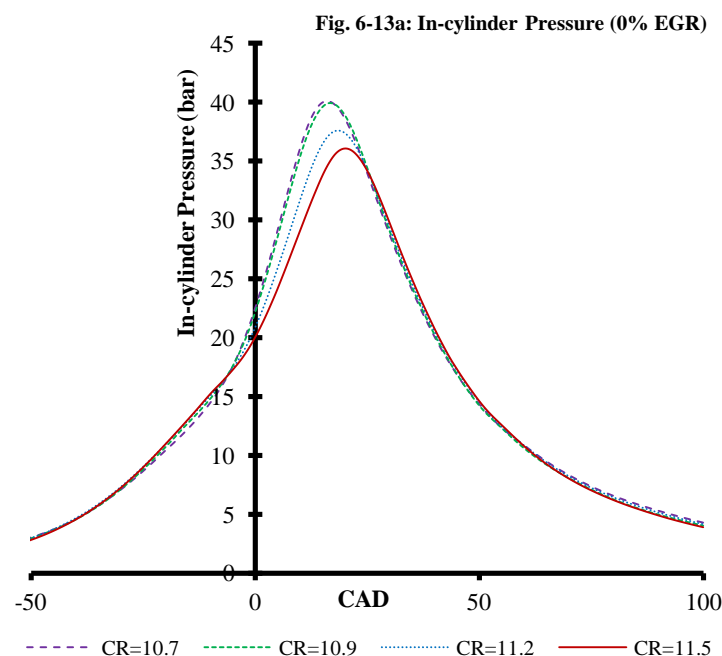| Compression Ratio / EGR Addition (%)	10.7	10.9	11.2	11.5
0	22	20	18	16
7	26	24	22	18
14	30	28	26	24

6.3.2.2 In-cylinder Pressures and Temperatures

The in-cylinder pressures at the KLMBT spark timings, as shown in Figures 6-12a, 6-12b and 6-12c for the three EGR conditions, generally reduced as the compression ratio was increased and the KLMBT spark timings (Table 6-4) had to be consequently retarded to avoid engine knock. It must be noted that knocking could have been avoided if the compression ratio was fully optimized for the fuel used. However, this was not pursued in order to investigate the effect of the parameter changes on engine knock limit and the consequent combustion and emission parameters at this limit.

At the compression ratio of 10.9, the in-cylinder pressure at 0 and 7% EGR addition did not reduce as compared to that at the compression ratio of 10.7, and it increased at 14% EGR addition. It is proposed that although the KLMBT spark timing had to be retarded with the compression ratio increase, the rate of heat release (ROHR) increased due to the more highly compressed fuel-air charge. At 14% EGR addition, this was also sufficient to overcome the retarded KLMBT spark timing, as the compression ratio was increased to 10.9. However, further increases in the ROHR produced by compression ratio increases beyond 10.9 were not sufficient to overcome the retarded combustion phasing resulting from the KLMBT spark timing retards, causing the in-cylinder pressure to reduce as the compression ratio was further increased.

The overall effect of compression ratio increase and EGR addition was reduced in-cylinder pressures as can be seen by comparing Figures 6-12a and 6-12c. It would appear the reduced ROHR produced by the EGR addition was more significant than the advanced combustion phasing resulting from the 2 CAD KLMBT spark timing advance (Table 6-4). Similarly (Alger et al., 2015) observed that in-cylinder pressure increases resulting from an increased compression ratio were cancelled out by the consequent spark retard required to avoid engine knock.

Smaller in-cylinder pressure decreases with EGR addition would have been likely if intake manifold temperature increases, resulting from the EGR addition, could have been eliminated. This is because, as mentioned, it would likely have led to a greater KLMBT spark timing advance and thus more of the energy released from the fuel would have contributed to the in-cylinder pressure increases.
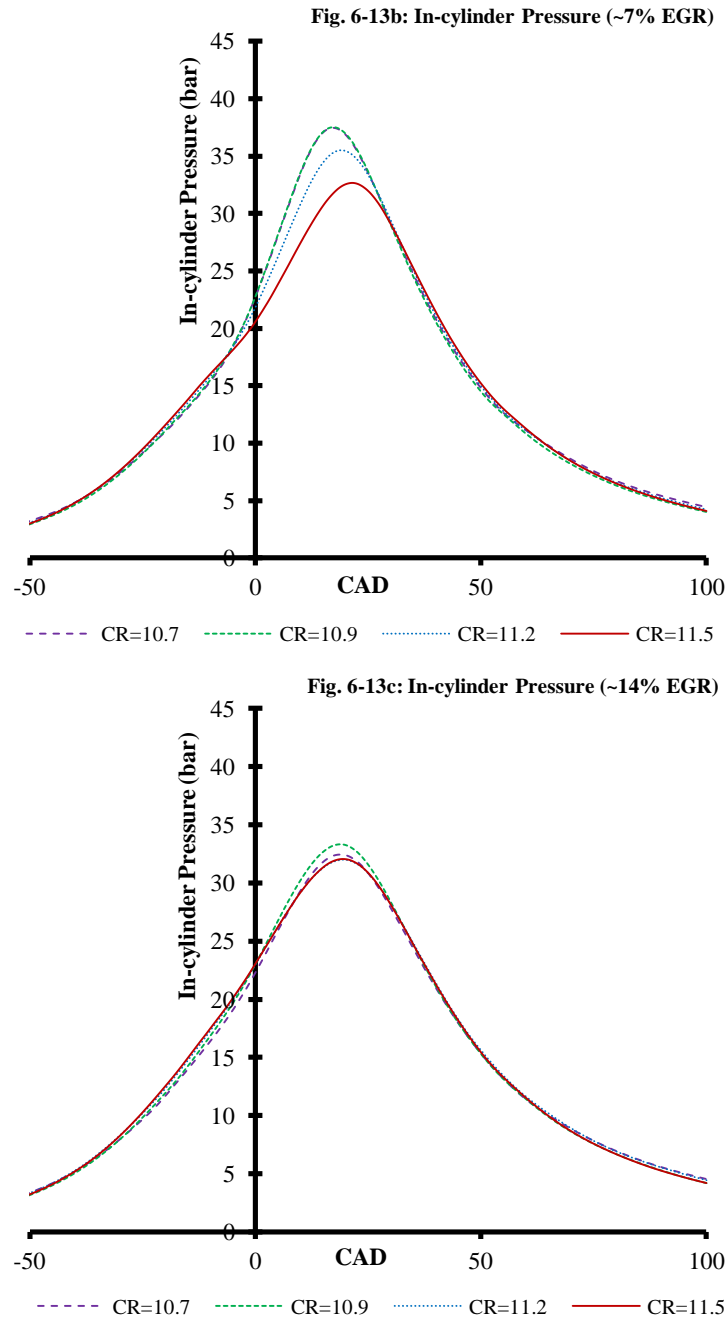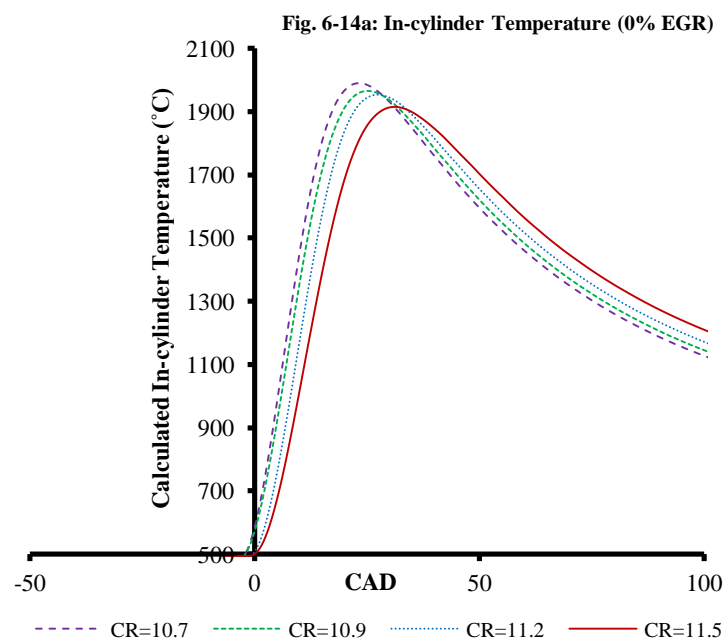

Fig. 6-13a: In-cylinder Pressure (0% EGR)

Fig. 6-13b: In-cylinder Pressure (~7% EGR)

CR=10.7   CR=10.9   CR=11.2   CR=11.5

Fig. 6-13c: In-cylinder Pressure (~14% EGR)

CR=10.7   CR=10.9   CR=11.2   CR=11.5

Figure 6-12   In-cylinder pressure versus CAD at KLMBT spark timings for **a)** 0% EGR, **b)** 7% EGR, **c)** 14% EGR

The calculated average in-cylinder temperatures at the KLMBT spark timings for the three EGR conditions, as shown in Figures 6-13a, 6-13b and 6-13c, generally reduced with compression ratio increases and consequent spark timing retards. This is again due to the KLMBT spark timing retards required with the compression ratio increases, as with the in-cylinder pressure reductions. The overall effect of increased compression ratio and EGR

addition was to reduce the average calculated in-cylinder temperatures as can be seen by comparing Figures 6-13a and 6-13c. This is the result of the KLMBT spark timing retards required to avoid engine knock at the increased compression ratios and the temperature suppression ability of the EGR gases due to their higher heat capacity as compared to air.

It is believed that the increased intake manifold temperatures resulting from the EGR addition were compensated for by the less optimized combustion phasing resulting from the consequently reduced KLMBT spark timing advance, compared to the maximum spark advance possible, as explained in the first part of Chapter 4. Thus, it is thought the two effects of increased intake manifold temperature and reduced subsequent KLMBT spark timing advances cancelled one another out, meaning there was no overall effect on the peak of the calculated average in-cylinder temperatures. Again, it is thought that the improved KLMBT spark timing would have quickly compensated for the intake gas temperature decrease by the time temperatures reached the beginning of the range reported (500˚C); thus, the effect would have been minimal.
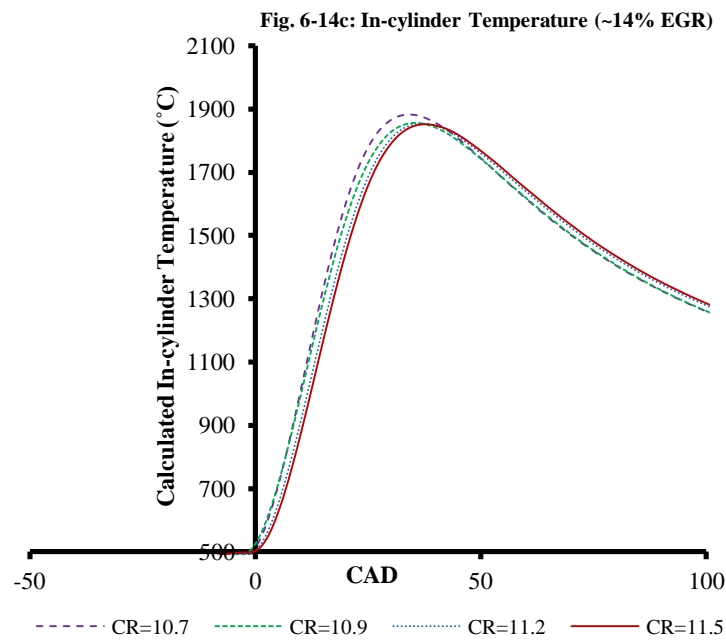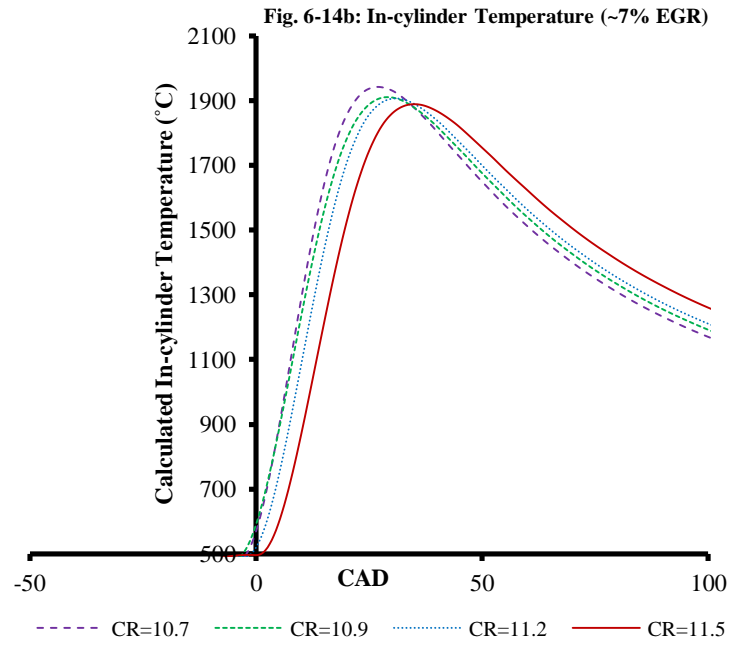

Fig. 6-14a: In-cylinder Temperature (0% EGR)

Fig. 6-14b: In-cylinder Temperature (~7% EGR)

CR=10.7   CR=10.9   CR=11.2   CR=11.5

Fig. 6-14c: In-cylinder Temperature (~14% EGR)

CR=10.7   CR=10.9   CR=11.2   CR=11.5

Figure 6-13   Calculated average in-cylinder temperatures versus CAD at KLMBT spark timings for **a)** 0% EGR, **b)** 7% EGR and **c)** 14% EGR

6.3.2.3 MFB

The MFB profiles at the KLMBT spark timings for the three EGR conditions are shown in Figures 6-14a, 6-14b and 6-14c. The profiles became retarded as the compression ratio was increased because of the KLMBT spark retard that was required in order to avoid engine knock. From the MFB profile for 14% EGR addition (Figure 6-14c) it can be seen that there

was a less significant difference between the profiles at different compression ratios as compared to the MFB profiles for 0% and 7% EGR addition. It is thought that the knock suppression ability of the EGR gases allowed the MFB50s at the different compression ratios to be more advanced towards their optimum phasing, resulting in the MFB profiles becoming more similar to each other at the highest EGR addition.

From comparing Figures 6-14a and 6-14c, it can be seen that the overall effect of the compression ratio increase and EGR addition was to retard and elongate the MFB profile, due to the KLMBT spark timing retard required with the compression ratio increase and the combustion slowing effects of the EGR gases (Rhodes and Keck, 1985).

Again, KLMBT spark timing advances would likely have been greater if intake manifold temperature increases, resulting from the EGR addition, could have been eliminated; thus, the retardation of the MFB profiles would likely have been reduced. The MFB profiles will have become slightly more elongated too because the slightly cooler fuel-air charge will have burned more slowly. If the compression ratio was fully optimised for the fuel used, the combustion phasing would have been optimised for each EGR ratio tested, therefore, it would be expected that the combustion would have been quicker at each condition due to higher in-cylinder turbulence at the time of ignition.
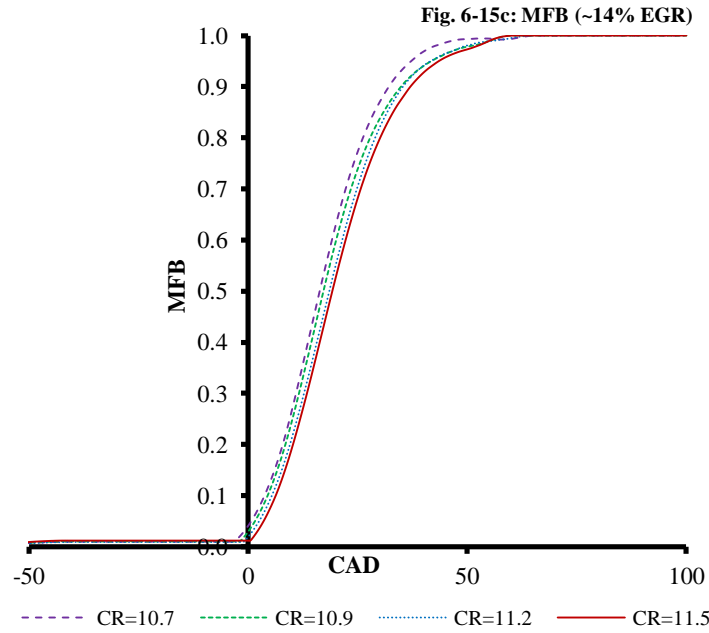
Fig. 6-15a: MFB (0% EGR)

Fig. 6-15b: MFB (~7% EGR)

211
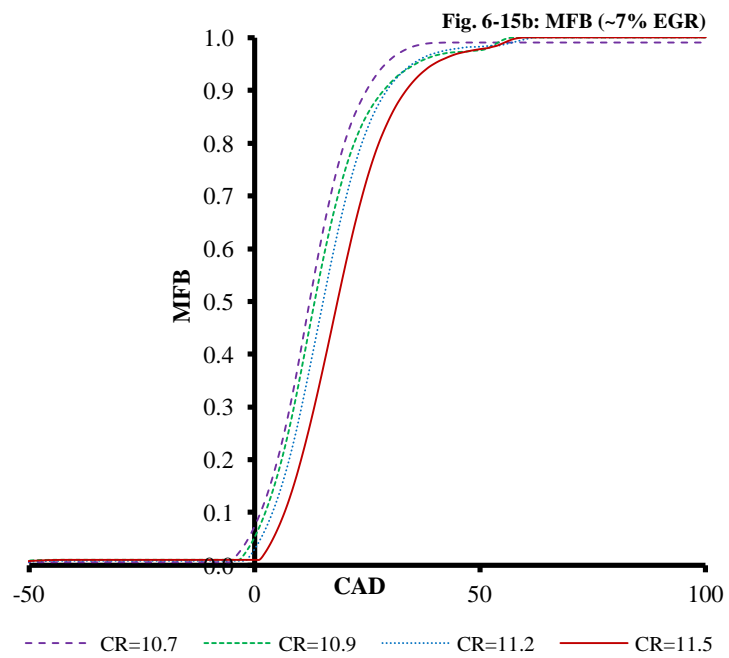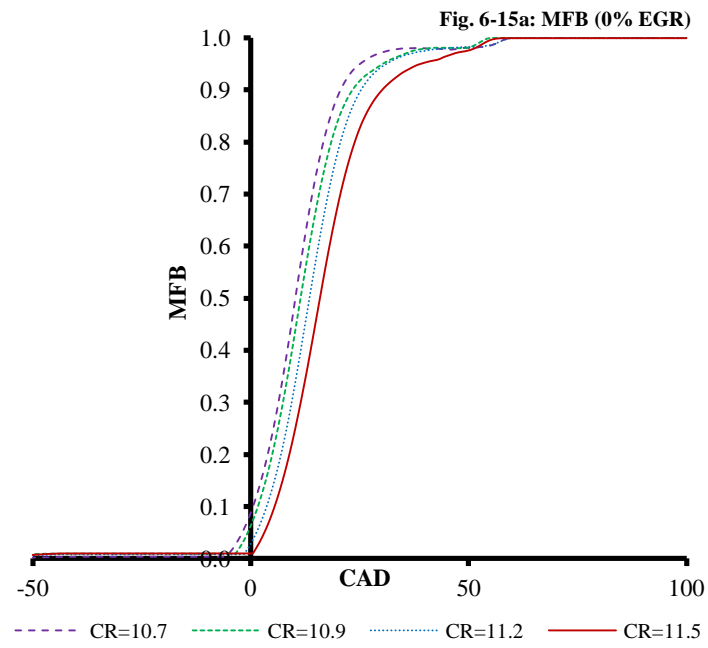
Figure 6-14 MFB versus CAD at KLMBT spark timings for **a)** 0% EGR, **b)** 7% EGR and **c)** 14% EGR

6.3.2.4 Fuel Consumption

Gravimetric $ISFC_{net}$ at the KLMBT spark timings, as shown in Figure 6-15, increased across the compression ratio range due to the KLMBT spark timing retards that were required. This caused the MFB50 (Figures 6-14a-c) to become retarded away from its optimum 8-10˚aTDC phase (de O. Carvalho et al., 2012), thus causing the fuel consumption increase observed. Fuel consumption increased by 4.4, 4.5 and 4.4% for the 0, 7 and 14% EGR additions, respectively. Therefore, increasing the compression ratio at 7.0 bar IMEP resulted in worse fuel consumption behavior.

Across the EGR range the fuel consumption decreased significantly, due to the KLMBT spark timing advances and PMEP reductions that could be achieved. It decreased by 4.6, 4.6, 4.3 and 4.6% for the compression ratios of 10.7, 10.9, 11.2 and 11.5 respectively. While the KLMBT spark timing advances were not sufficient to advance the MFB profile (Figures 6-14a-c), the PMEP was reduced significantly across the EGR range. The PMEP reduced from

0.36 to 0.28 bar, 0.36 to 0.27 bar, 0.38 to 0.26 bar, and 0.34 to 0.25 bar for the compression ratios of 10.7, 10.9, 11.2 and 11.5, respectively. Furthermore, the reduced combustion temperatures with EGR addition improved thermal efficiency (Ratnak et al., 2015, Siokos et al., 2015), contributing to the fuel economy improvements observed.

Overall, the indicated fuel consumption decreased by 0.4% across the compression ratio and EGR range; i.e. the fuel consumption was decreased by 0.4% at the compression ratio of 11.5 and EGR addition of 14% as compared to that observed at the compression ratio of 10.7 and EGR addition of 0%. This is because of the reduction in pumping losses and the 2 CAD KLMBT spark timing advance. Again, KLMBT spark timing advances would likely have been greater if intake manifold temperature increases resulting from the EGR addition could have been eliminated; thus, the fuel consumption reductions would likely have been greater. Although the fuel consumption reduction observed is considered to be significant, it must be noted that the VAF had an average error of 1.6%. Thus, the reduction of 0.4% could have resulted from this error, meaning that the result observed is limited.
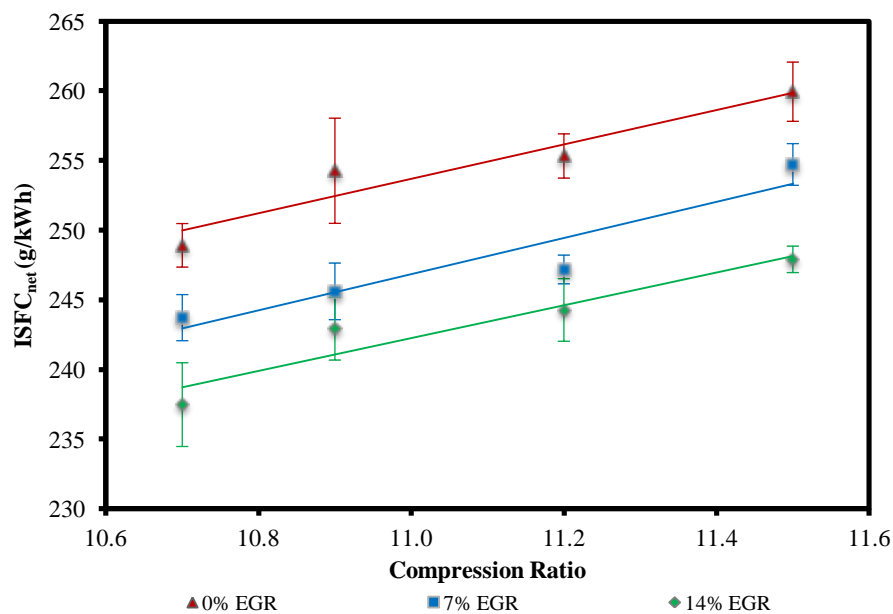

Figure 6-15   Gravimetric $ISFC_{net}$ versus compression ratio at KLMBT spark timings

6.3.2.5 PM Emissions

The PN emissions at the KLMBT spark timings for the three tested EGR conditions are shown in Figures 6-16a, 6-16b and 6-16c. For the 0 and 7% EGR additions, there was a significant increase in nucleation mode particles across the compression ratio range. There was also a small but significant increase in accumulation mode particles across the compression ratio range at 0% EGR addition, while at 7% EGR addition, there was no significant change in the accumulation mode particles across the range. Furthermore, the accumulation mode particles significantly increased across the compression ratio range with 14% EGR addition, but there was no significant change in the nucleation mode particles at this EGR addition.
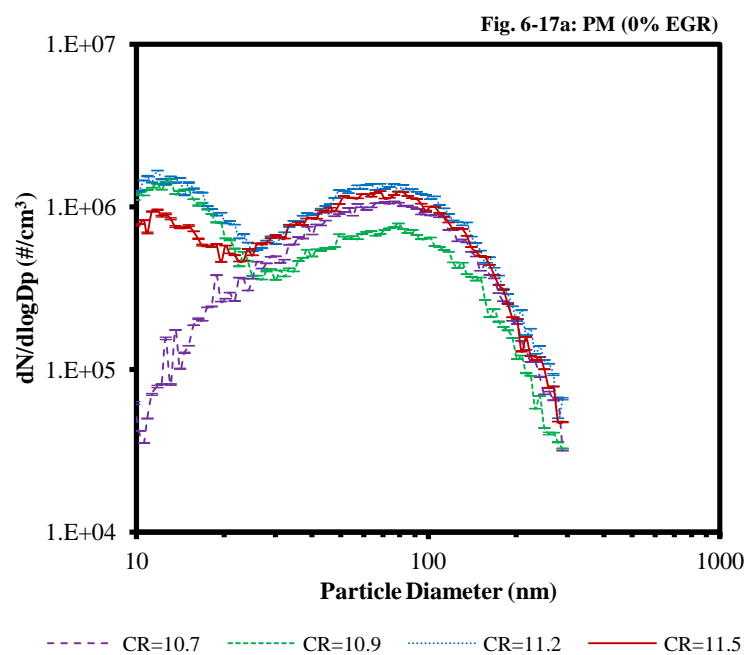
It is proposed that the reduced calculated average in-cylinder temperatures (Figures 6-13a-c) caused by the KLMBT spark timing retards (Table 6-4) reduced the oxidization of particles in the combustion chamber in the expansion and exhaust strokes, resulting in the observed behavior. This appears to have been more significant than the reduced primary carbon particle formation, resulting from the reduced in-cylinder temperatures (Zhang et al., 2014b). In addition, the time for post-combustion oxidization was reduced (Figures 6-14a-c) due to the MFB profile becoming more retarded, contributing to the increased PNs observed. It is believed that the accumulation mode particles did not significantly increase at 7% EGR addition because the KLMBT spark timing became more retarded across the compression ratio range (Table 6-4) as compared to the other EGR additions. This provided more time for fuel-air mixing in comparison which reduced the number of pockets of a high local equivalence ratio, meaning the fuel was burned more completely, cancelling out the effect of the reduced oxidization produced by the average in-cylinder temperature reductions.

Across the EGR range there was a small but significant decrease in the nucleation and accumulation particles observed for the compression ratios tested. It is proposed that the calculated average in-cylinder temperature decreases across the EGR range (Figures 6-13a-c) reduced primary carbon particle formation by the thermal pyrolysis and dehydrogenation reaction of fuel vapour/droplets, resulting in the PN decreases observed (Zhang et al., 2014b). In addition, the slower combustion produced by the EGR addition (Figures 6-14a-c) provided more time for the particulates to oxidize in the hot flames, contributing to the reductions observed. These effects appear to have been more significant than the reduced fuel-air mixing time due to the KLMBT spark timing advances (Table 6-4). This alone would have created more pockets of a high local equivalence ratio which would have produced higher PNs.

The overall effect of the compression ratio increase and EGR addition was a small but significant increase in the nucleation mode particle number and a significant reduction in the accumulation mode PN. The KLMBT spark timing was only advanced by 2 CAD (Table 6-4) therefore, it is not thought that the relative homogeneity of the two mixtures was significantly different. However, the primary carbon particle formation was reduced (Zhang et al., 2014b), due to the in-cylinder temperature decreases across the EGR range. This resulted in the reduced PN observed. In addition, the slower combustion produced by the EGR addition provided more time for the particulates to oxidize in the hot flames, contributing to the PN reductions. It is thought that due to the lower numbers of accumulation mode particles across the compression ratio range, less nuclei adsorption happened, which caused the observed increases in the nucleation mode particles.

If the intake manifold temperature increases with EGR addition could have been eliminated, then it is expected that the PM emissions would have been further reduced with EGR addition due to the greater post-combustion oxidation time available with the expected greater

expected KLMBT spark timing advances (Daniel et al., 2012e). The slightly longer expected combustion duration would also decrease the PM observed. However, poorer mixture preparation resulting from the greater KLMBT spark timing advances would be expected to limit the PM reductions, especially since this effect would be expected to result in an overall PM increase in the results from the first part of Chapter 4. As discussed, the intake manifold temperature effect on the calculated average in-cylinder temperature is believed to have been minimal; therefore, this is not thought to have affected the PM.
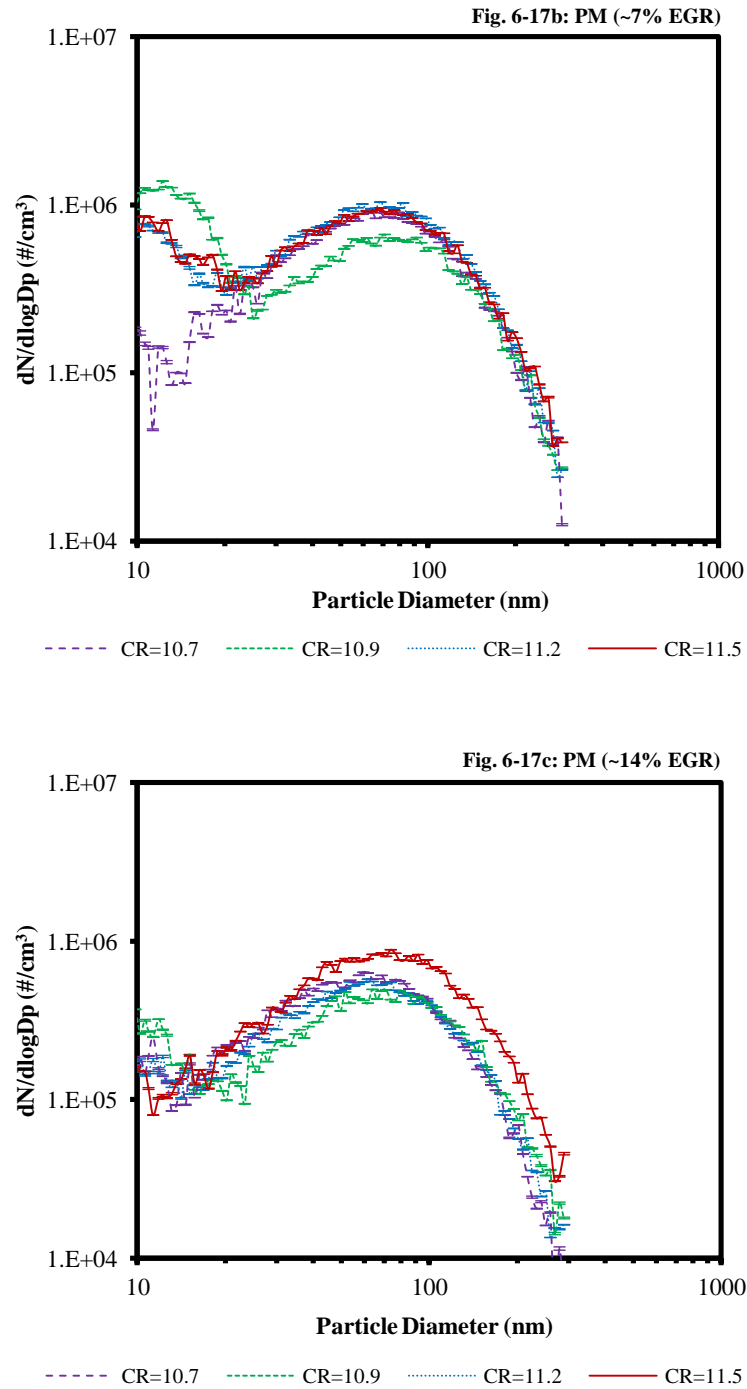

Fig. 6-17a: PM (0% EGR)

Fig. 6-17b: PM (~7% EGR)

----- CR=10.7   ------- CR=10.9   ············ CR=11.2   ——— CR=11.5

Fig. 6-17c: PM (~14% EGR)

----- CR=10.7   ------- CR=10.9   ············ CR=11.2   ——— CR=11.5

Figure 6-16   PN emissions versus particle diameter at KLMBT spark timings for **a)** 0% EGR, **b)** 7% EGR and **c)** 14% EGR

6.4 Data Continuity

For a detailed analysis regarding the continuity of the data between this chapter and Chapters 4 and 5, please refer to **Appendix B3**.

6.5 Conclusions

The effect of compression ratio and fuel on the combustion and emissions of a single cylinder DISI research engine was investigated in this chapter and the following conclusions have been made.

1. 1-butanol and ethanol addition to gasoline advanced the MFB50 phasing as well as reducing the overall combustion duration across the compression ratio range; 1-butanol had the greatest effect on these parameters.

2. 1-butanol addition to gasoline significantly reduced the accumulation mode PN emission, mainly due to the earlier combustion phasing and thus increased post-combustion oxidization time; ethanol addition to gasoline had little effect on the emission.

3. 1-butanol and ethanol addition to gasoline significantly reduced the NO_x and HC emission across the compression ratio range, with ethanol being the most effective.

4. Overall, if combustion and PN emission parameters are the priority, then the Bu20 fuel blend has the most potential, while if NO_x and HC emission parameters are the priority, then the E20 fuel blend has the most potential. Synergies between compression ratio increase and alcohol addition to gasoline enable PM and gaseous emissions to be simultaneously controlled while increasing indicated efficiency with respect to standard gasoline combustion.

The main findings from this section are also summarized in Table 6-5.

Table 6-5   Results summary (compression ratio & fuel) (==highlighted===improvement, <u>underlined</u>=worsening)

Result Summary Compression Ratio/Fuel	KLMBT	Indicated Efficiency	EGT	PM		NO$_x$	HC
				Nucleation	**Accumulation**		
Bu20 (at compression ratio of 11.5, compared to 10.7)	0 CAD	==1.3%==	==21.0°C==	No sig. change	No sig. change	<u>17.9%</u>	<u>20.9%</u>
E20 (at compression ratio of 11.5, compared to 10.7)	0 CAD	==1.3%==	==16.2°C==	No sig. change	No sig. change	<u>21.7%</u>	<u>20.8%</u>
ULG95 (at compression ratio of 11.5, compared to 10.7)	0 CAD	==1.1%==	==13.4°C==	No sig. change	No sig. change	<u>23.5%</u>	<u>26.2%</u>
Bu20 (compared to ULG95 at compression ratio of 11.5)	==4 CAD==	==4.5%==	==21.3°C==	==Reduction==	==Reduction==	==10.0%==	==7.7%==
E20 (compared to ULG95 at compression ratio of 11.5)	==2 CAD==	==2.4%==	==14.6°C==	No sig. change	No sig. change	==20.9%==	==12.1%==

The effect of compression ratio and hot EGR on the combustion and PM emissions of a single cylinder DISI research engine was also investigated in this chapter and the following conclusions have been made.

5. EGR addition of 14% overcame the increased knock produced as the compression ratio was increased from 10.7 to 11.5, resulting in an overall KLMBT spark timing advance of 2 CAD with the compression ratio increases and EGR addition.

6. Fuel consumption was reduced significantly by 0.4% as the compression ratio was increased from 10.7 to 11.5 and the EGR addition was increased from 0 to 14%; reduced pumping losses, lower in-cylinder temperatures (improved thermal efficiency) and the KLMBT spark timing advance resulted in the decrease observed.

7. PM was significantly reduced with compression ratio increase and EGR addition due to the reduced primary carbon particle formation resulting from the in-cylinder temperature decreases across the EGR range. In addition, the increased time available

for PM to oxidize in the hot flames, due to the slower combustion which resulted from

EGR addition, contributed to the PM decreases observed.

The main findings from this section are also summarized in Table 6-6.

Table 6-6   Results summary (compression ratio & EGR addition)
(highlighted=improvement, underlined=worsening)

Result Summary Compression Ratio/EGR	KLMBT	ISFC$_{net}$	PM	
			Nucleation	**Accumulation**
Compression ratio of 11.5, 0% EGR addition (compared to 10.7, 0% EGR addition)	6 CAD	4.4%	Increase	Increase
Compression ratio of 11.5, 14% EGR addition (compared to 11.5, 0% EGR addition)	8 CAD	4.6%	Reduction	Reduction
Compression ratio of 11.5, 14% EGR addition (compared to 10.7, 0% EGR addition)	2 CAD	0.4%	Increase	Reduction

Chapter 7

Summary, Conclusions and Suggestions for Future Work

The main aim of this thesis was to study the effect of EGR on the combustion and emissions of a DISI engine. In particular, the PM emissions were studied, and the results and discussion from this work are shown in the preceding chapters. The simplicity of EGR should allow for its adoption in all automotive gasoline engines rather than the partial adoption we see today, allowing increased compression ratios to be used as well as increased swirl and tumble ratios. However, PM still remains a challenge which could be overcome with increased swirl ratios and by blending 1-butanol into gasoline fuel. The aim of this chapter is to present the summary and conclusions of this current investigation and to make suggestions for future work.

7.1   Summary and Conclusions

This thesis contains numerous results from three chapters of experimental data from a 4-valve, 4-stroke, single-cylinder spray-guided DISI research engine, with a variable compression ratio of 10.7-11.5:1. The most significant findings of the investigation are presented below according to the area of study they came from.

It must be noted that the compression ratio was not optimized for each fuel used and for each engine condition tested. For the conditions which did not knock (e.g. 5.5 bar IMEP) the compression ratio could have been increased to improve thermal efficiency and the optimum combustion phasing would not have been affected. For the conditions which did knock, the compression ratio could have been reduced in order to obtain the optimum combustion phasing to improve thermal efficiency, although this would have been limited by the

reduction in thermal efficiency resulting from the compression ratio reduction. The least optimized load was 8.5 bar IMEP when gasoline fuel was used with no EGR addition since this required significant spark retards in order to avoid engine knock.

The Effect of EGR and its Type on Engine Combustion and Emissions

EGR addition of up to 13% enabled the KLMBT spark timing to be significantly advanced due to the suppression of end-zone temperatures, which was sufficient to advance the MFB profiles at 7.0 and 8.5 bar IMEP, but because the load of 5.5 bar IMEP was not knock limited, the MFB profile was already optimized so improvements could not be made. The more optimum MFB50 combustion phasing at 7.0 and 8.5 bar IMEP along with pumping reductions at all tested loads due to the throttle being more opened reduced the fuel consumption across the EGR ranges (2.2% at 5.5 bar IMEP, 4.1% at 7.0 bar IMEP, and 1.0% at 8.5 bar IMEP). PM accumulation mode emissions generally increased at 5.5 and 7.0 bar IMEP due to the lower in-cylinder and exhaust temperatures while they reduced in the nucleation mode through increased nuclei adsorption due to the greater number of accumulation mode particles present. The low EGR addition of 3% at 8.5 bar IMEP resulted in no significant changes in the PM. Finally, NO_x emissions decreased significantly due to the lower in-cylinder temperatures and HC emissions increased significantly due to the lower in-cylinder and EGTs.

Extending the work further allowed the hot EGR system from the first experiment to be compared against a cooled EGR system, along with a hot and cooled EGR system with a simulated TWC, at 7.0 bar IMEP, with EGR addition of up to 14%. The KLMBT spark timing could be most advanced with the cooled EGR after TWC EGR type due to the cooler gases suppressing end-zone temperatures and because the EGR gases did not contain NO which induces knock. The fuel consumption improvement (3.8%) was greatest for cooled

EGR, mostly due to its most improved MFB50 combustion phasing as compared to the other EGR types. Gaseous emissions (NO_x and HC) were best optimized with the cooled EGR after TWC EGR type (45.3% NO_x decrease and 10.1% HC increase). This is mainly because its MFB50 combustion phasing did not advance across the EGR range as significantly as the cooled EGR type. This resulted in less NO_x formation in comparison, because with the less advanced MFB50, the fuel-air mixture burned at a later point in the engine cycle where the in-cylinder turbulence was weaker, causing the combustion to proceed less quickly. This is believed to have resulted in lower local temperatures in comparison to the cooled EGR condition which resulted in the lower NO_x and thus greater NO_x reductions across the EGR range. Also, because the simulated gas came from a gas bottle, it did not introduce additional HCs into the combustion chamber (reflecting the behaviour of a TWC with 100% efficiency) as the hot and cooled EGR types did, reducing the HC increases observed.

The Effect of Intake Airflow and EGR on Engine Combustion and PM Emissions

Swirl and high tumble intake airflows significantly retarded the KLMBT spark timing at 7.0 bar IMEP. However, significant improvements could be made for all the intake airflow conditions with EGR addition of up to 11%. Fuel consumption increased significantly with swirl (6.4%) and high tumble (15.5%) intake airflows as compared to the reference low tumble condition because of the KLMBT spark timing retards required. However, the improvements made with EGR addition reduced the fuel consumption penalty significantly compared to the reference condition (4.8% and 6.2% increase, respectively, at maximum EGR additions).

PM was significantly reduced with the swirl intake airflow due to improved mixture formation resulting from the KLMBT spark timing retard providing more fuel-air mixing time and from the increased in-cylinder turbulence produced by the airflow. The high tumble

condition resulted in reduced nucleation but similar accumulation mode particles compared to the reference low tumble condition. This is because the post-combustion oxidization time was significantly reduced by the KLMBT spark timing retard and the improved mixture formation was not sufficient to overcome this. EGR addition reduced PM for the reference low tumble condition due to an increased post-combustion oxidization time resulting from the KLMBT spark timing advances. However, it remained approximately the same across the EGR range for the swirl and high tumble conditions. It is thought that the KLMBT spark timing advances resulted in poorer fuel-air mixture preparation due to reduced mixture preparation time available, which in addition to the reduced calculated average in-cylinder temperatures for the swirl condition across the EGR range, cancelled out the effect of the increased post-combustion oxidization time. It also cancelled out the effect of decreased primary carbon particle formation resulting from the in-cylinder temperature reductions for the swirl condition.

The Effect of Compression Ratio, Fuel and EGR on Engine Combustion and Emissions

At 8.5 bar IMEP, compression ratio increases from 10.7 to 11.5 did not result in KLMBT spark timing changes because the load condition of 8.5 bar IMEP was already prone to knock, so it did not worsen despite increasing the compression ratio. Bu20 had the most advanced KLMBT spark timing, followed by E20, then ULG95, mainly due to the 5%vol ethanol pre-mixed in it, giving it a 25%vol total alcohol content, as compared to only 20%vol for E20. Indicated efficiency was most improved for Bu20 and E20 due to their greater KLMBT spark timing advances as compared to ULG95. Compression ratio had little effect on the PM emission, with the most significant effect being the Bu20 fuel blend which reduced PN. This was mainly due to its most advanced spark timing and shorter combustion duration significantly increasing the post-combustion oxidation time available. Increasing the

ethanol addition from 5%vol (ULG95) to 20%vol (E20) had no significant effect on the PM emission.

At 7.0 bar IMEP, compression ratio increases from 10.7 to 11.5 resulted in the KLMBT spark timing becoming more retarded. This is because the engine was less prone to knock at this load, so small changes in the compression ratio made a significant difference to the knock tendency. EGR addition of 14% however enabled this effect to be overcome, enabling the KLMBT spark timing to be advanced overall by 2 CAD with compression ratio increases and EGR addition. Fuel consumption was significantly improved by 0.4% with the compression ratio increases and EGR addition due to the reduced pumping losses with EGR addition and the KLMBT spark timing advances. Finally, PM emissions were reduced overall with the compression ratio increases and EGR addition, because of the improved oxidation of particulates in the slower flame, and the reduced primary carbon particle formation resulting from in-cylinder temperatures decreases.

7.2 Suggestions for Future Work

This study has explored a wide range of combustion and emission aspects of EGR use in DISI engines, along with that of swirl and tumble intake airflows, compression ratio increase and oxygenated fuels. However, before the approaches outlined in this thesis can be fully implemented in commercial DISI engines, further research is required to better understand the behaviour of these parameters and to tackle the main challenges that have been identified in their use. The author has thus outlined some of the outstanding issues below to serve as recommendations for future work.

In general, the investigation should be extended to quantify the effects of EGR and its type, swirl and tumble intake airflows, compression ratio and oxygenated fuels over the entire

engine load and speed range. Split-injection strategies, different fuel injection timings and different valve timings/lifts should be studied to optimize the combustion and emissions. Synergies between these different techniques (e.g. swirl & tumble and EGR along with increased compression ratio) should be investigated once they have all been explored individually on a deep level. Results should be obtained not only at KLMBT spark timings but at a 10 CAD retard from the KLMBT too, because these are used in cold-start for catalyst warming and in turbocharged engines for knock reduction.

The compression ratio should be optimized for each fuel to ensure that the MFB50 does not become too retarded from its optimum phasing. However, it should be noted that any decrease in the compression ratio will lead to lower indicated efficiencies at the engine loads that did not knock while potentially increasing the indicated efficiencies at the higher engine loads which did knock. This will only happen if the benefits of increased burning speed due to the increased in-cylinder turbulence during the combustion are greater than the reduced thermal efficiency resulting from the lower compression ratio.

This investigation should be done ideally in a modern prototype development engine with turbocharging to increase the usefulness of the data for current engine development. It should also be conducted with more accurate fuel consumption measurement equipment to accurately quantify the fuel consumption improvements observed in this investigation. Transient tests should be conducted including NEDC and the upcoming RDE tests both in engine and vehicle test rigs to understand how the different techniques affect real-world emissions.

Tests should be conducted to investigate whether the use of the thermodenuder makes the nucleation mode particles recorded more consistent or not, since it is designed to remove

them. Furthermore, the tests should be conducted on 3 consecutive days in varying order to take day-to-day variability, resulting from changing ambient conditions and engine drift (Beck et al., 2006) into account, since this can potentially affect the data; especially PM. Specific further investigation for each particular research area is detailed in **Appendix C1**.

Appendix A1: Analysis of the Uncertainties in the Recorded Data

The data collected in this investigation is accurate; however, there will always be a limit to how accurate the data is. Therefore, the accuracy of the main components of the engine test rig and emissions measurements systems have been collected from the relevant manufacturer instruction manuals and they are discussed in the following section. This builds on the work of a previous research student in the engine group who conducted the initial analysis (Turner, 2010).

In order to control the engine dynamometer, a Mentor II Digital DC drive manufactured by Control Technologies was used. The encoder had an accuracy which is better than 0.01% and the drive can maintain the dynamometer speed to an accuracy of 0.1%. The VVT system had a steady state positional accuracy of $\pm 0.1\ CAD$ as shown on the LabView control panel for the system. The Kistler 6041A water cooled pressure transducer had a linearity error of less than $\pm 0.5\%$ of the full scale. Its short term drift, as measured by a reference sensor in the engine, when it is operating at 1500 rpm and at an engine load of 9 bar IMEP, quantified as a pressure and as a percentage, were ± 0.25 bar and $\pm 2\%$, respectively. The Kistler 5011B charge amplifier used to amplify the pressure signal had a linearity error of less than $\pm 0.05\%$ of the full scale.

The VAF meter produced AFR readings which had an average error of 1.6% for the AFRs used in this investigation. The inaccuracies resulted mainly from the limited resolution of the inclined u-tube manometer (1 mm) and the limited pressure difference produced by a given flow rate for the orifice plate, as discussed previously.

Regarding the PM emission measurement, the DMS500 manufactured by Cambustion Ltd. had a particle count accuracy of $\pm$16%. For the SMPS system, the condensing particle counter (model 3775) manufactured by TSi had a particle count accuracy of $\pm$10% for particle concentrations lower than 5×10^4 particles/cm^3 and $\pm$20% for particle concentrations larger than 5×10^4 but smaller than 1×10^7 particles/cm^3. The gaseous emission measurements obtained with the Horiba MEXA-7100DEGR were accurate to within $\pm$1% of the full scale.

Overall, this data highlights the limited accuracy of the equipment used in this investigation; particularly that of the particulate emission measurements. This should be taken into consideration in regards to the repeatability of the results reported in this thesis.

Appendix B1: Data Continuity (Chapter 4)

The results from the 7.0 bar IMEP condition in the first part of the chapter are directly comparable with the results from the hot EGR condition in the second half of the chapter, because they were recorded at the same engine condition (7.0 bar IMEP, hot EGR). As can be expected, there are some differences between the data. 14% EGR addition was achieved with the hot EGR condition while only 12% EGR addition was achieved at the 7.0 bar IMEP condition because two EGR lines rather than one were used, which enabled the flow rate of EGR gases to be increased. As a result, the KLMBT spark timing advances (Table 4-4 vs. Table 4-3) were greater and the EGT reductions were also greater (Figure 4-16 vs. Figure 4-5), which resulted from the increased EGR addition and the subsequently improved KLMBT spark timing advances.

Despite this, the MFB50 was retarded across the EGR range for the hot EGR condition in the second part of this chapter (Figure 4-12) while it was advanced across the EGR range at the 7.0 bar IMEP condition (Figure 4-3b). This was due to the flame speed reducing in the final 10% MFB as can be seen by comparing the profiles. It is believed that the more advanced KLMBT spark timing resulted in poorer mixture preparation, producing the observed difference. The fuel consumption improvements were greater in the first part of the chapter (Figure 4-4) with the 7.0 bar IMEP condition than they were in the second part of the chapter with the hot EGR condition (Figure 4-14), despite the more advanced spark timing. It is thought that the 1.6% error in fuel consumption measurements discussed previously resulted in the difference observed.

The HC emission increase was greater in the first part of the chapter with the 7.0 bar IMEP condition (Figure 4-8 vs. Figure 4-20), despite the lower EGR addition that was achieved for

the hot EGR condition in the second part of the chapter. It is believed that the research fuel used in the second part of the chapter had a higher oxygen content than the pump fuel used in the first part of the chapter, helping to suppress the HC emission increases more effectively through improved HC oxidation. Experimental error may also account for some of the difference observed.

Appendix B2: Data Continuity (Chapter 5)

The results from the 7.0 bar IMEP condition in the first part of Chapter 4 are directly comparable with the results from the low tumble condition in this chapter, because they were recorded at the same engine condition (7.0 bar IMEP, low tumble intake airflow). As can be expected, there are some differences between the data.

11% EGR addition was achieved in this chapter even though 12% EGR addition was achieved in the first part of Chapter 4. This was deliberately done in order to achieve the same maximum EGR addition as that for the swirl intake airflow condition in this chapter, to enable a direct comparison to be made. The KLMBT spark timings (Table 5-2) were more advanced than they were in the results from the 7.0 bar IMEP condition in the first part of Chapter 4 (Table 4-3), most likely because of experimental error. The in-cylinder pressures were increased more significantly across the EGR range (Figure 5-1b) than they were in the first part of Chapter 4 (Figure 4-1b), because of the greater spark advance achieved (2 CAD greater with 1% less EGR), in comparison. This is also why the calculated average in-cylinder temperatures (Figure 5-2b) could be increased across the EGR range, while only maintained across the EGR range in the results from the first part of Chapter 4 (Figure 4-2b).

The fuel consumption improvement (Figure 5-4) was less than that achieved in the first part of Chapter 4 (Figure 4-4) because of the 1.6% error in fuel consumption measurements. The EGT reductions (Figure 5-5) were greater than those achieved in the first part of Chapter 4 (Figure 4-5) because of the improved combustion phasing with EGR addition, resulting from the greater KLMBT spark timing advances achieved. This improved the efficiency of pressure and heat transfer into piston work in comparison, resulting in the greater EGT reductions.

PM was reduced with EGR addition (Figure 5-6b) while it was increased with EGR addition in the first part of Chapter 4 (Figure 4-6b), because of the calculated average in-cylinder temperature increases achieved with EGR addition, while they could only be maintained across the EGR range with EGR addition in the first part of Chapter 4. This improved the oxidation of PM across the EGR range, resulting in the observed differences. The PN was significantly lower than that observed in the first part of Chapter 4 mainly because of the effect of the thermodenuder which was used with the SMPS 3936, while for the DMS 500 it was not used. Differences in the equipment design and slight differences in the measuring principle (i.e. differential mobility sizer method vs. scanning mobility particle sizer method) are also likely to have contributed to the lower PN.

Indeed, (Abdul-Khalek et al., 1999) found that the number count of particles less than 50 nm in diameter are heavily influenced by the dilution conditions such as dilution ratio, temperature, relative humidity and residence time, which would vary slightly between the SMPS 3936 and DMS500. While those particles larger than 50 nm are not heavily influenced by the dilution conditions, it is believed they would still be influenced by them to a certain degree, thus helping to explain the observed differences between the data.

Appendix B3: Data Continuity (Chapter 6)

The results from the 7.0 bar IMEP condition in the first part of Chapter 4 are directly comparable with the results from the compression ratio of 11.5 in the second half of this chapter, because they were recorded at the same engine condition (7.0 bar IMEP, compression ratio=11.5). As can be expected, there are some differences between the data.

The KLMBT spark timing advance with EGR addition in the second part of this chapter (Table 6-4) is less than that achieved in the first part of Chapter 4 (Table 4-3) even though the EGR addition was increased (2% increase). It is believed that experimental error accounts for some of the differences observed. Also, the EGR line insulation was improved for the experiments in this chapter, which increased the intake manifold temperature, contributing to the decreased spark advance achieved, in comparison. The in-cylinder pressure decreased in the results from the second part of this chapter (Figures 6-12a-c), while it increased slightly in the first part of Chapter 4 (Figure 4-1b), with EGR addition, due to the reduced KLMBT spark timing advances, in comparison. The increased intake manifold temperatures also decreased the calculated average in-cylinder temperature reductions achieved with EGR addition in the second part of this chapter, as compared to those achieved in the first part of Chapter 4.

The PM accumulation mode decreased with EGR addition in the second part of this chapter (Figures 6-16a-c) while it increased with EGR addition in the first part of Chapter 4 (Figure 4-6b), because of the smaller calculated average in-cylinder temperature reductions achieved which resulted in improved PM oxidation across the EGR range. The reduced KLMBT spark timing advance with EGR addition compared to that achieved in the first part of Chapter 4 improved mixture formation, also contributing to the observed differences in PM behaviour.

The PN was significantly lower than that observed in the first part of Chapter 4 mainly because of the effect of the thermodenuder which was used with the SMPS, while for the DMS500 it was not used. Differences in the equipment design and slight differences in the measuring principle (i.e. differential mobility sizer method vs. scanning mobility particle sizer method) are also likely to have contributed to the lower PN.

Again, (Abdul-Khalek et al., 1999) found that the number count of particles less than 50 nm in diameter are heavily influenced by the dilution conditions such as dilution ratio, temperature, relative humidity and residence time, which would vary slightly between the SMPS and DMS500. While those particles larger than 50 nm are not heavily influenced by the dilution conditions, it is believed they would still be influenced by them to a certain degree, thus helping to explain the observed differences between the data.

Appendix C1: Detailed Specific Further Investigation for Each Research Area

EGR and EGR Type

A real TWC should be used in the suggested extended investigation because the simulated TWC does not introduce any additional HCs into the engine, which has an effect on the results. While a real TWC would convert most of the HCs, it would not be 100% efficient, thus it would introduce some HCs back into the engine, affecting the combustion and emissions. However, the EGR ratio variations resulting from the varying conversion efficiency of the TWC would have to be taken into consideration in the results. A real TWC also increases the exhaust back-pressure resulting in increased pumping losses which is another reason why it should be used in the suggested extended investigation.

The EGR addition should also be increased using an exhaust back pressure valve, for example, in order to quantify the effect of higher EGR ratios on the engine combustion and emissions. The trade-off between increased exhaust back-pressure resulting from the valve and higher EGR ratios should be studied to investigate whether it would be beneficial to increase exhaust back-pressure in engines for the purpose of achieving increased EGR ratios. This trade-off should also be investigated to see whether it is beneficial to remove the NO from the EGR gases for knock reduction, considering any improvements in fuel economy from subsequent KLMBT spark timing advances may be cancelled out by the effects of the increased back-pressure from the TWC. EGR should be studied at a range of temperatures to study the effect EGR temperature has on engine combustion and emissions in more detail.

The PM emissions should also be studied fully with the different EGR types; limited equipment availability prevented this from being done in this investigation. The effect of the

thermodenuder on the PM emission should be more deeply investigated as well as the differences between the DMS 500 and SMPS 3936 PM measurement equipment. Work should also be extended to optical investigations, particularly with Planar Laser Induced Fluorescence (PLIF), to investigate further the effect EGR has on soot formation.

Swirl and Tumble Intake Airflows

Different swirl and tumble ratios should be tested in the suggested extended investigation in order to optimize the ratios to achieve improved engine combustion and PM emissions behaviour. Particularly, they should be further investigated in the optical DISI engine, in order to fully quantify the effect of swirl and tumble ratios on the initial flame propagation and the last remaining 10% MFB, in order to optimize the combustion process. The swirl and tumble ratios should be quantified in the optical engine at 60 CAD intervals during the intake, compression and ignition strokes in order to fully quantify the effect of the intake airflow on the mixture preparation and combustion. A comparison should be made between the estimated and actual swirl and tumble ratios to quantify the accuracy of the estimation process undertaken in this investigation.

The PM change resulting from the retarded spark timings required with the additional intake airflows of swirl and tumble and the PM change resulting from the increased in-cylinder swirl/tumble ratios themselves should be quantified separately in order to investigate the effect of these parameters on PM individually. Further to this, the relationship between flame speed and knock tendency should be investigated further to find the optimum flame speed for minimum knock.

An exhaust back pressure valve should be used on the thermal engine to enable higher EGR ratios to be achieved to study the effect of the laminar flame speed increases resulting from

the increased swirl and tumble ratios being fully suppressed by the EGR gases. Finally, butanol and ethanol fuels should be studied with swirl and tumble intake airflows since they have the potential to compensate for the increased engine knock resulting from the faster laminar flame speeds.

Compression Ratio

The engine should be tested with a greater compression ratio range because some of the effects observed, particularly regarding PM behaviour, were not significant due to the relatively small range tested in this investigation. In addition, it is believed that Bu20 performed better than E20 in this investigation because they were only tested over a small compression ratio range. E20 would be expected to perform better than Bu20 over a larger compression ratio range because of its superior properties (higher octane number, higher HoV), particularly at compression ratios higher than 11.5. The larger compression ratio range should also be investigated in a turbocharged DISI engine along with EGR, to quantify the improvement in compression ratio that can be achieved with the knock suppression effect of the EGR gases. This is because compression ratios in turbocharged engines are reduced in comparison to their equivalent NA engines (Su et al., 2014), in order to achieve a high IMEP. Thus, EGR has the potential to enable the compression ratio to be maintained or increased when turbocharging an engine.

Oxygenated Fuels

1-butanol should be tested with and without 5%vol ethanol pre-mixed in the gasoline fuel to quantify exactly what effect the pre-mixed ethanol has on the engine combustion and emissions. In addition, 1-butanol and ethanol should be tested at different blend ratios in gasoline, including blends with both 1-butanol and ethanol in gasoline, in order to find which blends provide the best combustion and emissions characteristics. This is important because

rather than competing with ethanol, 1-butanol and ethanol could be blended together in gasoline to provide potential improvements over using just one of these fuels blended in gasoline. The work should also be extended to optical investigations; particularly that of laminar flame speed measurement, to quantify the effect of fuel blending on this parameter. This is because laminar flame speed significantly influences KLMBT which consequently affects indicated efficiency, exhaust temperature, and PM and gaseous emissions. A suitable FTIR detector should be used when testing the oxygenated fuels to ensure that the oxygenated hydrocarbons can successfully be measured.

List of References

ABD-ALLA, G. H. 2002. Using exhaust gas recirculation in internal combustion engines: a review. Energy Conversion and Management. 43 (8), 1027–1042, doi:10.1016/S0196-8904(01)00091-7.

ABDUL-KHALEK, I., KITTELSON, D. AND BREAR, F. 1999. The Influence of Dilution Conditions on Diesel Exhaust Particle Size Distribution Measurements. SAE Paper 1999-01-1142, doi:10.4271/1999-01-1142.

AGARWAL, A. K., PANDEY, A., GUPTA, A. K., AGGARWAL, S. K. AND KUSHARI, A. 2014. Novel Combustion Concepts for Sustainable Energy Development. New Delhi: Springer India.

ALEIFERIS, P. G., SERRAS-PEREIRA, J. AND RICHARDSON, D. 2013. Characterisation of flame development with ethanol, butanol, iso-octane, gasoline and methane in adirect-injection spark-ignition engine. Fuel, 109, 256-278, doi:http://dx.doi.org/10.1016/j.fuel.2012.12.088.

ALGER, T., HALL, M. AND MATTHEWS, R. 2000. Effects of Swirl and Tumble on In-Cylinder Fuel Distribution in a Central Injected DISI Engine. SAE Technical Paper 2000-01-0533, doi:10.4271/2000-01-0533.

ALGER, T., CHAUVET, T. AND DIMITROVA, Z. 2009a. Synergies between High EGR Operation and GDI Systems. SAE Int. J. Engines 1(1):101-114, doi:10.4271/2008-01-0134.

ALGER, T. AND MANGOLD, B. 2009. Dedicated EGR: A New Concept in High Efficiency Engines. SAE Int. J. Engines 2(1):620-631, doi:10.4271/2009-01-0694.

ALGER, T., GINGRICH, J., KHALEK, I., AND MANGOLD, B. 2010. The Role of EGR in PM Emissions from Gasoline Engines. SAE Int. J. Fuels Lubr. 3(1):85-98, doi:10.4271/2010-01-0353.

ALGER, T., GUKELBERGER, R., GINGRICH, J. AND MANGOLD, B. 2015. The Impact of Cooled EGR on Peak Cylinder Pressure in a Turbocharged, Spark Ignited Engine. SAE Int. J. Engines 8(2):455-463, doi:10.4271/2015-01-0744.

AL-HASAN, M. 2003. Effect of ethanol–unleaded gasoline blends on engine performance and exhaust emission. Energy Conversion and Management. 44 (9), 1547–1561, doi:10.1016/S0196-8904(02)00166-8.

AMANN, M. AND ALGER, T. 2012. Lubricant Reactivity Effects on Gasoline Spark Ignition Engine Knock. SAE Int. J. Fuels Lubr. 5(2):760-771, doi:10.4271/2012-01-1140.

ANALIIT AA. 2015. Gasoline EN 228. Available: http://www.analiit.ee/index.php?option=com_content&view=article&id=48&lang=en. Last accessed 27th February 2015.

ANDERSON, J., LEONE, T., SHELBY, M., WALLINGTON, T., BIZUB, J. J. AND FOSTER, M. 2012a. Octane Numbers of Ethanol-Gasoline Blends: Measurements and Novel Estimation Method from Molar Composition. SAE Technical Paper 2012-01-1274, doi:10.4271/2012-01-1274.

ANDERSON, J. O., THUNDIYIL, J. G. AND STOLBACH, A. 2012b. Clearing the Air: A Review of the Effects of Particulate Matter Air Pollution on Human Health. Journal of Medical Toxicology, 8, 166-175, doi:10.1007/s13181-011-0203-1.

ARCOUMANIS, C. AND KAMIMOTO, T. 2009. Flow and Combusiton in Reciprocating Engines. Berlin: Springer-Verlag.

BALABIN, R. M., SYUNYAEV, R. Z. AND KARPOV, S. A. 2007. Molar enthalpy of vaporization of ethanol–gasoline mixtures and their colloid state. Fuel, 86, 323-327, doi:10.1016/j.fuel.2006.08.008.

BAYRAKTAR, H. 2005. Experimental and theoretical investigation of using gasoline–ethanol blends in spark-ignition engines. Renewable Energy. 30 (11), 1733–1747, doi:10.1016/j.renene.2005.01.006.

BECK, C., STEVENSON, P. AND ZIMAN, P. 2006. The Impact of Gasoline Octane on Fuel Economy in Modern Vehicles. SAE Technical Paper 2006-01-3407, doi:10.4271/2006-01-3407.

BENNETT, S. 2010. Diesel Engines- Modern Diesel Technology. New York: Delmar.

BENNETT, S. 2013. Medium/Heavy Duty Truck Engines, Fuel & Computerized Management Systems. New York: Delmar.

BIELACZYC, P., SZCZOTKA, A. AND WOODBURN, J. 2014. The Impact of Fuel Ethanol Content on Particulate Emissions from Light-Duty Vehicles Featuring Spark Ignition Engines. SAE Int. J. Fuels Lubr. 7(1):224-235, doi:10.4271/2014-01-1463.

BOCK, B., BELL, A. AND FLOWEDAY, G. 2013. Investigation into the Influence of Charge Cooling and Autoignition Chemistry on the Greater Knock Resistance of Ethanol over Iso-octane. SAE Technical Paper 2013-01-2615, doi:10.4271/2013-01-2615.

BP. 2015. Oil reserves. Available: http://www.bp.com/en/global/corporate/about-bp/energy-economics/statistical-review-of-world-energy/review-by-energy-type/oil/oil-reserves.html. Last accessed 15th Sep 2015.

BRADLEY, D., MORLEY, C. AND WALMSLEY, H. 2004. Relevance of Research and Motor Octane Numbers to the Prediction of Engine Autoignition. SAE Technical Paper 2004-01-1970, doi:10.4271/2004-01-1970.

BRUSIANI, F., FALFARI, S. AND CAZZOLI, G. 2014. Tumble Motion Generation in Small Gasoline Engines: A New Methodological Approach for the Analysis of the Influence of the Intake Duct Geometrical Parameters. Energy Procedia. 45, 997–1006, doi:10.1016/j.egypro.2014.01.105.

BURTON, G., HOLMAN, J., LAZONBY, J., PILLING, G. AND WADDINGTON, D. 2000. Chemical Storylines. Oxford: Heinemann.

BURTSCHER, H. 2005. Physical characterization of particulate emissions from diesel engines: a review. Journal of Aerosol Science, 36, 896-932, doi:10.1016/j.jaerosci.2004.12.001.

CAIRNS, A., BLAXILL, H. AND IRLAM, G. 2006. Exhaust Gas Recirculation for Improved Part and Full Load Fuel Economy in a Turbocharged Gasoline Engine. SAE Technical Paper 2006-01-0047, doi:10.4271/2006-01-0047.

CAMBUSTION LTD. 2011. DMS500 Fast Particulate Spectrometer with Heated Sample Line High Ratio Diluter User Manual Version 3.5 Software Version UI v4.11.

CASTAGNÉ, M., DUMAS, J., HENRIOT, S. AND LAFOSSAS, F. A. 2003. New Knock Localization Methodology for SI Engines. SAE Technical Paper 2003-01-1118, doi:10.4271/2003-01-1118.

CATAPANO, F., DI IORIO, S., SEMENTA, P. AND VAGLIECO, B. 2014. Characterization of Ethanol-Gasoline Blends Combustion processes and Particle Emissions in a GDI/PFI Small Engine. SAE Technical Paper 2014-01-1382, doi:10.4271/2014-01-1382.

CENGEL, Y. A. AND BOLES, M. A. 2007. Thermodynamics An Engineering Approach. New York: McGraw-Hill.

CHECKEL, M. AND DALE, J. 1989. Pressure Trace Knock Measurement in a Current S.I. Production Engine. SAE Technical Paper 890243, doi:10.4271/890243.

CHEN, R., OKAZUMI, R., NISHIDA, K. AND OGATA, Y. 2015. Effect of Ethanol Ratio on Ignition and Combustion of Ethanol-Gasoline Blend Spray in DISI Engine-Like Condition. SAE Int. J. Fuels Lubr. 8(2):264-276, 2015, doi:10.4271/2015-01-0774.

CHENG, W. K., SUMMER, T AND COLLINGS, N. 1998. The Fast-response Flame Ionization Detector. Progress in Energy and Combustion Science, 24, 89-124, doi:10.1016/S0360-1285(97)00025-7.

CHEVRON. 2009. Motor Gasolines Technical Review. Available: http://www.chevron.com/documents/pdf/MotorGasTechReview.pdf. Last accessed 27th February 2015.

COSTAGLIOLA, M. A., DE SIMIO, L., IANNACCONE, S. AND PRATI, M. V. 2013. Combustion efficiency and engine out emissions of a S.I. engine fueled with alcohol/gasoline blends. Applied Energy, 111, 1162-1171, doi:http://dx.doi.org/10.1016/j.apenergy.2012.09.042.

DANIEL, R., TIAN, G., XU, H., WYSZYNSKI, M.L., WU, X. AND HUANG, Z. 2011. Effect of spark timing and load on a DISI engine fuelled with 2,5-dimethylfuran. Fuel, 90, 449-458, doi:10.1016/j.fuel.2010.10.008.

DANIEL, R., XU, H., WANG, C., RICHARDSON, D. AND SHUAI, S. 2012a. Combustion performance of 2,5-dimethylfuran blends using dual-injection compared to direct-injection in a SI engine. Applied Energy, 98, 59-68, doi:http://dx.doi.org/10.1016/j.apenergy.2012.02.073

DANIEL, R., WANG, C., XU, H., TIAN, G. AND RICHARDSON, D. 2012b. Dual-Injection as a Knock Mitigation Strategy Using Pure Ethanol and Methanol. SAE Int. J. Fuels Lubr. 5(2):772-784, doi:10.4271/2012-01-1152.

DANIEL, R., WANG, C., XU, H. AND TIAN, G. 2012c. Effects of Combustion Phasing, Injection Timing, Relative Air-Fuel Ratio and Variable Valve Timing on SI Engine Performance and Emissions using 2,5-Dimethylfuran. SAE Int. J. Fuels Lubr. 5(2):855-866, doi:10.4271/2012-01-1285.

DANIEL, R. 2012d. Combustion and emissions performance of oxygenated fuels in a modern spark ignition engine. PhD Thesis, University of Birmingham.

DANIEL, R., TIAN, G., XU, H. AND SHUAI, S. 2012e. Ignition timing sensitivities of oxygenated biofuels compared to gasoline in a direct-injection SI engine. Fuel. 99, 72-82, doi:http://dx.doi.org/10.1016/j.fuel.2012.01.053.

DAVIS, G. AND BORGNAKKE, C. 1982. The Effect of In-Cylinder Flow Processes (Swirl, Squish and Turbulence Intensity) on Engine Efficiency — Model Predictions. SAE Technical Paper 820045, doi:10.4271/820045.

DE ABRANTES, R., DE ASSUNÇÃO, J. V., PESQUERO, C. R., BRUNS, R. E. AND NÓBREGA, R. P. 2009. Emission of polycyclic aromatic hydrocarbons from gasohol and ethanol vehicles. Atmospheric Environment. 43 (3), 648–654, doi:10.1016/j.atmosenv.2008.10.014.

DE O. CARVALHO, L., DE MELO, T. AND DE AZEVEDO CRUZ NETO, R. 2012. Investigation on the Fuel and Engine Parameters that Affect the Half Mass Fraction Burned (CA50) Optimum Crank Angle. SAE Technical Paper 2012-36-0498, doi:10.4271/2012-36-0498.

DELPHI 2012. Worldwide Emissions Standards - Passenger Cars and Light Duty Vehicles.

DENG, B., YANG, J. AND ZHANG, D. 2013a. The challenges and strategies of butanol application in conventional engines: The sensitivity study of ignition and valve timing. Applied Energy, 108, 248-260, doi:http://dx.doi.org/10.1016/j.apenergy.2013.03.018.

DENG, B., FU, J., ZHANG, D., YANG, J., FENG, R., LIU, J., LI, K. AND LIU, X. 2013b. The heat release analysis of bio-butanol/gasoline blends on a high speed SI (spark ignition) engine. Energy. 60, 230–241, doi:10.1016/j.energy.2013.07.055.

DI IORIO, S., LAZZARO, M., SEMENTA, P., VAGLIECO, B. AND CATAPANO, F. 2011. Particle Size Distributions from a DI High Performance SI Engine Fuelled with Gasoline-Ethanol Blended Fuels. SAE Technical Paper 2011-24-0211, doi:10.4271/2011-24-0211.

DIANA, S., GIGLIO, V., IORIO, B. AND POLICE, G. 1996. A Strategy to Improve the Efficiency of Stoichiometric Spark Ignition Engines. SAE Technical Paper 961953, doi:10.4271/961953.

DIRECTIVE 2009/28/EC. 2009. On the promotion of the use of energy from renewable sources. Official Journal of the European Union; 2009.

DUNN-RANKIN, D. 2008. Lean Combustion- Technology and Control. Burlington, MA: Elsevier.

EASTOP, T. D. AND MCCONKEY, A. 1993. Applied Thermodynamics for Engineering Technologists, London: Longman.

EASTWOOD, P. 2008. Particulate Emissions from Vehicles, Chichester, John Wiley & Sons Ltd.

ENDRES, H., NEUBER, H. AND WURMS, R. 1992. Influence of Swirl and Tumble on Economy and Emissions of Multi Valve SI Engines. SAE Technical Paper 920516, doi:10.4271/920516.

ELFASAKHANY, A. 2014. Experimental study on emissions and performance of an internal combustion engine fueled with gasoline and gasoline/n-butanol blends. Energy Conversion and Management. 88, 277–283, doi:10.1016/j.enconman.2014.08.031.

EUROPEAN COUNCIL. 2016. Vehicle emissions in real driving conditions: Council gives green light to second package. Available: http://www.consilium.europa.eu/en/press/press-releases/2016/02/12-vehicle-emissions-in-real-driving-conditions-2nd-package/. Last accessed 6th Apr 2016.

FENG, R., YANG, J., ZHANG, D., DENG, B., FU, J., LIU, J. AND LIU, X. 2013. Experimental study on SI engine fuelled with butanol–gasoline blend and H2O addition. Energy Conversion and Management. 74, 192–200, doi:10.1016/j.enconman.2013.05.021.

FLOCH, A., VAN FRANK, J. AND AHMED, A. 1995. Comparison of the Effects of Intake-Generated Swirl and Tumble on Turbulence Characteristics in a 4-Valve Engine. SAE Technical Paper 952457, doi:10.4271/952457.

DENG, B., FU, J., ZHANG, D., YANG, J., FENG, R., LIU, J., LI, K. AND LIU, X. 2013b. The heat release analysis of bio-butanol/gasoline blends on a high speed SI (spark ignition) engine. Energy. 60, 230–241, doi:10.1016/j.energy.2013.07.055.

FOUNTAIN, H. 2012. Corn Ethanol Makers Weigh Switch to Butanol. Available: http://www.nytimes.com/2012/10/24/business/energy-environment/weighing-butanol-as-an-alternative-to-ethanol.html?_r=0. Last accessed 27th February 2015.

FRANCQUEVILLE, L. AND MICHEL, J. 2014. On the Effects of EGR on Spark-Ignited Gasoline Combustion at High Load. SAE Int. J. Engines 7(4):1808-1823, doi:10.4271/2014-01-2628.

FRENNET, A. AND BASTIN, J.-M. 1995. Catalysis and Automotive Pollution Control III. Amsterdam: Elsevier.

FU, J., DENG, B., WANG, Y., YANG, J., ZHANG, D., XU, Z. AND LIU, J. 2014. Numerical study and correlation development on laminar burning velocities of n-butanol, iso-octane and their blends: Focusing on diluent and blend ratio effects. Fuel. 124, 102–112, doi:10.1016/j.fuel.2014.01.092.

FUJIMOTO, M. AND TABATA, M. 1993. Effect of Swirl Rate on Mixture Formation in a Spark Ignition Engine Based on Laser 2-D Visualization Techniques. SAE Technical Paper 931905, doi:10.4271/931905.

GILL, S., TURNER, D., TSOLAKIS, A. AND YORK, A. 2011. Understanding the Role of Filtered EGR on PM Emissions. SAE Technical Paper 2011-01-2080, doi:10.4271/2011-01-2080.

GALLONI, E., FONTANA, G. AND PALMACCIO, R. 2013. Effects of exhaust gas recycle in a downsized gasoline engine. Applied Energy. 105, 99–107, doi:10.1016/j.apenergy.2012.12.046.

GOLDING, B. T. AND WATSON, W. P. 1999. Possible mechanisms of carcinogenesis after exposure to benzene. IARC scientific publications, 150, 75-88, doi: unavailable.

GOSWAMI, A., VASHIST, S. AND NAYYAR, A. 2015. Effect of Compression Ratio on the Performance Characteristics of Spark Ignition Engine Fueled with Alternative Fuels: A Review. SAE Technical Paper 2015-01-0766, doi:10.4271/2015-01-0766.

GOV UK. 2011. Public attitudes towards climate change and the impact of transport: 2010. Available: https://www.gov.uk/government/uploads/system/uploads/attachment_data/file/8916/climate-change-2010-report.pdf. Last accessed 27th February 2015.

GRAHAM, L. A., BELISLE, S. L. AND BAAS, C.-L. 2008. Emissions from light duty gasoline vehicles operating on low blend ethanol gasoline and E85. Atmospheric Environment. 42 (19), 4498–4516, doi:10.1016/j.atmosenv.2008.01.061.

GRANDIN, B., ÅNGSTRÖM, H., STÅLHAMMAR, P. AND OLOFSSON, E. 1998. Knock Suppression in a Turbocharged SI Engine by Using Cooled EGR. SAE Technical Paper 982476, doi:10.4271/982476.

GREEN CAR CONGRESS. 2006. Mercedes-Benz Premiers New Gasoline Direct Injection System for More Power and Lower Fuel Consumption. Available: http://www.greencarcongress.com/2006/02/mercedesbenz_pr.html. Last accessed 26th Feb 2015.

GREEN CAR CONGRESS. 2013. 2013 SAE International High Octane Fuels Symposium: the potential for high octane fuels (Part 1). Available: http://www.greencarcongress.com/2013/01/hofs-20130131.html. Last accessed 25th Feb 2015.

GU, X., HUANG, Z., CAI, J., GONG, J., WU, X. AND LEE, C.-F. 2012. Emission characteristics of a spark-ignition engine fuelled with gasoline-n-butanol blends in combination with EGR. Fuel, 93, 611-617, doi:10.1016/j.fuel.2011.11.040.

GUMBLETON, J., NIEPOTH, G. AND CURRIE, J. 1976. Effect of Energy and Emission Constraints on Compression Ratio. SAE Technical Paper 760826, doi:10.4271/760826.

GUPTA, H. N. 2013. Fundamentals of Internal Combustion Engines. 2nd ed. Delhi, India: Phi Learning.

HAMILTON, L., ROSTEDT, M., CATON, P. AND COWART, J. 2008. Pre-Ignition Characteristics of Ethanol and E85 in a Spark Ignition Engine. SAE Int. J. Fuels Lubr. 1(1):145-154, doi:10.4271/2008-01-0321.

HARADA, J., TOMITA, T., MIZUNO, H., MASHIKI, Z. AND ITO, Y. 1997. Development of Direct Injection Gasoline Engine. SAE Technical Paper 970540, doi:10.4271/970540.

HARRINGTON, J. A. AND SHISHU, R.C. 1973. A Single-Cylinder Engine Study of the Effects of Fuel Type, Fuel Stoichiometry, and Hydrogen-to-Carbon Ratio and CO, NO, and HC Exhaust Emissions. SAE 730476, doi:10.4271/730476.

HE, B.-Q., WANG, J.-X., HAO, J.-M., YAN, X.-G. AND XIAO, J.-H. 2003. A study on emission characteristics of an EFI engine with ethanol blended gasoline fuels. Atmospheric Environment. 37 (7), 949–957, doi:10.1016/S1352-2310(02)00973-1.

HE, X., IRELAND, J., ZIGLER, B., RATCLIFF, M. A., KNOLL, K. E., ALLEMAN, T. L. AND TESTER, J. T. 2010. The Impacts of Mid-level Biofuel Content in Gasoline on SIDI Engine-out and Tailpipe Particulate Matter Emissions. SAE Technical Paper 2010-01-2125, doi:10.4271/2010-01-2125.

HE, B.-Q., LIU, M.-B. AND ZHAO, H. 2015. Comparison of combustion characteristics of n-butanol/ ethanol–gasoline blends in a HCCI engine. Energy Conversion and Management. 95, 101–109, doi:10.1016/j.enconman.2015.02.019.

HEDGE, M., WEBER, P., GINGRICH, J., ALGER, T. AND KHALEK, I. 2011. Effect of EGR on Particle Emissions from a GDI Engine. SAE Int. J. Engines 4(1):650-666, doi:10.4271/2011-01-0636.

HEFFEL, J. W. 2003. NO_x emission and performance data for a hydrogen fueled internal combustion engine at using exhaust gas recirculation. International Journal of Hydrogen Energy. 28, 901–908, doi:10.1016/S0360-3199(02)00157-X.

HEYWOOD, J. 1988, Internal Combustion Engine Fundamentals, Singapore, McGraw-Hill.

HEYWOOD, J. AND WELLING, O. 2009. Trends in Performance Characteristics of Modern Automobile SI and Diesel Engines. SAE Int. J. Engines 2(1):1650-1662, doi:10.4271/2009-01-1892.

HIROOKA, H., MORI, S. AND SHIMIZU, R. 2004. Effects of High Turbulence Flow on Knock Characteristics. SAE Technical Paper 2004-01-0977, doi:10.4271/2004-01-0977.

HOFFMEYER, H., MONTEFRANCESCO, E., BECK, L., WILLAND, J., ZIEBART, F. AND MAUSS, F. 2009. CARE – CAtalytic Reformated Exhaust Gases in Turbocharged DISI-Engines, SAE Int. J. Fuels Lubr. 2(1):139-148, doi:10.4271/2009-01-0503.

HOUNTALAS, D. T. AND ANESTIS, A. 1998. Effect of pressure transducer position on measured cylinder pressure diagram of high speed diesel engines. Energy Conversion and Management, 39, 589–607, doi:10.1016/S0196-8904(97)10009-7.

HSIEH, W.-D., CHEN, R.-H., WU, T.-L. AND LIN, T.-H. 2002. Engine performance and pollutant emission of an SI engine using ethanol–gasoline blended fuels. Atmospheric Environment. 36 (3), 403–410, doi:10.1016/S1352-2310(01)00508-8.

HU, E., HU, X., WANG, X., XU, Y., DEARN, K. D. AND XU, H. 2012. On the fundamental lubricity of 2,5-dimethylfuran as a synthetic engine fuel. Tribology International, 55, 119–125, doi:http://dx.doi.org/10.1016/j.triboint.2012.06.005

HULL, A., GOLUBKOV, I., KRONBERG, B., MARANDZHEVA, T. AND VAN STAM, J. 2005. An alternative fuel for spark ignition engines. International Journal of Engine Research, 7 , 203-214, doi:10.1243/14680874JER02504.

IKEYA, K., TAKAZAWA, M., YAMADA, T., PARK, S. AND TAGISHI, R. 2015. Thermal Efficiency Enhancement of a Gasoline Engine. SAE Int. J. Engines 8(4), doi:10.4271/2015-01-1263.

ISERMANN, R. 2014. Engine Modeling and Control- Modeling and Electronic Management of Internal Combustion Engines. New York: Springer-Verlag.

INSTITUTION OF MECHANICAL ENGINEERS. 2013. Internal Combustion Engines: Performance, Fuel Economy and Emissions. Cambridge: Woodhead Publishing.

IRIMESCU, A., MARCHITTO, L., MEROLA, S. S., TORNATORE, C. AND VALENTINO, G. 2015. Combustion process investigations in an optically accessible DISI engine fuelled with n-butanol during part load operation. Renewable Energy. 77, 363–376, doi:10.1016/j.renene.2014.12.029.

JOHNSON, T. 2010. Review of CO_2 Emissions and Technologies in the Road Transportation Sector. SAE Int. J. Engines 3(1):1079-1098, doi:10.4271/2010-01-1276.

KALGHATGI, G. 2013. Fuel/Engine Interactions, Warrendale (USA), SAE International.

KALGHATGI, G. 2014. The outlook for fuels for internal combustion engines. International Journal of Engine Research. Special Article, 1-17, doi: 10.1177/1468087414526189.

KARAVALAKIS, G., SHORT, D., HAJBABAEI, M., VU, D., VILLELA, M., RUSSELL, R., DURBIN, T. AND ASA-AWUKU, A. 2013. Criteria Emissions, Particle Number Emissions, Size Distributions, and Black Carbon Measurements from PFI Gasoline Vehicles Fuelled with Different Ethanol and Butanol Blends. SAE Technical Paper 2013-01-1147, doi:10.4271/2013-01-1147.

KARAVALAKIS, G., SHORT, D., VU, D., VILLELA, M., ASA-AWUKU, A. AND DURBIN, T. D. 2014. Evaluating the regulated emissions, air toxics, ultrafine particles, and black carbon from SI-PFI and SI-DI vehicles operating on different ethanol and iso-butanol blends. Fuel. 128, 410–421, doi:10.1016/j.fuel.2014.03.016.

KAWABATA, Y., SAKONJI, T. AND AMANO, T. 1999. The Effect of NO_x on Knock in Spark-ignition Engines. SAE Technical Paper 1999-01-0572, doi:10.4271/1999-01-0572.

KESKIN, A. AND GÜRÜ, M. 2011. The Effects of Ethanol and Propanol Additions Into Unleaded Gasoline on Exhaust and Noise Emissions of a Spark Ignition Engine. Energy Sources, Part A: Recovery, Utilization, and Environmental Effects. 33 (23), 2194-2205, doi: 10.1080/15567030903530558.

KIM, S. AND KIM, S. 1995. Effects of Swirl and Spark Plug Shape on Combustion Characteristic in a High Speed Single-Shot Visualized SI Engine. SAE Technical Paper 951003, doi:10.4271/951003.

KIM, M., LEE, S. AND KIM, W. 2006. Tumble Flow Measurements Using Three Different Methods and its Effects on Fuel Economy and Emissions. SAE Technical Paper 2006-01-3345, 2006, doi:10.4271/2006-01-3345.

KITTELSON, D. B. 1998. Engines and nanoparticles: a review. Journal of Aerosol Science, 29, 575–588, doi:10.1016/S0021-8502(97)10037-4.

KRAMER, F., SCHWARZ, C. AND WITT, A. 2000. Effect of Compression Ratio on the Combustion of a Pressure Charged Gasoline Direct Injection Engine. SAE Technical Paper 2000-01-0250, doi:10.4271/2000-01-0250.

KUMANO, K. AND YAMAOKA, S. 2014. Analysis of Knocking Suppression Effect of Cooled EGR in Turbo-Charged Gasoline Engine. SAE Technical Paper 2014-01-1217, doi:10.4271/2014-01-1217.

LATTIMORE, T., WANG, C., XU, H., WYSZYNSKI, M. L. AND SHUAI, S. 2016a. Investigation of EGR Effect on Combustion and PM Emissions in a DISI Engine, Applied Energy, 161, 2016, 256-267, doi:10.1016/j.apenergy.2015.09.080.

LATTIMORE, T., HERREROS, J. M., XU, H. AND SHUAI, S. 2016b. Investigation of Compression Ratio and Fuel Effect on Combustion and PM Emissions in a DISI Engine, Fuel, 169, 68-78, doi: 10.1016/j.fuel.2015.10.044.

LECOINTE, B. AND MONNIER, G. 2003. Downsizing a Gasoline Engine Using Turbocharging with Direct Injection. SAE Technical Paper 2003-01-0542, doi:10.4271/2003-01-0542.

LEE, S., TONG, K., QUAY, B., ZELLO, J. AND SANTAVICCA, D. A. 2000. Effects of Swirl and Tumble on Mixture Preparation During Cold Start of a Gasoline Direct-Injection Engine. SAE Technical Paper 2000-01-1900, doi:10.4271/2000-01-1900.

LEE, K., BAE, C. AND KANG, K. 2007. The effects of tumble and swirl flows on flame propagation in a four-valve S.I. engine. Applied Thermal Engineering. 27 (11-12), 2122–2130, doi:10.1016/j.applthermaleng.2006.11.011.

LEPPARD, W. 1982. Individual-Cylinder Knock Occurence and Intensity in Multicylinder Engines. SAE Technical Paper 820074, doi:10.4271/820074.

LEWIS, A., AKEHURST, S., TURNER, J., PATEL, R. AND POPPLEWELL, A. 2014. Observations on the Measurement and Performance Impact of Catalyzed vs. Non Catalyzed EGR on a Heavily Downsized DISI Engine. SAE Int. J. Engines 7(1):458-467, doi:10.4271/2014-01-1196.

LI, Y., ZHAO, H., PENG, Z., AND LADOMMATOS, N. 2001. Analysis of Tumble and Swirl Motions in a Four-Valve SI Engine. SAE Technical Paper 2001-01-3555, doi:10.4271/2001-01-3555.

LIIVA, P., VALENTINE, J., COBB, J., AND ACKER, W. 1992. Use of Multiple Pressure Transducers to Find In-Cylinder Knock Location. SAE Technical Paper 922368, doi:10.4271/922368.

LIU, H., LI, S., ZHENG, Z., XU, J. AND YAO, M. 2013. Effects of n -butanol, 2-butanol, and methyl octynoate addition to diesel fuel on combustion and emissions over a wide range of exhaust gas recirculation (EGR) rates. Applied Energy. 112, 246-256, doi:10.1016/j.apenergy.2013.06.023.

LUSZCZ, P. 2009. Combustion diagnostics in Homogeneous Charge Compression Ignition optical and thermal single cylinder engines. PhD Thesis, University of Birmingham.

MA, X., ZHANG, F., XU, H. AND SHUAI, S. 2014. Throttleless and EGR-controlled stoichiometric combustion in a diesel–gasoline dual-fuel compression ignition engine, Fuel, 115, 765–777, doi:10.1016/j.fuel.2013.07.052.

MAJI, S., BABU, M. AND GUPTA, N. 2001. A Single Cylinder Engine Study of Power, Fuel Consumption and Exhaust Emissions with Ethanol. SAE Technical Paper 2001-28-0029, doi:10.4271/2001-28-0029.

MASUM, B. M., MASJUKI, H. H., KALAM, M.A., RIZWANUL FATTAH, I.M., PALASH, S.M. AND ABEDIN, M.J. 2013. Effect of ethanol–gasoline blend on NO_x emission in SI engine. Renewable and Sustainable Energy Reviews. 24, 209–222, doi:10.1016/j.rser.2013.03.046.

MASUM, B. M., KALAM, M. A., MASJUKI, H. H., PALASH, S. M. AND FATTAH, M. R. 2014. Performance and emission analysis of a multi cylinder gasoline engine operating at different alcohol–gasoline blends. RSC Advances. 4, 27898-27904, doi:10.1039/c4ra04580g.

MATHIS, U., MOHR, M. AND FORSS, A. M. 2005. Comprehensive particle characterization of modern gasoline and diesel passenger cars at low ambient temperatures. Atmospheric Environment, 39, 107-117, doi:10.1016/j.atmosenv.2004.09.029.

MATSUSHITA, S., INOUE, T., NAKANISHI, K., OKUMURA, T. AND ISOGAI, K. 1985. Effects of Helical Port with Swirl Control Valve on the Combustion and Performance of S. I. Engine. SAE Technical Paper 850046, doi:10.4271/850046.

MATTIMARICQ, M. 2012. Soot formation in ethanol/gasoline fuel blend diffusion flames. Combustion and Flame, 159, 170-180, doi:10.1016/j.combustflame.2011.07.010.

MEHTA, D., ALGER, T., HALL, M., MATTHEWS, R. D., AND NG, H. 2001. Particulate Characterization of a DISI Research Engine using a Nephelometer and In-Cylinder Visualizationǁ. SAE Technical Paper 2001-01-1976, doi:10.4271/2001-01-1976.

MIKULEC, A., KENT, J. AND TABACZYNSKI, R. 1988. The Effect of Swirl on Combustion in a Pancake Chamber Spark Ignition Engine: The Case of Constant Inducted Kinetic Energy. SAE Technical Paper 880200, doi:10.4271/880200.

MITSUBISHI MOTORS. 1999. GDI Engine Production Tops 400,000. Available: http://www.mitsubishi-motors.com/en/corporate/pressrelease/corporate/detail791.html. Last accessed 26th Feb 2015.

MITTAL, V., REVIER, B. AND HEYWOOD, J. 2007. Phenomena that Determine Knock Onset in Spark-Ignition Engines. SAE Technical Paper 2007-01-0007, doi:10.4271/2007-01-0007.

NAGAYAMA, I., ARAKI, Y. AND IIOKA, Y. 1977. Effects of Swirl and Squish on S.I. Engine Combustion and Emission. SAE Technical Paper 770217, doi:10.4271/770217.

NATIONAL INSTITUTE OF STANDARDS AND TECHNOLOGY. 2011a. 1-Butanol. Available: http://webbook.nist.gov/cgi/cbook.cgi?ID=C71363&Mask=4. Last accessed 16th Jan 2015.

NATIONAL INSTITUTE OF STANDARDS AND TECHNOLOGY. 2011b. 1-Ethanol. Available: http://webbook.nist.gov/cgi/cbook.cgi?ID=C64175&Mask=4. Last accessed 16th Jan 2015.

NIASS, T., AMER, A., XU, W., VOGEL, S., HORTMANN, K. K., ADOMEIT, P. AND BRASSAT, A. 2012. Butanol Blending - a Promising Approach to Enhance the Thermodynamic Potential of Gasoline - Part 1. SAE Int. J. Fuels Lubr. 5(1):265-273, doi:10.4271/2011-01-1990.

NIEMAN, D., DEMPSEY, A., AND REITZ, R. 2012. Heavy-Duty RCCI Operation Using Natural Gas and Diesel. SAE Int. J. Engines 5(2):270-285, doi:10.4271/2012-01-0379.

NISHIDA, M., INOUE, N., SUZUKI, H., AND KUMAGAI, S. 1988. Closed Loop Control of the EGR Rate Using the Oxygen Sensor. SAE Technical Paper 880133, doi:10.4271/880133.

OJAPAH, M., ZHAO, H. AND ZHANG, Y. 2014. Effects of Ethanol on Performance and Exhaust Emissions from a DI Spark Ignition Engine with Throttled and Unthrottled Operations. SAE Technical Paper 2014-01-1393, doi:10.4271/2014-01-1393.

OKAMOTO, K., ICHIKAWA, T., SAITOH, K., OYAMA, K., HIRAYA, K. AND URUSHIHARA, T. 2003. Study of Antiknock Performance Under Various Octane Numbers and Compression Ratios in a DISI Engine. SAE Technical Paper 2003-01-1804, doi:10.4271/2003-01-1804.

OPPENHEIM, A. K. 2004. Combustion in Piston Engines, Berlin, Springer-Verlag.

OWEN, K. AND COLEY, T. 1995. Automotive Fuels Reference Book, Warrendale, Society of Automotive Engineers.

PAN, M., SHU, G., WEI, H., ZHU, T., LIANG, Y. AND LIU, C. 2014. Effects of EGR, compression ratio and boost pressure on cyclic variation of PFI gasoline engine at WOT operation. Applied Thermal Engineering, 64, 491-498, doi:10.1016/j.applthermaleng.2013.11.013.

PARAG, S. AND RAGHAVAN, V. 2009. Experimental investigation of burning rates of pure ethanol and ethanol blended fuels. Combustion and Flame, 156, 997-1005, doi:10.1016/j.combustflame.2008.10.011.

PARSONS, D., AKEHURST, S. AND BRACE, C. 2015. The potential of catalysed exhaust gas recirculation to improve high-load operation in spark ignition engines. International Journal of Engine Research. 16 (4), 592-605, doi:10.1177/1468087414554628.

PAWLOWSKI, A. AND SPLITTER, D. 2015. SI Engine Trends: A Historical Analysis with Future Projections. SAE Technical Paper 2015-01-0972, doi:10.4271/2015-01-0972.

PCB Piezeotronics. 2013. Introduction to Piezoelectric Pressure Sensors. Available: http://www.pcb.com/TechSupport/Tech_Pres.aspx. Last accessed 4th Mar 2015.

PIOCK, W., HOFFMANN, G., BERNDORFER, A., SALEMI, P. AND FUSSHOELLER, B. 2011. Strategies Towards Meeting Future Particulate Matter Emission Requirements in Homogeneous Gasoline Direct Injection Engines. SAE Int. J. Engines 4(1):1455-1468, doi:10.4271/2011-01-1212.

POITRAS, M., ROSENBLATT, D. AND GOODMAN, J. 2015. Impact of Ethanol and Isobutanol Gasoline Blends on Emissions from a Closed-Loop Small Spark-Ignited Engine. SAE Technical Paper 2015-01-1732, doi:10.4271/2015-01-1732.

RAJPUT, R. K. 2005. A Textbook of Internal Combustion Engines. New Delhi: Laxmi Publications.

RAMADHAS, A. S. 2011. Alternative Fuels for Transportation. Boca Raton, FL: CRC Press.

RATNAK, S., KATORI, K., KUSAKA, J., DAISHO, Y., YOSHIMURA, K. AND KENJIRO, N. 2015. Computational Study to Improve Thermal Efficiency of Spark Ignition Engine. SAE Technical Paper 2015-01-0011, doi:10.4271/2015-01-0011.

REITZE JR., A. W. 2001. Air Pollution Control Law: Compliance & Enforcement. Washington D. C.: Environmental Law Institute.

RHODES, D. AND KECK, J. 1985. Laminar Burning Speed Measurements of Indolene-Air-Diluent Mixtures at High Pressures and Temperatures. SAE Technical Paper 850047, doi:10.4271/850047.

ROBERT BOSCH GMBH. 2006. Gasoline-Engine Management, 3rd edition, Chichester, John Wiley & Sons Ltd.

ROTH, D., KELLER, P. AND BECKER, M. 2010. Requirements of External EGR Systems for Dual Cam Phaser Turbo GDI Engines. SAE Technical Paper 2010-01-0588, doi:10.4271/2010-01-0588.

ROTHE, M., HEIDENREICH, T., SPICHER, U. AND SCHUBERT, A. 2006. Knock Behavior of SI-Engines: Thermodynamic Analysis of Knock Onset Locations and Knock Intensities. SAE Technical Paper 2006-01-0225, doi:10.4271/2006-01-0225.

SERRAS-PEREIRA, J., ALEIFERIS, P. G. AND RICHARDSON, D. 2013. An Analysis of the Combustion Behavior of Ethanol, Butanol, Iso-Octane, Gasoline, and Methane in a Direct-Injection Spark-Ignition Research Engine. Combustion Science and Technology. 185 (3), 484-513, doi:10.1080/00102202.2012.728650.

SHIMOTANI, K., OIKAWA, K., HORADA, O. AND KAGAWA, Y. 1995. Characteristics of gasoline in-cylinder direct injection engine. JSAE Review. 17 (3), 267-272, doi:10.1016/0389-4304(96)00021-5.

SIOKOS, K., KOLI, R., PRUCKA, R., SCHWANKE, J. AND MIERSCH, J. 2015. Assessment of Cooled Low Pressure EGR in a Turbocharged Direct Injection Gasoline Engine. SAE Int. J. Engines 8(4), doi:10.4271/2015-01-1253.

SONG, D., JIA, N., GUO, X., MA, X., MA, Z., GAO, D., LI, K., LAI, H. AND ZHANG, C. 2014. Low Pressure Cooled EGR for Improved Fuel Economy on a Turbocharged PFI Gasoline Engine. SAE Technical Paper 2014-01-1240, doi:10.4271/2014-01-1240.

SPLITTER, D. AND SZYBIST, J. 2014. Intermediate Alcohol-Gasoline Blends, Fuels for Enabling Increased Engine Efficiency and Powertrain Possibilities. SAE Int. J. Fuels Lubr. 7(1):29-47, doi:10.4271/2014-01-1231.

SRINIVASAN, S. 2001. Automotive Engines. New Delhi: Tata McGraw-Hill.
STEIN, R., ANDERSON, J. AND WALLINGTON, T. 2013. An Overview of the Effects of Ethanol-Gasoline Blends on SI Engine Performance, Fuel Efficiency, and Emissions. SAE Int. J. Engines 6(1), doi:10.4271/2013-01-1635

STONE, C. AND LADOMMATOS, N. 1992. The Measurement and Analysis of Swirl in Steady Flow. SAE Technical Paper 921642, doi:10.4271/921642.

STONE, R. 1999. Introduction to Internal Combustion Engines, 3rd edition, Basingstoke: Macmillan Press Ltd.

STONE, R., CHEN, L., HINTON, N. LEACH, F. AND XU, F. 2012. GDI Engine Operation with Ethanol/Gasoline Blends and Aqueous Ethanol. Journal of Automotive Safety and Energy. 3 (3), 257-264, doi:10.3969/j.issn.1674-8484.2012.03.009.

STOREY, J., BARONE, T., NORMAN, K. AND LEWIS, S. 2010. Ethanol Blend Effects On Direct Injection Spark-Ignition Gasoline Vehicle Particulate Matter Emissions. SAE Int. J. Fuels Lubr. 3(2):650-659, doi:10.4271/2010-01-2129.

STROJARSKI FAKULTET. 2015. Properties of some common fuels and hydrocarbons. Available: https://www.sfsb.hr/test/testhome/Test/solve/basics/tables/tablesComb/trash/hhv.html. Last accessed 10th Mar 2015.

SU, J., XU, M., LI, T., GAO, Y. AND WANG, J. 2014. Combined effects of cooled EGR and a higher geometric compression ratio on thermal efficiency improvement of a downsized boosted spark-ignition direct-injection engine. Energy Conversion and Management. 78, 65–73, doi:10.1016/j.enconman.2013.10.041.

SZWAJA, S. AND NABER, J. D. 2010. Combustion of n-butanol in a spark-ignition IC engine. Fuel, 89, 1573–1582, doi:10.1016/j.fuel.2009.08.043

TAKAGI, Y. AND SKIPPON, S. 1998. Effects of In-Cylinder Fuel Spray Formation on Emissions and Cyclic Variability in a Lean-Burn Engine. Part 1: Background and Methodology. SAE Technical Paper 982618, doi:10.4271/982618.

TAKAHASHI, D., NAKATA, K., YOSHIHARA, Y., OHTA, Y. AND NISHIURA, H. 2015. Combustion Development to Achieve Engine Thermal Efficiency of 40% for Hybrid Vehicles. SAE Technical Paper 2015-01-1254, doi:10.4271/2015-01-1254.

TAKAKI, D., TSUCHIDA, H., KOBARA, T., AKAGI, M., TSUYUKI, T. AND NAGAMINE, M. 2014. Study of an EGR System for Downsizing Turbocharged Gasoline Engine to Improve Fuel Economy. SAE Technical Paper 2014-01-1199, doi:10.4271/2014-01-1199.

TERAJI, A., KAKUHO, A., TSUDA, T. AND HASHIZUME, Y. 2009. A Study of the Knocking Mechanism in Terms of Flame Propagation Behavior Based on 3D Numerical Simulations. SAE Int. J. Engines 2(1):666-673, doi:10.4271/2009-01-0699.

THE INSTITUTE OF HISTORICAL RESEARCH, UNIVERSITY OF LONDON 2004. History of Technology (Volume Twenty-Five). London: Thoemmes Continuum.

TIAN, G., LI, H, XU, H., LI, Y, AND SATISH M.R. 2010. Spray Characteristics Study of DMF Using Phase Doppler Particle Analyzer. SAE 2010-01-1505, doi:10.4271/2010-01-1505.

TOMITA, M., IWAKIRI, Y., SAKAI, E., URUSHIHARA, T., INOUE, R. AND KOJIMA, K. 1996. Effects of Gas Flow and Mixture Properties on Engine-Out HC Emissions. SAE Technical Paper 961952, doi:10.4271/961952.

TURNER, D. 2010. The combustion and emissions performance of fuel blends in modern combustion systems. PhD Thesis, University of Birmingham.

TURNER, D., XU, H., CRACKNELL, R. F., NATARAJAN, V. AND CHEN, X. 2011. Combustion performance of bio-ethanol at various blend ratios in a gasoline direct injection engine. Fuel. 90, 1999-2006, doi:10.1016/j.fuel.2010.12.025.

ULSOY, A. G., PENG, H. AND ÇAKMAKCI, M. 2012. Automotive Control Systems. Cambridge: Cambridge University Press.

UNITED STATES ENVIRONMENTAL PROTECTION AGENCY. 2010. Light-Duty Vehicle Greenhouse Gas Emission Standards and Corporate Average Fuel Economy Standards; Final Rule. Available: http://www.nhtsa.gov/staticfiles/rulemaking/pdf/cafe/CAFE-GHG_MY_2012-2016_Final_Rule_FR.pdf. Last accessed 27th February 2015.

UNITED STATES ENVIRONMENTAL PROTECTION AGENCY. 2014. Health. Available: http://www.epa.gov/pm/health.html. Last accessed 16th Jan 2015.

URUSHIHARA, T., MURAYAMA, T., TAKAGI, Y. AND LEE, K. 1995. Turbulence and Cycle-by-Cycle Variation of Mean Velocity Generated by Swirl and Tumble Flow and Their Effects on Combustion. SAE Technical Paper 950813, doi:10.4271/950813.

VAROL, Y., ÖNER, C., ÖZTOP, H. F. AND ALTUN, Ş. 2014. Comparison of Methanol, Ethanol, or n-Butanol Blending with Unleaded Gasoline on Exhaust Emissions of an SI Engine. Energy Sources, Part A: Recovery, Utilization, and Environmental Effects. 36 (9), 938-948, doi:10.1080/15567036.2011.572141.

VUK, C. AND VANDER GRIEND, S. 2013. Fuel Property Effects on Particulates In Spark Ignition Engines. SAE Technical Paper 2013-01-1124, doi:10.4271/2013-01-1124.

WALLNER, T. AND MIERS, S.A 2008. Combustion Behavior of Gasoline and Gasoline/Ethanol Blends in a Modern Direct-Injection 4-Cylinder Engine. SAE 2008-01-0077, doi:10.4271/2008-01-0077.

WALLNER, T., ICKES, A., LAWYER, K., MIERS, S., NABER, J., ERTL, D., WILLIAMSON, R., MIERS, S. A. AND NABER, J. D. 2013. Blend Ratio Optimization of Fuels Containing Gasoline Blendstock, Ethanol, and Higher Alcohols (C3-C6): Part II - Blend Properties and Target Value Sensitivity. SAE International 2013-01-1126, doi:10.4271/2013-01-1126.

WANG, C., XU, H., DANIEL, R., GHAFOURIAN, A., HERREROS, J. M., SHUAI, S. AND MA, X. 2013. Combustion characteristics and emissions of 2-methylfuran compared to 2,5-dimethylfuran, gasoline and ethanol in a DISI engine. Fuel, 103, 200-211, doi:http://dx.doi.org/10.1016/j.fuel.2012.05.043.

WANG, C., XU, H., HERREROS, J. M., WANG, J. AND CRACKNELL, R. 2014a. Impact of fuel and injection system on particle emissions from a GDI engine. Applied Energy, 132, 178–191, doi:http://dx.doi.org/10.1016/j.apenergy.2014.06.012.

WANG, C. 2014b. Combustion and emissions of a direct injection gasoline engine using biofuels. PhD Thesis, University of Birmingham.

WANG, C., XU, H., HERREROS, J. M., LATTIMORE, T. AND SHUAI, S. 2014c. Fuel Effect on Particulate Matter Composition and Soot Oxidation in a Direct-Injection Spark Ignition (DISI) Engine. Energy & Fuels, 28, 2003-2012, doi:10.1021/ef402234z.

WEI, H., ZHU, T., SHU, G., TAN, L. AND WANG, Y. 2012. Gasoline engine exhaust gas recirculation – A review. Applied Energy. 99, 534–544, doi:10.1016/j.apenergy.2012.05.011.

WILLIAMSON, R. 2013. Meeting RFS2 Targets with an E10/E15-like Fuel - Experimental and Analytical Assessment of Higher Alcohols in Multi-component Blends with Gasoline. SAE Int. J. Fuels Lubr. 6(3):691-701, doi:10.4271/2013-01-2612.

WU, C. 2007. Thermodynamics and Heat Powered Cycles: A Cognitive Engineering Approach. New York: Nova Science.

YANG, J. AND ANDERSON, R.W. 1998. Fuel Injection Strategies to Increase Full-Load Torque Output of a Direct-Injection SI Engine. SAE Technical Paper 980495, doi:10.4271/980495.

YEJIAN, Q., CHENGJI, Z., HONGMING, X., JIAN, T. AND QIN, T. 2007. Experimental Investigation of Using Ethanol-gasoline in Electronic Control Gasoline-injection Engine. HKIE Transactions. 14 (2), 26-30, doi:10.1080/1023697X.2007.10668074.

YUAN, H., FOONG, T., CHEN, Z., YANG, Y., BREAR, M., LEONE, T. AND ANDERSON, J. E. 2015. Modeling of Trace Knock in a Modern SI Engine Fuelled by Ethanol/Gasoline Blends. SAE Technical Paper 2015-01-1242, doi:10.4271/2015-01-1242.

ZACCARDI, J., DUVAL, L. AND PAGOT, A. 2009. Development of Specific Tools for Analysis and Quantification of Pre-ignition in a Boosted SI Engine. SAE Int. J. Engines 2(1):1587-1600, doi:10.4271/2009-01-1795.

ZENG, W., SJOBERG, M. AND REUSS, D. L. 2015. PIV examination of spray-enhanced swirl flow for combustion stabilization in a spray-guided stratified-charge direct-injection spark-ignition engine. International Journal of Engine Research. 16 (3), 306–322, doi:10.1177/1468087414564605.

ZHANG, Z., WANG, T., JIA, M., WEI, Q., MENG, X. AND SHU, G. 2014a. Combustion and particle number emissions of a direct injection spark ignition engine operating on ethanol/gasoline and n-butanol/gasoline blends with exhaust gas recirculation. Fuel, 130, 177-188, doi:http://dx.doi.org/10.1016/j.fuel.2014.04.052.

ZHANG, Z., ZHANG, H., WANG, T. AND JIA, M. 2014b. Effects of tumble combined with EGR (exhaust gas recirculation) on the combustion and emissions in a spark ignition engine at part loads. Energy. 65, 18–24, doi:10.1016/j.energy.2013.11.062.

ZHANG, J., NITHYANANDAN, K., LI, Y., LEE, C.-F. AND HUANG, Z. 2015. Comparative Study of High-Alcohol-Content Gasoline Blends in an SI Engine. SAE Technical Paper 2015-01-0891, doi:10.4271/2015-01-0891.

ZHONG, L., MUSIAL, M., REESE, R. AND BLACK, G. 2013. EGR Systems Evaluation in Turbocharged Engines. SAE Technical Paper 2013-01-0936, doi:10.4271/2013-01-0936.

ZHU, G. G., HASKARA, I. AND WINKELMAN, J. 2007. Closed-Loop Ignition Timing Control for SI Engines Using Ionization Current Feedback. EEE Transactions on Control Systems Technology, 15 (3), 416-427, doi:10.1109/TCST.2007.894634.